

Faculty of Engineering - Department of Civil Engineering

Dynamic Filtration at Soil-Geotextile Interfaces

By

MUHAMMAD WALEED KHAN

Thesis submitted to the University of Nottingham for the degree of Doctor of Philosophy in Civil Engineering

January 2017

ABSTRACT

The soil-geotextile filtration mechanism is a complex process which depends on physical compatibility between the geotextile and the soil to be retained. Geotextiles often perform well under steady state conditions like those found in dams. However, when the soil-geotextile interface is subjected to dynamic loading, the requirements for successful filtering are uncertain and/ or conservative as the controlling factors are not well understood in these circumstances. There are few filter design criteria available for dynamic flow conditions. These criteria do not properly address the internal instability of soils for which the rearrangement of particles adjacent to the filter interface is complex. Unstable soils may exist in roadway bases adjacent to pavement edge drain. Therefore, this research work was carried out to better understand the filtration behaviour of non-woven geotextiles with internally stable and unstable soils beneath roads.

To carry out the filtration tests, a flexible wall gradient ratio (GR) apparatus was developed. The GR tests were performed to investigate the effect of different factors on the filtration performance of the soil-geotextile interface under dynamic conditions. The factors included hydraulic gradient, vertical stress and frequency of loading, soil gradation and geotextile properties. Test results were interpreted in terms of head loss within the soil and across the geotextile, GR values, permeability ratio, mass and gradation of particles passed through geotextiles, microscopic images of geotextiles after test, partial geotextile clogging levels and hydrometer sieve analyses of soil samples to compare the gradation of samples after test with the original gradation.

All the tests were performed under a hydraulic gradient of five. The internal stability of soil samples were evaluated by three geometric criteria. The test results showed that a

high hydraulic gradient has the ability to lead to the internal instability of soils which resulted in migration of fines towards the geotextiles. The dynamic loading resulted in increase of soil migration within the base soil as well as washing out of soil particles through geotextiles. No significant effect of increase in frequency and vertical stress was observed on filtration behaviour of soil-geotextile combinations. The geotextile pore size was found to be the main factor controlling the filtration behaviour as compared to other geotextile properties. The Kenney and Lau (1985) and the Kezdi (1979) criteria predicted well the internal instability of soils under dynamic conditions.

In this research study, a new method was suggested which is able to measure the pore sizes along the entire thickness of geotextiles. The filtration tests showed that geotextiles having the same large openings but different pore size distributions may result in different filtration performances. Based on the test results, filter design criteria were suggested for piping and blinding limits which were compared with the existing design criteria. These new filter criteria were found to be more appropriate in terms of piping and blinding limit states.

To my family

ACKNOWLEDGEMENTS

First and foremost, praises and thanks to Almighty God, for His showers of blessings throughout my research work to accomplish it successfully.

I would like to thank the University of Nottingham for rewarding a highly competitive scholarship to support this PhD study.

This thesis owes its existence to the help and support of several people.

I would like to express my sincere gratitude and appreciation to my supervisors Mr. Andrew Dawson and Dr. Alec Marshall for providing me continuous guidance, insight, constructive criticism, assistance, scholarly inputs and consistent encouragement that kept me motivated throughout this research work. Special thank is due to Mr. Andrew Dawson for putting his effort in reviewing my thesis chapters, and who responded to my questions and queries so promptly.

I would like to express my appreciation towards my internal examiner Dr. Mohammad Rezania who gave positive criticism and guidance during my first and second year PhD reviews.

Special thanks are given to all the academic staff in Nottingham Transportation Engineering Center (NTEC). Significant part of this research was based on experimental work and I would like to extend my thanks to all the technicians at NTEC and Nottingham Center for Geomechanics (NCG) for their valuable assistance to carry out experimental work especially Mr. Richard Blakemore, Mr. Martyn Barrett, and Mr. John Watson. I would also like to extend my thanks to Mr. Balbir Loyla (Structures Laboratory) for his continuous help to fix the pressure sensors.

I would also like to thank all my friends and fellow researchers at NTEC, with whom I have shared many enjoyable times.

Finally, I am extremely grateful to my parents, my sisters, and my brothers for their patience and continued support throughout the research period. I could not have pursued this degree without the love and support of my family.

DECLARATION

This research described in this thesis was conducted at the Civil Engineering Department, the University of Nottingham between October 2012 and September 2016. I declare that the work is my own and has not been submitted for a degree at another university.

Muhammad Waleed Khan

University of Nottingham

TABLE OF CONTENTS

ABSTRACT ..... **I**

ACKNOWLEDGEMENTS ..... **IV**

DECLARATION ..... **V**

TABLE OF CONTENTS ..... **VI**

LIST OF FIGURES ..... **XII**

LIST OF TABLES ..... **XVII**

LIST OF ABBREVIATIONS ..... **XIX**

1. INTRODUCTION **1**

1.1. Background 1

1.2. Problem Statement 2

1.3. Aim & Objectives 4

1.4. Research Methodology 5

1.5. Thesis Organization 9

2. LITERATURE REVIEW **11**

2.1. Soil Filtration Using Geotextiles 11

2.2. Seepage Flow 14

2.2.1. Saturated Soil 16

2.2.2. Partially Saturated Soils 18

2.3. Geotextile Filters in Pavements 20

2.4. Mechanism of Geotextile Filtration 22

2.5. Internal Stability of Cohesionless Soils 26

2.5.1. Evaluation of Soil Internal Stability: Geometric Criteria 28

2.5.2. Initiaition of Soil Instability: Hydraulic Criteria 36

2.5.3. Summary 38

2.6. Factors Affecting the Internal Stability of Cohesionless Soils 40

2.6.1. Particle Shape and Size 40
2.6.2. Density 40
2.6.3. Confining Stress 40
2.6.4. Mechanical Loading 41
2.6.5. Hydraulic Loading 41
2.7. Effect of Geotextile Properties on Filtration Performance 42
2.7.1. Filter Opening Size 42
2.7.2. Weaving Pattern 52
2.7.3. Porosity 54
2.7.4. Thickness 54
2.7.5. Compressibility 56
2.8. Boundary Conditions Affecting Soil-Geotextile Filtration Behaviour 56
2.8.1. Top Load 56
2.8.2. Hydraulic Gradient 57
2.8.3. Dynamic Conditions 58
2.9. Filter Design Criteria 61
2.9.1. Retention criterion 61
2.9.2. Permeability Criterion 66
2.9.3. Clogging Criterion 68
2.10. Previous Laboratory Studies 69
2.10.1. Gradient Ratio (GR) Test (Steady State Conditions) 69
2.10.2. Dynamic Flow Conditions 74
2.11. Summary 79
2.12. Research Implications 81
3. MATERIAL PROPERTIES 83
3.1. Introduction 83
3.2. Geotextile Properties 83
3.3. Soil Properties 84

3.3.1. Medium Sand 85
3.3.2. PFA Soil 86
3.3.3. Different Soil Gradations 87
3.4. Internal Stability of Soils 89
3.4.1. Kezdi's Criterion 90
3.4.2. Kenney and Lau's Criterion 90
3.4.3. Burenkova's Criterion 91
3.5. Test Program 93
4. DYNAMIC GR TEST APPARATUS AND TEST PROCEDURE 94
4.1. Dynamic GR Apparatus 94
4.1.1. Modified Triaxial Cell 96
4.1.2. Pore Pressure Transducers 102
4.1.3. Dynamic Load Cell Actuator 105
4.1.4. Hydraulic Supply System 105
4.1.5. Confining Pressure 106
4.1.6. Filter Holder For Collecting Particles 106
4.1.7. Flow Rate Measurement 107
4.2. Test Procedure 108
4.2.1. Test Sample Preparation 108
4.2.2. Sample Saturation 111
4.2.3. Test Setup 113
4.2.4. Test Programme 114
4.2.5. Post Test Procedure 118
4.2.6. Microscopic Images of Geotextile and Soil After Test 118
5. DYNAMIC GR TEST RESULTS 123
5.1. Introduction 123
5.2. Head Losses in the Sample 124
5.3. Filtration Behaviour of Narrow Graded Soils 126

5.3.1. Water Head Distribution 126
5.3.2. Gradient Ratio 134
5.3.3. Permeability 136
5.3.4. Post-Test Procedure 138
5.4. Filtration Behaviour of Broadly Graded Soils 145
5.4.1. Water Head Distribution 146
5.4.2. Gradient Ratio 150
5.4.3. Permeability 152
5.4.4. Post Test Procedure 155
5.5. Test Repeatability 164
5.6. Test without Geotextile 166
5.7. Summary 167
6. EVALUATING PORE SIZES OF NON-WOVEN GEOTEXTILES 169
6.1. Introduction 169
6.2. Scope of the Chapter 171
6.3. Image Analysis Technique 172
6.4. Two-Dimensional PSD 173
6.4.1. Sample Preparation 173
6.4.2. Image Acquisition 176
6.4.3. Image Enhancement and Correction 177
6.4.4. Image Segmentation 178
6.4.5. Bubble Analysis 180
6.4.6. Results 181
6.5. Three-Dimensional Constriction Size Measurement 183
6.5.1. Image Acquisition 183
6.5.2. Image Processing 185
6.5.3. Plotting Pores in Matlab 189
6.5.4. Results 192

6.6. Theoretical Constriction Size Measurement 196
6.6.1. Results....197
6.7. Merury Intrusion Porosimetry....198
6.7.1. Results....199
6.8. Comparison of Pore Sizes from Different Techniques....200
6.9. Summary and Conclusions....203
7. DISCUSSION....205
7.1. Introduction....205
7.2. Filtration Behaviour of Narrow Graded Soils....205
7.2.1. Gradation of Particles Passed....206
7.2.2. Influence of Flow Regime....207
7.2.3. Clogging Ratios....211
7.3. Filtration Behaviour of Broadly Graded Soils....214
7.3.1. Gradation of Particles Passed....214
7.3.2. Influence of Flow Regime....216
7.3.3. Clogging Ratios....219
7.4. Effect of Geotextile PSD on Filtration Performance....221
7.5. Soil/Geotextile Compatibility....224
7.5.1. Piping....225
7.5.2. Clogging/ Blinding....236
7.6. Summary of Suggested Criteria....240
7.6.1. Piping....240
7.6.2. Clogging/Blinding....241
7.7. Critical Review of Suggested Criteria....241
8. CONCLUSION AND RECOMMENDATIONS....245
8.1. Conclusions....245
8.1.1. Dynamic GR Apparatus....245
8.1.2. Test Procedure....246

8.1.3. A New Method to Find the PSD of Geotextiles 246
8.1.4. Dynamic Filtration Tests 247
8.1.5. Filter Design Criteria 250
8.2. Recommendations for Future Research 251
REFERENCES 253
APPENDICES 268
Appendix A: Evaluation of Internal Stability of Soils 269
Appendix B: Calibration of Pressure Transducers 272
Appendix C: Test Results 273
Appendix D: Pre and Post-Test Gradation 294
Appendix E: Summary of all Filtration Tests 305

LIST OF FIGURES

Figure 1.1 Flow chart of the research methodology 8

Figure 2.1 Geotextile in drainage applications (Holtz et al., 2008)..... 14

Figure 2.2 Water rise in a capillary tube (adapted after Nimmo (2005)..... 19

Figure 2.3 Moisture distribution in soil below ground 20

Figure 2.4 Components of a typical pavement subsurface drainage system (FHWA, 1992) 21

Figure 2.5 Piping (a), bridging (b) and blinding (c) mechanisms (after Lafleur, 1999). 25

Figure 2.6 Clogging and blinding of geotextiles (Bell & Hicks, 1980)..... 26

Figure 2.7 Description of Kenney-Lau approach and the inset contains H-F curve (adapted from Kenney and Lau (1985,1986)) 31

Figure 2.8 Classification of Broadly Graded Soils (Lafleur et al., 1989)..... 32

Figure 2.9 Classification of soils (adapted after Burenkova (1993))..... 34

Figure 2.10 Wan and Fell criterion for evaluation of internal stability of broadly-graded soils 35

Figure 2.11 Pore structure terminology to define void space between geotextile fibers (Fischer et al., 1996) 43

Figure 2.12 Schematic cross section of a non-woven geotextile (Giroud, 2010)..... 55

Figure 2.13 Tradition GR test apparatus (after Fannin et al. (1994)) 71

Figure 2.14 Dynamic test setup (after Glynn and Cochrane, 1987) 75

Figure 2.15 Cyclic flow test set-up (after Cazzuffi et al. (1999)) 77

Figure 3.1 Particle size distribution of medium sand and PFA..... 84

Figure 3.2 SEM images of medium sand particles 85

Figure 3.3 SEM Images of PFA 87

Figure 3.4 Particle size distribution curves of different proportions of medium sand and PFA 88
Figure 3.5 Burenkova stability criterion to evaluate soil internal stability 92
Figure 4.1 Dynamic gradient ratio test apparatus setup 95
Figure 4.2 Modified triaxial cell for gradient ratio test 97
Figure 4.3 Holes punched in rubber membrane to connect ports of differential pressure transducers 99
Figure 4.4 Modified steel mould to support rubber membrane 100
Figure 4.5 Modified bottom pedestal in triaxial cell 101
Figure 4.6 Pore pressure transducers to measure water heads 104
Figure 4.7 Apparatus for saturation and calibration for miniature PPT 104
Figure 4.8 Mariotte bottle for supplying constant water pressure 106
Figure 4.9 Designed metallic hammer for compacting soil 109
Figure 4.10 Sample preparation steps 110
Figure 4.11 B value vs degree of saturation curves by various researchers 113
Figure 4.12 The dynamic GR device 115
Figure 4.13 KENLAYER analysis for (a) 450mm and (b) 350mm thick pavements .. 116
Figure 4.14 Sinusoidal load with an amplitude of 30kPa at 1Hz frequency 117
Figure 4.15 Nikon Microscope with a captured image of block specimen 121
Figure 4.16 Microscopic image of a geotextile specimen after test 121
Figure 5.1 Head difference along samples with variation in Flow rate, Q 125
Figure 5.2 Measuring mean cyclic head difference 127
Figure 5.3 Summary of water head distribution responses 128
Figure 5.4 Water head distribution of medium sand with different geotextiles 131
Figure 5.5 Water head distribution of fine sand with NW20 and NW8 geotextiles 132

Figure 5.6 Water head distribution of 90% sand 10% PFA mix with NW20 and NW8 geotextiles..... 133
Figure 5.7 Relationship between O_{90}/d_{30} and mass collected for narrow graded soils. 139
Figure 5.8 Possible scenarios of post-test gradations 140
Figure 5.9 Microscopic images of geotextile samples after filtration test with medium sand 144
Figure 5.10 Microscopic images of geotextile samples after filtration test with fine sand 144
Figure 5.11 Microscopic images of geotextile samples after filtration test with 90% sand 10% PFA 145
Figure 5.12 Water head distribution of 85% sand 15% PFA with NW20 geotextile... 146
Figure 5.13 80% Sand 20% PFA: Rate of head loss across soil-geotextile interface and within soil..... 147
Figure 5.14 Water head distribution of 70% sand 30% PFA with NW20 geotextile... 148
Figure 5.15 60% Sand 40% PFA: Rate of head loss across soil-geotextile interface and within soil..... 149
Figure 5.16 Water head distribution of 40% sand 60% PFA with NW20 geotextile... 149
Figure 5.17 PFA: Rate of head loss across soil-geotextile interface and within soil ... 150
Figure 5.18 Relationship between O_{90}/d_{30} and mass collected for broadly-graded soils 157
Figure 5.19 Microscopic images of geotextile samples after filtration test with 85% sand 15% PFA mix 160
Figure 5.20 Microscopic images of geotextile samples after filtration test with 80% sand 20% PFA 161

Figure 5.21 Microscopic images of geotextile samples after filtration test with 60% sand 40% PFA 162
Figure 5.22 Microscopic images of geotextile samples after filtration test with PFA . 163
Figure 5.23 Repeatability Tests: Water head distribution..... 165
Figure 5.24 Test without geotextile: Water head distribution..... 167
Figure 6.1 Different stages to measure 2-D PSD of geotextiles..... 173
Figure 6.2 SEM Images of geotextile specimen using scattered electron method..... 174
Figure 6.3 SEM images of NW8 geotextile specimen (1.2mm thickness) at different depths using back scattered method..... 175
Figure 6.4 Microscopic image of geotextile specimen using Nikon microscope..... 176
Figure 6.5 8-bit grey image before (left) and after (right) normalization 177
Figure 6.6 8-bit grey image after smoothing filter (left) and median filter (right)..... 178
Figure 6.7 Image histograms before (a) and after (b) Gaussian filter..... 179
Figure 6.8 Binary image of cross-sectional image after thresholding 180
Figure 6.9 Bubble analysis of binary image in two steps; the black shades are fibers and white shades show pore spaces..... 181
Figure 6.10 Two-dimensional PSD of different geotextiles from cross-sectional images 182
Figure 6.11 Image control information for X-ray image acquisition 184
Figure 6.12 2-D slice images of NW20 (left) and ST170 (right) 184
Figure 6.13 Grey images of NW20 before (a) and after (b) Median filter..... 185
Figure 6.14 Image histogram of NW20 geotextile 186
Figure 6.15 Image segmentation by finding the optimum threshold value..... 188
Figure 6.16 3-D plotting of spheres (pores) in Matlab 190
Figure 6.17 Sphere-sphere intersection (Weisstein, 2007) 191

Figure 6.18 Flowchart of the detailed steps to find 3-D constriction size distribution of geotextiles 192
Figure 6.19 Constriction size distributions of NW20 and ST170 specimens 193
Figure 6.20 X-ray image of NW20 clogged with PFA before (a) and after (b) segmentation 194
Figure 6.21 Orthoslices of NW20 images in xy, xz, and yz directions to observe clogging 195
Figure 6.22 PFA particles clogged inside NW20 and ST170 geotextiles specimens ... 196
Figure 6.23 Comparison of constriction sizes C_{95} from theoretical equations 198
Figure 6.24 Comparison of PSD measured from MIP technique 199
Figure 6.25 Comparison of O_{95} and C_{95} measured from different techniques 201
Figure 6.26 Comparison of O_{90} and C_{90} measured from different techniques 202
Figure 7.1 GR and KR values for broadly-graded soils 220
Figure 7.2 Retention criteria on basis of O_{90} 227
Figure 7.3 Retention criteria on basis of C_{50} 229
Figure 7.4 The interaction ratio based on Holtz et al. (1997) criterion with current test results 232
Figure 7.5 The interaction ratio based on Heerten (1982) criterion with current test results 233
Figure 7.6 The interaction ratio based on Lafleur (1999) criterion with current test results 234
Figure 7.7 The interaction ratio based on Moraci et al. (2012) criterion with current test results 236
Figure 7.8 Summary of filtration tests in terms of blinding/ non-blinding 239

LIST OF TABLES

Table 2.1 Critical hydraulic gradient values for migration or piping in sandy gravels (Skempton and Brogan, 1994) 37

Table 2.2 Summary of selected studies of geometric and hydraulic criteria 39

Table 2.3 Important features of different pore size determination techniques (after Fischer, 1994) 53

Table 2.4 Hydraulic gradient in soil next to filters (Giroud, 2010) 58

Table 2.5 Existing filter retention criteria for steady state flow conditions 62

Table 2.6 Existing filter retention criteria for dynamic flow conditions 64

Table 2.7 Existing geotextile permeability criteria 67

Table 2.8 Existing geotextile clogging criteria 68

Table 2.9 Typical values of GR by previous researchers 73

Table 2.10 Previous laboratory tests to assess the soil-geotextile filtration compatibility 78

Table 3.1 Properties of geotextiles provided by the manufacturers 84

Table 3.2 Physical properties of medium sand 85

Table 3.3 Properties of PFA 87

Table 3.4 Description of soils 89

Table 3.5 Stability analysis of soils by Kenney and Lau's (1985) and Kezdi's criteria. 91

Table 3.6 Summary of soil internal stability classification based on geometric criteria 92

Table 3.7 Dynamic filtration test program 93

Table 5.1 Narrow graded soils: GR values 135

Table 5.2 Narrow graded soils: Coefficient of permeability values (x 10^{-5} m/s) 137

Table 5.3 Narrow graded soils: Mass of particles collected after each test 138

Table 5.4 Narrow graded soils: d_{90p} of washed out particles 139

Table 5.5 Narrow graded soils: Summary of pre and post-test gradation..... 142

Table 5.6 Narrow graded soils: Partial clogging of geotextiles 145

Table 5.7 Broadly-graded soils: GR values 151

Table 5.8 Permeability values (x 10^{-7} m/s) for 80% Sand 20% PFA samples..... 152

Table 5.9 Permeability values (x 10^{-7} m/s) for 60% Sand 40% PFA samples..... 153

Table 5.10 Permeability values (x 10^{-7} m/s) for PFA samples..... 153

Table 5.11 Permeability values (x 10^{-7} m/s) of test samples with NW20..... 154

Table 5.12 Permeability values (x 10^{-5} m/s) for 70% sand 30% PFA sample 155

Table 5.13 Broadly-graded soils: Mass of soil particles collected after each test..... 156

Table 5.14 Broadly-graded soils: d_{90p} of washed out particles 157

Table 5.15 Broadly-graded soils: Summary of pre and post-test gradation..... 159

Table 5.16 Broadly-graded soils: Partial clogging of geotextiles 164

Table 5.17 Repeatability Tests 166

Table 5.18 Test without geotextile 167

Table 7.1 Comparison of d_{90p} and original sample for narrow graded soils 207

Table 7.2 GR and KR values for narrow graded soils 213

Table 7.3 Comparison of d_{90p} and original sample for broadly-graded soils 215

Table 7.4 Summary of filtration tests for NW20 and ST170 geotextile samples..... 223

Table 7.5 The interaction ration (IR) for widely used retention criteria in practice..... 230

LIST OF ABBREVIATIONS

A	Cross-sectional area of test sample
AOS	Apparent Opening Size
B	Capillary constant
BPT	Bubble Point Test
BSE	Back Scattered Electron
CDA	Canadian Dam Association
C_c	Coefficient of curvature
C_u	Coefficient of uniformity
C_{50}	Constriction size measured from 3-D Constriction Size
D_a	Diameter of average particle
D_c	Critical diameter of suffusion
DPT	Differential pressure transducer
D_i	Indicative grain size (D_{85}, D_{50}, D_{30} or D_{15})
D_5	Diameter for which 5% grains by weight of coarse fraction is smaller
D_{15}	Diameter for which 15% grains by weight of coarse fraction is smaller
D_{85}	Diameter for which 85% grains by weight of coarse fraction is smaller
d_{90p}	90% of particles passing through geotextiles
d_{90}/d_{60}	Slope of coarse fraction of soil gradation
d_{20}/d_5	Slope of fine fraction of soil gradation
EOS	Equivalent Opening Size
F	Percentage mass of soil particles smaller than a given diameter D
FOS	Filtration Opening Size
GEO	Geotechnical Engineering Office
GSD	Grain size distribution

GR	Gradient ratio
h	Head loss
H	Percentage mass of soil particles between D and 4D
h_{35}	Differential water head between Port 3 and Port 5 in GR apparatus
h_{57}	Differential water head between Port 5 and Port 7 in GR apparatus
h_1	Factor of uniformity to describe heterogeneity of soil (d_{90}/d_{60})
h_2	Factor of uniformity to describe heterogeneity of soil (d_{90}/d_{15})
$\triangle h$	Difference in head across the test sample
Hz	Hertz
i	Hydraulic gradient
i_c	Critical hydraulic gradient
i_s	Hydraulic gradient within base soil
i_{sg}	Hydraulic gradient across soil-geotextile interface
i_{35}	Hydraulic gradient between port 3 and port 5 in GR apparatus
i_{67}	Hydraulic gradient between port 3 and port 5 in GR apparatus
ICOLD	International Commission on Large Dams
ID	Inner diameter
IR	Interaction ratio
kB	Initial soil hydraulic conductivity
kF	Virgin geotextile hydraulic conductivity
kPa	Kilo pascal
KR	Permeability ratio
k_s	Permeability of soil
k_{sg}	Permeability of soil-geotextile interface
k_{sys}	Permeability of soil-geotextile system

L	Length of the sample
MIP	Mercury Intrusion Porosimetry
NP	Needle punched
NW	Non-woven geotextile
OD	Outer diameter
OF	Filter Opening Size
Q_d	Dry flow rate
O_i	Geotextile opening size in which i% of pores are smaller
O_{90}	Characteristic pore size (90% finer) based on wet sieving
Q_w	Wet flow rate
P	Pressure required to force mercury into capillary pores
POA	Percent Open Area of geotextiles
PFA	Pulverised fuel ash
PPT	Pore pressure transducer
PSD	Pore size distribution
PVD	Pore volume distribution
q	Volumetric flow rate
R	Hydrodynamic Number
Re	Reynolds number
SEM	Scanning Electron Microscopy
T	Surface tension
USDA	U.S. Department of Agriculture
USSD	U.S. Society of Dams
W	Woven geotextile
n	Porosity

ν	Kinematic viscosity of water
ρ	Bulk density of the material
ρ_w	Density of water
Θ	Angle of contact
ν	discharge velocity
ρ	density of the fluid
η	Viscosity of fluid
Ψ	Permittivity
ψ	Matric potential of soil

Chapter 1

Introduction

1.1. Background

Filters are used in civil engineering to drain water from surrounding soils or waste materials and to collect it downstream. A filter should perform the following two functions i.e. retain the soil particles to avoid the erosion of soil, and allow water to move through the filter freely, without development of pore water pressure. A traditional technique has been to use selected graded granular material such as gravel and sand as a filter material in civil engineering projects such as retaining walls, roadways, earth dams or bank revetments. Successful use of filters requires consideration of application, filter properties, soil properties, flow conditions and stresses.

A number of filter selection criteria have been formulated which are currently being used for a wide range of civil engineering applications. These filter criteria are empirical formulae which relate the filter grain size to that of surrounding material. In the last few decades, geosynthetic (i.e. geotextiles) are rapidly replacing graded granular filters due to their cost advantages. Geotextiles have been successfully used as filters in many applications while much thinner and more permeable than granular filters (Giroud, 1996). The geotextile market is projected to reach $8.18 Billion by 2024, growing at a mean annual growth rate of 10.4% from 2016 to 2024 (Grand View Research, 2016) .

The selection of the geotextile filter is a complex process which depends on the specific application. The factors governing the interaction between soil and geotextile filters include geotextile properties, soil properties, and external conditions (confining stress, hydraulic gradient, flow regime etc.). The geotextile properties (pore size, thickness, porosity, and others) are usually provided by the manufacturer. The compatibility of geotextiles with a specific soil should be performed using a standard test method such as the Gradient Ratio (GR) test (ASTM D5101). The performance test should simulate conditions in the field.

1.2. Problem Statement

Geotextiles, like graded granular filters, should stop the migration of particles upstream while allowing the water to flow freely downstream. Geotextile filter design with respect to retention of soil is usually performed by using empirical formulae in which the characteristic pore size of geotextile is compared with an index size of the surrounding soil. The commonly used characteristic pore sizes of geotextiles in empirical formulae are Apparent Opening Size (AOS), Equivalent Opening Size (EOS), and Filtration Opening size (FOS).The value of each depends on the method to find these pore sizes (see Section 2.7.1.1). These pore sizes are representative of the size of the nearly-largest pores in the geotextiles. The filter design criteria to meet the retention requirement is well established for steady-state flow conditions.

However, when the soil-geotextile interface is subjected to dynamic loading, the requirements for successful filtering are uncertain and/or conservative as the controlling factors are not well understood in these circumstances. Dynamic conditions may be caused by mechanical disturbance (e.g. vehicles, trains or aircrafts) or hydraulic disturbance (e.g., wave loading against bank revetment, seawalls, etc.). Dynamic

conditions can cause erosion of soil particles through geotextiles which may result in unstable soil structure upstream of the geotextiles. This erosion of soil under dynamic conditions may be significant if the soil upstream of the geotextile is internally unstable (i.e. some grains can move through the soil voids under the action of water flow). The loss of fine portion of a soil may then allow the load carrying soil skeleton to become unstable, depending on the portion of fines lost from the surrounding soil (Yideti et al., 2013, Kenney and Lau, 1985). Therefore, the selection of an appropriate geotextile under dynamic condition becomes a major challenge.

There are fewer retention criteria available for geotextiles under dynamic flow conditions and these are mostly based on theoretical work. These criteria do not take into account the internal stability of soils. The most commonly used retention criterion is not supported by any systematic mechanics-based study of soil-geotextile behaviour in dynamic, cyclic or pulsating flow. Furthermore, no criteria exists for assessing the clogging potential of geotextile filters with soil under dynamic conditions.

The retention criteria for geotextiles is mostly based on a single characteristic pore size of geotextiles, but geotextiles having the same large opening size may have different pore size distribution which may result in their performances differing from each other (Fischer et al., 1990, Elton et al., 2007).

Very little laboratory work has been done in studying the soil-geotextile filtration compatibility in roads under dynamic conditions. The apparatuses used in the studies by other researchers were lacking control over the flow regime as well as precision of measurements. Exception were Hammeri (2000), and Fannin and Pishe (2001) where a traditional GR test equipment was modified to perform cyclic tests. The traditional GR test equipment use a rigid wall permeameter. There are issues associated with the rigid

wall permeameter to carry out filtration tests such as side wall leakage as well as incomplete control over stresses (Acar et al., 1985; Harney & Holtz, 2001; Lee & Bourdeau, 2006; Madsen & Mitchell, 1989).

The geotextile as filters around pavement edge drains and beneath permeable bases is mostly designed on the basis of Holtz et al. (1997) criterion which is suggested for internally stable soils. Unstable soils may exist in roadway bases adjacent to pavement edge drain (Holtz et al., 2008). Therefore, the filtration compatibility of geotextiles with internally unstable soil need to be evaluated for dynamic conditions.

1.3. Aim & Objectives

This research takes an experimental-based approach to investigate the different mechanisms involved in filtration behaviour at soil-geotextile interfaces under dynamic flow conditions. The major challenges in filtration compatibility of soil-geotextile interface include conditions of mechanical disturbance, and soils that are internally unstable. The current retention criteria for geotextiles under dynamic flow conditions are mostly based on theoretical work and do not take into account the internally unstable soils. The ultimate aim of this research is to enhance the long term filtration performance of geotextile filters in highways by developing a more appropriate filter design criteria.

Specifically, the objectives of this study were to:

1. To investigate the effect of different factors on the filtration performance at soil-geotextile interface under dynamic conditions. The factors that will be studied include: hydraulic gradient, vertical stress, frequency of loading, soil gradation, and geotextile properties.

2. To develop a dynamic filter design criteria, potentially on the basis of a characteristic pore size of geotextile and an index grain size of soil by analysing the results of dynamic gradient ratio tests.
3. To evaluate the effect of pore size distribution of geotextiles on the filtration performance at the soil-geotextile interface.
4. To assess the newly proposed design criteria against the current criteria used for design under dynamic conditions.

1.4. Research Methodology

The research methodology employed is illustrated in Figure 1.1 to achieve the objectives and consisted of eight tasks.

Task 1:

A dynamic gradient ratio test device was developed to perform the filtration tests under dynamic conditions. The current ASTM standard test method for static conditions (ASTM D5101) were taken into account and compatible procedure were developed for dynamic conditions. ASTM D5101 is a standard test procedure for measuring the filtration compatibility of soil-geotextile system. The test apparatus and procedure in this study used a flexible wall in place of the rigid wall recommended by ASTM D5101 because of the disadvantages associated with traditional gradient ratio apparatus (see Section 2.10.1). Task 1 was a preliminary to Task 4.

Task 2:

Suitable geotextiles and soil samples were selected to perform filtration tests. The geotextile samples were selected due to their frequent use as filters for applications such as pavement edge drains, reservoirs and dams, and under revetments. Different gradation

soils were prepared to assess the filtration compatibility of geotextiles with internally stable and unstable soils.

Task 3:

A new method was suggested for evaluating more realistically the three-dimensional (3-D) PSD of geotextiles using X-ray CT and image processing techniques. Also, a new approach was developed to find the two-dimensional (2-D) PSD of non-woven geotextiles from cross-sectional images. The pore sizes from the 3-D method were compared with pore sizes measured from 2-D method, mercury intrusion porosimetry, wet sieving, and theoretical equations.

Task 4:

Gradient ratio tests were performed according to ASTM D5101-12. The tests were performed for static stage followed by cyclic stages. The effect of different factors on filtration performance of soil-geotextile interface under dynamic conditions were investigated using the developed dynamic gradient ratio test device. The factors included applied hydraulic gradient, vertical stress, frequency of loading, soil gradation, and geotextile properties. Task 3 was performed to achieve Objective 1**.**

Task 5:

The post-test procedure included measuring the mass of soil particles passed through the filters, finding the gradation of particles passed through filters, taking microscopic images of geotextiles after each test to look for clogged particles, and hydrometer sieve analysis of soil samples taken at 0-8mm and 25-40mm above the geotextile to compare the gradation of soil samples after each test with the original gradation.

Task 6:

The test results were analysed after each filtration test. Data analysis included: total head loss along sample, variation of mean static and cyclic head loss within the soil and across the geotextile with time, static and cyclic GR with time, flow rate, and analysis of results from post-test procedure. Task 6 was a preliminary to Task 7.

Task 7:

The filtration performance of internally stable and unstable soils with different geotextiles was assessed by analysing the results of dynamic GR tests. A filtration design criteria was prepared based on the ratio of characteristic pore size of geotextile measured from wet sieving method (Section 2.7.1.1) and an index grain size of soil. The effect of pore size distribution of geotextiles on filtration performance was also evaluated and a filter retention criterion was suggested on the basis of median pore size of geotextile measured from the suggested 3-D method (Task 3) and an index grain size of soil. Task 7 was performed to achieve Objective 2 and Objective 3.

Task 8

The new filter design criteria were compared with the existing filtration design criteria which are representative of those most widely used in practice to check that improvements had been achieved. Task 8 was performed to achieve Objective 4.

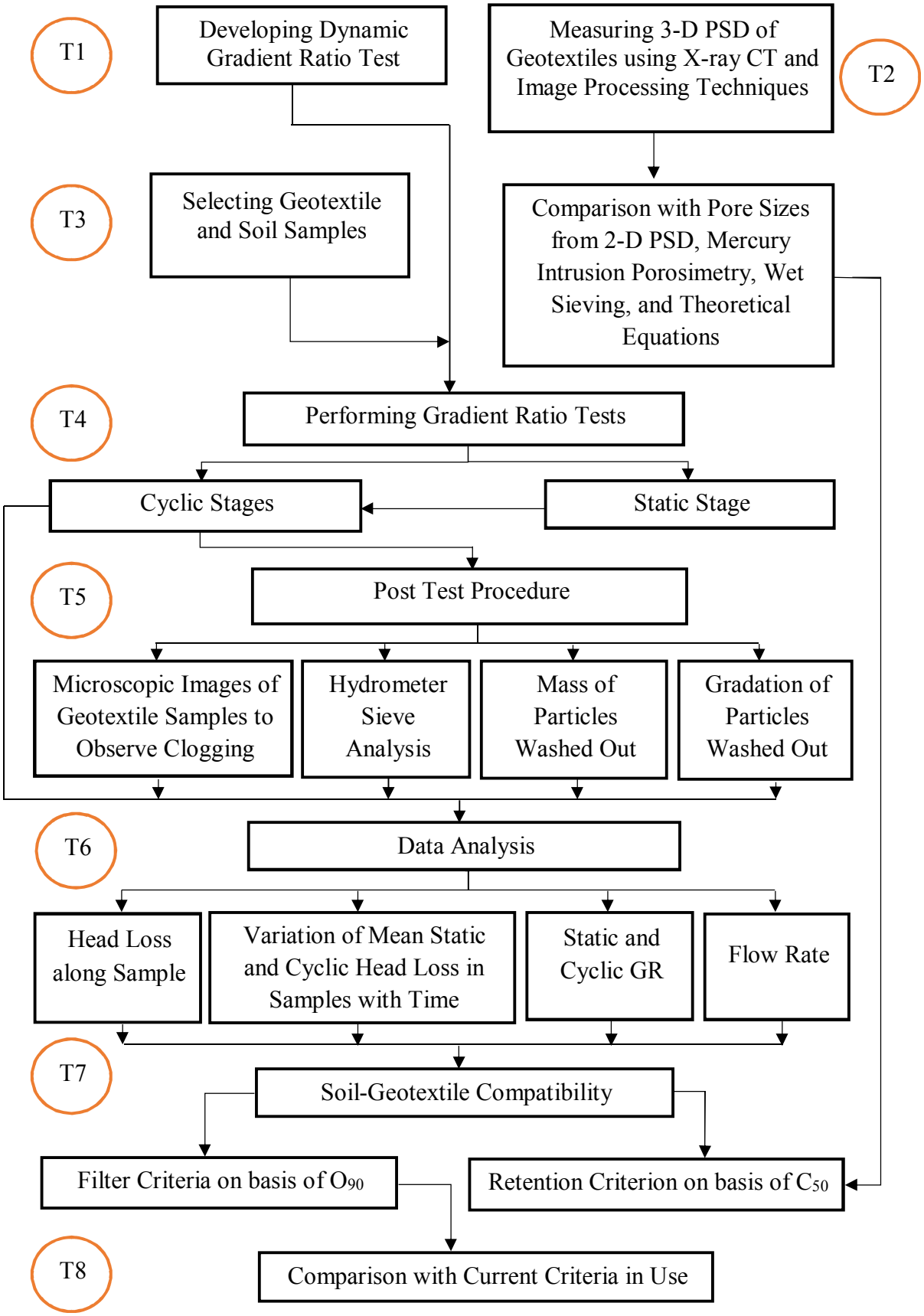


Figure 1.1 Flow chart of the research methodology

1.5. Thesis Organization

There are eight chapters in this thesis. After this first **Chapter**, the other chapters are organised as follows:

Chapter 2 provides a background to the project. It delivers a basic understanding of the filtration mechanisms at the soil-geotextile interface as well as the internal stability of soils. The chapter also reviews the different factors affecting soil-geotextile filtration behaviour. Previous filter design criteria for static and dynamic conditions are also discussed in this chapter. Finally, previous laboratory studies and further research needs are reviewed in Chapter 2.

Chapter 3 in this thesis characterizes the materials used in the study. The internal stability/ instability of soil gradations, as evaluated by different methods, are also included in Chapter 3.

Chapter 4 describes the design and development of a flexible wall gradient ratio test apparatus, as well as the test-set up to perform filtration tests. It also includes the test procedure to carry out dynamic filtration tests. Furthermore, the post-test procedure are also included in this chapter.

Chapter 5 reports the dynamic filtration test results. The results are discussed separately for narrow and broadly graded soils.

Chapter 6 explains the evaluation of pore sizes of geotextiles from different currently available methods. It also describes a new method which is suggested for evaluating more realistically the pore size distribution of geotextiles using X-ray CT and image processing techniques. Comparison of pore sizes of geotextiles from all these methods are also presented in the chapter.

Chapter 7 discusses the dynamic filtration results reported in Chapter 5. It also discusses the filtration performance of geotextiles in terms of pore size distribution which were measured from a newly suggested method that was described in chapter 6. Finally, a filtration design criteria is suggested for dynamic flow conditions which is compared with the current design criteria in use.

Chapter 8 is the last chapter of this thesis. It details the conclusions and recommendations based on the entire study.

Chapter 2

Literature Review

Filters are used in civil engineering to drain water from surrounding soils or waste materials and to collect it downstream. A traditional graded granular filter should perform the following two functions i.e. retaining the soil particles to avoid the piping of soil, and allowing water to move through the filter without development of pore water pressure. The use of filters involves aspects of application, filter properties, soil properties, flow conditions and stresses. The two types of filters in common use are granular filters and geotextile filters.

2.1. Soil Filtration Using Geotextiles

Geotextiles are either woven or non-woven planar sheet textile materials made from synthetic fibers mostly from polypropylene, although some are manufactured from polyethylene or polyester polymers as well. The different geotextile manufacturing choices are monofilament, multifilament, staple yarn, continuous yarn, slit-film monofilament or slit-film multifilament. Geotextile type is determined by the method used to combine the filaments into a planar structure. The woven geotextiles are made using the conventional textile weaving machinery. Woven geotextiles have a regular structure which consists of two orthogonal orientations of fibers Woven geotextiles have a quite narrow pore size range. Nonwoven geotextiles are manufactured by a modern process and

bonded by entanglement, heat treatment or glue. Non-woven geotextiles have a random structure and are characterized by a wider range of pore sizes than woven geotextiles.

Geotextile always performs one of the four discrete functions i.e. separation, filtration, reinforcement and drainage. The open porous structure and its permanence enable geotextiles to filter soil particles while allowing free flow of pore fluid. Geotextiles can perform better as filters than granular materials, and there is definite advantage provided by their easy installation and relative low cost of construction (Giroud, 1996). Geotextiles as a filter material are replacing graded granular filters at a tremendous rate in almost any geotechnical design. Geotextile are usually preferred over (or in conjunction with) conventional graded granular filter material in most drainage and filtration applications because of cost advantages from (Christopher & Holtz, 1989):

- the use of less-costly drainage aggregate: more open graded drainage aggregate could be considered for use
- expedient construction;
- lower risk of contamination and segregation of drainage aggregate during construction;
- reduced excavation: reduction of aggregate thickness required to stabilize the subgrade

Few examples of geotextile filters in erosion control systems include (Koerner, 1993):

- Replacement of granular soil filters
- Filters beneath pavement bases, and base courses

- Filters around trench drains and pavement edge drains
- Beneath ballast under railroads
- Around crushed stone surrounding underdrains
- Around perforated underdrain pipe
- Beneath landfills that generated leachate
- Filtering hydraulic fills

Figure 2.1 shows few examples of geotextile as a filter material in subsurface drainage systems. Geotextiles as a filter material require proper engineering design otherwise they may not perform as desired. The design of soil-geotextile filtration depends on the severity and critical nature of the application. The concept of critical and severe nature of projects was developed for the first time by Carroll (1983). The nature of the project is considered critical if one of the following conditions occur:

- When risk of life and structural damage due to drainage failure is much high or
- When repair costs versus installation costs of drain is very high or
- When failure occurs before the clogging of drains.

Similarly, for severity condition, any of the following conditions should exist;

- The soil to be drained is unstable or
- The hydraulic gradient is high or
- When dynamic, cyclic or pulsating loading occurs.

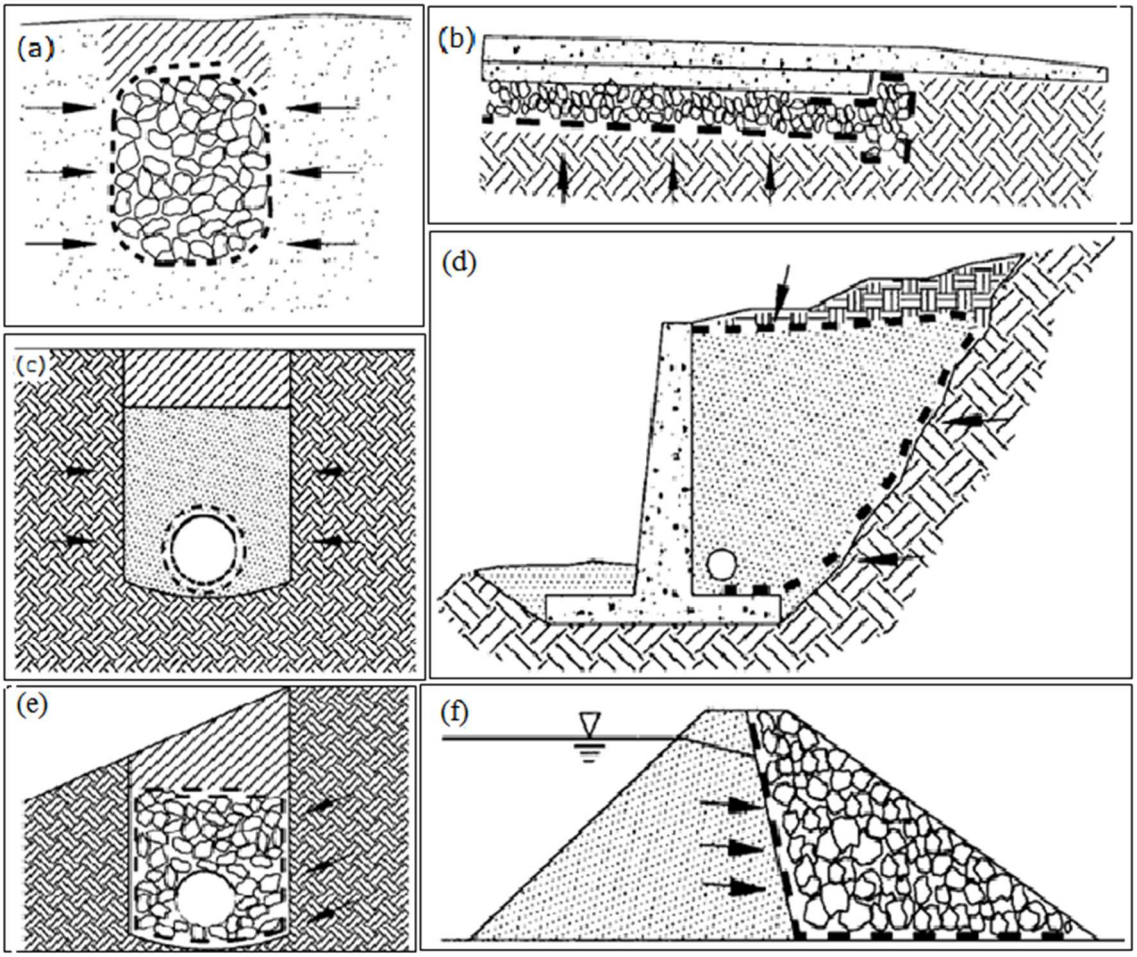


Figure 2.1 Geotextile in drainage applications (Holtz et al., 2008)

(a) Filters around trench drains and edge drains (b) Filters beneath pavement permeable bases and base courses (c) Filter wraps for slotted or jointed drain and well pipes (d) Drains for retaining walls and bridge abutments (e) Interceptor, toe drains and surface drains (f) Chimney and toe drains for earth dams and levees

2.2. Seepage Flow

A soil mass can be classified as three phase system consisting of soil particles, water and air. A soil is termed to be dry when all the pores of soil are filled with air. A soil is saturated when all pores are occupied by water and there is no air in the voids. However, when the pores of soil are filled with a mixture of air and water, the soil is said to be partially saturated.

Water present in soil voids can be classified into free water and held water. The free water or gravitational water percolates downward in soil due to gravity and ultimately reach the saturated zone. The water held in the voids of soil mass cannot move under gravitational force as the water is held by some forces which exist within the pores. The held water maybe sub-divided into adsorbed water/ hygroscopic water and capillary water.

The adsorbed water is a thin film of water held tightly by the soil particles by the force of adhesion. It is adsorbed freely from atmosphere by the physical forces of attraction. The soil particles carry a net negative charge due to which they attract water. This water is different from the pore water as it is under the influence of soil attractive forces. The attractive forces are quite strong so that the water show immobility under normal hydrodynamic forces. The amount of adsorbed water depends on the characteristics of soil particles. It is lower for coarse grained soils and higher for finer grained soils such as clay.

The capillary water is water held in the soil pores due to capillary forces. The small pores of soil act as capillary tubes through which water rises above the ground water table. The water molecules are attracted to the walls of tube by hydrogen bonds which results in capillary rise. The water is said to be under tension (see Section 2.2.2).

Any soil mass consists of particles of different sizes with interconnected pores. Water flows in these pores from a higher energy to a lower energy which is termed as seepage flow. Soil permeability is the property of soil to transmit water through its interconnecting voids. The factors affecting the permeability of soil are (Punmia & Jain, 2005):

- **Grain Size:** The permeability of a soil varies approximately as the square of grain size due to large pore openings. Allen Hazen (1892) found experimentally that, for sands of particle sizes between 0.1 and 0.3mm, the permeability is directly related to

the square of its D_{10} (where D_{10} corresponds to diameter for which 10% grains by weight of soil fraction is smaller).

- **Properties of Pore Fluid:** The soil permeability is directly related to the unit weight of pore fluid while inversely proportional to its viscosity.
- **Temperature:** Permeability increases with increase in temperature as the viscosity of the pore fluid decreases with increase in temperature. However, this effect is small for the range of temperature normally found in-situ. The unit weight of pore fluid is not much affected by variation in temperature.
- **Void Ratio:** The permeability is directly related to the void ratio (ratio of volume of voids to the total volume) of soil.
- **Stratification of Soils:** Stratified soils are those soils which are formed by layer upon layer deposited on each other. The permeability is always maximum in direction parallel to the layers of stratification, while minimum in direction perpendicular to stratification.
- **Degree of Saturation:** The presence of air entrapped in the voids of soil reduces its degree of saturation and thus decreasing the permeability. Once all water is held (by adhesion and capillarity), permeability becomes close to zero as water can then only move by diffusion and not by flow.
- **Adsorbed Water:** The adsorbed water is attached firmly to the soil particles by the forces of adhesion which reduces the effective pore space available for water flow and, therefore, decreasing the permeability of soil.

2.2.1. Saturated Soil

During rainfall or irrigation application, there is possibility of all soil pores filled with water and the soil is said to be saturated. Soil below the water table is saturated since all

the pores are occupied by the water (Figure 2.3). The flow of water through saturated soil was first studied by Darcy (1856) who demonstrated experimentally that:

$$q = k\,i\,A \tag{2.1}$$

where q = discharge per unit time (m^3/s),

A = cross-sectional area of soil (m^2),

i = hydraulic gradient (m/m),

k = coefficient of permeability (m/s)

A hydraulic gradient is gradient between hydraulic heads measurement over the length of flow path. When a differential head (h_2-h_1) occurs for a soil sample of length L, then the Darcy's law can be written as:

$$q = k\,\frac{h_1 - h_2}{L}\,A \tag{2.2}$$

Darcy's law is valid for steady state, laminar and irrotational flow conditions in saturated soils. The validity of Darcy's law for rotational flow conditions (i.e. where flow eddies occur) is questionable and should be used with caution. The flow through soils depends on the pore space dimensions. Rotational flow conditions may exist in highly permeable granular material as pore dimensions are larger in these soils. Darcy's law has been found to be valid for soils finer than gravels and coarse sands with permeability up to 0.011m/s (CDOT Drainage Design Manual). Fancher et al. (1933) showed experimentally that Darcy's law is valid if the Reynolds number (Equation 2.2) is less than one:

$$\mathrm{Re} = \frac{\rho v D_a}{\eta} \leq 1 \tag{2.2}$$

where Re = Reynolds number (dimensionless)

ρ = density of the fluid (kg/m^3)

v = discharge velocity (m/s)

Da = diameter of average particle (m)

η = viscosity of fluid (kg/(m.s)

The upper limit of Re can be taken as 1 to 10 to validate the Darcy's law (Lindquist, 1933; Rose, 1945). Darcy's law is valid for most of the natural ground water conditions. However, it is possible to get higher flow velocities in areas such as vicinity of a pumping well where steep hydraulic gradients are expected which results in higher Reynolds number (Fetter, 2001).

2.2.2. Partially Saturated Soils

As described earlier, the partially saturated soils consists of soil skeleton and pores between soils are filled with air and water. The water inside the capillary tubes is under tension. A meniscus is formed at the interface of water-air interface due to the surface tension (see Figure 2.2). This surface tension results in the difference between water pressure and air pressure which is termed as matric suction or capillary pressure. It is called suction (or negative pressure) as the pressure inside the water is less than the air pressure. The water inside the soil is retained due to this capillary pressure. As the soil dries, the radius of curvature of meniscus decreases which result in increase in matric suction. When the soil is more dry, then matric suction is dominated by the adsorbed water as soil pores always carry adsorbed water. In other words, the matric suction is dominated by capillary rise when the soil is wet and is dominated by the adsorbed water when the

soil is dry. Fine grained soils have finer pores due to which the radius of meniscus is smaller and consequently the matric suction is higher.

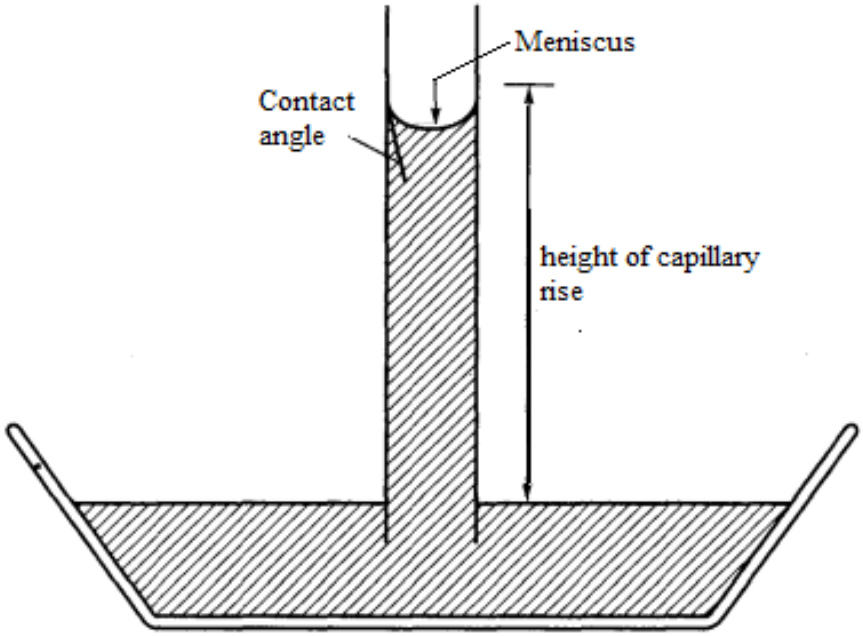


Figure 2.2 Water rise in a capillary tube (after Nimmo (2005))

The different zones of water below the surface are shown in Figure 2.3. It is divided into three zones: 1) the vadose zone, 2) the intermediate zone (capillary fringe), and 3) the saturated zone (or ground water). The vadose zone is the partially saturated zone where water exists as held water. The soil in this zone may become saturated during the time of high rainfall. The capillary fringe is located immediately above the ground water table. It is the area of saturated zone where the water is held by surface tension and capillarity. It is also called tension saturated zone since the water pressure in this zone is less than the atmospheric pressure. The soil pores in ground water zone is occupied by water all the time. Water table rise during times of high rainfall could, therefore, make the vadose zone saturated.

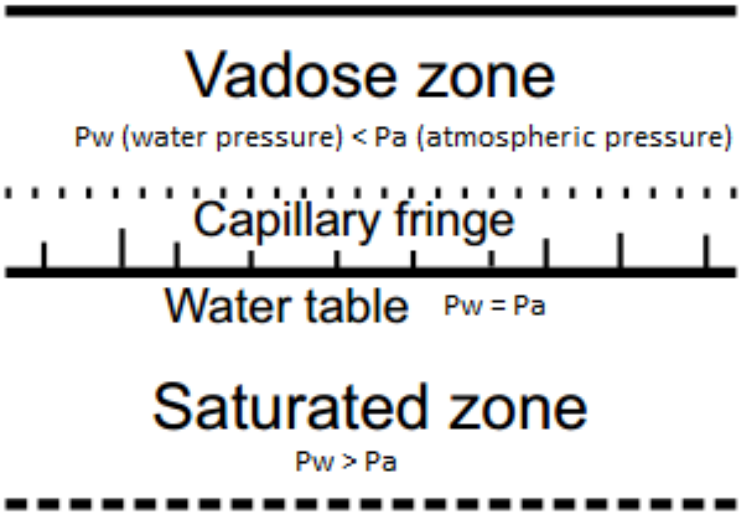


Figure 2.3 Moisture distribution in soil below ground (after (Thorsteinsson, 2013))

The Darcy's law is not applicable for partially saturated soils. As compared to saturated flow conditions where the flow is due to positive heads (Equation 2.2), the flow in partially saturated soils is due to negative gradient, water content, and gravitational potential. It is unlikely that the gradient is constant throughout the soil layer. Therefore, the hydraulic gradient cannot be taken as the difference of differential heads divided by the length of soil (Equation 2.2). Instead, the flow rate is measured iteratively for specific gradients at a given location. For partially-saturated soils, the Darcy's law can be expressed as:

$$q=K\frac{k}{\rho g}\left[\frac{d\psi}{dz}+\rho g\right] \tag{2.4}$$

Where ψ is matric potential of soil which is established by adsorption and capillary forces, g is acceleration due to gravity, and z is upward distance.

2.3. Geotextile Filters in Pavements

Changes in the moisture content in pavement layers is one of the important cause of pavement damage (Espinoza-Melendrez et al., 2005). Water enters the pavements despite the efforts to prevent it. The major source of water in pavements is infiltration of rainfall

through surface through joints, cracks and other defects, especially through old and deteriorated pavements and shoulders (Dawson, 2008). Other sources of water in pavements are capillary rise due to high water table, lateral movement of water from pavement edges, and moisture changes due to freezing/ thawing cycles.

The drainage of water is one of the most important aspects in road constructions. Drainage of water is achieved by providing subsurface drainage system which is placed lower than the section of road (Figure 2.4). A subsurface drainage system is composed of:

- A permeable base course layer with high permeability to allow water to reach longitudinal drains (edge drains) quickly
- A separator layer (graded granular filter or a geotextile filter) to prevent migration of fines from subgrade layer into permeable base and edge drains
- A longitudinal drain to collect water from permeable base layer and to convey it to the outlet
- A longitudinal drain to convey the collected water from longitudinal drains to the surface drainage system

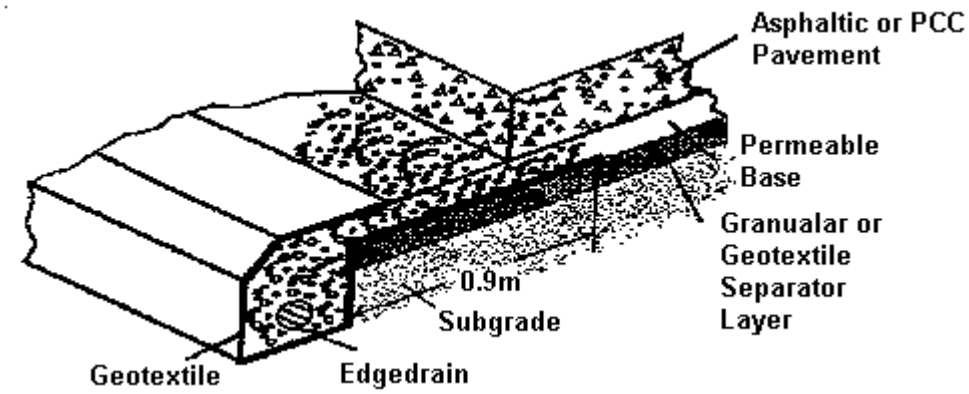


Figure 2.4 Components of a typical pavement subsurface drainage system (FHWA, 1992)

A subsurface drainage system is only able to remove free water and cannot remove water in pavement structure that is held by capillary forces. An improper or incomplete drainage of pavements, combined with traffic loads, often results in pavement deterioration caused by water presence in the structure. Water in pavements can also cause pumping of fines from subgrade soil into sub-base layer under traffic loading (see Section 2.8.3.1).

Although the primary function of a geotextile in a drainage system is separation, however, it also performs filtration function since the subgrade soil maybe wet and saturated. The water is passed through geotextiles into base course and edge drains so that the pore water pressure in subgrade soil is dissipated quickly but the soil is prevented from moving. The pore water dissipation also helps the strength of subgrade soil to gain over time, especially for subgrade soils with higher fines, since the strength of such soils is highly influenced by moisture (Holtz et al., 2008). Used in this way, geotextiles and the water adjacent to them, can be expected to experience dynamic forces due to traffic. These will partly be experienced as water pressure pulses.

2.4. Mechanism of Geotextile Filtration

The filtration mechanism at soil-geotextile interface is a complex process. The soil particles movement towards the filter under the action of seepage forces result in changes in soil grain size distribution, as well as change in porosity and permeability of soil and filter material. Several mechanisms are observed with geotextile filtration performance. These include piping, bridging, blinding, blocking and clogging which are discussed below:

Piping:

Piping occurs when the pore sizes of geotextiles are too large to retain the soil particles. It is severe in case of unstable soils which is much prone to internal erosion (see Section 2.5). Piping may result in significant changes in volume inside the soil and/ or failure of the structure. The limit state of piping occurs when the primary fabric of base soil move through the geotextile filter by the hydraulic flow (Moraci & Mandaglio, 2008). Vice versa, the limit state of piping is not reached if the soil which passed through geotextile does not belong to the primary fabric of base soil (internally unstable soils). The piping of soil through geotextiles may be significant if no bridging develops near the filter interface (Lafleur, 1999). The piping results in increase in local hydraulic conductivities (near geotextile surface) due to which there is a gradual increase of the permeability of soil-geotextile system (Figure 2.5).

Bridging:

Bridging is a filtration mechanism by which base soil forms a self-filtration layer at the geotextile interface. The bridge network formation occurs when the fine particles close to the filter interface pass through the filter and the coarse particles are retained by the filter. These particles in turn will retain the smaller particles and thus an auto-filtration layer is formed. The local hydraulic conductivities increase with the washout of fines near the filter. The hydraulic equilibrium of the soil/ geotextile system is reached after the formation of bridging network (Bhatia & Huang, 1995; Giroud, 2010; Moraci, 2010). The system hydraulic conductivity at the interface lies at a value between the soil hydraulic conductivity and the geotextile hydraulic conductivity (Figure 2.5). This network formation usually occurs in non-cohesive soils.

Blinding:

The limit state of blinding occurs when hydraulic flow drags base soil particles with dimensions smaller than geotextile pores (Gourc & Faure, 1990; Moraci, 2010; Moraci & Mandaglio, 2008). The accumulation of particles near the geotextile interface results in a low permeability zone (filter cake). The decrease in permeability results in development of excessive pore water pressures and subsequently affects the structure stability of soil. Blinding state cause porosity to be increased at the area from where fine particles are migrating, resulting in increase of hydraulic conductivity there (Moraci and Mandaglio, 2008) (see Figure 2.5).

Blocking:

Block mechanism occurs when the coarse particles close to the geotextile plugged in the filter openings at the upstream side, obstructing fine particles as well as fluid to pass through the geotextile. It occurs when the soil particles of equal size or greater than pore opening size reach the geotextile under high flow. Blocking is expected when the soil is not in contact with the geotextiles and soil particles are in low concentration.

Clogging:

Clogging (also called internal clogging) occurs when soil particles passing through the filters find the drainage path too narrow to pass through, thus entrapping inside the filter (Figure 2.6). The blocking of drainage paths results in a decrease in drainage capacity of the filtering system and subsequently increases the pore water pressure, thus, causing the instability problem. The clogging level depends on the amount of fines passing through the filter, the filtration velocity and the clogging positions (funnel type openings).

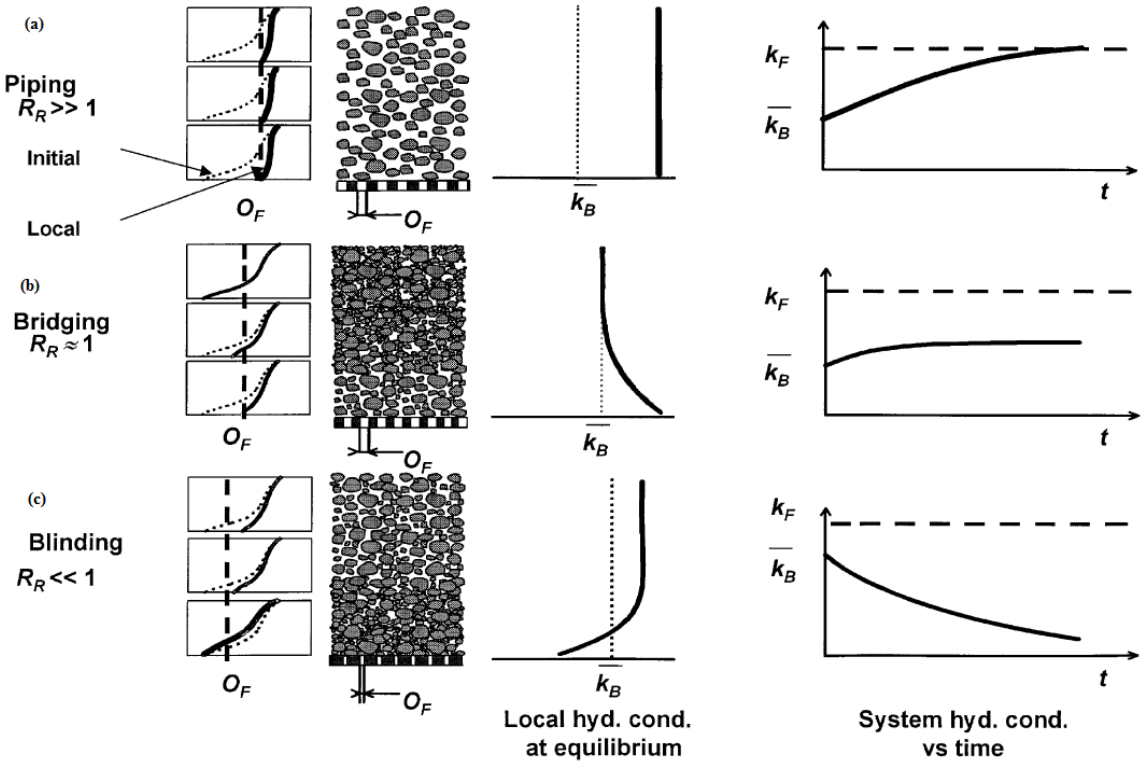


Figure 2.5 Piping (a), bridging (b) and blinding (c) mechanisms (after Lafleur, 1999) Left hand side: Grain size distribution (GSD) of base soil and its variation in the vicinity of geotextile (Initial GSD; doted curve, Final GSD; plain curve, O_F;Filter opening size), Center-left: Granular structure of base soil, Center-right: soil hydraulic conductivity (k_B : initial soil hydraulic conductivity (dotted line)) – Right hand side: system hydraulic conductivity (k_F: virgin geotextile hydraulic conductivity)

Rollin and Lombard (1988) and Hameiri (2000) extended the term clogging to internal clogging, as well as blinding and blocking since all these three mechanisms results in the decrease in system permeability. Out of five filtration mechanisms discussed above, only bridging network is considered a highly desirable condition.

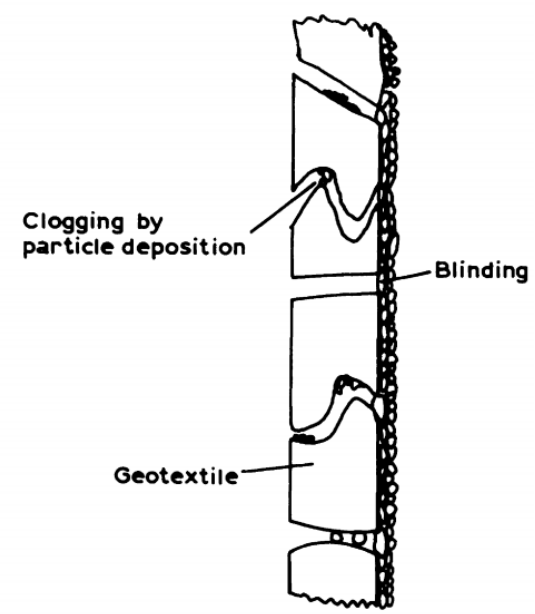


Figure 2.6 Clogging and blinding of geotextiles (Bell & Hicks, 1980)

2.5. Internal Stability of Cohesionless Soils

Most of the filter design criteria do not consider the internal stability of the soils to be protected. A soil skeletal structure consists of coarse fraction and fine fraction. The coarse fraction (or primary structure) of soil interlock with each other which act as a primary load carrying structure. Fine fraction (or secondary structure) of soil fill the gaps between the coarse fraction and may provide stability to the coarse fraction, depending on its proportion. The fine contents plays an important role in the internal stability of soils (Bendahmane et al., 2008; Wan & Fell, 2008). If the fine contents is less, it only fills the pores formed by coarse fraction and do not effect the internal stability of soil. If the fine content is significantly increased, the coarse particles loose contact with each other and can only float in the matrix of fines. Skempton and Brogan (1994) recommended fine contents above 35% for the fine fraction to dominate the soil properties. The optimum amount of fine content largely fills the pores formed by the coarse particles which makes

the soil structure more stable than soils with less or significantly high fines (Yideti et al., 2013).

A soil is referred to be internally stable if the coarse fraction of soil is able to stop the movement of fine particles through its void spaces due to disturbing forces such as seepage flow or vibration (Chang & Zhang, 2013; Kenney & Lau, 1985; Kumar Shukla & Yin, 2006; Wan & Fell, 2008). The fine particles in internally unstable soils are washed out due to suffusion. Suffusion is the detachement and transport of fine particles through the constrictions of coarse particles matrix under seepage flow (Head, 1992; Indraratna et al., 2011; Kézdi, 1979; Wan & Fell, 2008). Internal suffusion is the movement of fines within the soil which affects only the local permeability. External suffusion is the movement of fines form one layer (base soil) into adjacent layer (filter), without affecting the stability of soil skeleton. Suffusion ocurrs in natural soil deposits as well as geotechnical structures such as earth dams, levees, road embankments etc. Piping (internal erosion) is another term used for soil migration which leaves free spaces within the surrounding soil. On the contrary to suffusion, piping may involve migration of fine particles as well as coarse particles from the soil matrix.

The possibility of fine grains passing through the coarse fraction of soils depends on the constriction sizes along the pore paths of coarse fraction. Since it is not possible to measure the constriction sizes, the assessment is usually based on grain size distribution bacause grain sizes can be correlated to constriction sizes. The potential for internal stability of a cohesionless soil depends on its geometric criteria (grain size distribution, filter rules, and pore constriction size) whereas the hydraulic criteria (hydraulic gradient) governs the initiation of instability, if any.

2.5.1. Evaluation of Soil Internal Stability: Geometric Criteria

Grain size distribution of a soil is considered to be one of the most important geometric factors. A lot of work has been done on finding the internal stability of soil from a particle packing point of view e.g. Burenkova (1993); Istomina (1957); Kenney and Lau (1985); Kézdi (1979); Lafleur et al. (1989); Wan and Fell (2008). These criteria are explained in detail in the following section.

i. Istomina Criterion

Istomina (1957) (see Kovacs, 1981) proposed a criterion for evaluating the internal stability of sandy gravels on the basis of coefficient of uniformity ($C_u = D_{60}/D_{10}$). According to his criterion, soils having C_u less than 10 are internally stable while soils having C_u greater than 20 are internally unstable. Soils having C_u between 10 and 20 are considered to be in a transitional zone.

Istomina's criterion has been adopted by Geotechnical Engineering Office (GEO) (1993), U.S. Department of Agriculture (USDA) (1994) and U.S. Society of Dams (USSD) (2011) to evaluate possible erosion of filters.

ii. Kezdi Criterion

Kezdi proposed a criterion in 1969 to assess the internal stability of soils which is further explained in detail by Kezdi (1979). He proposed that the internal stability of soil can be measured by the splitting up the grain size distribution into coarser and finer fractions at an arbitrary grain diameter. The soil is said to be internally stable if both coarse and fine components satisfy Terzaghi type ratio i.e. $D_{15}/d_{85} = 4$. The D_{15} corresponds to diameter for which 15% grains by weight of coarse fraction is smaller while d_{85} corresponds to diameter for which 85% grains by weight of fine fraction is

smaller. The Kezdi's criterion suggests that the constriction size $D_{15}/4$ should retain d_{85} of fine fraction which results in self-filtration of soil. A ratio of $D_{15}/d_{85} > 4$ indicates that the fine fraction particles can pass through the pore constriction sizes which would make the soil potentially unstable under seepage.

Fannin and Moffat (2006) found the $D_{15}/d_{85} = 4$ ratio consistent in terms of evaluating the internal stability of gap-graded and widely graded soils. Sherard (1979) suggested a filter ratio $D_{15}/d_{85} = 4\sim5$ for assessing the internal stability of soils. Kezdi's criterion does not take into account factors like relative density or anisotropy, although these factors have an affect on soil behaviour (Shire et al., 2012). Kezdi's criterion was recommended by USSD (2011) to evaluate the internal stability of base soils.

iii. Kenney and Lau Criterion

The Kenney and Lau approach (Kenney & Lau, 1985; Kenney & Lau, 1986) is the most widely used method for assessing the internal stability of soils. The method was proposed on the basis of interpretation of experimental work performed on 16 well-graded sandy gravels. The soil samples were tested in two permeameters, having diameters of 245mm and 580mm, under downward seepage flow. Vibration was applied to the permeameter during the test with the help of a rubber hammer. A drainage layer consisting of sufficiently coarse particles was placed at the bottom of the permeameter. The corresponding seepage flux, that is, a hydrodynamic number R' > 10 was used by Kenney and Lau (1985). The hydrodynamic number R' is given by Equation 2.5, where q is a unit flux, D_5 is the particle size for which 5% mass is smaller, n is the porosity, and ν is the kinematic viscosity of water (10^{-6} m^2/s):

$$R' = \frac{q \times D_5}{n \times 9} \tag{2.5}$$

The test was stopped when insignificant amount of fine particles were discharged into the bottom sedimentation tank. Soil samples were removed in 5 to 8 layers from the permeameter and sieve analysis were performed on the samples to determine whether internal instability took place.

The Kenney and Lau approach involves a shape analysis of the grain size distribution curve. Terzaghi rule assumes that the constriction size of filter grains is one-quarter of the average size of the surrounding filter grains. This means that a soil particle can only pass through the pores between filter grains if its size is four times smaller than the average size of surrounding filter grains. The Kenney and Lau approach suggests the need for a F-H curve for soils to measure its potential for internal instability, where F is the percentage mass of soil particles smaller than a given diameter D and H is the percentage mass of soil particles between D and 4D (see Figure 2.7). Kenney and Lau (1985) found out that the amount of critical fine content, which completely fill the voids between coarse particles, is at most 20% for widely graded soil ($C_u > 3$) and 30% for uniformly graded soil. The Kenney and Lau criterion recommends production of a F-H curve for the amount of mass passing at 20% for widely graded soils and passing 30% for uniformly graded soils. Initially Kenney and Lau (1985) recommended a $(H/F)_{min}$ ratio greater than 1.3 for internally stable soil. However, this ratio was found conservative to be conservative which was revised to 1 by Kenney and Lau (1986).

The Kenney and Lau method was recommended by International Commission on Large Dams (ICOLD, 1994) to evaluate internal stability of base soils. The method was adopted by GEO (1993) and Canadian Dam Association (CDA, 2007) to assess possible segregation of granular filters.

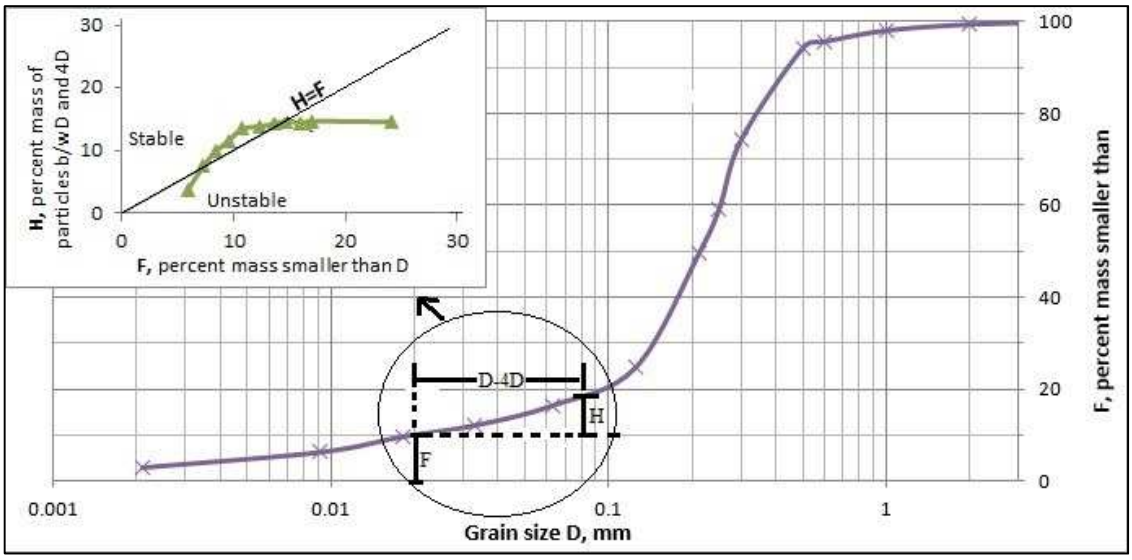


Figure 2.7 Description of Kenney-Lau approach and the inset contains H-F curve (after Kenney and Lau (1985,1986))

iv. Lafleur et al. Criterion

Lafleur et al. (1989) showed that the self-filtration mechanism of broadly graded cohesionless soils is related to the profile of their gradation curve. They defined three categories of broadly graded soil i.e. linearly graded, gap-graded and internally unstable soils (Figure 2.8). Linearly graded soils have a straight line gradation curve. In linear graded soils, either all soil particles are uniformly distributed (Curve 1) or only the fine particles in the soil are uniformly distributed (Curve 2). Linearly graded soils, having gradation curve similar to Curve 2, have very few coarse particles within a matrix of fine particles and coarse particles do not take part in the filtration process. Linearly graded soils are usually internally stable. The gradation curve of gap-graded soils (Curve 3) lacks some particles within a range of sizes. A gap width ratio can be defined as the ratio of largest diameter to the smallest diameter in the gap range. Honjo et al. (1996) considered a gap width ratio of 4 as an upper bound limit for gap-graded soils internal stability. Internally unstable soils usually have concave upward gradation curve (Curve 4). There are more chances that fine particles within internally unstable

soils will move between their coarse particles which might result in accumulation of fines (also known as blinding) near the filter interface during the filtration process.

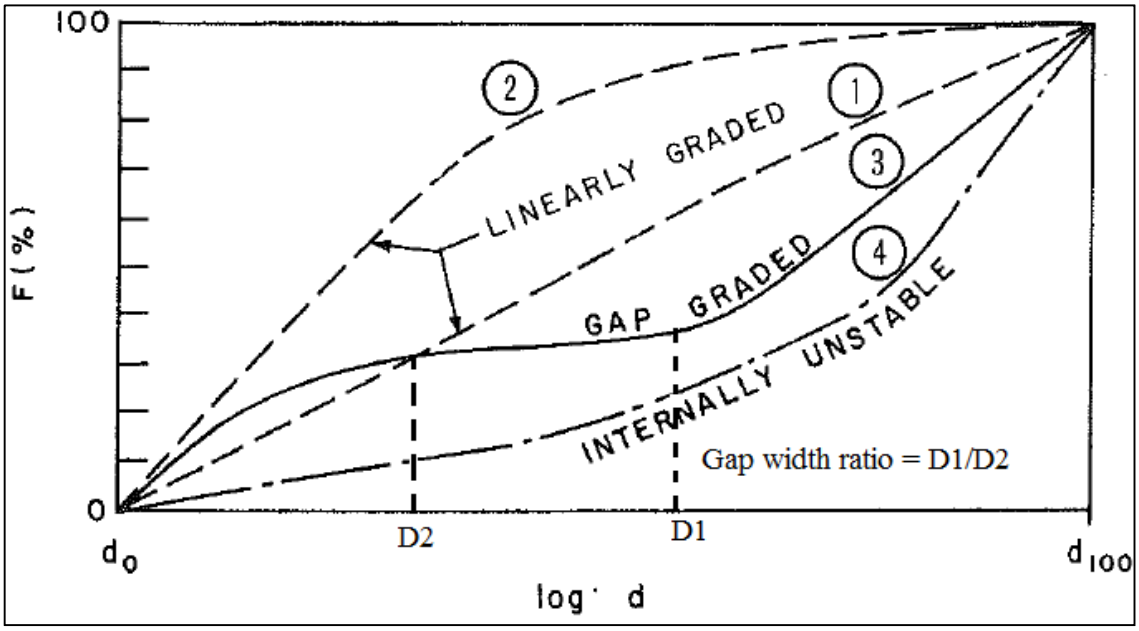


Figure 2.8 Classification of Broadly Graded Soils (Lafleur et al., 1989)

v. Burenkova Criterion

Burenkova (1993) proposed a criterion for measuring the internal stability of cohesionless soils. A total of 22 widely graded, sand-gravel soils were tested in laboratory, with a maximum grain size of 100mm and C_u upto 200. The Burenkova criterion divides soil into coarse fractions (supporting soil skeleton) and fine fractions (loose filling). The tested soils were divided into fractions of the same grain sizes. The basic assumption is that smaller size fractions will form part of supporting soil skeleton only if there is an increase in volume when mixed with a coarse size fraction. The volume of the coarsest size fraction was measured and next finer fraction was mixed with it and volume measured again. If there was increase in volume after adding finer fraction, the finer fraction was considered to be the part of supporting soil skeleton, otherwise it would be a potentially loose filling which is able to move through

supporting soil skeleton. The increase in volume with finer fraction was probably due to coarse particles loosing contact with an excess amount of finer particles, therefore, resulting in coarse particles disruption.

Burenkona used two conditional factors of uniformity to describe the heterogeneity of soils. These factors of uniformity are based on fractions d_{90}, d_{60} and d_{15}.

$$h_1 = \frac{d_{90}}{d_{60}} \tag{2.6}$$

$$h_2 = \frac{d_{90}}{d_{15}} \tag{2.7}$$

According to Burenkova (1993) criterion, a soil is considered non-suffosive (internally stable) if it satisfies Eq. 2.8:

$$0.76.\log(h_2)+1 \le h_1 \le 1.86.\log(h_2)+1 \tag{2.8}$$

Figure 2.9 shows classification of soils based on Burenkova's (1993) criterion. Zone 1 and zone 3 shows suffosive (internally unstable soils) while zone 4 shows artificial soils. Zone 2 represents non-suffosive soils. Based on the tests conducted by Burenkova, the verification method is applicable to the soils for which $1 \le h_1 \le 5$ and $3 \le h_2 \le 130$.

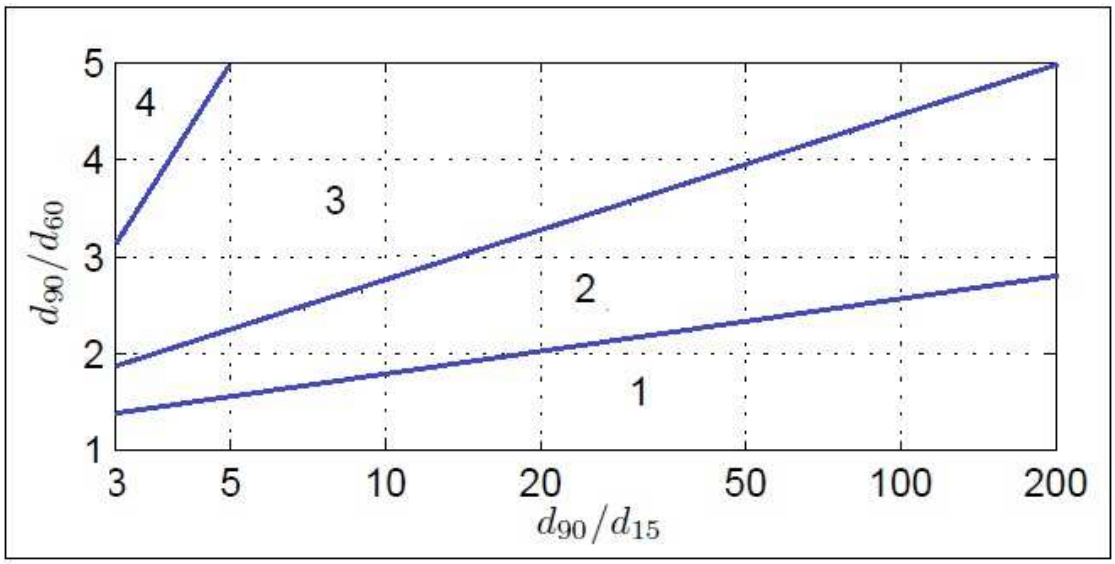


Figure 2.9 Classification of soils (adapted after Burenkova (1993))

vi. Wan and Fell Criterion

Wan and Fell (2008) proposed a criterion for assessing the internal stability of broadly-graded soils (Figure 2.10). Tests were carried out on 300mm thick compacted soil samples. The flow was kept downward during the testing program under a hydraulic gradient of 8. The gradient was kept higher than the expected gradient in core or foundation of dam. The test was stopped when no fine particles were collected from the test sample.

The Wan and Fell (2008) criterion is not valid for gap-graded soils. The proposed criterion is based on the assumption that a soil is more likely to be internally unstable if its coarse fraction has a steep slope and fine fraction has a flat slope. The d_{90}/d_{60} ratio was defined to represent slope of coarse fraction and d_{20}/d_5 ratio to represent fine fraction slope. A soil is considered to be internally stable if it satisfies the following boundary conditions;

$$\frac{30}{\log\left(\frac{d_{90}}{d_{60}}\right)} < 80 \qquad (2.\ 9)$$

or $$\frac{30}{\mathrm{Log}\left(\frac{d_{90}}{d_{60}}\right)} > 80 \qquad (2.\ 10)$$

and $$\frac{15}{\log\left(\frac{d_{20}}{d_{5}}\right)} > 22 \qquad (2.\ 11)$$

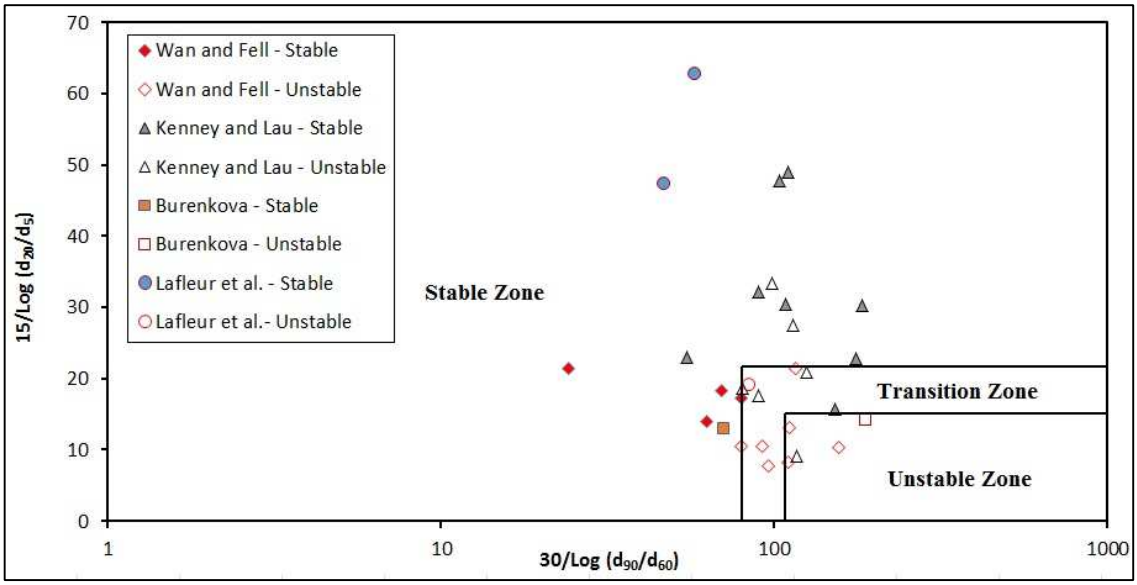


Figure 2.10 Wan and Fell criterion for evaluation of internal stability of broadly-graded soils

Figure 2.10 shows the soil gradations from various authors (discussed above) assessed by the Wan and Fell (2008) criterion. Some of the soil gradations which were evaluated as unstable by Kenney and Lau (1985) method were assessed as internally stable by the Wan and Fell (2008) criterion. The soil gradations which were evaluated as internally stable/ unstable by Lafleur et al. (1989) and Burenkova (1993) criteria were in agreement with Wan and Fell stability criterion.

2.5.2. Initiaition of Soil Instability: Hydraulic Criteria

The hydraulic criteria for instability are directly related to the geometric conditions of a soil for internal erosion. It is the hydraulic load which forces the soil particles to move. Even if the geometric condition of a soil is such that its fine particles are smaller than the constrictions provided by the coarse fraction, hydraulic load is needed to overcome the drag force, that is the weight of particle and inter-particle skeletal frictional forces, to move the particle. Unlike geometric criteria, very limited studies have been carried out to study the hydraulic criteria which describe the onset of soil instability (Adel et al., 1988; Richards & Reddy, 2007; Skempton & Brogan, 1994).

i. Terzaghi's Theoretical Critical Gradient

Terzaghi (1939) proposed a theory that the hydraulic gradient at which zero effective stress condition is reached, that is when the pore pressure acting at a certain level equals the vertical total stress at that level, which he called the critical hydraulic gradient. The critical hydraulic gradient i_c can be expressed by;

$$i_c = \frac{\rho - \rho_w}{\rho_w} \tag{2.12}$$

Where ρ is bulk density of the material and ρ_w is density of water. According to Equation 2.12, the critical hydraulic gradient is 1. The critical hydraulic gradient results in heave failure i.e. all the particles are free to move under the hydraulic gradient. Therefore, as far as instability of a fine fraction that is not providing the primary soil skeleton and, hence, not experiencing the full vertical total stress, a value of 1 must be considered the maximum value of hydraulic gradient at which instability will be evidenced with the likelihood being that it will occur at a lower value.

ii. Adel et al. (1988)

Adel et al. (1988) carried out tests on large dimension specimens in an equipment set up for testing under horizontal flow conditions. Three minestone specimens were used in the study which were loosely packed. The critical hydraulic gradient values were determined for the samples which was defined as the hydraulic gradient for which the loss of fine particles was observed at 1 g/ (s.m^2) over a 30 min time interval. The critical hydraulic gradient values were reported to be 0.16 or 0.17 for internally unstable soils and 0.7 for internally stable soils (smaller than what Terzaghi theory predicts).

iii. Skempton and Brogan (1994)

Skempton and Brogan (1994) carried out tests on well-graded and gap-graded sandy gravels. The test method was based on vertical upward flow conditions as compared to the horizontal flow tests by Adel et al. (1988). They observed a critical hydraulic gradient value of 1 for internally stable soil which is in agreement with Terzaghi's theoretical value. However, they experienced lower critical hydraulic gradient values for internally unstable soils which were 1/3 to 1/5 of those of stable materials. Table 2.1 shows a comparison of experimental values for critical hydraulic gradient observed by Aden et al. (1988) and Skempton and Brogan (1994). The table shows that there is a very little difference between the critical gradient values for horizontal and vertical flows.

Table 2.1 Critical hydraulic gradient values for migration or piping in sandy gravels (Skempton and Brogan, 1994)

State	Horizontal Flow Aden et al. (1988)	Vertical Flow Skempton and Brogan (1994)
Stable	0.7	1.0
Unstable	0.16-0.17	0.2-0.3

iv. Richards and Reddy (2010)

Richards and Reddy (2010) developed a new triaxial apparatus to evaluate the non-cohesive soils prone to erosion. Uniformly graded fine sands were tested in the triaxial apparatus and the direction of flow was kept vertically downward. Sand particles passing through a caorse filter were collected in a pan at the base of the apparatus. It was observed that both the critical gradient and critical hydraulic conductivity changed irregularly during the repeatibility tests while their product according to Darcy's law, that is critical flow, was found to be fairly constant. They concluded that critical velocity parameter, instead of critical gradient, should be measured to evaluate the piping problem.

2.5.3. Summary

The selected studies of geometric criteria (section 2.5.1) and hydraulic criteria (section 2.5.2) is summarized in Table 2.2. Geometric criteria evaluates the internal instability of soils where the ability of fine particles to pass through constrictions of coarse particles is investigated. Hydraulic criteria evaulates the initiation of internal instability of soils where the critical hydraulic gradient is able to move the soil particles.

These criteria are based on different hypotheses and experimental work and, therefore, may provide different assessment of the same gradation (see Figure 2.10). Among all the geometric criteria explained in Section 2.5.1, the Kezdi (1979), Kenney and Lau (1985, 1986) and Burenkova (1993) are the most widely used criteria for evaluating the internal stability of soils in engineering practice (Chang & Zhang, 2013; Elandaloussi et al., 2014; Li, 2008). Very limited studies have been carried out to study the hydraulic criteria as compared to geometric criteria. The test procedure, materials,

flow direction by various researchers (Section 2.5.2) to measure the critical hydraulic gradient varies. The lack of a standard test procedure to measure the critical hydraulic gradient results in different values.

Table 2.2 Summary of selected studies of geometric and hydraulic criteria

Year	References	Material Description	Hydraulic Gradient	Flow Direction	Criteria
1957	*Istomina	Sandy Gravel	-	-	Geometric
1979	*Kezdi	All soils	-	-	Geometric
1985	Kenney and Lau	Granular soils	**R' > 10	Downward	Geometric
1988	Adel et al.	Minestones	0-1	Horizontal	Hydraulic
1989	Lafleur et al.	Broadly-graded cohesionless soils	2.5-6.5	Downward	Geometric
1993	Burenkova	Cohesionless and graded soils	-	-	Geometric
1994	Skempton and Brogan	Well-graded and gap graded sandy gravels	0-1	Upward	Hydraulic
1996	*Terzaghi et al.	Cohesionless soils	1	Upward	Hydraulic
2008	Wan and Fell	Well-graded soils	8	Downward	Geometric
2010	Richards and Reddy	Uniformly-graded sand	0.13-0.24	Downward	Hydraulic

*Based on theoretical approach
**hydrodynamic number (see Kenney and Lau criterion, section 2.5.1)

2.6. Factors Affecting the Internal Stability of Cohesionless Soils

The internal stability of cohesionless soils depends on many factors including particle shape, density, confining stress, mechanical loading, and hydraulic loading. These factors are explained in detail in the below sections.

2.6.1. Particle Shape and Size

By testing angular and sub-rounded sands, Bertram (1940) showed that particle shape has no effect on the soil internal stability. Kenney and Lau (1985) demonstrated experimentally that as long as particles are coarser than silt size, particles sizes have little influence on internal stability as comapred to the shape of gradation curves. Lafleur et al. (1989) reported that the angularity of fine particles contributes to make the granular bridge network thicker in successful filtration cases. Current soil stability evaluation criteria do not take into account the particle shape.

2.6.2. Density

Sherard and Dunnigan (1989) showed that the density of soils have a significant effect on the stability of well graded soils. They observed that the movement of particles increased with a decrease in soil density. Uniformly graded soils are stable and less sensitive to density. Bertram (1940) showed that the density had little effect on the filtration performance of uniformly graded sands. According to Giroud (2010), soil particles in a dense state cannot pass through filter if the opening size of filter is as large as the particle size. Therefore, the internal stability of soil depends on its density.

2.6.3. Confining Stress

The internal stability of base soil depends on the friction between particles, which in turn depends on the magnitude of compressive stresses. However, the base soil and

filter may reach a critical state if the magnitude of compressive stresses reaches zero. It may result in particles movement through filter. This critical condition usually occurs during cyclic flow, earthquake, and repeated traffic loads (Giroud, 1996). Moffat et al. (2011) developed a hydro-mechanical relation governing the internal stability of cohesionless soils. The onset of internal instability was triggered by a decrease in effective stress. Similar behaviour was also observed by Hameiri (2000) and Hawley (2001). Although confining pressure plays an important role in the stability of cohesionless soils, however, high confining stresses may cause intrusion of fine particles into the filter which may result in the reduction of filter permeability (Luettich, 1993).

2.6.4. Mechanical Loading

Kenney and Lau (1985, 1986) and Lafleur et al. (1989) performed tests on granular soils by applying light vibration to the test samples. The purpose behind applying mechanical loading was to induce more severe conditions on test samples than generally expected in practice. Kenney and Lau (1985) indicated that the mechanical disturbance had a significant effect on filtration behaviour of few tested materials which started losing fine particles even under a mild vibration. Geometrically assessed internally stable soil gradations may experience washing out of fines similar to internally unstable soils under dynamic conditions (Trani & Indraratna, 2010). Internally stable soils can experience heave and heave-piping phenomenon under heavy haul loadings (Israr et al., 2016).

2.6.5. Hydraulic Loading

Lafleur (1984) suggested that the filtration tests performed under downward flow conditions has significant effect on the erosion of soils as compared to the upward flow due to drag of water in the same direction as gravity. de Graauw et al. (1984) showed that

the critical hydraulic gradient to start erosion of fine particles is lower in cyclic flow conditions as compared to steady flow conditions. Kayser et al. (2016) showed that granular soils are more stable under unidirectional conditions as compared to oscillatory flow. Internally unstable soils should not be placed in conjunction with geotextiles under dynamic conditions as there is a high risk of geotextile clogging (Holtz et al., 2008).

2.7. Effect of Geotextile Properties on Filtration Performance

The properties of geotextiles which has a direct effect on the filtration performance of geotextiles are discussed in the sections below. Among these properties, the filter opening size is usually considered a key parameter in controlling the filtration performance of geotextile since most of the retention criteria are based on characteristic opening size of geotextiles (see Table 2.5 and Table 2.6).

2.7.1. Filter Opening Size

A pore channel in a geotextile is a continuous opening between fibers throughout the thickness of geotextile. Water and soil particles follow this pore channel to travel from one side of geotextile to the other side. A pore channel is made up of various pores which is the size of pore channel at any location (Fischer et al., 1996). The minimum pore size along the pore channel is called constriction size (Kenney et al., 1985). Every pore channel has one constriction size. The filter opening size (also known as pore opening size) is the nearly largest constriction size of pore channels. It means that the filter opening size determines the diameter of the largest sphere that can pass through the filter (Giroud, 2010). There are some pore spaces which are not involved in pore channel. These pore spaces are called dead end pores. The pore structure terminology which represents the void space between geotextile fibers is shown in the Figure 2.11.

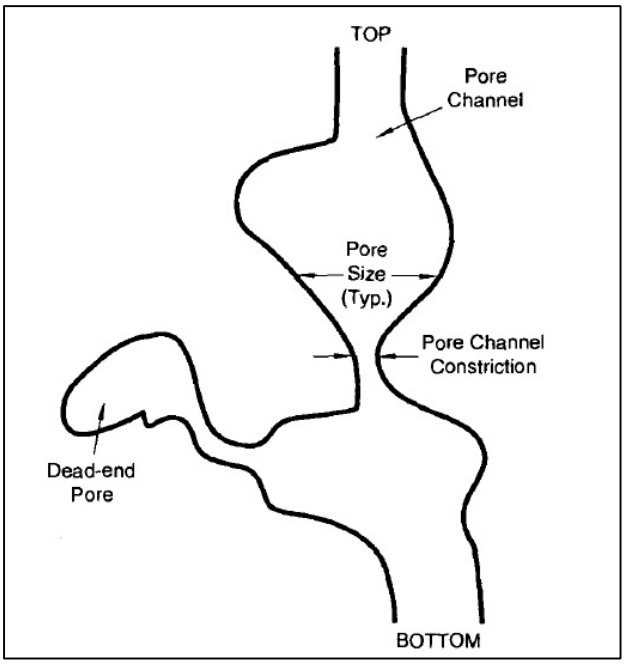


Figure 2.11 Pore structure terminology to define void space between geotextile fibers (Fischer et al., 1996)

The characteristic pore size of geotextile is a very important parameter to select a geotextile for filtration (Mlynarek, 1999). Geotextile filter design criteria are based on the ratios of geotextile pore sizes to soil grain sizes. It is important to have knowledge about at least one characteristic opening size of geotextile to ensure soil retention. The first attempt to find the pore sizes of geotextile was made by Calhoun (1972) who developed a test to evaluate the pore sizes of woven fabrics. In the test procedure, rounded sand particles of specified sizes were shaken over woven fabrics. Equivalent opening size (EOS) was taken as the size of sand for which less than 5 percent were passed through woven fabrics after shaking. That procedure was then implemented by U.S. Army Corps of Engineers (1977), by replacing sand with glass beads to eliminate possible variations between sand samples, to measure the apparent opening size (AOS) of woven geotextiles. This method was later extended to non-woven geotextiles. According to CW-02215 (US Army, 1977), AOS or EOS is the standard U.S. sieve number that has openings closest in size to the openings in the geotextile. The term

"apparent" is used with pore size because results do not signify a precise equivalence between US standard sieve aperture sizes and geotextile pore sizes.

2.7.1.1. Methods to Find Pore Sizes of Geotextiles

Various techniques have been developed to find the pore size distribution (PSD) of geotextiles. The indirect technique includes dry sieving method (Calhoun,1972, ASTM D4751), wet sieving method (Saathoff & Kehlhase, 1986) and hydrodynamic sieving method (Fayoux, 1977). Direct techniques include mercury intrusion porosimetry (Prapaharan et al., 1989), the bubble point test (Hoffman, 1983, Bhatia & Smith, 1985, Miller et al, 1986, Fischer et al., 1994, ASTM F316) , and image analysis (Faure et al., 1990; Lombard & Rollin, 1987). However, none of these methods is universally accepted because of the disadvantages associated with these methods. The PSD calculated from these methods vary within and between each other. Bhatia and Smith (1996) have identified various problems with different PSD measurement methods. Fischer et al. (1996) concluded that the pore size of geotextile is a unique property of the method of measurement, instead of the unique property of geotextile.

i. Dry sieving

Dry sieving is the most commonly used method to find the AOS of geotextiles. ASTM D 4751 is the standard test procedure to find the AOS of geotextiles. In this test procedure, 50g of glass beads of a certain size are placed on the geotextile specimen. The sieving equipment is adjusted at a frequency of 50 Hz and amplitude of 0.75mm (a total height of 1.5mm). The test recommends shaking sieves for 10 min. The amount of glass beads passed through geotextile is collected in a pan. The test is repeated with progressively larger size beads until 5% or less pass through geotextile specimen. AOS

or O_{95} is calculated which corresponds to 95% glass beads retained on the geotextile specimen.

AOS is the nearly largest pore opening of a geotextile. Although dry sieving is a low cost method, however, there are many problems with the testing procedure (Fischer & Holtz, 1991; Giroud, 1996; Myers, 2010). The main disadvantages of dry sieve method include its inability to find smaller pore openings, chances of electrostatic forces between fibers and glass beads in the absence of static-eliminating devices, and the possibility of glass beads becoming trapped inside the geotextile. Dry sieving is difficult to apply to geotextiles having a characteristic pore size smaller than 100µm because of the risk of electrostatic force between fine particles and geotextile fibers which results in erroneous results (Dierickx & Myles, 1996). The dry sieving test is conducted in dry conditions, whereas geotextiles as a filter material involve liquids (Koerner & Koerner, 2014). Moreover, Bergado et al. (2002) studied the effect of environmental conditions on the dry sieving method and concluded that humidity of the test environment affects the AOS values of non-woven geotextiles.

ii. Wet sieving:

Wet is currently the European Standard for measuring the characteristic opening size of geotextiles (BS-EN-ISO-12956). The characteristic opening size calculated from wet sieving is known as equivalent opening size (EOS) or O_{90} of a geotextile. Wet sieving involves the same equipment as with the dry sieving method. In this method, well-graded granular soil is used instead of fractions of glass beads. The granular soil should not be gap graded and its coefficient of uniformity (C_u) should be between 3 and 20 such that the expected O_{90} of geotextile is between its d_{20} and d_{80} i.e. the particle size for which 20% and 80% of all particles respectively have a smaller size. In this

method, spray nozzles are used to uniformly spray water over the soil specimen to keep the granular soil wet during the sieving process. The water flow reduces the electrostatic attraction between fibers and soil particles. The sieving equipment is adjusted at amplitude of 1.5mm (3mm height) which acts a source of frictional drag on the aggregate particles. The Standard recommends adjusting the flow of spray water such that there is no probability of water standing over the geotextile which might act as a dragging force on the aggregate particles. Particles passed through the geotextile specimen are oven-dried and particle size distribution of the transmitted soil is assessed. The test is carried out in triplicate for data analysis. Wet sieving considers D_{90} of the passing soil as the largest significant particle and, therefore, considers D_{90} of the passing soil as O_{90} of the geotextile. The O_{90} value is mostly situated in the transition zone between steep and gentle slope of the gradation curve of passing particles, as compared to O_{95} which lies in the gentle slope of the curve which, therefore, makes O_{90} value less sensitive to variations as compared to O_{95} (Dierickx and Myles, 1996).

The use of water spray over soil specimen to reduce electrostatic force makes wet sieving method advantageous compared with the dry sieve method. Unlike dry sieving, wet sieving can be used for geotextiles having characteristic opening size less than 100µm. The main disadvantage of wet sieve method is that it finds just a single pore size instead of PSD of geotextiles. The shaking of sieving equipment at amplitude of 3mm during wet sieving does not reflect actual field conditions. Particle agglomeration inside geotextile specimen is also a big problem in wet sieving method (Bhatia and Smith, 1996, Ziabari et al., 2008). Moreover, the lack of precision in the Standard (BS-EN-ISO-12956) could result in different interpretations which might affect the accuracy and repeatability of the method.

iii. Hydrodynamic Sieving

Hydrodynamic sieving is a standard method used in the Eastern Provinces of Canada (CAN/ CGSB 148.1 No.10). The opening size calculated from hydrodynamic sieving is known as the filtration opening size (FOS). This method involves passing well-graded glass beads through a geotextile specimen which is subjected to hydrodynamic (immersion and withdrawal) action. The test recommends a glass bead mixture with a C_u greater than 6 and the size of the maximum glass bead to be twice greater than the expected FOS. The main reason behind hydrodynamic action during hydrodynamic sieving is to simulate the filtration mechanism where a soil-geotextile system is considered as a dynamic process. The hydrodynamic conditions more strongly force the glass beads to pass through geotextile than gravity and simple water flow do in the dry and wet sieving methods previously described. The FOS is calculated as the 95 percentile diameter of the glass beads passed through geotextile.

The advantages of hydrodynamic sieving includes; glass beads are wet during the sieving process, good repeatability of results, this method can be used for geotextiles having characteristic pore size smaller than 100um, and large geotextile specimen is involved which, therefore, has more representative pore openings (Mlynarek et al., 1993) The main disadvantage of this method is the time duration to complete sieving because a large geotextile area is involved. The use of a larger geotextile specimen in hydrodynamic sieving makes it difficult for geotextile products installed in narrow strips such as filters wrapped around drainage pipes (Blond & Veermersch, 2015). The test equipment in this method is expensive and differs from one laboratory to another (Dierickx and Myles, 1996). There is risk of blinding during hydrodynamic sieving

where the transmission of fine particles is stopped by large particles which have entered and settled first (Bhatia and Smith, 1996, Ziabari et al., 2008) .

iv. Mercury Intrusion Porosimetry

Mercury intrusion porosimetry (MIP) is already a standard procedure (ASTM-D4404) to find the pore volume distribution (PVD) of soils, rock, and related materials. Prapaharan et al. (1989) used MIP to find the PSD of non-woven geotextiles and the MIP results were in good agreement with image analysis results. The MIP method works on Washburn principle which states that the entry of liquid into the pores of material is opposed by the surface tension of a non-wetting liquid (e.g. mercury). This resistance could be overcome by applying an external pressure and that external pressure is inversely proportional to the pore sizes in the material. The Washburn equation is given by the equation;

$$P = -\frac{4TB\cos\theta}{d} \tag{2.13}$$

Where P is the pressure required to force mercury into capillary pore of diameter d, T is the surface tension, B is capillary constant and θ is angle of contact.

MIP is a simple and rapid test which takes only 30-45 minutes to find the volumetric PSD of geotextiles. Moreover, the test does not need any form of sample preparation. The disadvantage of MIP is that it doesn't give any idea about the number of pores or the constriction size of geotextile pore channels. MIP measures all the free volume of pores including the dead end pores and thus does not give a specific idea about the volume available for flow which influences the filtration behaviour (Fischer et al., 1996). Mercury is a hazardous substance which makes the MIP method environmentally problematic (Tu et al., 2002).

v. Bubble Point Test

Bubble Point Test (BPT) is a current standard procedure (ASTM-D6767) to find the pore size characteristics of geotextiles by capillary flow test. The test procedure involves measuring the flow rate of air instead of measuring the volume of liquid, as in MIP. The technique is based on differential analysis of two test runs; a dry run and a wet run. In the dry run, the flow rate of air is measured over a range of pressures through a dry geotextile. While in the wet run, air pass through saturated geotextile when the applied air pressure exceeds the capillary attraction of non-wetting liquid (mineral oil) inside the pores. The air pressure will force liquid from large pores first, followed by small pores with increasing pressure. A flow rate vs pressure graph over the intended range of use is plotted for both dry and wet run. The pore sizes are measured from the pressure difference between the dry and the wet run using the Washburn equation (Equation 2.14). The percent finer of a given pore size is calculated from the flow rate difference between wet and dry run at the given pore size. The percent finer of a particular pore size is measured using Eq. 2.10 at the same pressure;

$$\% \text{ Finer} = \left(1 - \frac{Q_w}{Q_d}\right) 100 \tag{2.14}$$

Where Q_w is wet flow rate and Q_d is dry flow rate.

The BPT is a quick and efficient method to find the PSD of geotextiles. The BPT method is advantageous over other methods since it measures the constriction area of pores (Fischer et al, 1996, Bhatia and Smith, 1996, Elton et al., 2007, Aydilek et al., 2007). It is the constriction size of pores which controls the filtration behaviour of geotextiles (JP Giroud, 1996, Kenney et al., 1985, Vermeersch and Mlynarek, 1996) . The Washburn equation used in the BPT to find the pore sizes from pressure difference

assume pores to be cylindrical. The PSD calculated from the BPT is not the true PSD because the flow rates measured during the dry and wet runs are proportional to the cross-sectional area of pore constrictions instead of their equivalent diameter (Fischer et al., 1996). ASTM D6767 has only been verified for constriction sizes up to 200µm and there is a need to evaluate the applicability of ASTM D6767 for constriction sizes greater than 200µm. The results of the BPT depend on the viscosity of the wetting liquid for non-woven geotextiles (Elton et al., 2007). ASTM method (D6767) to carry out bubble point test does not consider temperature variation which may have an effect on the capillary action and constriction sizes (Aydilek et al., 2007).

vi. Image Analysis

Image analysis technique is considered to be a more direct approach for determining the constriction sizes of non-woven geotextiles since it measure the actual distance between geotextile fibers. Various investigators (Lombard & Rollin, 1987, Faure et al., 1990) have used image analysis to find the two-dimensional PSD of geotextiles. Image analysis appears to be more suitable for woven geotextiles because of the largely two-dimensional structure and large pore sizes. Elsharief and Lovell (1996), and Bhatia and Smith (1996) measured the two-dimensional PSD of non-woven geotextiles from cross-sectional images. However, the method does not fully take into account the randomness in non-woven geotextile fibers due to fiber arrangement in all directions. Image analysis is highly sensitive to light intensity and it is highly likely to measure large pore sizes with an increase in brightness. Also the pore dimensions measured are image-specific rather than the actual pore sizes in the geotextile (Aydilek, 2004; Aydilek et al., 2005).

vii. Theoretical Pore Size

An alternative method to define the pore sizes of geotextiles is theoretical modelling (Faure et al., 1986, Faure et al., 1990, Giroud, 1996). The pore sizes calculated on the basis of theoretical modelling requires information of thickness and mass per unit area of geotextile, and density and diameter of fibers. These parameters are easy to calculate. The disadvantage of theoretical modelling is that pore sizes are not actually measured.

2.7.1.2. Evaluation of Pore Size Determination Techniques

The important features of different pore size determination techniques are given in the Table 2.3. A detailed description of each test method along with its advantages and disadvantages are already explained in above. Most methods find only the largest opening size AOS, EOS or FOS depending on the technique, instead of finding the PSD of geotextile. Sieving methods provide somewhat arbitrary results as there are random chances that glass beads or soil particles will pass through the desired pore openings. If glass beads or soil particles come across pore openings smaller than their diameter, they will not pass and vice versa. It is possible that glass beads or soil particles can pass through a single large pore in geotextile if enough timing is provided for vibration or repeated immersion cycles. In that case, a true characteristic opening size or PSD will not be obtained. At best, sieving methods can provide the largest opening size of geotextile because it is measured from the largest glass bead or soil particle passed through geotextile, but it cannot provide the PSD of geotextiles. If sieving methods are to be used, sequential use of increasing particle sizes is much preferred to prevent pore channel blocking by large particles before smaller particles arrive. Currently, bubble point appears to be the best method amongst all the methods

because it measures the constriction size of geotextile but the method still needs to be validated for constriction sizes larger than 200µm. Image analysis measures the actual pore dimensions of geotextiles but there is no standard procedure available to consider the randomness in non-woven geotextiles.

2.7.2. Weaving Pattern

Woven and non-woven geotextiles (Section 2.1) have sub-categories which depend on the particular manufacturing process. The major types of woven geotextiles are monofilament, slit film, and multi-yarn fibrillated. The filaments of non-woven geotextiles are bonded together by thermal, chemical or mechanical means (i.e. heat bonded, resin bonded, or needle-punched). The manufacturing process has an effect on the filtration performance of non-woven geotextiles. Heat-bonded geotextiles occasionally may not be successful in filtration applications due to their smoother surface (Haliburton and Wood, 1982, Aydilek and Edil, 2003, Elsharief, 2016). The complex needle-punched structure of the geotextile enables the retention of soils.

The difference in fabric structure of woven and non-woven geotextiles results in different filtration performance. For instance, mono-slit woven geotextiles is used in applications where there is a high risk of clogging by organic matter. The woven geotextiles are also used as reinforcement in pavements constructed over weaker soils due to its high tensile strength (Holtz et al., 2008). On the other hand, the heterogeneous pore structure of nonwoven geotextiles gives better soil retention results. There is a high potential of fine passing though woven geotextiles as compared to non-woven in coastal application under hydrodynamic flow conditions (Chew et al., 2000).

Table 2.3 Important features of different pore size determination techniques (after Fischer, 1994)

Test Method	Pore Type measurement	Measurement of PSD	Finer Pores Measurement	Length of Test (h)	Cost of Test
Dry Sieving	Indication of pore size	No	No	2	Low
Wet Sieving	Indication of pore size	No	No	2	Low
Hydro-dynamic Sieving	Indication of pore size	Yes	No	24	High
Mercury Intrusion Porosimetry	Pore Volume	Yes	Yes	1	Average
Bubble Point	Constriction size	Yes	Yes	1	Average
Image Analysis	Pore Dimension	Yes	Yes	48-72	High
Theoretical	Pore Dimension	Yes	Yes	0.5-1	Low

2.7.3. Porosity

Porosity of a material is the fraction of the volume of its voids over the total volume. The porosity criterion of a geotextile filter ensures that the number of filter openings is sufficient. High porosity means geotextile has large pore space which causes high flow rate and contact between fine particles and fibers will be for less duration. Sufficient number of openings also ensures that the flow will be less disturbed if clogging of some of the filtration paths of geotextile occur. Porosity is closely related to geotextile density (mass per total volume)(Lee & Bourdeau, 2006). A geotextile may meet the permeability criterion even if the filter has small number of openings per unit area. Since base soil has greater number of pore channels per unit area as compared to geotextile, therefore, a geotextile having small no. of pore openings per unit area causes disturbance of flow at the soil-geotextile interface which could result in the moving of soil particles inside the filter, causing clogging (Giroud, 2010).

Giroud (1996) suggested porosity value of greater than 55% for nonwoven geotextiles and relative open area (i.e. two-dimensional porosity) of 10% for woven geotextiles while Bhatia and Smith (1996a) suggested porosity value greater than 30-40% for non-woven geotextiles. Normally geotextiles have a porosity value of 70-90% in uncompressed state and 60-80% in compressed state. Geotextiles have more porosity than graded granular filters due to which the deposition rate of particles on geotextile fibers can be considered negligible (Reddi et al., 2000; Xiao & Reddi, 2000).

2.7.4. Thickness

Thickness of geotextile has more significant effect on the filtration response of non-woven geotextiles as compared to woven geotextiles. Woven geotextiles have nearly similar pore sizes so they are not affected by thickness parameter. Giroud (2010)

showed that the pore opening size of a non-woven geotextile increases with decrease in its thickness. This is due to the fact the number of constrictions (passage between fibers) increases with the thickness of a geotextile which, therefore, increases the possibility of more small constrictions in geotextiles (see Figure 2.12).

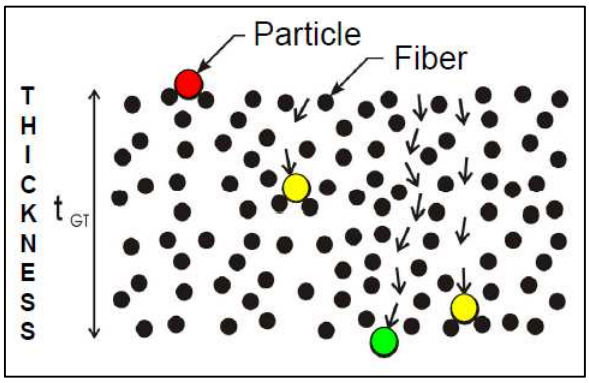


Figure 2.12 Schematic cross section of a non-woven geotextile (Giroud, 2010) showing particles stopped on the top and inside the filter, while one particle passed through the filter

The increase in a geotextile thickness results in entrapment of more fine particles inside the filter, thus enhancing the chances of clogging. Faure et al. (2010) concluded that thick geotextile samples should be used to control erosion in bank revetments under cyclic loading. Qureshi et al. (1990) found that thicker geotextiles gave higher permeability values and less severe clogging were observed for fine soils. The findings were based on 6 geotextiles in combination with 18 gap-graded soils. On other hand, Mannsbart and Christopher (1997) showed that for fine soils, the amount of clogging decreases with decreasing the thickness of geotextiles. The continuous openings of thicker geotextile may be tortuous which increases its potential to clog more as compared to thinner geotextiles (Bell and Hicks, 1980). The thicker geotextiles are effective in reducing the critical hydraulic gradient at the soil-geotextile interface and dissipating excessive pore water pressure (Alobaidi & Hoare, 1996; Palmeira & Tatto, 2015).

2.7.5. Compressibility

The compressibility of a geotextile refers to its thickness at different applied normal stresses. The compressibility has a direct effect on the hydraulic conductivity of geotextiles. The compressibility is important in case of needle-punched geotextiles since these geotextiles are also used as a drainage layer to convey liquids within the plane of their structure (Koerner, 1993). The compression of non-woven geotextiles occurs for normal stresses up to 200kPa which results in decrease in its hydraulic properties (Pak & Zahmatkesh, 2011; Palmeira & Gardoni, 2002). Palmeira (2002) also observed decrease in pore channel constriction diameters for normal stresses upto 100kPa, however, the increase in normal stresses was significant on large pore sizes instead on small pore sizes.

2.8. Boundary Conditions Affecting Soil-Geotextile Filtration Behaviour

2.8.1. Top Load

The significance of confining stresses on the hydraulic behaviour of geotextiles has been pointed out by many researchers (Chen et al., 2008; Hufenus & Schrade, 2006; Pak & Zahmatkesh, 2011; Palmeira & Gardoni, 2002). Pore sizes and thickness of nonwoven geotextiles may be affected by confining stresses, depending on its compressibility. The decrease in pore sizes enhances the retention capability of geotextiles which, in turn, easily stop the particles smaller than its pore diameter (Shan et al., 2001). This makes the retention criterion more conservative. However, in situation if the base soil is unstable or particles are in suspension and moving towards geotextile, then the pore sizes (reduced by confinement) used for evaluating the clogging potential will enhance the chances of clogging of geotextiles.

Pak and Zahmatkesh (2011) studied the physical and hydraulic properties of needle punched nonwoven geotextiles under various hydraulic gradients and normal stresses. A markable decrease in the value of permeability was observed with increasing the normal stresses in the range below 100kPa. Palmeira and Gardoni (2002) also observed much reduction in large pore constriction diameters of filter materials by increasing normal stresses up to 100kPa as compared to small pore constriction sizes. Cazzuffi et al. (1999) concluded that a stable soil-geotextile interface can become unstable if a decrease in normal effective stress occurs.

Although high confining stresses has a stabilizing effect on the soil-geotextile interface by reducing the filter voids, however, it can also be a destabilizing factor. If the filter interface is not subjected to any confining stress, the base particles can form bridging network by inter-particle frictional forces. High confining stresses can overcome the frictional forces and destabilize the bridging network.

2.8.2. Hydraulic Gradient

The filtration tests performed under large hydraulic gradients can be justified as a compensating factor for short time laboratory experiments relative to life over which filter is expected to perform (Bertram, 1940). Field hydraulic conditions vary from site to site. The typical hydraulic gradient values in different applications are given in Table 2.4.

Critical hydraulic gradient causes the erosion of soil particles (see Section 2.5.2). Tomlinson and Vaid (2000) concluded that the stability of filter bridge is mainly affected by the value of gradient instead of duration. Sudden increase in hydraulic gradient causes rapid migration of fine particles towards filter. This causes the temporary clogging of the filter and increases the pore water pressure, thus

destabilizing the bridging network. The same effect is also observed by Elsharief (2016) that high flow rates associated with high hydraulic gradients enhance the blinding process at geotextile interface. The presence of less pervious subgrade soil would lead in high hydraulic gradients. Bhatia and Huang (1995) observed that change in the hydraulic gradient destabilize the bridging network. They concluded that the rapid increase in hydraulic gradient has less effect on stable soils as compared to unstable soils. Some geotextiles require high gradient to allow the flow through it and this is not possible through low hydraulic gradients (Bell & Hicks, 1980).

Table 2.4 Hydraulic gradient in soil next to filters (Giroud, 2010)

Application	**Typical Hydraulic Gradient**
Dewatering trench	≤1.0
Vertical wall drain	1.5
Pavement edge drain	≤1.0
Inland waterway protection	≤1.0
Landfill drains	1.5
Dam toe drain	2.0
Drain behind dam clay core	3 to >10
Liquid reservoir with clay liner	>10

2.8.3. Dynamic Conditions

Geotextiles may be subjected to steady or dynamic conditions. Steady flow is considered as non-severe condition while flow under dynamic, cyclic or pulsating load is considered as severe condition (Carroll, 1983). Under static condition of flow, the soil next to geotextile forms a bridging network which prevents other soil particles and the flow stabilizes. In dynamic conditions, the geotextile may be subjected to hydraulic disturbance or mechanical disturbance (Hameiri, 2000). Dynamic conditions may

impair the formation of bridging network, causing the pumping of particles that are smaller in size than the filter opening size.

2.8.3.1. Mechanical Disturbance

The most common use of geotextiles in highways and railways is to work as a separator layer to stop intermixing of sub-grade particles with the base-soil/sub-ballast layer. While performing as a separator, geotextile also act as a filter to allow water from subgrade into the sub-base/ sub-ballast layer. Geotextiles are also used as filters around trench drains and edge drains to stop erosion of subgrade soils into the drainage aggregate. Mechanical disturbance caused by traffic load (for instance: vehicles, trains or aircrafts), construction work or earthquake results in pumping load and vibration action. The traffic induced cyclic loading is treated as one-way cyclic loading where the stress alternates between zero and a positive value (Miura et al., 1990; Unnikrishnan et al., 2002).

According to Hameiri (2000), the mechanical disturbance has the ability to disturb the internal stability of soil as well as the soil-geotextile interface. Dynamic loading causes the pumping of fines from subgrade into the sub-base layer, contaminating the sub-base soil which may impair their performance as well as result in the reduction of subgrade strength (Alobaidi & Hoare, 1996; Bell et al., 1982; Hoare, 1982; Narejo, 2003). The authors have used fine grained soil (silt to clay) during the filtration tests. Narejo and Koerner (1992) used a flow rate test to study the effect of dynamic loading on soil-geotextile filtration. The test was conducted under worst case hydraulic conditions where the soil was added into test set-up in slurry form which, eventually, resulted in excessive soil loss through geotextiles. Not enough literature review is

available to evaluate the dynamic filtration compatibility of geotextile with soils in roads.

Very few researchers have performed filtration tests with geotextiles under sub-ballast layer in railways (Fatahi et al., 2011; Ip et al., 2012). The authors have used geotextiles as an extra filter layer to stop pumping of fines from subgrade into sub-ballast layer as well as to reduce the thickness of sub-ballast layer. Not a detailed experimental work has been performed in terms of retention and clogging criteria for geotextiles in railways.

2.8.3.2. Hydraulic Disturbance

Hydraulic disturbance is caused by dynamic cyclic flow usually in coastal structures like revetment, seawalls, navigation channels, barriers etc. The change of flow direction in such a flow tends to destabilize the bridging network. de Graauw et al. (1984) showed that the bridging (arching) of particles at the filter interface may not be possible under cyclic conditions due to the changing direction of flow. According to Tondello (1998), high dynamic cyclic flow cyclically displaces the geotextile due to the variation in pore water pressure at the both side of geotextile which causes the migration of fines through the geotextile. Studies by Cazzuffi et al. (1999) showed that compared with one-way flow, the change in direction of cyclic flow will increase migration of soil particles and the disturbance on soil-geotextile interfaces and decrease the possibility of clogging. However, they also observed that the effect of cyclic flow is related to the normal effective stress on the geotextile and the continuity of the contact between soil and geotextile.

Hameiri (2000) concluded that the existing design criteria do not take into account the confining stresses, the maximum hydraulic gradient, and the internal instability of soils

for cyclic flow conditions. Chen et al. (2008) observed that a bridging network is able to form under the long term cyclic flow conditions which is not the same finding as what Tondello (1998) and Cazzuffi et al. (1999) have suggested. Moreover, they observed that the decrease in cyclic flow period increase the pore water pressure. The clogging under cyclic flow was not as serious as under unidirectional flow.

Palmeira and Tatto (2015) concluded that geotextile filters should be used in bank revetments under the action of waves to avoid piping of soil. They also observed that geotextiles with greater thickness and lower permeability perform better in cyclic flow conditions since these geotextiles help to reduce the maximum pore pressure.

2.9. Filter Design Criteria

A design criterion is based on the ability of the filter to retain soil particles from washing out while allowing water to move freely through the filter without developing pore water pressure. Giroud (1981) suggested that the permeability of geotextile should be greater than permeability of soil and a safety factor 10 is recommended. Most of the researchers have shown that the retention criteria depends on the Apparent opening size (AOS) of geotextile (Table 2.5). Carroll (1983), for the first time, recognized that clogging potential of geotextiles should be assessed along with retention and permeability criteria. Thus, most of the design methods recommend performing laboratory tests in order to assess the long term clogging potential of the geotextile.

2.9.1. Retention criterion

Retention criterion is the most important and complex part of filter design criteria. The retention criterion ensures that minor loss of fines occurs so that a state of equilibrium is developed at the soil-geotextile interface. Lafleur et al. (1989) reported that piping

failure of broadly graded cohesionless soils occurs for particles migration in excess of 2500 g/m^2 during a long term filtration test. However, this amount of fines passing into the downstream drain maybe large in some instances (Lafleur, 1999). Hameiri (2000) suggested that piping failure of soil occurs when the particles passed through filter constitute the primary fabric of soil. The retention criterion of geotextiles is usually expressed as:

$$O_i < C\ D_i \tag{2.15}$$

Where O_i is the characteristic opening size of geotextile, C is a constant, and D_i is the indicative grain size (D_{85}, D_{50}, D_{30} or D_{15}).

The retention criterion is considered as the upper limit in terms of filtration design criterion. Some of the existing design criteria for steady state flow conditions (Table 2.5) and unsteady flow conditions are given below.

Table 2.5 Existing filter retention criteria for steady state flow conditions

Author	**Geotextile**	**Hydraulic Gradient**	**Base Soil**		**Retention Criterion**
			Relative Density	**Grain Size Distribution**	
Calhoun (1972)	W			Soils with < 50% passing #200 sieve	$O_{95}/D_{85} \leq 1$
Zitscher (1975)	W			Soils with $C_u \leq 2$ D_{50} = 0.1-0.3 mm	$O_{50}/D_{50} \leq 1.7$-2.7
Ogink (1975)	W	7		Uniform Sand	$O_{90}/ D_{90} \leq 1.8$
				Graded Sand	
Ognik (1975)	NW	7		Uniform Sand	$O_{90}/ D_{90} \leq 1.8$
				Graded Sand	
Schober and Teindl (1979)	W Thin NW	10		Quartz Sand	$O_{90}/D_{50} \leq 1.7$ - 3 (depending on C_u)

Author	Geotextile	Hydraulic Gradient	Base Soil		Retention Criterion
			Relative Density	Grain Size Distribution	
Schober and Teindl (1979)	Thick NW	10		Silt	$O_{90}/D_{50} \leq$ 3-5 (depending on C_u)
				Sand soil with C_u <5	
Heerten (1982)	W NW			Granular soil with C_u < 5	$O_{90}/D_{50} \leq 2$ $O_{90}/D_{90} \leq 1$
Heerten (1982)	W NW			Granular soil with $C_u \geq 5$	$O_{90}/D_{50} \leq 10$ $O_{90}/D_{90} \leq 1$
Faure et al. (1986)	W NW	1		Uniform sand 1.4 < C_u < 1.5	O_F/D_{85}<1.5-2
Faure et al. (1986)	NW	10		Uniform sand and silt 1.2 < C_u < 3.6	O_F/D_{85}<1-1.2
Faure et al. (1986)	W NW	1		Broadly-graded soil 1.4<C_u<10	O_F/D_{85}<1.5-2
Fannin et al. (1994)	NW	1-7	$\leq$ 70%	1 < C_u < 2	O_F/D_{85}<1.5 O_F/D_{50}<1.8
Fannin et al. (1994)	NW	1-8	$\leq$ 70%	3 < C_u < 7	O_F/D_{50} < 2
Holtz et al. (1997)	NW			Granular soil	$O_{95}/D_{85} \leq$ 1 to 2 (Depending on C_u)
Lafleur (1999)	NP-NW			$C_u \leq 6$	O_F/D_{85}<1
Lafleur (1999)	NP-NW			Linearly graded C_u > 6	O_F/D_{50}<1
				Gap-graded C_u > 6	O_F/D_G<1
				Concave upward C_u > 6	O_F/D_{30}<1
Moraci et al. (2012)	NW			C_u > 6 Broadly-graded unstable soils	O_F/D_c<3 Where D_c is suffusion diameter

W-woven: NW-Non-woven, NP-NW-Needle punched non-woven

Table 2.5 shows that significant number of retention criteria exists for steady state flow conditions. Most of the retention criteria take into account the soil particle size d_{85} which can be interpreted that the 15% coarser fraction of the soil particles should be prevented to enter the filter and these coarse particles will help in forming a stable network. The boundary conditions and the relative density of soils are different or sometimes not defined for the base soil erosion limit. Except Lafleur (1999) and Moraci et al. (2012) criteria, the rest of retention criteria does not consider the internal stability of soils. Therefore, it is necessary to carefully evaluate the retention criteria to the real design and boundary conditions.

Little test data is available to describe the soil-geotextile interaction for dynamic flow condition. A review of these criteria is shown in the Table 2.6.

Table 2.6 Existing filter retention criteria for dynamic flow conditions

Author	**Geotextile**	**Hydraulic Gradient**	**Base Soil**		**Retention Criterion**
			Relative Density	**Grain Size Distribution**	
Ogink (1975)	W-NW	7		Sand	$O_{98}/ D_{85} \leq 1$ Formation of natural filter
				Sand	
Ognik (1975)	NW	7		Sand	$O_{90}/ D_{15} \leq 1$ No formation of natural filter
				Sand	
Schober and Teindl (1979)	W-NW			Sand $1<C_u<3$	$O_{90}/D_{85} \leq 1\text{-}2$ $O_{90}/D_{50} \leq 1$
Heerten (1982)	W-NW			Granular soil	$O_{90}/D_{50} \leq 1$
Lawson (1982)					$O_{90}/D_{50} \leq 1$
Mouw et al. (1986)				Sand	$O_{95}/D_{85} \leq 2$
Faure (1988)	W-NW		Loose	Granular soil	$O_F/D_{85} \leq 0.5$
Faure (1988)			Dense	Granular soil	$O_F/D_{85} \leq 0.75$

Author	**Geotextile**	**Hydraulic Gradient**	**Base Soil**		**Retention Criterion**
			Relative Density	**Grain Size Distribution**	
Hameiri (2000)	NW		Dense	Granular soil	$O_F/D_{85} \leq 1$ (Confined conditions)
Hameiri (2000)	NW		Dense	Granular soil	$O_F/D_{85} \leq 0.5$ (Unconfined conditions)
Narejo (2003)	W-NW			Fine silts and clays	$O_{95}/D_{85} \leq 0.5$ Dynamic conditions in pavements
Aydilek (2006)	W			Contaminated sediments	$O_{95}/D_{85} \leq 0.5$ For all POA
Holtz et al. (1997)	NW			Internally Stable Soils	$O_{95}/D_{85} \leq 0.5$
Hameiri (2000)	NW			Internally unstable soils	$FOS < 0.5D_{85}$
Khachan et al. (2012)	W			Sand with Cu ≤ 4.2 Silt with C_u = 14.5	$O_{95}/D_{85} \leq 1.62$

The pore sizes of woven-geotextiles are determined in terms of percent open area (POA) which is determined using a light projection method. Like the steady state retention criteria, the geotextile type, the soil type, the boundary conditions, and the relative density of soils are either different or not defined for most of retention criteria under dynamic flow conditions. Each retention criterion is based on a specific test method. Moreover, most of the retention criteria do not take into account the internal stability of soils. As discussed in Section 2.5.1, the internally unstable soils are prone to pipe internally which increases the risk of piping if used as a base soil with geotextiles. It is always recommended to find the internal stability of the soil before using the retention criteria (Holtz et al., 2008).

It can be seen from Table 2.5 and Table 2.6 that mostly all researchers have developed the filtration design criteria on the basis of a single characteristic pore size. It was recommended for the first time by Fischer et al. (1990) that the retention criterion for geotextile filters, instead of a single pore size, should be based on PSD of geotextiles to develop a more accurate filter criterion. Elton et al. (2007) found that geotextiles having the same characteristic opening size may have different PSD which makes their performance different from each other and, therefore, design criterion on the basis of PSD needs to be developed.

2.9.2. Permeability Criterion

The permeability criteria are based on the concept that the permeability of the geotextile should be greater enough to avoid the development of excessive pore water pressure at the soil-geotextile interface. The permeability of geotextile can be determined by ASTM standard method for water permeability of geotextiles by permittivity (ASTM D4491-99). The permeability of geotextile can be determined using constant head or falling head test procedures. In the constant head test procedure, a water head of 50mm is maintained on the geotextile throughout the test period and the water flow rate is measured. In the falling head test procedure, a column of water is allowed to flow through the geotextile and the readings of head changes is measured versus time. The constant head test procedure is used when the water flow rate through geotextile is large such that it is difficult to measure the readings of head changes versus time in the falling head test method.

The permeability criteria suggested by different researchers for critical/ non-critical and severe/ non-severe conditions are given below in Table 2.7.

Table 2.7 Existing geotextile permeability criteria

Authors	**Criterion**	**Comments**
Calhoun (1972), Schober & Teindl (1979), Carroll (1983), (Haliburton & Wood, 1982), Christopher & Holtz (1985), Holtz et al. (2008)	$k_g \geq k_s$	Steady state Non-critical application Non-severe soil conditions
Carroll (1983), Christopher & Holtz (1985), Holtz et al. (2008)	$k_f > 10k_s$	Critical applications Severe soil conditions
Giroud (1982)	$k_g > 0.1k_s$	No factor of safety
(Koerner, 2012)	$\Psi_{allow} > FS\Psi_{required}$ Where Ψ is the permittivity of geotextile	FS is dependent on the critical/ non-critical application and soil severity conditions
Giroud (2010)	$k_f \geq \max(i_s k_s, k_s)$ where 'i_s' is the hydraulic gradient of soil next to filter	Steady state

Permittivity of a geotextile is the volumetric flow rate of water per unit cross sectional area per unit head under laminar flow conditions, in the normal direction through a geotextile. The permeability criterion is closely related to the porosity of geotextiles which meets the minimum requirement in most cases (Giroud, 2010). Margin of safety is required for critical or severe applications as pores clogged by the soil could decrease the permeability of the filter. This would assure that the geotextile has the required permeability through its entire life (Holtz et al., 2008).

2.9.3. Clogging Criterion

Clogging can be defined as the penetration of fine particles into the pores of geotextile and blocking off pore channels, thus reducing the permeability of geotextile (Christopher and Fischer, 1992). Carroll (1983) reported that a complete filter design criteria cannot be achieved by considering just retention and permeability criteria as the filtration system still could be failed by clogging. Few of the clogging criteria are shown in Table 2.8. These criteria are based on the relationship between opening size of geotextile and grain size of base soil, porosity, percent open area (for woven geotexitles), or performance tests for soil-geotextile interface. No clogging criteria has been suggested yet for dynamic flow conditions.

Table 2.8 Existing geotextile clogging criteria

Source	**Criterion**	**Remarks**
Calhoun, (1972); Haliburton & Wood, (1982); Giroud (1982); Carroll (1983); Christopher & Holtz, (1985); Holtz et al. (2008); Koerner (2012)	Performing soil/ filter filtration tests	For critical/ severe applications
Christopher & Holtz, (1985), Holtz et al. (2008)	$O_{95} \geq 3D_{15}$ for $C_u \geq 3$	Less critical/ nonsevere applications
Fischer et al., 1990	$O_{15}/ D_{15} \geq 0.8$-1.2 $O_{50}/ D_{50} \geq 0.2$-1	Less critical/ non-severe applications
Calhoun, (1972); Koerner (1990)	Percent Open Area (POA) $\geq$ 4% to 6%	Less critical/ nonsevere applications Woven Fabrics
Christopher & Holtz, (1985); Koerner (2012)	Porosity $\geq$ 30% to 40%	Less critical/ nonsevere applications Nonwoven Fabrics
Lafleur (1999)	$FOS/d_{30} \geq 1$	Internally unstable soils
Hameiri (2000)	$FOS/d_{30} \geq 1$	Internally unstable soils

2.10. Previous Laboratory Studies

Previous laboratory tests to evaluate the soil-geotextile compatibility are discussed in this section. One previous study related to static unidirectional flow conditions, as well as laboratory studies under dynamic conditions are discussed.

2.10.1. Gradient Ratio (GR) Test (Steady State Conditions)

Several methods have been proposed by different researches for assessing the filtration behaviour of soil-geotextile composite system under steady state conditions. This includes Long Term Flow (LTF) test (Aydilek & Edil, 2003; Koerner et al., 1994; Mannsbart & Christopher, 1997; Veylon et al., 2016), Hydraulic Conductivity Ratio (HCR) test (Emin Kutay & Aydilek, 2005; Williams & Abouzakhm, 1989), and Gradient Ratio test (Fannin et al., 1996; Fannin et al., 1994; Fischer et al., 1999; Palmeira et al., 2005). The LTF test is carried out in a test cylinder (252mm diameter) containing a geotextile specimen at the bottom and 8 g of soil placed above the geotextile specimen. The interaction between geotextile filter and soil is assessed from the permeability of the system, and the mass of soil retained on a filter paper. The test is run until an equilibrium condition of flow rate is obtained. The LTF test should be carried out for atleast one hundred hours for silty soils to ensure a stable filter formation (Koerner & Ko, 1982). The shortcomings of a LTF test includes long test duration, its inability to reproduce stress conditions in the field, and no information on the distribution of water head. The HCR test is performed in a triaxial cell which is based on permeability analyses of soil-geotextile composite systems. The HCR is defined as the ratio of the hydraulic conductivity of soil-geotextile composite to the hydraulic conductivity of soil alone. A decrease in HCR indicates flow reduction in the system. The hydraulic conductivity of soil is measured initially without geotextile. The

hydraulic conductivity of soil-geotextile composite is measured for equilibrium conditions and HCR is calculated. The ability to simulate field stress conditions, and possibility of back pressure saturation are the major advantages of the HCR test. Since the water head readings (hydraulic gradients) are not measured in HCR test, it is questionable whether the decrease in HCR values occurred due to clogging/ blinding of geotextiles or as a result of blinding within the soil matrix itself. The Gradient Ratio (GR) test is the most commonly used filtration test which is the standard test method for measuring the filtration compatibility of soil-geotextile system (ASTM D5101). According to Holtz et al. (2008), GR test is the most suitable test for measuring the filtration compatibility of soil-geotextile composite. This test was first proposed by U.S. Army Corps of Engineers (1977) for filtration testing which later on became an ASTM test method. The GR test is advantageous over LTF and HCR tests as it measures the soil-geotextile compatibility by measuring the distribution of water head across and near the geotextile with the help of piezometers on the apparatus (Figure 2.13). The disadvantages associated with other filtration tests makes them less suitable than GR test for measuring the filtration compatibility of soil-geotextile interface (Fischer, 1994).

The GR test apparatus comprises of a rigid wall permeameter which accommodates 100 mm length and diameter of base soil which is placed above geotextile (Figure 2.13). The base soil is saturated with water under differential head and hydraulic heads are measured at several positions by mean of piezometers installed at different positions along the permeameter and the variation of hydraulic gradients along the sample and geotextile is established. A GR is defined as the ratio of hydraulic gradient across the soil geotextile interface (i_{sg}) to the hydraulic gradient within the base soil (i_s) which can be expressed as follows:

$$GR = \frac{(h_{57} / L_{57})}{(h_{35} / L_{35})} \tag{2.16}$$

$$GR = \frac{i_{57}}{i_{35}} \tag{2.17}$$

Where h_{35} and h_{57} are the differential water heads, L_{35} is the distance between Ports 3 and 5, and L_{57} is the distance between Port 5 and support screen (including geotextile thickness) (see Figure 2.13).

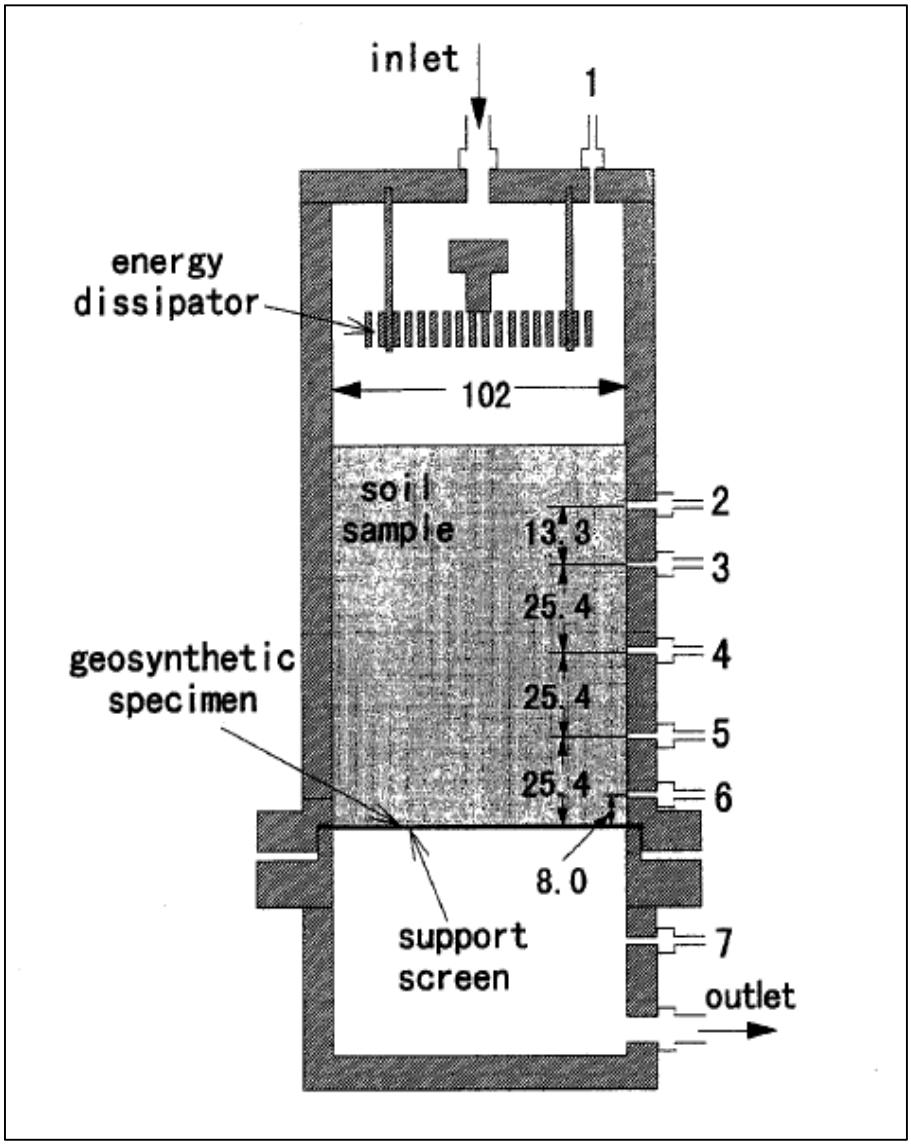


Figure 2.13 Tradition GR test apparatus (after Fannin et al. (1994))

Permeability of the composite system is calculated by measuring the flow rates through the system. The GR can also be defined in terms of permeability of soil (k_s) and permeability of soil-geotextile interface (k_{sg}) under steady flow:

$$GR = \frac{i_s}{i_{sg}} = \frac{k_s}{k_{sg}} \tag{2.18}$$

A GR value equal to one suggests that geotextile has not influenced the flow through the system. A GR value less than 1 indicates that soil-geotextile interface is more permeable than the base soil and vice versa. A continuous decrease in GR value shows that piping of soil is occurring through geotextile (Figure 2.5). If a GR value less than 1 occurs and gets stable, it shows that the fine particles near the filter interface are washed through the geotextile and a bridging network is developed at the filter interface by the coarse particles retained. A GR more than 1 indicated that flow reduction has occurred, possibly due to clogging of geotextile. Although a GR value more than 1 is not preferred, however, the U. S. Army Corps of Engineers (1977) considers a GR value more than 3 as excessive clogging. The GR limit of 3 was adopted after Haliburton and Wood (1982) who performed GR analyses on four woven and two non-woven geotextiles. Some typical values of GR by previous researchers using the traditional GR apparatus are given in Table 2.9. It can be seen that the GR was measured comparatively higher for soil-geotextile samples with a smaller O_{95}/d_{85} ratio as compared to test samples with higher O_{95}/d_{85} ratios. As discussed earlier, a GR more than 1 showing clogging of geotextiles. The effect of increasing hydraulic gradient on the GR can be seen from the Table. The test samples with GR more than 1 showed increase in GR with increase in the hydraulic gradient. High hydraulic gradients enhance the clogging/ blinding process at geotextile interfaces (see Section 2.8.2). Similarly test samples with GR less than 1 showed a decrease in GR with increase in

hydraulic gradient as high hydraulic gradients destabilize the bridging network at geotextile interface.

Table 2.9 Typical values of GR by previous researchers

Author	Geotextile Type	Soil Samples	Cu	O_{95}/d_{85}	Hydraulic Gradient	GR
Shi (1993)	NW	Silt	1.6	0.86	1.1	0.40
					2.3	0.55
	NW	Sandy Silt	4.6	0.18	1.4	1.10
					5.2	1.15
Fannin et al. (1994)	NW	Medium Sand	1.5	0.20	1	0.64
		Coarse Sand	1.4	0.21	1.3	0.59
Nishigata et al. (2000)	NP-NW	Silty Sand	13.2	0.13	5	1
			10	0.2	5	0.9
Shan et al. (2001)	HB-NW	Silty Sand	9.13	0.20	1	0.86
					5	0.39
	NP-NW	Silty Sand	9.13	0.20	1	0.60
					5	0.59

The results of GR test are totally based on hydraulic heads and it should be ensured that the hydraulic heads are not adversely disturbed by testing equipment, procedure etc. (Fannin et al., 1994). The compaction of samples result in less movement of soil particles and the permeability values stabilize earlier than the loose samples recommended by ASTM. Fannin et al. (1994) included additional ports 2, 4 and 6 to

better study the water head distribution in soil and modified gradient ratio was suggested which is more sensitive index of soil-geotextile compatibility:

$$GR = \frac{i_{67}}{i_{35}} \tag{2.19}$$

The advantages of the traditional GR test device includes its simplicity, and water head distribution measurement using piezometers. The GR value is based on water head readings closer to geotextile which measures more accurately the filtration mechanisms at the soil-geotextile interface. The main disadvantage is high risk of side wall leakage which may give inaccurate data about the head loss, especially for fine grained soils (Acar et al., 1985; Daniel et al., 1984; Harney & Holtz, 2001; Holtz et al., 2008; Madsen & Mitchell, 1989). The GR test is not recommended for fine grained soils since it is not possible to saturate fine grained soils in the traditional GR test equipment. Also, the GR test apparatus cannot simulate field confining stress conditions on test samples.

2.10.2. Dynamic Flow Conditions

2.10.2.1. Highways and Railways

The pumping of fines from cohesive subgrade in to upper layer may impair the stability of railroads or a highway (Bell, 1982). A geotextile is used as a separator to stop the contamination of sub-ballast layer in railroads and sub-base layer in highways. Different experimental research works have been carried out to observe the pumping of fines from subgrade into sub-base layer through geotextile separator (see Section 2.8.3). The principle of these tests is shown in Figure 2.14. The test-set up measures the migration of fines from subgrade into sub-base layer by measuring the particle size

distribution of sub-base layer after the test. There is no mean to observe the excessive pore water pressure at the soil-subgrade interface.

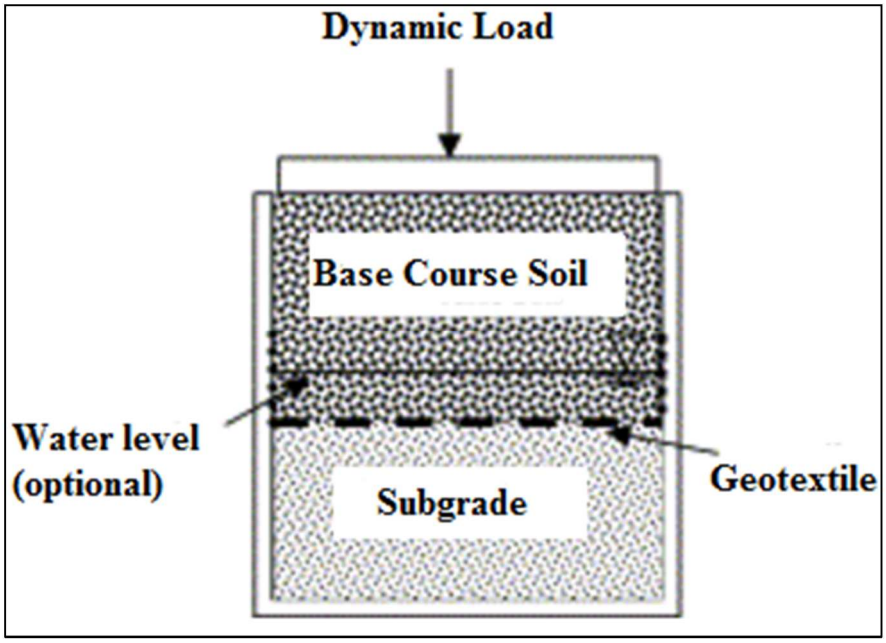


Figure 2.14 Dynamic test setup (after Glynn and Cochrane, 1987)

Hameiri (2000) used a gradient ratio test equipment instead to perform filtration tests by applying vibration (mechanical disturbance) to the test samples which can be present in railways and pavements due to traffic loading and construction works. The test equipment was modified after Fannin et al. (1994) (see Figure 2.13) for cyclic loading. The test equipment is more advantageous in terms of stress control. A vibration device was added to the top of equipment for applying vibration to the test sample. The vibration was applied in a series of 180, 720, and 1440 blows to the test samples. The tests were performed under severe conditions as the confining stress factor was not considered in the test program. The base-soil and filter may reach a critical state when the magnitude of compressive stresses reach zero (see Section 2.6.3). The disadvantage of test equipment is use of piezometers which has high risk of air trapping inside. Also, the piezometers are not suited to measure the excessive pore

water pressure at the soil-geotextile interface which, therefore, is only able to characterize the sample before and after the vibration.

2.10.2.2. Revetments and Armoured Banks

Cyclic flow experiments have been carried out to investigate the performance of geotextile filters under conditions typical that of in revetments and armoured banks of reservoirs (Cazzuffi et al., 1999; Chen et al., 2008; Kayser et al., 2016; Palmeira & Tatto, 2015; Srikongsri & Fannin, 2011). The test apparatus used by all authors is based on the concept of Cazzuffi et al. (1999) test equipment with slight modifications. Figure 2.11 shows the cyclic test equipment used by Cazzuffi et al. (1999). The main advantages of the test equipment are; field behaviour can be modelled, measurement of water head distributions, and control over stresses. The main disadvantage is incompetency of the equipment to provide head control flow regime, as well as limited range of frequencies. Moreover, the upper chamber containing the base soil is rigid wall permeameter. As discussed earlier, there are side wall leakage issues associated with rigid wall permeameter which may result unreliable water head readings. The cyclic flow apparatus after Cazzuffi et al. (1999) has been modified significantly to eliminate the disadvantages associated with the test equipment. However, all the modified test set-ups consists of rigid wall permeameters.

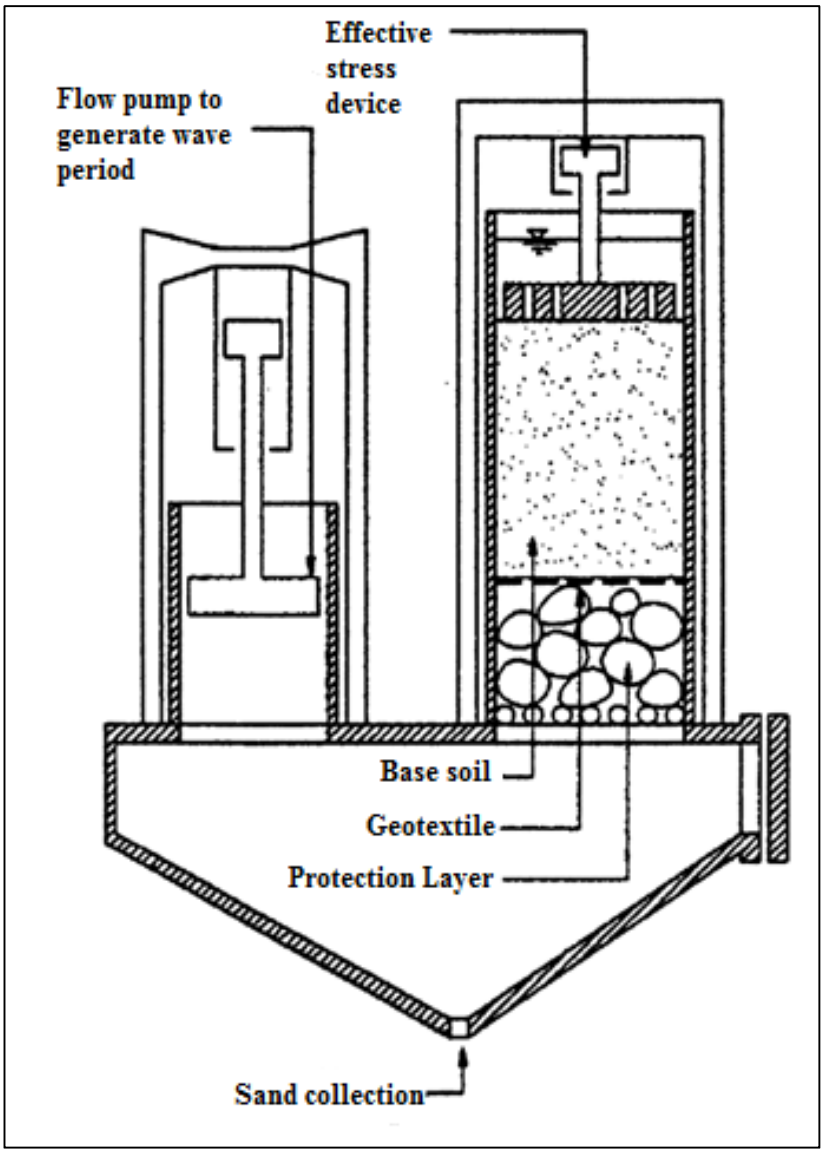


Figure 2.15 Cyclic flow test set-up (after Cazzuffi et al. (1999))

Table 2.10 shows the advantages and the disadvantages of the typical test apparatuses used for the filtration compatibility of soil-geotextile interfaces. A flexible wall GR test apparatus, which was designed and developed to carry out the research work (see Chapter 4), is also compared in the table. The table shows the flexible wall GR test apparatus is more advantageous over the typical test apparatuses.

Table 2.10 Previous laboratory tests to assess the soil-geotextile filtration compatibility

Parameters	**Dynamic Flow Conditions**		**Static Flow Conditions**			**Equipment Described in Chapter 4**
	Highways and Railways	**Revetments and Armoured Banks**	**Gradient Ratio Test**	**Long Term Flow Test**	**Hydraulic Conductivity Ratio Test**	
Control of stress conditions	×	✓	×	×	✓	✓
Possibility of edge leakage	✓	✓	✓	✓	×	×
Distribution of water head	×	✓	✓	×	×	✓
Accuracy of pore pressure measurement		✓	×			✓
Possibility of back pressure saturation	×	×	×	×	✓	✓

2.11. Summary

The following key points have been drawn on the basis of literature review in this chapter:

- Geotextiles can be successfully used as a filter material by replacing (or in conjunction with) graded granular filters
- The Kenny and Lau (1985), the Kezdi (1979), and the Burenkova (1993) criteria are the most widely used criteria for evaluating the internal stability of soils
- The literature review shows that the internal stability of soils depend on the coefficient of uniformity of soil gradation. Hydraulic drag is required to onset the erosion of fines through the voids of the primary fabric of soils. The seepage force to move the fine particles increase with increasing the hydraulic gradient. The internal stability of soil is also affected by density, confining stresses, mechanical loading, and hydraulic loading.
- Non-woven geotextiles are mostly used in applications to control erosion of soil due to its random structure and wider range of pore sizes.
- The characteristic opening size of geotextile is the most important property affecting the filtration performance.
- Non-woven geotextiles usually fulfil the porosity criterion. There are high risk of clogging with thick geotextiles. The number of constrictions increases with increasing the thickness of geotextiles.
- Most of the currently available methods to evaluate the pore size of geotextiles finds only the largest opening size, depending on the test method. There are advantages and disadvantages associated with each pore size determination method. The AOS, EOS, and FOS are the most commonly used geotextile pore sizes used in filter design criteria due to standard test procedure available for these pore sizes.

- There are fewer retention criteria available for geotextiles under dynamic conditions. Most of the retention criteria are based on the largest opening size of geotextile and d_{85} of soil. The retention criteria for dynamic conditions do not take into account the internal stability of soils. A retention criterion is needed for dynamic conditions which take into account the internal stability of soils.
- Geotextiles are usually more permeable than the base soil and meet the permeability criterion. There is no clogging criterion suggested yet for dynamic flow conditions and it is recommended to perform filtration tests to evaluate the clogging potential of geotextiles.
- The test apparatuses used for filtration tests under dynamic conditions use a rigid wall permeameter. There are chances of side wall leakage with rigid wall permeameter which may not give true water head readings if fine grained soils are used. A better approach in terms of a flexible wall permeameter is needed to perform filtration tests.
- Very little literature is available about the dynamic filtration performance of geotextiles in highways and railways. It has been discussed in Section 2.8.3.2 that there is possibility of subgrade particles passing through the geotextiles under mechanical disturbance. The previous tests for highways under dynamic conditions were performed for fine grained soils in a simple test set-up. Very limited studies has been done to observe the filtration performance of subgrade and sub-ballast layer in railways by adding geotextile as an extra filter layer.
- There is a better need for understanding the soil internal stability and geotextile filter performance under dynamic conditions.

2.12. Research Implications

It is apparent from the literature review that geotextiles have been used as filters under dynamic loading conditions. Geotextiles have been used in highways and railroads to stop migration of fines from subgrade layer in to sub-base and sub-ballast layers respectively (see Section 2.8.3). Dynamic conditions also exists in pavement edge drains where geotextiles are used as a filter to stop erosion of sub-base and subgrade soils into edge drains. Little literature review is available that evaluates the filtration compatibility of geotextiles with soils in roads under dynamic conditions. The geotextile as filters around pavement edge drains and beneath permeable bases is designed on the basis of retention criteria which are mostly based on theoretical work. Unstable soils (Section 2.5) may exist beneath roads, however, the current design criteria do not take in to account the internal stability of soils. There is a need for a better understanding of the soil internal stability and the geotextile performance under dynamic conditions in roads.

The review of previous experimental tests (Table 2.10) revealed that there is a need for the design and development of a flexible wall GR test apparatus to perform filtration tests under dynamic conditions. The research need is to investigate the effects of different factors on the filtration performance at soil-geotextile interface under dynamic conditions by using the flexible wall GR test apparatus. These factors include: hydraulic gradient, vertical stress, frequency of loading, soil gradation, and geotextile properties.

To meet the research needs, a flexible wall GR test apparatus was designed and developed (see Section 4.1). Filtration tests were performed on different combinations of geotextile filters with internally stable and unstable soils. Based on test results, filter design criteria are suggested which takes into account the internal stability of soils into account (see

Section 7.6). These criteria are compared with the existing filter design criteria to check that improvements have been achieved.

Chapter 3

Material Properties

3.1. Introduction

The materials used in the filtration testing program are geotextiles and soils with different gradations. As previously discussed in Chapter 2 (Section 2.5), if a soil is internally unstable, there is a risk of fine particles passing through geotextiles due to fine particles ability to move within the voids of the primary fabric of the soil. To meet the research needs (Section 2.12), the soil gradations were prepared to evaluate the performance of internally stable/ unstable soils with different geotextiles. The properties of soils and geotextiles are reported in this chapter.

3.2. Geotextile Properties

Four non-woven polyproylene geotextiles specimens were used in the filtration testing program. Geotextiles NW20, ST170 and NW8 were supplied by ABG geosynthetics and F1200M geotextile by Fibertex. The geotextile were selected due to their frequent use as filters for applications such as pavement edge drains, reservoirs and dams, and under revetments. NW20 and NW8 are needle-punched and thermally-bonded geotextiles while ST170 and F1200M are needle-punched geotextiles (no thermal bonding). The physical properties of these geotextiles are given in Table 3.1. The permeability of a geotextile

measures the volume of water which will pass through the geotextile for a given time at a given head of pressure.

Table 3.1 Properties of geotextiles provided by the manufacturers

Properties	**NW20**	**ST170**	**NW8**	**F1200M**
Tensile Strength, kN/m	20	14.4	9.5	7
Thickness, mm	1.7	1.1	1.2	8
Mass per unit area, g/m^2	250	237	120	110
Permeability, l/sm^2	80	75	115	15
O_{90}, µm	70	70	120	60

3.3. Soil Properties

The type of soils used in filtration test program with non-woven geotextiles are medium sand, pulverised fuel ash (PFA) and mixture of these soils in different proportions to make different gradations of test soils. The particle size distribution of medium sand and PFA is shown in Figure 3.1. It can be seen from Figure 3.1 that gradation of PFA fits well with medium sand to make different gradations of test soils (see Figure 3.4).

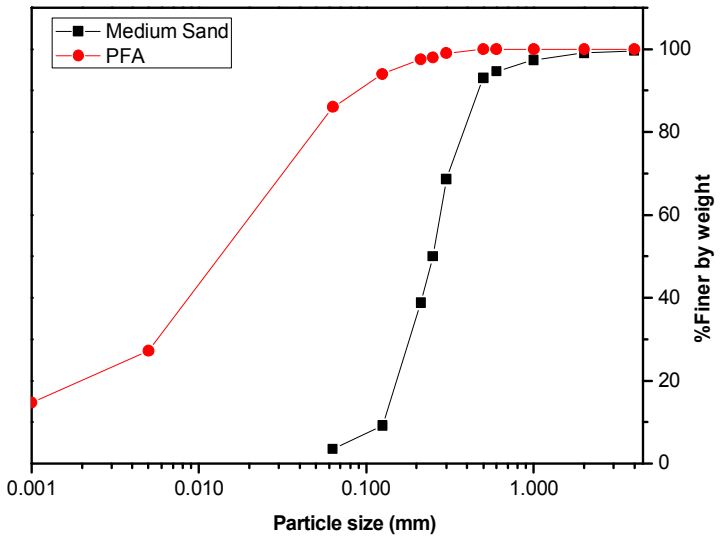


Figure 3.1 Particle size distribution of medium sand and PFA

3.3.1. Medium Sand

The sand used in filtration tests was supplied by Lafarge Aggregates Ltd, UK. The sand can be classified as medium sand according to British Standard BS5930 (Standard, 2015). The particle size distribution of medium sand is uniform with C_u of 1.9 and d_{85} of 0.4mm. Soils with C_u less than 2 are usually considered as one fraction regarding filtration criteria by U.S FHWA (Holtz et al., 1998), suggesting a more stringent retention criterion. The physical properties of medium sand, based on laboratory testing, are given in Table 3.2.

Table 3.2 Physical properties of medium sand

Max. Dry Density[a], kg/m^3	**Optimum Moisture Content[a], %**	**Permeability[b], m/s**	**Void Ratio[c], e**		**Specific Gravity[d]**
			e_{max}	**e_{min}**	
1936	12	2.92E-04	0.75	0.30	2.65

[ac]BS 1377-4:1990; [b] BS 1377-5:1990; [d]BS 1377-2:1990

Scanning electron microscopy (SEM) images of the medium sand sample were taken in order to visualize the angularity and shape of soil grains (Figure 3.2). The sand particles have relatively plane sides and the surfaces are unpolished. The particles have sharp to rounded edges and corners. Therefore, according to ASTM-D2488 (2009), these visual characteristics of sand particles classify them as angular to sub-angular particles.

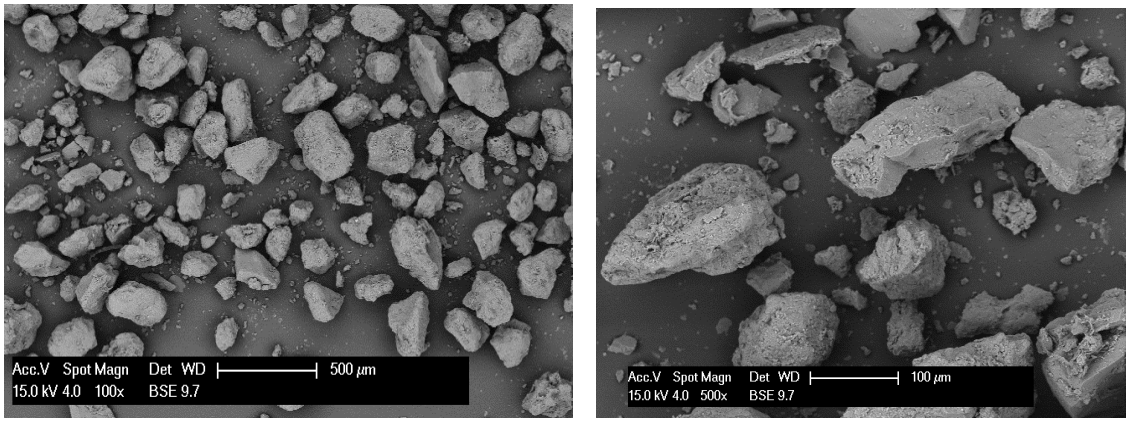


Figure 3.2 SEM images of medium sand particles

3.3.2. PFA Soil

Various researchers (Allen & Fleckenstein, 1991; Highlands et al., 1991; Koerner & Koerner, 2015) have reported excessive clogging of geo-composite drains with fine-grained soil. Fly ash or PFA is one of the coal combustion products with majority of its particles smaller than 63μm. In 2010, about 100 million tonnes of fly ash was produced across the European member states (Caldas-Vieira & FEUEBORN, 2013). The disposal of this huge amount of fly ash is a serious environmental issue due to which reuse markets are utilizing fly ash as a replacement for natural materials mainly in building material industry, landfill liner, in civil engineering, in underground coal mining, and transportation applications such as highway embankments and road bases.

The PFA used in the filtration tests was provided by ABG Geosynthetics, UK. It was identified after consulting with ABG Geosynthetics as a potentially problematic soil regarding filtration point of view, in conjunction with geotextiles. Very little literature review is available regarding the filtration compatibility of PFA with geotextiles (Gabr & Akram, 1996). It can be seen from the Figure 3.1 that PFA is quite fine material with a D_{85} of 0.063mm. Some SEM images of PFA were taken to visualize the particle shapes. It can be shown from Figure 3.3 that PFA mostly consists of spherical particles with round edges. The physical properties of PFA were found out in laboratory which is given in the Table 3.3.

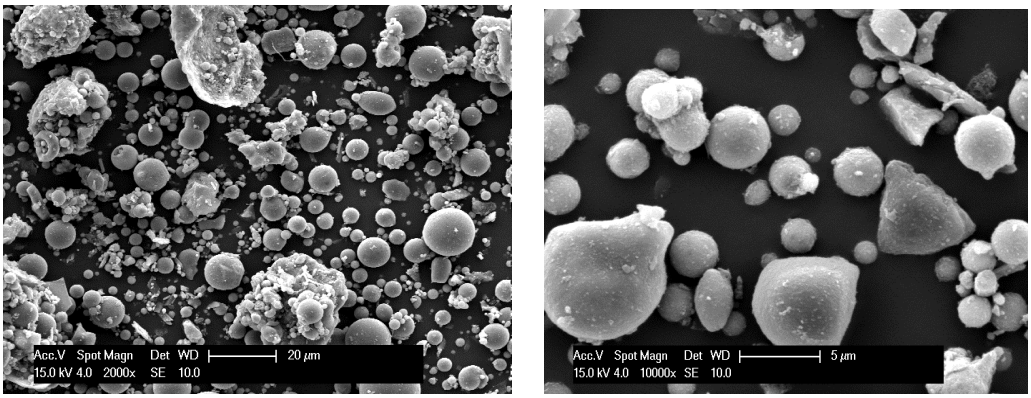


Figure 3.3 SEM Images of PFA

Table 3.3 Properties of PFA

Property	**Average Value**
Specific Gravity[a]	1.87
Liquid Limit[a], %	38.5
Plastic Limit[a], %	Non-plastic
Max. Dry Density[b], kg/m3	1436
OMC[b], %	27.5
Axial Stress at Optimum Moisture Content[c], kPa	85
Axial strain at Optimum Moisture Content[c], m/m	6.4
Angle of frictional resistance[c], [°]	31

[a]BS 1377-2:1990; [b]BS 1377-4:1990; [c]BS 1377-8:1990

3.3.3. Different Soil Gradations

Medium sand and PFA were mixed in different proportions to assess the filtration compatibility of non-woven geotextiles with different gradation soils (Figure 3.4). The 90% sand 10% PFA soil indicates that 90% medium sand and 10% PFA by weight are mixed with each other to make a soil gradation, and similarly for the other proportions.

The fine sand was obtained from medium sand by removing coarse particles and, therefore, has more fines passing through the 63µm sieve as compared to the medium sand. The gap-graded soil was obtained by mixing 70% medium sand with 30% PFA by weight. The gap-graded soil has a gap location at 30% finer and a gap width ratio of 2.77. Gap width ratio is the ratio of diameter at the end of gap to the diameter at the beginning of the gap. It can be seen from the gradation of gap-graded soil that particles sizes between 0.09mm (start of the gap) and 0.250mm (end of the gap) are missing.

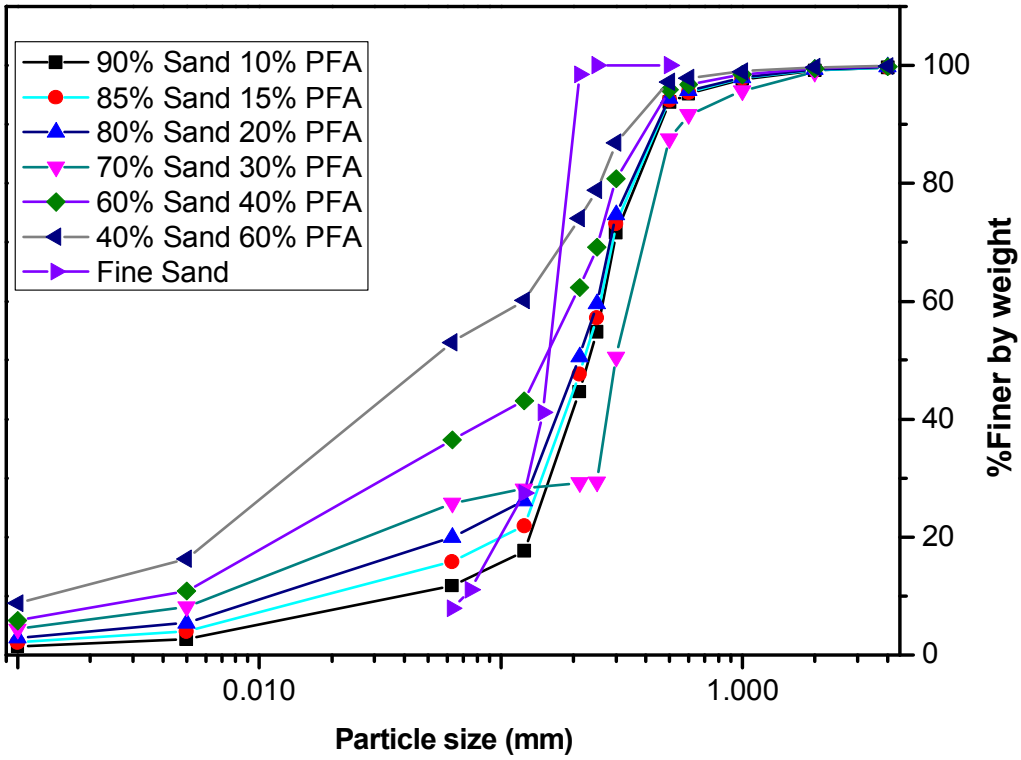


Figure 3.4 Particle size distribution curves of different proportions of medium sand and PFA

A soil with C_u (= d_{60}/d_{10}) greater than 6 is generally termed as broadly graded soil (Lafleur, 1999). Table 3.4 shows that medium sand, fine sand and 90%sand 10%PFA are narrowly graded soils while the rest are broadly graded soils.

Table 3.4 Description of soils

Soil	D_{85} mm	D_{60} mm	D_{50} mm	D_{30} mm	D_{15} mm	D_{10} mm	C_u	Gap width ratio
Medium Sand	0.420	0.270	0.250	0.190	0.150	0.140	1.9	-
Fine Sand	0.195	0.175	0.17	0.14	.085	0.072	2.4	-
90% Sand 10% PFA	0.400	0.260	0.230	0.170	0.115	0.044	5.9	-
85% Sand 15% PFA	0.400	0.270	0.220	0.160	0.055	0.020	13.5	-
80% Sand 20% PFA	0.380	0.260	0.210	0.150	0.030	0.013	20	-
Gap Graded	0.470	0.340	0.300	0.260	0.015	0.0065	52.3	2.77
60% Sand 40% PFA	0.340	0.200	0.160	0.034	0.008	0.0043	46.5	-
40% Sand 60% PFA	0.285	0.130	0.052	0.014	0.005	0.0016	81.2	-
PFA	0.063	0.023	0.015	0.006	0.001	0.0006	38.3	-

3.4. Internal Stability of Soils

The different geometric criteria to evaluate the internal stabiliy of soils have already been discussed in detail in Section 2.5.1. The Kezdi (1979), Kenney and Lau (1985, 1986) and Burenkova (1993) are the most most widely used criteria for evaluating the internal stability of soils in engineering practice (Li, 2008; Elandaloussi, 2014). These three geometric criteria were used to evaluate the internal stability of the different gradation soils used in this research.

3.4.1. Kezdi's Criterion

The Kezdi's (1979) criterion divides a soil into a coarser and finer component (see Appendix A). A summary of the maximum values of D_{15}/d_{85} for all soil gradations is shown in Table 3.5. According to the Kezdi's (1979)criterion, a soil is termed as internally stable for which $(D_{15}/d_{85})_{max}$ is greater than 4. It can be seen from Table 3.5 that except medium sand and fine sand, all the other soils showed a $(D_{15}/d_{85})_{max}$ greater than 4 for 30% finer by weight of soil gradations. Three soil gradations (85% sand 15% PFA, 80% sand 20% PFA, and 60% sand 40% PFA) showed $D_{15}/d_{85} > 4$ over a wide range of % finer by weight as compared to other soils.

3.4.2. Kenney and Lau's Criterion

The H/F curves for all soil gradations on the basis of Kenney and Lau's (1985) criterion are shown in Appendix A. A summary of the minimum values of H/F for all soil gradations is shown in Table 3.5. According to the Kenney and Lau's (1985)criterion, a soil is termed as internally stable for which $(H/F)_{min}$ is more than 1 at most 30% finer by weight for uniformly graded soils and at 20% for widely graded soils .It can be seen from Table 3.5 that only three soil gradations i.e. medium sand, fine sand, and 90% sand 10% PFA gave $(H/F)_{min}$ value more than 1. Except for two soil gradations (90% sand 10% PFA, and 40% sand 60% PFA), the Kenney and Lau (1985) and the Kezdi (1979) criteria almost showed the same range of % finer by weight over which soils is expected to show instability.

Table 3.5 Stability analysis of soils by Kenney and Lau's (1985) and Kezdi's criteria

Soil Type	**Kezdi Criterion (1979)**			**Kenney and Lau Criterion (1985)**		
	$(D_{15}/d_{85})_{max}$	**% finer by weight at $(D_{15}/d_{85})_{max}$**	**% finer by weight showing $D_{15}/d_{85}>4$**	**$(H/F)_{min}$**	**% finer by weight at $(H/F)_{min}$**	**% finer by weight showing H/F <1**
Medium Sand	1.9	5	-	1.8	34	-
Fine Sand	1.8	10	-	2.3	30	-
90% Sand 10% PFA	16.3	5	5-12	1.2	0.5	-
85% Sand 15% PFA	27.5	5	5-15	0.7	10	5-11
80% Sand 10% PFA	20	5	5-20	0.6	15	7-18
70% Sand 30% PFA	20	5	5-30	0.2	25	10-26
60% Sand 40% PFA	8	10	10-30	0.4	30	15-30
40% Sand 60% PFA	8.5	10	15-17	0.7	30	20-30
PFA	7.5	12	12-19	0.6	15	10-17

3.4.3. Burenkova's Criterion

The Burenkova's criterion, unlike the Kezdi (1979) and Kenney and Lau (1985) criteria, does not provide information about the size of particles which are expected to be unstable. Figure 3.5 shows the Burenkova's (1993) criterion to evaluate internal stability of soil gradations on the basis of two ratios of grain diameters i.e. d_{90}/d_{60} and d_{90}/d_{15}. The soils which are evaluated as non-suffosive (internally stable) are medium sand, 90% sand 10% PFA, 40% sand 60% PFA, and PFA.

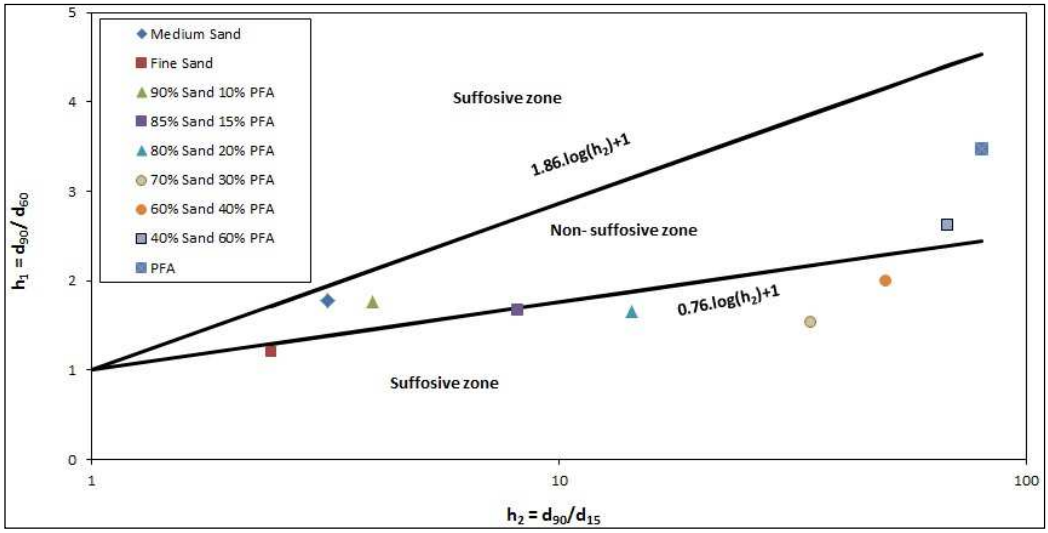


Figure 3.5 Burenkova stability criterion to evaluate soil internal stability

The results of evaulating soil internal stability by the Kezdi (1979), Kenney and Lau (1985) and Burenkova (1993) criteria are summarized in Table 3.6. For the given soils, the identical soil stability classification can be observed only for medium sand. The Kezdi (1979) and Kenney and Lau (1985) predicted similar stability classification for broadly graded soils.

Table 3.6 Summary of soil internal stability classification based on geometric criteria

Soil Type	**Kezdi**	**Kenney and Lau**	**Burenkova**
Medium Sand	S	S	S
Fine Sand	S	S	U
90% Sand 10% PFA	U	S	S
85% Sand 15% PFA	U	U	U
80% Sand 20% PFA	U	U	U
60% Sand 40% PFA	U	U	U
40% Sand 60% PFA	U	U	S
PFA	U	U	S
Gap Graded	U	U	U

[a]S = stable; U = unstable

3.5. Test Program

The combinations of geotextiles and soil samples which were tested are shown in Table 3.7. Two repeatability tests were performed to assess the experimental repeatability and reliability of test results.

Table 3.7 Dynamic filtration test program

Soil	NW8	NW20	ST170	F1200M	Without Geotextile
Medium Sand	✓	✓	✓		✓
Fine Sand	✓	✓			
90% Sand 10% PFA	✓	✓			
85% Sand 15% PFA		✓			
80% Sand 20% PFA	✓	✓		✓✓	
70% Sand 30% PFA				✓	
60% Sand 40% PFA	✓	✓	✓	✓✓	
40% Sand 60% PFA		✓			
PFA		✓	✓	✓	

✓✓ = repeatability tests

Chapter 4

Dynamic Gradient Ratio Test Apparatus and Test Procedure

A typical gradient ratio (GR) test apparatus is composed of a soil-geotextile permeameter, constant head water tanks, piezometers to find the water head distribution within the soil and across the geotextile and a collection trough to collect the soil particles passed through the geotextile (Figure 2.13).

In this study, a flexible wall GR test apparatus was designed and developed to carry out dynamic GR filtration tests on different soil-geotextile combinations. The dynamic GR test apparatus and test procedure are described in the following sections.

4.1. Dynamic GR Apparatus

Figure 4.1 shows an overall schematic diagram of the dynamic GR test apparatus. The dynamic GR test apparatus was developed since there are issues associated with the traditional GR test apparatus (see Section 2.10.1). The dynamic GR apparatus included; use of a modified triaxial cell (flexible wall) instead of rigid wall permeameter, pore pressure transducers instead of piezometer tubes, application of desired confining pressure using compressed air, and application of cyclic loading using an INSTRON machine.

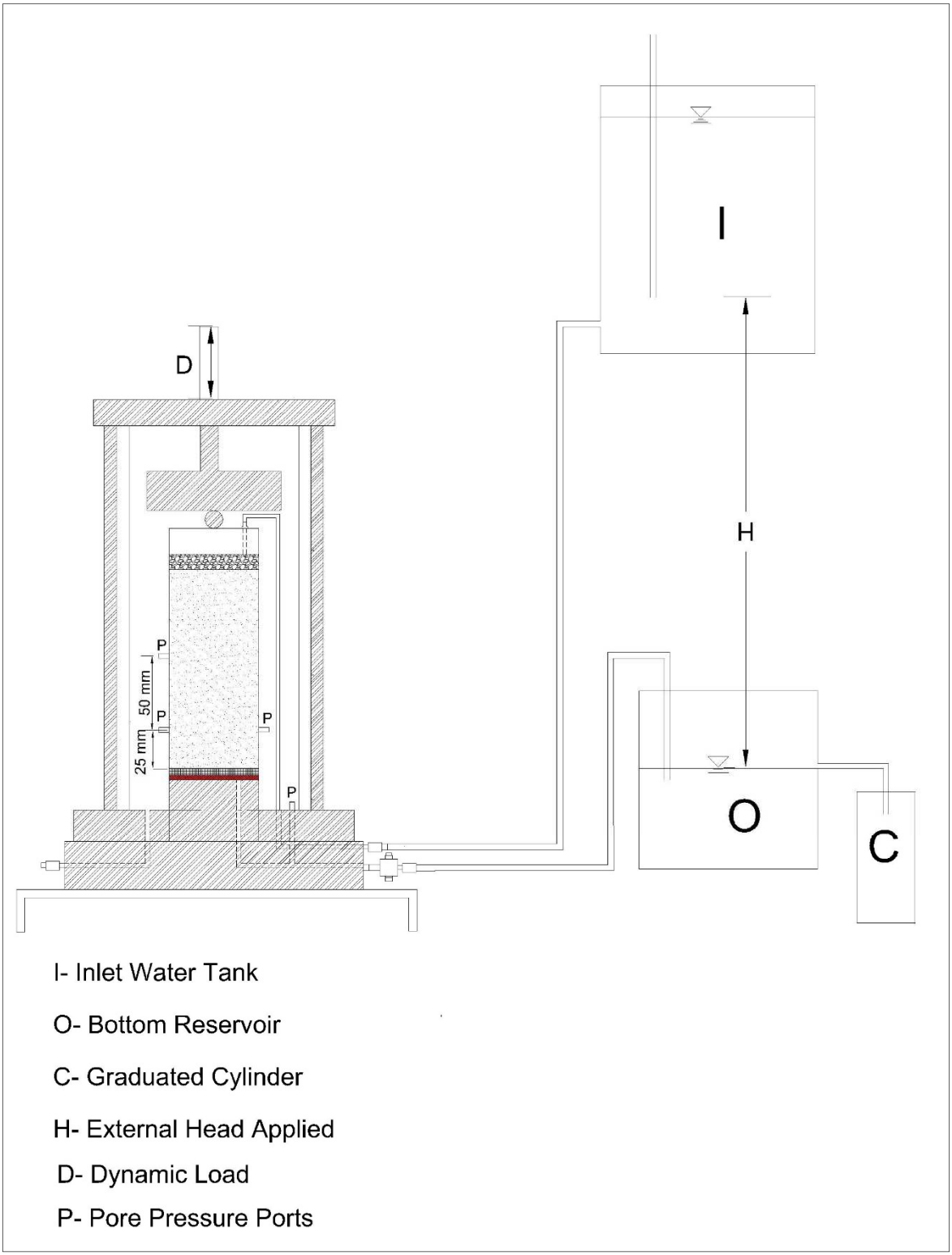


Figure 4.1 Dynamic gradient ratio test apparatus setup

4.1.1. Modified Triaxial Cell

The traditional GR test apparatus consists of a rigid-wall permeameter (see Section 2.10.1). There are issues associated with the rigid-wall permeameter such as side wall leakage and incomplete control over stresses (Daniel et al., 1984, Acar et al., 1985, Madsen and Mitchell, 1987, Harney and Holtz, 2001, Holtz et al., 2008). Moreover, the test conditions in a typical GR test apparatus are limited to a very low confining stress which is representative of shallow depths. To avoid these problems with a rigid-wall permeameter, Daniel et al. (1984) and Harney and Holtz (2001) recommended a flexible wall gradient ratio test in order to control the applied confining stresses and minimize the undesirable side wall leakage. In this test program, a triaxial cell was modified to perform dynamic GR tests on different soil-geotextile combinations (Figure 4.2). A 0.64mm thick rubber latex membrane, which acts as a flexible wall, was used to hold the soil sample and geotextile.

The apparatus is capable of accommodating a sample of 50mm diameter and 100mm height, giving a height to diameter ratio of 2. The main challenge with the apparatus was to connect differential pore pressure transducers (DPTs) to measure water head losses within the soil, and across the soil-geotextile interface (Section 4.1.2). As indicated from the Figure 4.2, a total of 4 ports were required for the two DPTs i.e. three ports inside the rubber membrane and one port below the geotextile to measure water head losses within the soil (25-75mm) and at the soil-geotextile interface (0-25mm), respectively.

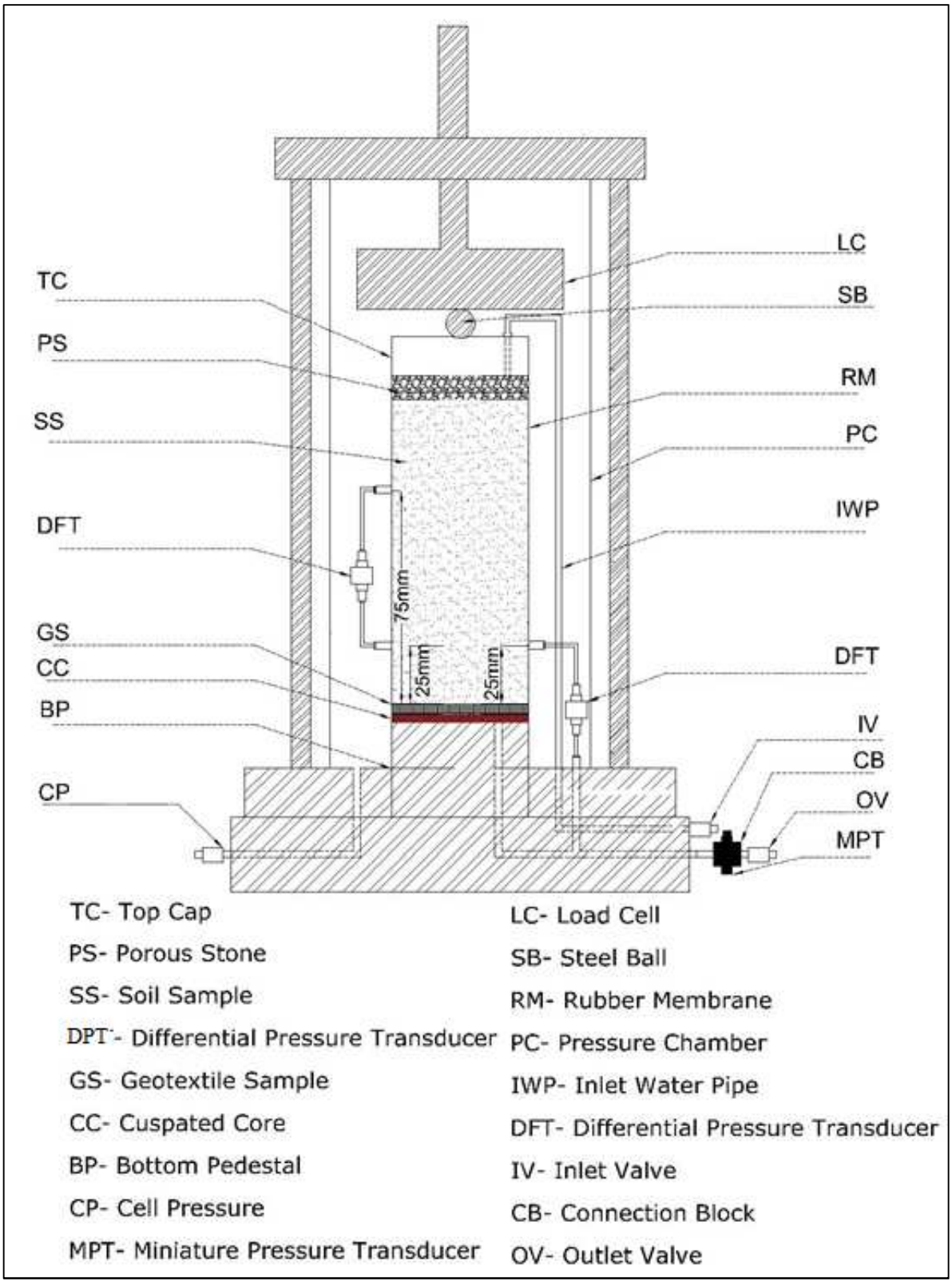
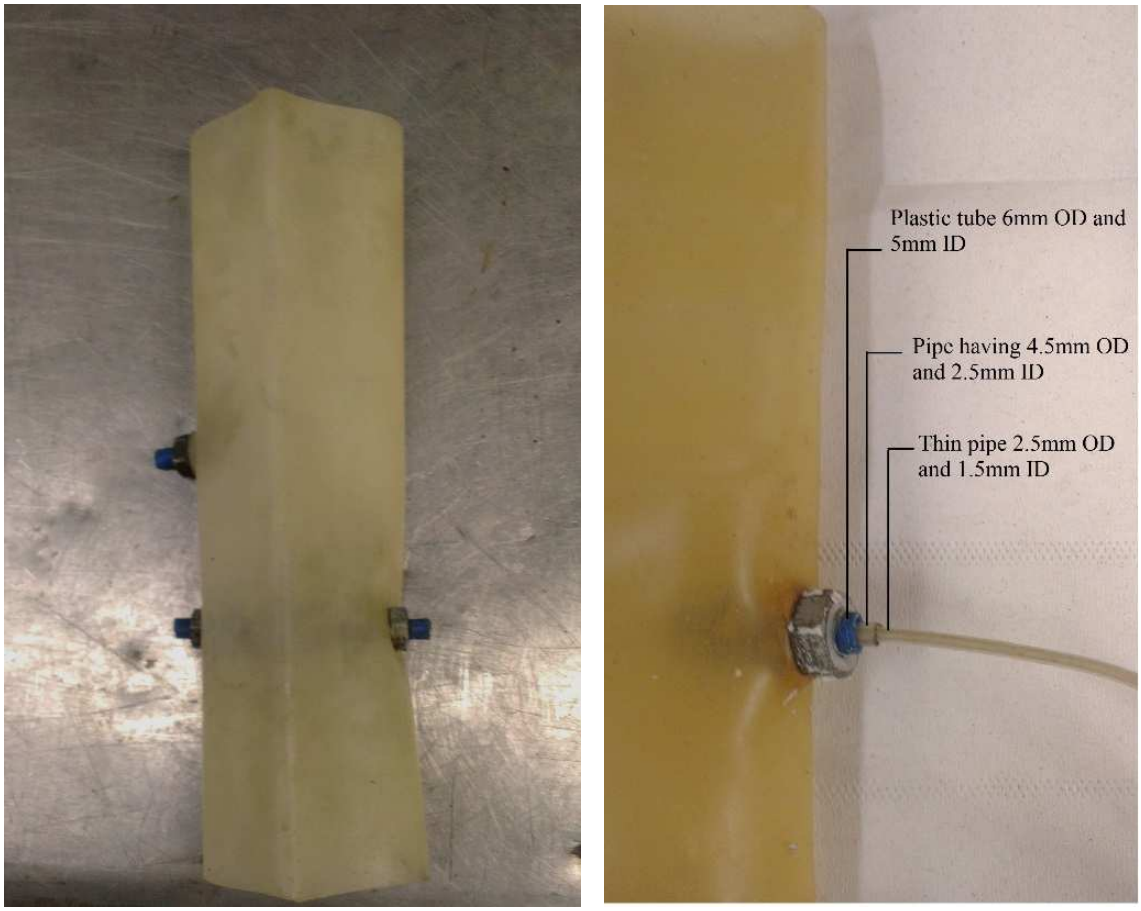


Figure 4.2 Modified triaxial cell for gradient ratio test

The ports inside the rubber membrane were attached by punching small holes in the rubber membrane to accommodate 5mm inner diameter (ID) plastic tubes (Figure 4.3a). The purpose of inserting the plastic tubes in to the rubber membrane was to connect the ports of DPTs to these plastic tubes. The plastic tubes extended 25 mm in to the soil sample in order to measure the pore pressure readings at the middle of the test specimen. Porous filters were inserted in to the tips of the plastic tubes inside the soil to prevent soil entering the tubes. These plastic tubes were tightly fixed by 5mm nuts on the inner and outer side of the rubber membrane. Silicon sealant was applied to the surface of the nuts before fixing the nuts tight against the rubber membrane. The role of the nuts was to keep the plastic tubes straight horizontally and minimize the water leakage along the perimeter of the plastic tubes and holes. It was important that the nuts were not fixed too tight in order to avoid tearing of the rubber membrane. Since the ports of DPTs have 1.5mm ID, they were attached to the plastic tubes through thin pipes which had 2.5mm outer diameter (OD) and 1.5mm ID. To match the connections of plastic tubes and thin pipes, pipes of 4.5mm OD and 2.5mm ID were attached to the end of the thin pipes and inserted inside the plastic tubes, as shown in the Figure 4.3b. All gaps around the pipes and nuts were sealed with silicone sealant on the outer side of the rubber membrane and left for 24 hours to ensure proper sealing.

The port below geotextile specimen was connected by drilling a 5mm diameter threaded hole in the bottom pedestal to a depth where the threaded hole encountered the water channel connected to the outlet valve. The threaded hole was equipped with a male connector having 5mm threaded connection and 4.5mm tube size. To match the connections of tube size of the male connector and thin pipe connected to the differential DPT, a small length of pipe of 4.5mm OD and 2.5mm ID was attached to the end of the

thin pipe and fixed inside the male connector tube. The connection was properly sealed with silicone sealant.



(a) (b)

Figure 4.3 Holes punched in rubber membrane to connect ports of differential pressure transducers

The steel split mould which is used to support the rubber membrane during sample preparation was modified to accommodate the pipes inserted into the rubber membrane (Figure 4.4). Three holes of 10mm diameter were drilled in to the steel mould.

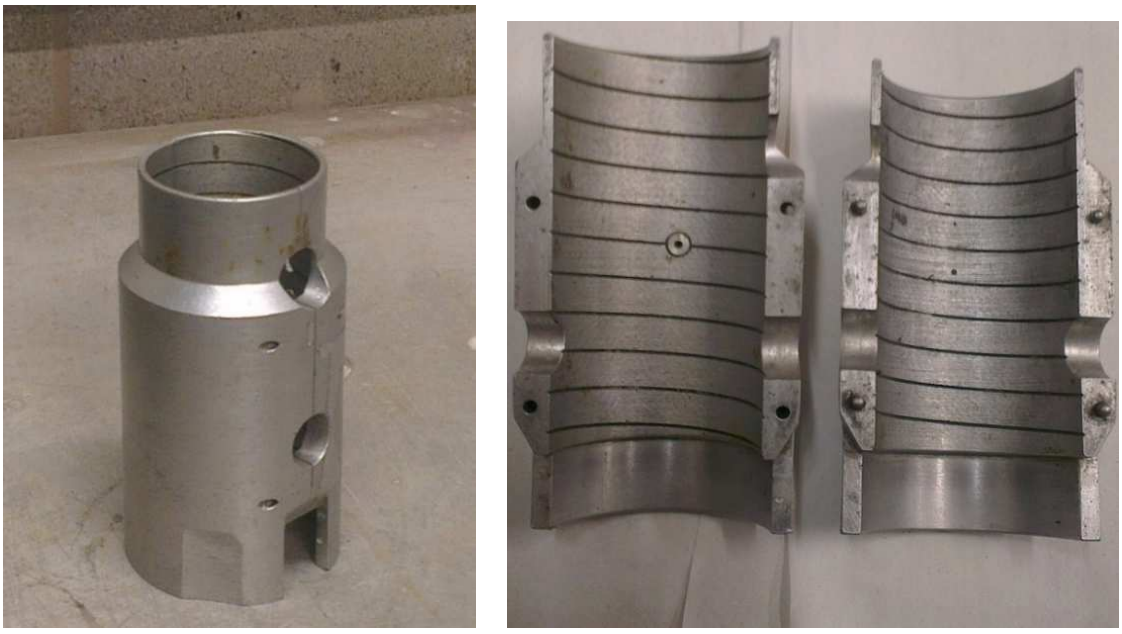
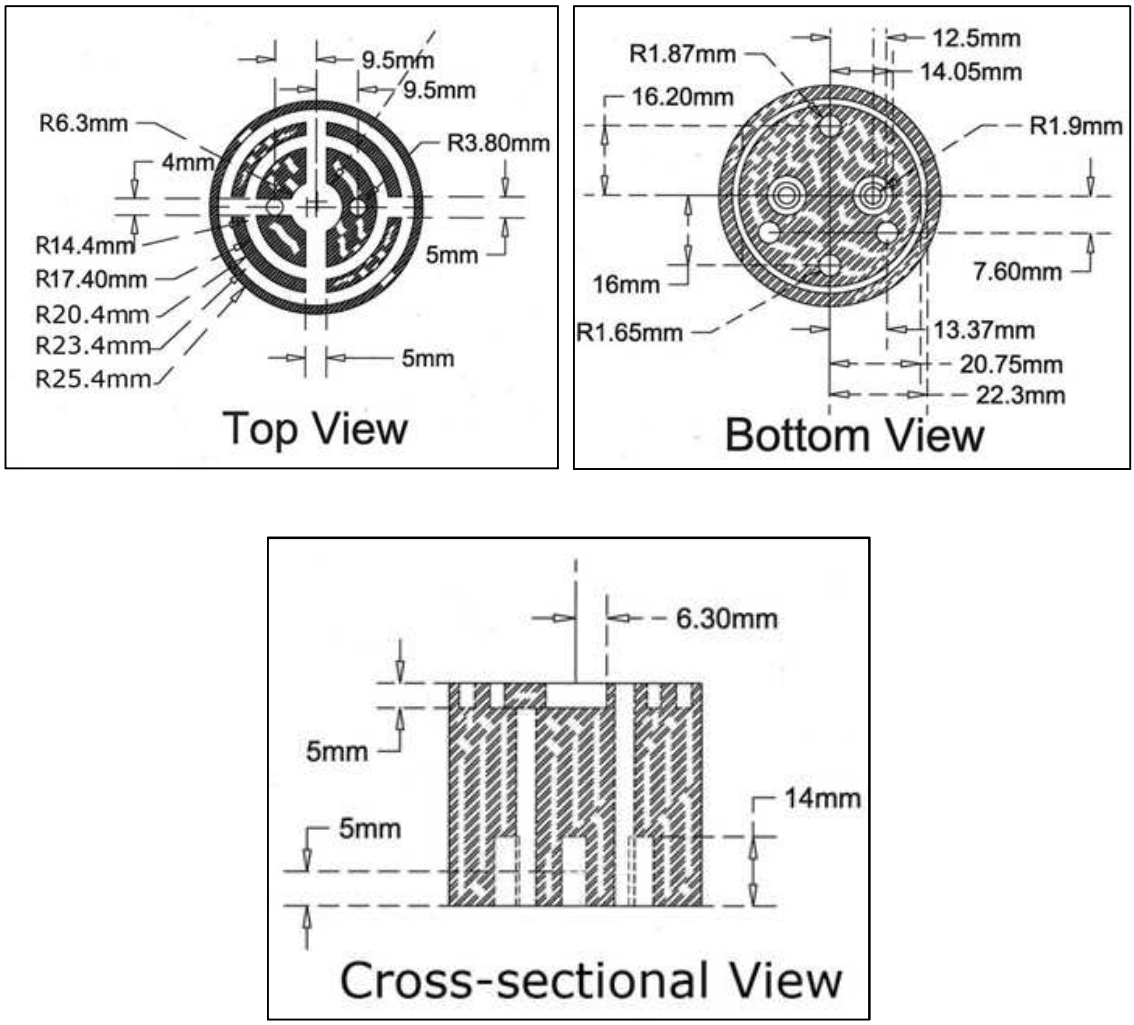
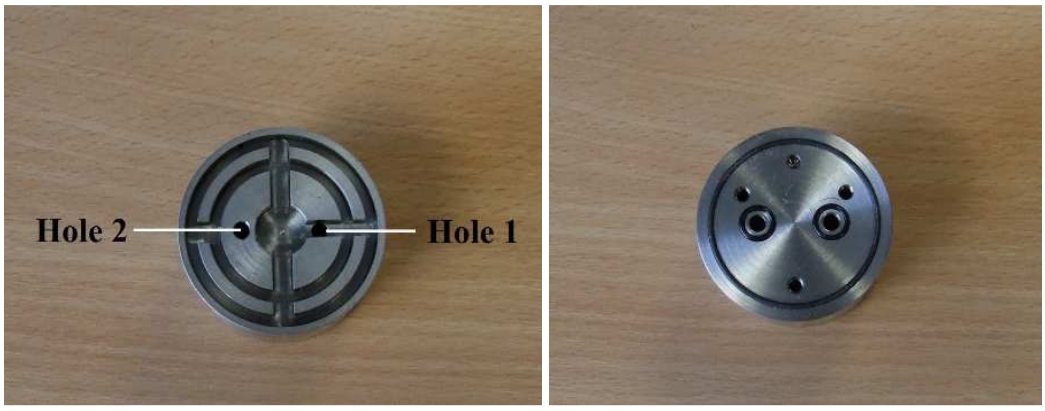


Figure 4.4 Modified steel mould to support rubber membrane

A bottom triaxial pedestal of 50mm diameter was designed to collect soil particles that pass through the geotextile. Figure 4.5a shows a schematic diagram of the designed bottom pedestal. Grooves, 5mm in depth, were machined into the pedestal to collect the soil particles that pass through the geotextile specimens. It can seen from Figure 4.5b that the bottom pedestal has two holes i.e. Hole 1 and Hole 2. The initial plan was to connect Hole 1 with the outlet valve and Hole 2 directly with a miniature pore pressure transducer (Section 4.1.2) to measure total water head below the geotextile. However, during the preliminary testing, it was found that there is a risk of Hole 2 blockage with soil particles passing through the geotexitle because the soil particles entering Hole 2 are not allowed to leave the hole until the end of filtration test. Therefore, Hole 2 was permanently sealed and miniature pore pressure transducer (PPT) was equipped at the outlet valve. The soil particles which are collected in the bottom pedestal grooves are passed through Hole 1 and collected in a bottom reservoir tank.



(a) Schematic diagram of modified bottom pedestal



(b) Top and bottom view of modified bottom pedestal

Figure 4.5 Modified bottom pedestal in triaxial cell

4.1.2. Pore Pressure Transducers

The traditional gradient ratio test device uses piezometers to measure water head loss within the soil and across the geotextile. It is not easy to remove air trapped within the piezometer tubings which could affect the pore pressure measurement (Chang & Nieh, 1996). The accuracy of pore pressure measurement can be improved by using electronic pressure transducers instead of piezometers (Chang et al., 2004).

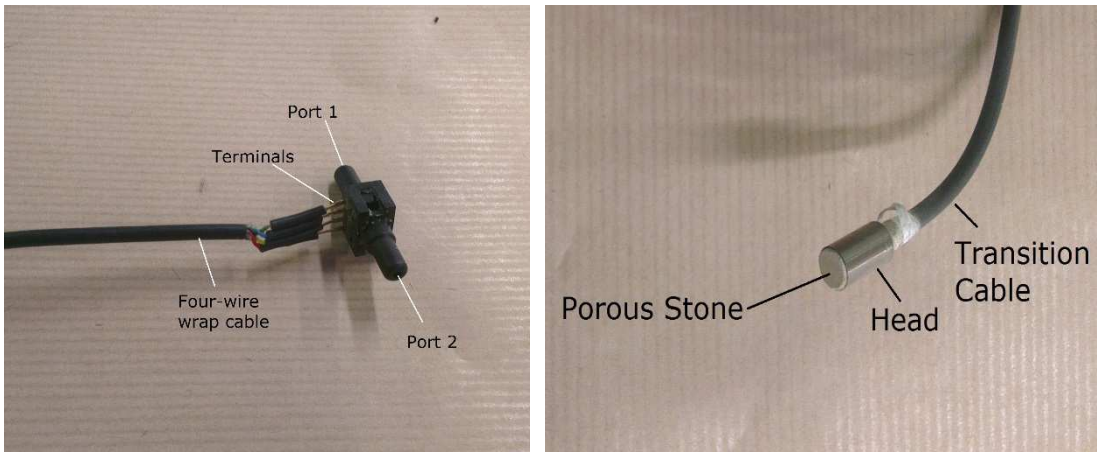
In this study, two DPTs were used to measure head loss within the soil (25-75mm) and across the getoextile (0-25mm) (Fig 4.6a). The DPTs (Honeywell 24PCBFA6D pressure sensor) have 0 to 34kPa range and a response time of 1 millisecond. The response time shows the interval required by the output signal of pressure sensor to display a change in the applied pressure. It can be seen from the Figure 4.6a that DPTs have two ports i.e. Port 1 and Port 2 which have a connection size of 1.5mm. Port 1 is located near the terminals and is the high port. The pressure sensing element is located between port 1 and port 2. The terminals of differential transducers were connected to a Four-wire wrap cable which was connected to a data acquisition system. The ports of DPTs were connected to the plastic pipes inside the rubber membrane and below the geotextile (section 4.1.1).

One miniature pore pressure transducer (PPT) was also connected to a connection block at the outlet valve of the triaxial cell (Fig 4.6b). The PPT has 0 to 100kPA range. The head of the PPT contains the Diaphragm with 4 strain gauges which is protected with a porous stone. The sensor is connected to the data acquisition system through a transition cable and then a thin cable. The PPT was used to measure the total water head below the geotextile. The PPT readings were also used to compute the total water head at 25mm and 75mm above the geotextile by adding the DPTs readings to the PPT readings.

The pressure transducers were connected to a HBM spider 8 data logger through four-wire wrap cables to record the output voltages. Spider 8 is an easy and reliable PC data acquistion system operated by CATMAN software. The output voltage is converted to the pressure heads after applying the calibration factor.

All three pressure transducers were calibrated prior to each test to get accurate pore water pressure readings. DPTs were calibrated by connecting the ports to two water tanks. Output voltages were recorded in the data logger for the corresponding pressure heads applied by raising or lowering one tank relative to other tank. Lines of best fit were applied to the applied pressure and the output voltage readings in excel to find the calibration factors (Appendix A). The PPT was very well saturated and calibrated with the use of a dedicated apparatus (Matziaris et al., 2015), as shown in the Figure 4.7.

The design of calibration apparatus is based on the work of previous research (Take & Bolton, 2003). It can be seen from the Figure 4.7 that the saturation and calibration apparatus is capable of saturating and calibrating 8 PPTs simultaneously. The PPT is placed in one of the slots and connected to a data logger. The PPT was saturated in the same apparatus before calibration because a good saturation of the porous stone of the PPT was necessary to measure precisely the pore pressure readings. These parameters were calculated by performing regression analysis on the output signal vs actual pressure graph (Appendix A). The detailed procedure about saturation and calibration of PPTs can be found in Matziaris et al. (2015).



(a) differential pressure transducer (b) miniature pressure transducer

Figure 4.6 Pore pressure transducers to measure water heads

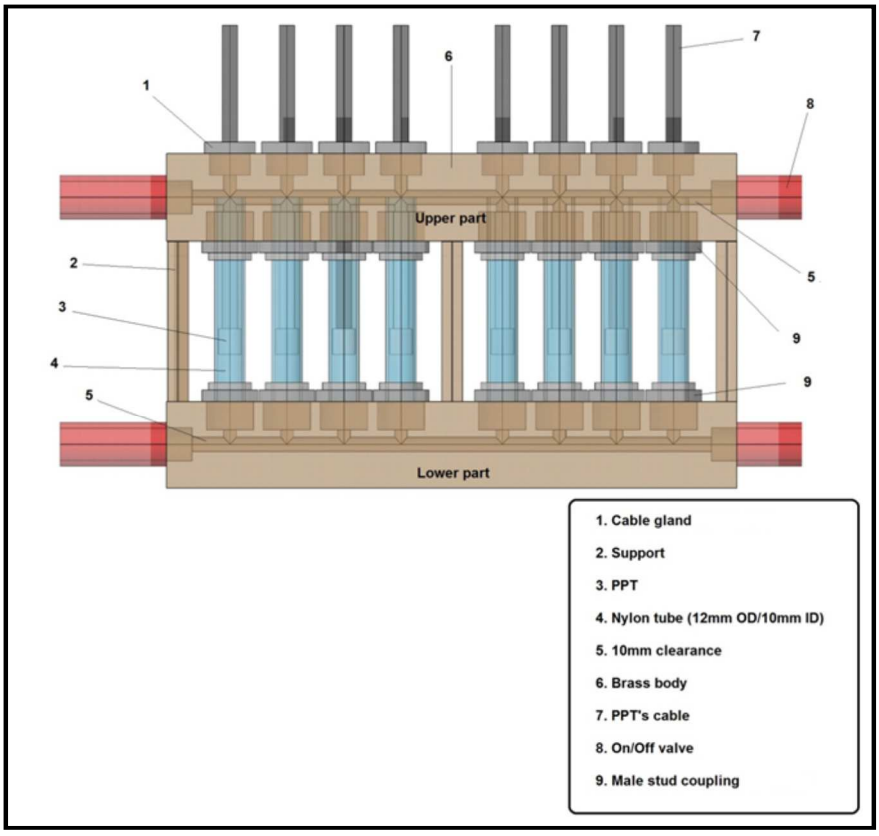


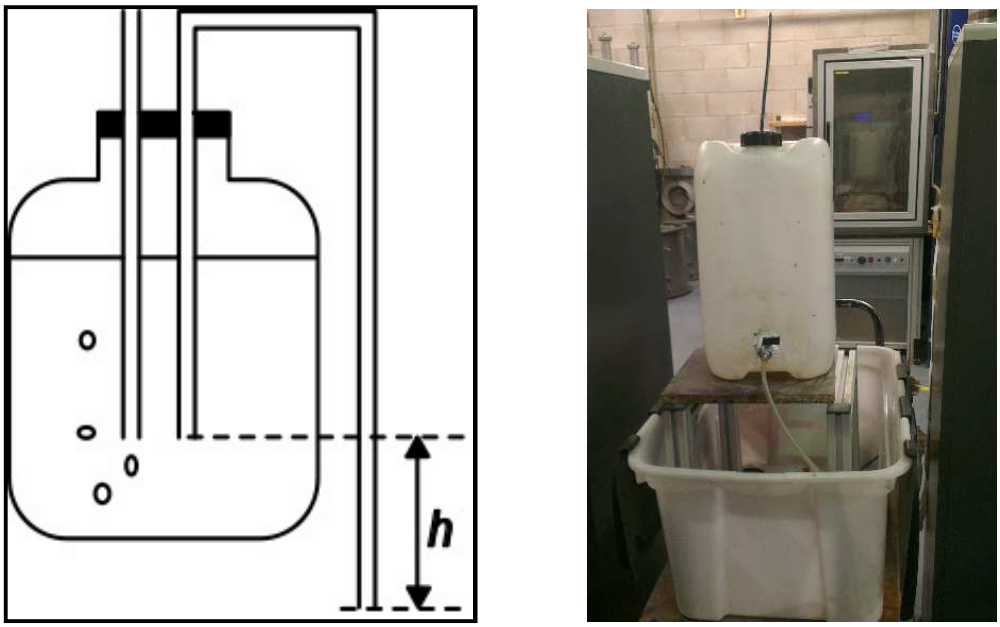
Figure 4.7 Apparatus for saturation and calibration for miniature PPT (Matziaris et al., 2015)

4.1.3. Dynamic Load Cell Actuator

An INSTRON machine with a servo-controlled hydraulic actuator and capable of applying a vertical load of 100kN was used to induce cyclic loading condition. The INSTRON loading frame is connected to oil hydraulic system controlled by PC Rubicon software via a switchbox. Cyclic loading conditions and the number of loads were selected using the Rubicon Software. Repeated cyclic load on test samples was generated by the dynamic actuator within the INSTRON test cyclinder.

4.1.4. Hydraulic Supply System

The constant head difference on the test sample was applied by two water tanks i.e. a Mariotte bottle and a bottom tank. The Mariotte bottle is a device which delievers liquid at a constant pressure. The vessel is closed except for an opening at the top of the vessel and another opening for the exit tube, as shown in Figure 4.8(a). The pressure at the bottom of the air inlet is the same as outside the tank i.e. atmospheric pressure. As long as the liquid level is above the bottom of the air inlet pipe, it will always supply water at a constant pressure regardless of the level of the liquid in the vessel. In Figure 4.8(a), the air inlet is below the water level and the exit tube is at a level h below the air inlet tube. The pressure at the exit tube will remain constant at ρgh as long as the water level is above the air inlet. In all the filtration tests, the Mariotte bottle was used to supply water at a constant pressure to keep the externally applied gradient constant through the sample during the test (Figure 4.8b and Figure 4.1).



(a) concept of mariotte bottle (b) mariotte bottle used in lab

Figure 4.8 Mariotte bottle for supplying constant water pressure

4.1.5. Confining Pressure

The required low confining pressure to keep the sample in position was applied by compressed air. This can be regulated very quickly as compared to water and can be controlled easily by using air regulator valves. The great compressibility of the compressed air leads to easy up-down movement of the axial piston and the fluctuation of ambient pressure due to piston entry and exit from the cell is negligible. A low range pressure gauge was fixed at the top of the triaxial cell to monitor the desired pressure inside the triaxial cell. Two rubber o-rings were used at the top and bottom pedestal instead of a single o-ring to avoid air leakage inside the rubber membrane.

4.1.6. Filter Holder For Collecting Particles

The soil particles passing through the geotextile were collected in the bottom reservoir tank. After each test was finished, water from the bottom tank was passed through a polypropylene filter holder capable of accommodating a filter paper of 47mm diameter to

collect the soil particles washed out. A wet strength filter paper was used inside the filter holder to avoid tearing of the filter papers. The dry weight of the filter paper and soil particles was measured to find the weight of soil particles that wash out.

4.1.7. Flow Rate Measurement

As shown in the Figure 4.1, water from the soil-geotextile composite system was collected in a bottom reservoir through a hose pipe from the outlet valve. A graduated cylinder was connected to the overflow of the bottom reservoir tank. The rate of discharge was determined by the volume of water collected in the graduated cylinder and the elapsed time. Permeability of the soil-geotextile composite system was calculated from the discharge rate by using Darcy's law:

$$Q = -k A \frac{\Delta h}{L} \tag{4.1}$$

Where Q = total discharge (units of volume per time e.g. m^3/s)

k = permeability (m/s)

A = cross-sectional area of the test sample (units of area, m^2)

Δh= Difference in head across the sample (m)

L= Length of the sample (m)

4.2. Test Procedure

Filtration tests were performed to find the head losses in the soil and across the soil-geotextile interface using the modified gradient ratio (GR) test device. The test procedure consists of preparing a geotextile and soil sample, saturating the sample, setting up the apparatus, running the static and cyclic GR test, collecting the soil particles that wash out, perform a hydrometer sieve analysis of the soil sample between 0-8mm and 25-40mm after the test, finding the particle size distribution of the soil particles that wash out, finding the weight of particles retained inside the geotextiles, and observing the clogging sites in the geotextiles after the test using microscopy.

4.2.1. Test Sample Preparation

Each geotextile sample was first cut into a 55 mm diameter circle. It was slightly bigger than the diameter of the rubber membrane to ensure a proper seal at the bottom of the rubber membrane so that there is no flow path around the edges of the geotextile (between it and the membrane). The geotextile sample was then boiled for two hours in a beaker to ensure saturation. The geotextile was squeezed manually during the boiling to make sure that no air is trapped inside the pores. The geotextile sample was then transferred to a bath of de-aired water and left overnight to ensure full saturation.

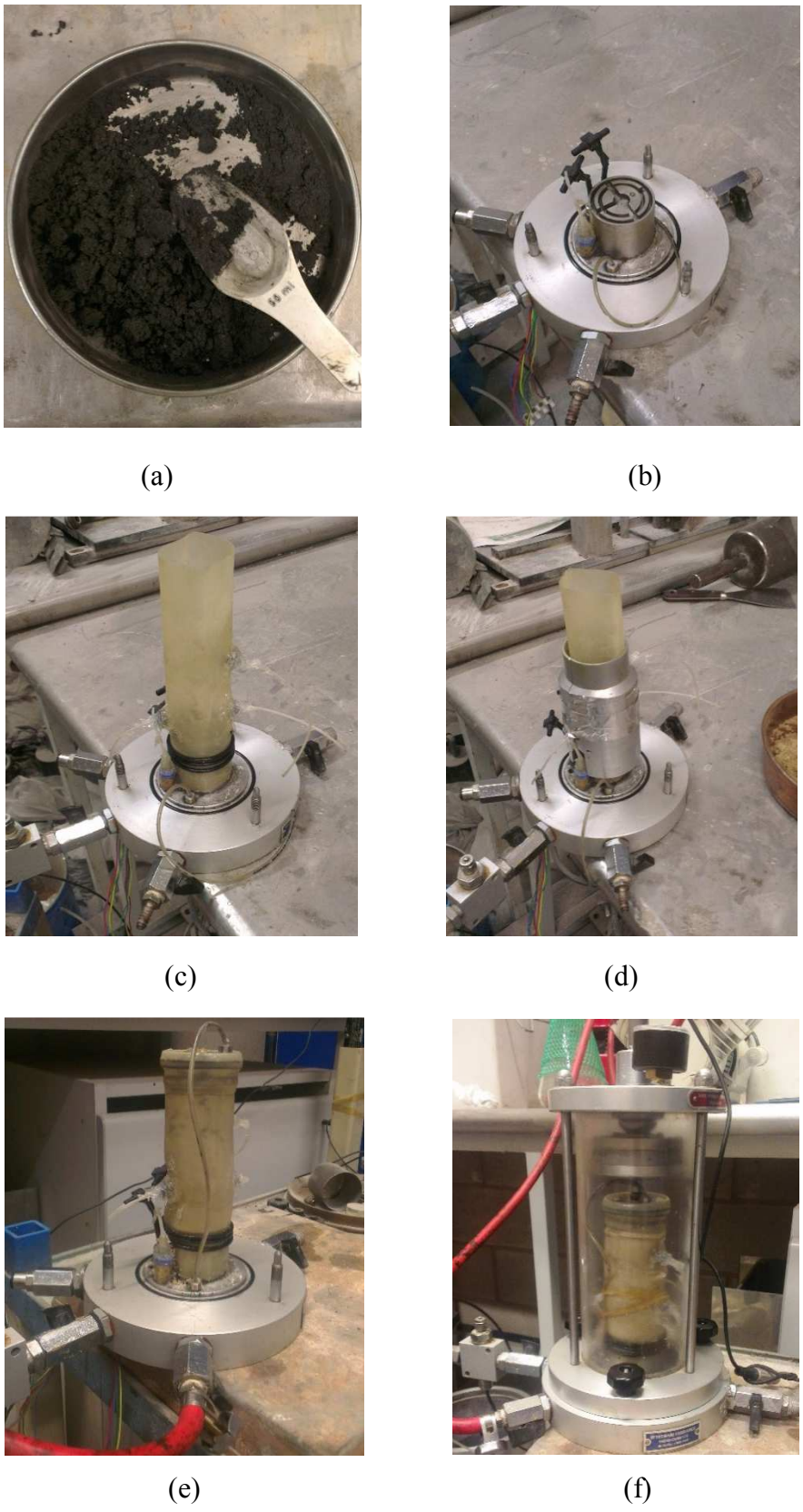
To simulate field conditions, soil samples were prepared inside the rubber membrane at max dry density. The maximum dry density and optimum moisture content of soil samples were obtained by standard proctor compaction test (ASTM-D698, 2012).

Soil was mixed with water at optimum moisture content for at-least ten minutes to ensure proper mixing. The rubber membrane was put into the bottom pedestal of the triaxial cell and sealed with two rubber o-rings from the bottom. The steel mould was then clamped

around the rubber membrane and the rubber membrane was stretched around the mould. A cuspated core having 50mm diameter was put on top of the bottom pedestal inside the rubber membrane. The purpose of cuspated core is to provide a supporting frame for the geotextile, while allowing water to pass through it. The geotextile sample from the water bath was placed on the cuspated core. Soil was then placed in the rubber membrane in 4 equal layers of 25mm. Each layer of the soil sample was compacted using 25 blows of a designed metallic hammer, having 50mm drop height (Figure 4.9). All the soil samples were compacted between 90 and 95% of the maximum dry density. After compacting the last layer of soil, the pre-saturated porous stone and top pedestal were carefully placed on the top of the soil sample. The rubber membrane was rolled up around the top pedestal and sealed by two O-rings. The pipes from the rubber membrane and below the geotextile were connected to DPTs and the PPT was fixed to the connection block. A suction of 20kPa was applied to the specimen to avoid collapse of the specimen. The steel mould was then carefully removed from the rubber membrane. During the vacuum suction process, the triaxial pressure chamber was carefully placed over the base plate and fully tightened with screws. The different steps of sample preparation are shown in Figure 4.10.



Figure 4.9 Designed metallic hammer for compacting soil



(a) (b)

(c) (d)

(e) (f)

Figure 4.10 Sample preparation steps
(a) mixing soil with water (b) getting bottom pedestal ready (c) putting rubber membrane into bottom pedestal (d) clamping steel mould around rubber membrane (e) applying suction to specimen (f) placing pressure chamber

4.2.2. Sample Saturation

The in-situ soil may be fully saturated in some circumstances, but not always. It is preferable to saturate test samples for control purposes as it would not be possible to ascertain how much results are affected by suction if the test sample is not fully saturated. The saturation process ensures air trapped inside the specimen is dissolved into the water in specimen. ASTM D5101 recommends flushing the specimen with CO_2 to remove the air from the test sample. As CO_2 was not available in the lab, a vacuum pump was used to apply suction to the specimen. To avoid the volume change of the test specimen, a small vacuum suction of 20kPa was applied to the specimen for one hour by connecting the outlet valve to a vacuum pump while keeping the inlet valve closed. The vacuum suction also helped to keep the sample stable.

After applying the vacuum suction, the back pressure technique was applied to fully saturate the specimen. The desired back pressure was applied by adjusting the height of the Mariotte bottle and the cell pressure was applied by compressed air. The back pressure technique involves two processes: (1) forcing the water inside the specimen and (2) checking the Skempton's B value. The B value is the ratio of increase in the pore water pressure with increase in cell pressure, i.e. $\Delta u/ \Delta\sigma_3$ (Skempton, 1954). A 'B' value of 1 show that soil is fully saturated.

The Mariotte bottle was filled with de-aired water and the height was adjusted to apply 20kPa back pressure to the specimen. The Mariotte bottle was connected to the outlet valve of the triaxial cell, keeping both inlet and outlet valves closed. The compressed air was connected to the triaxial cell, applying a confining pressure of 30kPa. Both inlet and outlet valves were opened and water started travelling through the specimen from bottom to top. The inlet valve was closed when water started coming through it. The inlet valve

was opened and closed at regular intervals to allow the trapped air inside to come out. The back pressure line was then connected to the inlet valve and the specimen was left for two days to complete the saturation process. It is important to keep the back pressure line open only for saturation process and it should be closed to check the Skempton's B value. After leaving the specimen for two days for saturation, the inlet valve was closed to stop applying back pressure to the specimen. The cell pressure was increased by 10kPa and the miniature PPT readings were recorded to check the increase in pore pressure readings. The pore pressure readings were recorded once the readings became steady. The B value was calculated from the increase in pore pressure to increase in cell pressure ($B= \Delta u/ \Delta \sigma_3$).

The B value depends on the type of soil which is 1 for soft soils and less than 1 for stiff soils. Black and Lee (1973) determined B values for different soils and they found that very dense sands get fully saturated at a B value of 0.91. It is recommended to use a back pressure of more than 200kPa to achieve a B value more than 0.95. Since the applied back pressure was less than 200kPa, the soil specimens were left for more than one day to ensure complete saturation. All the test specimens showed a B value ranging between 0.8 and 0.9 which is more than 99% degree of saturation, as indicated by the relationship between B values and degree of saturation determined by various researchers (Figure 4.11).

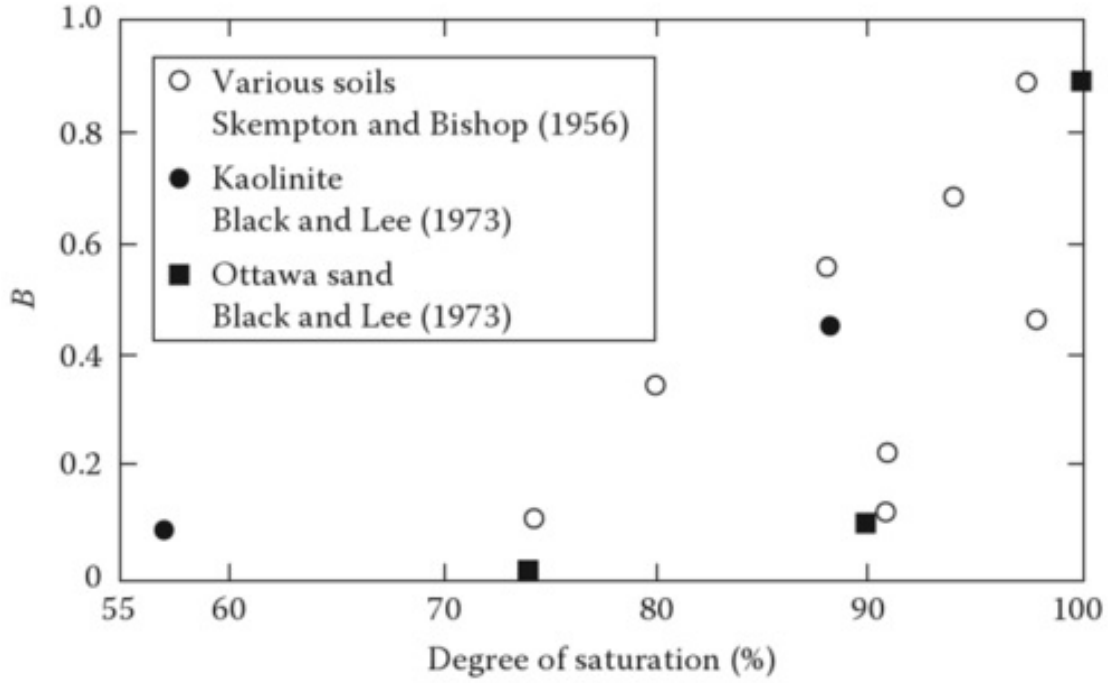


Figure 4.11 B value vs degree of saturation curves by various researchers

4.2.3. Test Setup

The next step after saturation was to set up the apparatus before starting the test. This involved adjusting the heights of the Mariotte bottle and bottom reservoir tank to apply the desired hydraulic gradient across the sample, connecting the Mariotte bottle and bottom reservoir tank to inlet and outlet valves, respectively through hose pipes, adjusting the load cell of the INSTRON machine for cyclic loading, connecting the pore pressure transducers and load cell wires to the data logger, and connecting the bottom overflow reservoir to the graduated cylinder so as to be able to calculate the permeability of the soil-geotextile composite system.

The most important step before starting the filtration test was to make sure that no air is trapped inside the small pipes connecting the sample to the DPTs. This was necessary to get true water pressure readings inside the sample and across the geotextile. The pipes were disconnected from pressure transducers, tapped to remove any air inside, and again

connected to the differential pressure transducers. The cell pressure was applied by compressed air and the inlet valve was opened to allow the water to enter the test specimen. The outlet valve was kept closed and the system was allowed to remain in a no flow condition until the pore pressure readings became steady. Once constant readings were obtained, the outlet valve was opened to start the test.

4.2.4. Test Programme

Multi-stage testing was performed on all the specimens to measure the filtration compatibility of different soil-geotextile combinations. A static stage was followed by cyclic stages in all filtration tests. A very low confining pressure (σ_3) of 20 kPa was applied in all tests to hold the specimen in place without significantly affecting the pore pressure readings. All tests were performed under a hydraulic gradient of 5 which was chosen to be larger than the expected gradient under field conditions so as to apply severe conditions on the specimens and the conclusions drawn are on safe side. A hydraulic gradient of 1 or less than 1 is expected in pavement edge drains (see Table 2.4). However, a higher hydraulic gradient is possible in realistic field conditions, for example, if partial leakage is allowed through pavement boundary. Lee and Bourdeau (2006) recommended a hydraulic gradient of 5 at pavement edge drains in their experimental work. The test setup is shown in Figure 4.12.



(a) Test set-up without vertical load (b) sample under vertical load

Figure 4.12 The dynamic GR device

During static flow, no vertical load was applied (σ_1=0), as indicated by Figure 4.12(a). The filtration behaviour of soil-geotextile specimens was observed under unidirectional flow during the static stage. The test was run for one to two hours until constant readings of pore pressure and permeability were observed.

The purpose behind the cyclic stage was to observe the filtration behaviour of soil-geotextile specimens under unidirectional flow conditions while applying cyclic loading. All the tests were run for 5000-10000 cycles depending on the stability of the pore pressure and permeability readings. Cyclic loadings were applied in 3 stages depending on the deviator stress ($q=\sigma_1- \sigma_3$) and loading frequency;

q=30kPa and loading frequency 1Hz.

q=30kPa and loading frequency 2Hz.

q=60kPa and loading frequency 1Hz.

KENLAYER, a pavement design/ analysis software, was used to calculate deviator stresses at subgrade for two pavements having 450mm and 350mm thicknesses. The purpose of using different thicknesses was to calculate stresses at the subgrade for arterials and collector roads, respectively. An axle equipped with single tyres having a standard axle load of 80kN was considered in the analysis. Commonly used tire pressure of 700kPa and tire radius of 150mm were used in the analysis. The stress analysis by KENLAYER showed a deviator stress of 30kPa for a 450mm, and 60kPa for a 350mm, thick pavement (Figure 4.13).

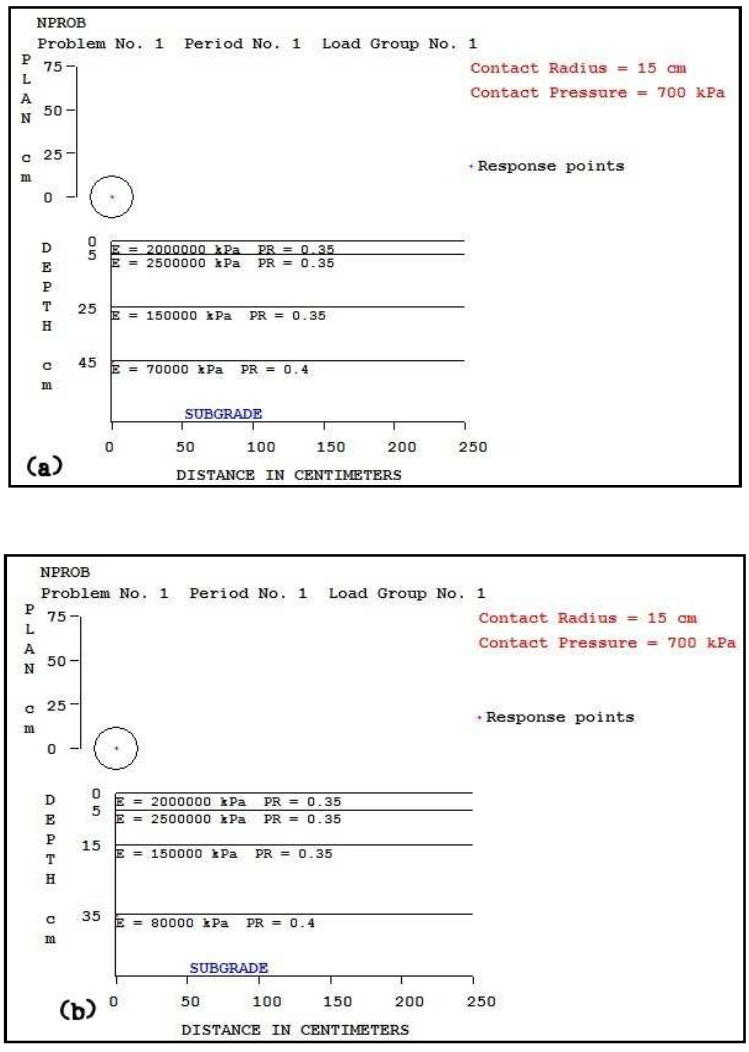


Figure 4.13 KENLAYER analysis for (a) 450mm and (b) 350mm thick pavements

Filtration tests were performed under frequencies of 1Hz and 2Hz to observe the effect of frequencies on the filtration behaviour of the soil-geotextile composite system. Brown et al. (1975) have reported some effect of loading frequencies on the behaviour of subgrade cohesive soils. A frequency ranging from 0.5 to 10Hz to observe fine particle movement was carried out by Hoare (1982) and Bell (1982). The effect of sample deformation was not considered as the tests were performed under stress-controlled conditions. The deviator stresses (Figure 4.13) applied were less than then the shearing stress of the test samples (see Table 3.3). The soil samples were prepared inside the rubber membrane at maximum dry density and there is less possibility of deformation in test samples by applying the deviator stresses. The deformation of samples is more relevant for fine materials such as clay where pumping phenomenon occurs under dynamic loading (see Section 2.8.3.1).

During the cyclic stages, a sinusoidal (Haversine) signal was selected as the load function for both frequencies (Figure 4.14). Usually frequencies below 1Hz are relevant to simulate truck loads on roads. Frequencies greater than 0.5Hz were selected to shorten the duration of the test.

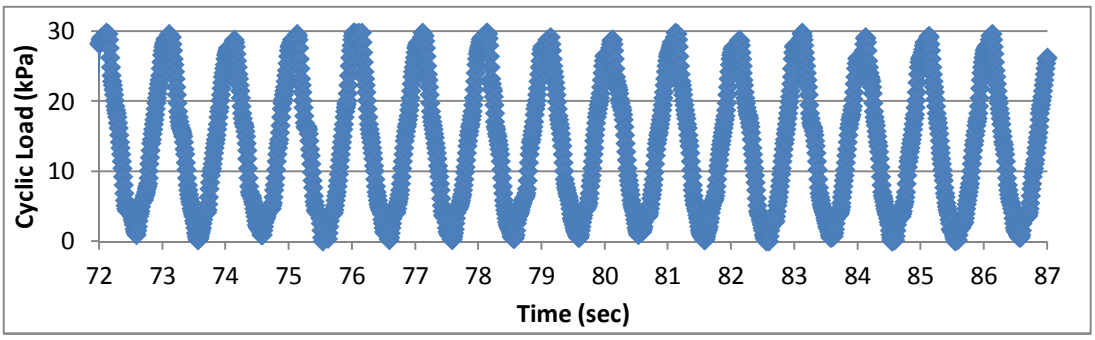


Figure 4.14 Sinusoidal load with an amplitude of 30kPa at 1Hz frequency

4.2.5. Post Test Procedure

After the test was finished, the inlet valve was closed immediately. The confining pressure line was removed and the outlet valve was kept open to drain any particles out into the bottom reservoir. The outlet valve was closed after a while and all the tubes connected to the triaxial cell were disconnected. The pressure chamber of the triaxial cell was carefully removed and the rubber membrane along with the geotextile was carefully taken out from the bottom pedestal. Soil samples were taken at 0-8 mm and 25-40mm from the top of the geotextile. The samples were oven-dried and then subject to a grading evaluation so as to observe the change in soil gradation after testing. The geotextile sample was left to dry and then inspected by microscopic image analysis to identify clogging sites, if any. The microscopic image analysis procedure is described in detail in Section 4.2.6.

The soil particles left in the bottom pedestal grooves were washed out with water and collected in the bottom reservoir to make sure all particles passing through the geotextile filter were collected. These particles were filtered using a wet filter paper, as described in Section 4.1.6. Soil particles collected on the filter paper were taken to a Nikon Microscope to perform a visual grading analysis (see Section 4.2.6).

Data obtained from pore pressure transducers and the load cell were recorded in the Spider 8 data logger. All the data were saved in ASCII format and later exported into excel. Calibration factors were applied to all readings so that data analysis could be performed.

4.2.6. Microscopic Images of Geotextile and Soil After Test

Images of geotextile samples and soil particles collected after each test were taken using a light microscope Nikon LV100ND. The microscope is capable of accommodating 150x150x38mm maximum sample size. A digital camera is attached to the microscope

which sends the images to a monitor. Images can be taken at 5x, 10x, 20x, 50x and 100x magnifications depending on the requirements. Separate methods were used for taking microscopic images of geotextiles and soil particles collected. These methods are explained in detail in the sections below.

4.2.6.1. Microscopic Images of Geotextile Samples

Microscopic imaging is influenced by the surface characteristic of the sample, with the ideal surface being polished. To achieve a polished surface for imaging, geotextile samples were prepared according to the procedures used for preparing thin sections of soil and rock. Preparation steps included: epoxy-resin impregnation, grinding and polishing.

Two sections of 20x25 mm were cut from the geotextile. Both sections were put into separate plastic circular moulds. Each plastic mould is 25mm in diameter and has a height of 25mm, with a flat bottom surface. Each specimen was cemented to the bottom of the mould with a cyanoacrylate adhesive. Epofix epoxy resin was mixed with epofix hardener at a ratio of 15:2 in a separate plastic jar for impregnating the samples. The resin-hardener mixture was slowly poured into the moulds with the help of a syringe. The specimens were left for 24 hours for air curing at room temperature.

The specimen blocks were removed from the moulds after 24 hours. The blocks were then ground using automatic grinding machines. The purpose of grinding was to remove irregularities from the specimen blocks, to remove resin covering the specimens, and to make the specimens smooth for polishing. Four automatic rotating grinding plates having grit sizes P240 (58.5μm), P400 (35μm), P800 (21.8μm) and P1200 (15.3μm) were used for grinding the sample blocks. The grit sizes are designated according to the coarseness of abrasive paper used on the plates. The blocks were ground in sequence from coarse to fine grits. It is important during the grinding process to prevent overheating of sample

blocks or the carrying over of abrasive from the previous step to the current step. All the specimens were properly washed and cleaned between each step of grinding.

The last stage in the specimen preparation was polishing the block specimens to remove damages due to the grinding process. It is also important for quantitative measurement in image analysis. The process of polishing was achieved with the help of automatic polishing discs. Polishing discs were covered with soft cloth impregnated with abrasive diamond particles. Coarse polishing was performed with 6µm diameter diamond particles and then finer polishing with 1µm diameter diamond particles.

All specimens were properly washed before polishing with the 6µm polishing disc. The polishing disc was sufficiently lubricated to provide a smooth surface for polishing. The blocks were gently polished until no deep scratches were observed on the samples. Care was taken during the polishing process to avoid excessive heating of the block specimens. The specimens were washed properly after finishing with 6um polishing. Polishing with the 1um polishing disc was necessary to produce a relative scratch-free surface. The same steps were performed for 1um polishing as were performed for 6µm polishing. The specimens were then washed again after finishing 1µm polishing. The specimens were then kept in front of air dryer for two minutes. The dry specimens were taken to the microscope to capture images.

After the specimen preparation step, the geotextile block specimen was kept under the objective lens and magnification was adjusted at 10x. The microscope stage was moved up and down until a clear image was observed on the monitor. Images were taken along the whole length of each specimen's cross section. The same process of grinding and polishing were repeated on the same specimen to take images at 50µm intervals of depth through the geotextile. Twenty images were taken for each specimen and possible

clogging sites were identified in the images. The Nikon microscope with a geotextile block specimen is shown in Figure 4.15. A sample cross-sectional image of a geotextile sample produced by is shown in Figure 4.16.

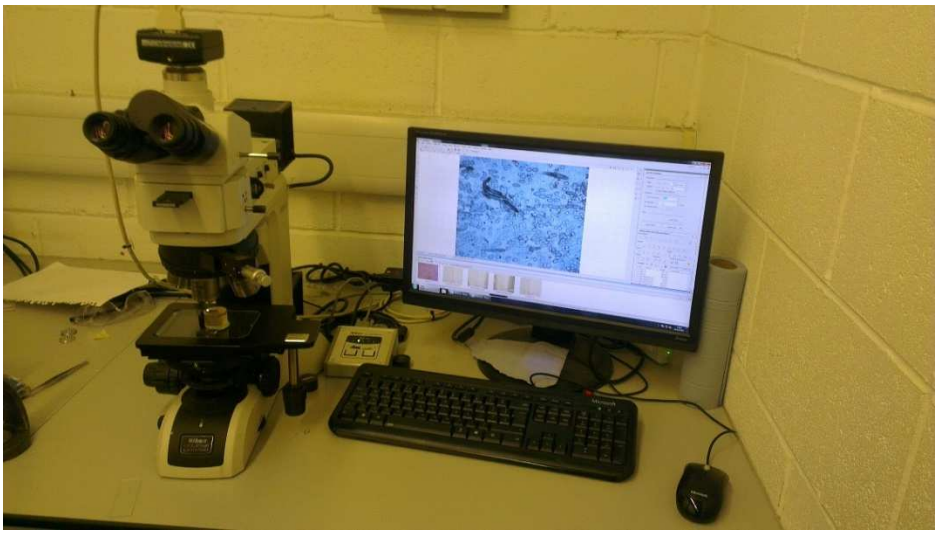


Figure 4.15 Nikon Microscope with a captured image of block specimen

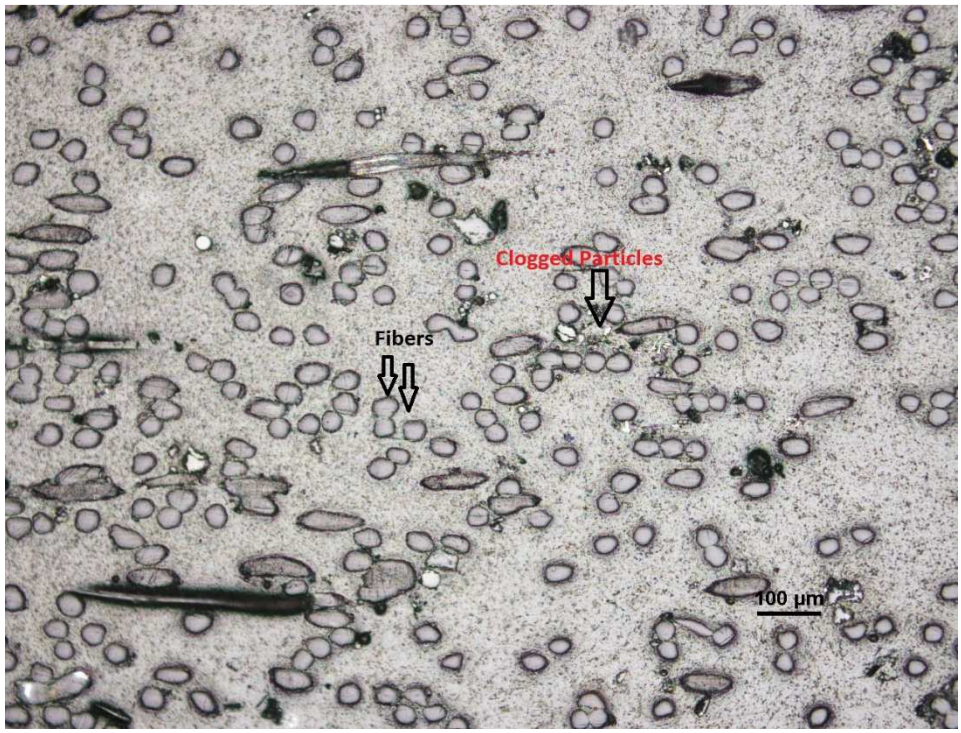


Figure 4.16 Microscopic image of a geotextile specimen after test

4.2.6.2. Microscopic Images of Soil Particles Collected

Images of soil particles collected after each test were also taken using the Nikon microscope, but without preparing thin sections as were prepared for the geotextile sample. The most important thing was to make sure the soil particles were not agglomerated before taking images. For this purpose, soil particles were mixed with a dispersant solution and gently mixed to avoid breaking of particles. Soil particles were then transferred to a glass slide and kept below the objective lens of the microscope. The objective lens was then adjusted to 20x and the microscope stage moved up and down until a clear image was observed on the monitor. Fifty images were taken for each soil sample collected after the filtration test.

The images were analysed using ImageJ. Images were thresholded to create binary images. The "Analyze Particles" function was applied on binary images to calculate the area of individual particles. All results were transferred to an Excel sheet to calculate the equivalent diameter of particles from their known areas. The particle size distribution was then calculated in the conventional manner, assuming a spherical shape and uniform particle density. The d_{90} of soil particles passed, defined as d_{90p}, was measured from the particle size distribution. The test results are given in Table 5.4 and Table 5.14 in terms of d_{90p}.

Chapter 5

Dynamic GR Test Results

5.1. Introduction

The dynamic GR test device, described in Chapter 4, was developed to assess the filtration compatibility of non-woven geotextiles with different soil gradations (see Table 3.7). The testing program consisted of applying static unidirectional flow stage using different soil/geotextile combinations, followed by cyclic stages in which unidirectional flow and cyclic loading were imposed simultaneously. Few tests were performed for multi-stage cyclic loading to observe the effect of increase in frequency and deviator stress on the soil/geotextile filtration performance. The test results are reported in this chapter.

The data was analysed after each test and total water head values were calculated. Data analysis includes:

(1) Total head loss along the sample

(2) Variation of mean static and cyclic head loss within the soil and across the geotextile with time

(3) Static and cyclic gradient ratio with time

(4) Flow rate

(5) Mass of soil particles passed through filters

(6) Gradation of particles passed through filters

(7) Microscopic images of the geotextiles after each test to look for the clogged particles

(8) Hydrometer sieve analysis of soil samples taken at 0-8mm and 25-40mm above geotextile to compare the gradation of samples after each test with the original gradation.

The test results for narrow graded soils are reported first, followed by broadly graded soils. The narrow graded soils were evaluated as internally stable by at least two of the three geometric criteria i.e. the Kezdi (1979), Kenney and Lau (1985) and Burenkova (1993) criteria (Table 3.6). The broadly graded soils were mostly evaluated as internally unstable by all the three geometric criteria. The repeatability of tests is included at the end of this chapter. One test carried out without any geotextile is also included in this chapter.

5.2. Head Losses in the Sample

The measured flow rate (Q) across the whole sample and the total head loss ($h_{0\text{-}75}$) from the bottom of geotextile to 75 mm higher in the sample for different tests is shown in Figure 5.1 (Note: In this thesis, the expression $h_{a\text{-}b}$ means the head difference between points a and b, where a and b are measured in mm and the zero position is at the bottom of the geosynthetic). The head loss across the whole sample was not possible to be measured since no pressure transducer was installed at the top of sample (see Figure 4.1). The hydraulic gradient across the test sample was applied by adjusting the heights of inlet water tank and bottom reservoir tank. For an externally applied hydraulic gradient of 5 (Section 4.2.4), the $h_{0\text{-}75}$ across the sample should be 375mm. It can be seen from Figure 5.1 that $h_{0\text{-}75}$ for different tests is not constant and it gradually reduces with Q. The same effect was measured by Hameiri (2000) and found that the total head difference across the samples (soils with higher permeability) decreased when Q was increased due to energy losses in the system. From the inspection of Figure 5.1, it can be seen that $h_{0\text{-}75}$ decreased

as the flow rate increased for static stage and each cyclic stage. Apart from two tests, the measured $h_{0\text{-}75}$ is between 250-400mm which makes the internally imposed hydraulic gradient approximately 3.33-5.33. This small variation in the imposed hydraulic gradient is probably associated with the flow-induced head losses in the modified triaxial cell. Such small variations in the imposed hydraulic gradient are acceptable to assess the filtration performance of soil/geotextile combinations (Fannin et al., 1994).

As discussed earlier, the head difference in the top soil layer ($h_{75\text{-}100}$) was not measured as there was no pressure transducer installed at the top of sample. By considering the rate of head loss within the top of sample ($h_{75\text{-}100}$ per mm) equal to $h_{25\text{-}75}$ per mm (as both layers are part of soil zone), the total head difference across the sample can be measured. The hydraulic gradient across the sample can be calculated by dividing the total head difference across the sample by the length of the sample. This hydraulic gradient will be used in Darcy's law (Equation 4.1) to find the permeability of the soil-geotextile composite system (see Section 5.3.3).

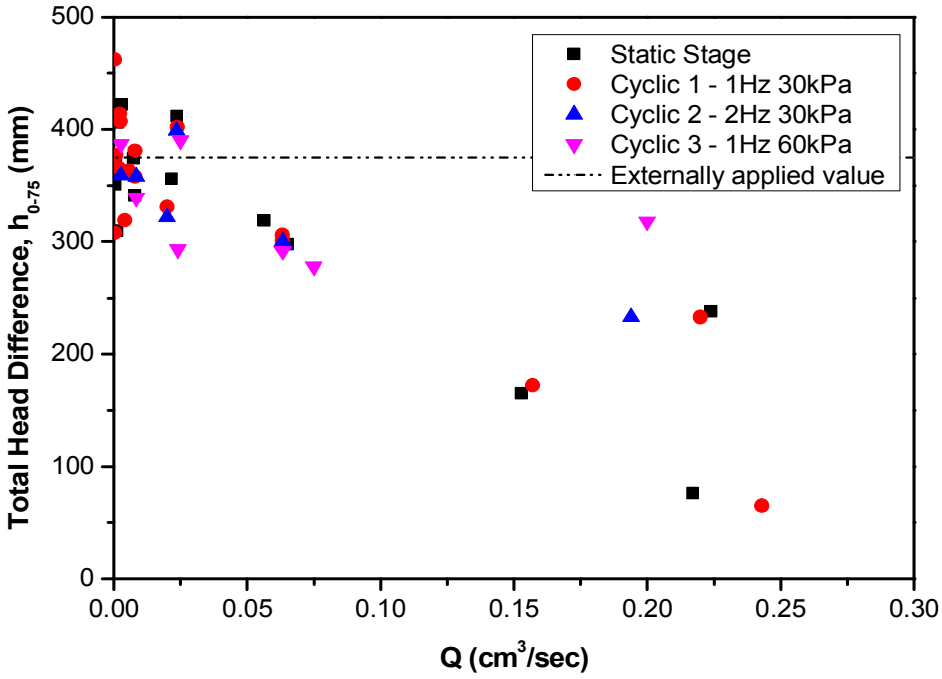


Figure 5.1 Head difference along samples with variation in Flow rate, Q

5.3. Filtration Behaviour of Narrow Graded Soils

Seven filtration tests were performed using narrow graded soils with three different geotextiles to assess the filtration behaviour under static and dynamic conditions. The three soils described in Chapter 3 i.e. medium sand, fine sand and 90% Sand 10% PFA were used in the test program with three geotextiles NW8, NW20 and ST170. The filtration tests were performed for different O_{90}/d_{85} ratios (Table 5.1) for static stage and cyclic stages. Two tests were performed for one stage of cyclic loading i.e. Cyclic 1 stage, while five tests were performed for performed for two additional cyclic stages i.e. 30kPa 2Hz (Cyclic 2) and 60kPa 1Hz (Cyclic 3). The filtration test results for static and cyclic stages are discussed in the sections below.

5.3.1. Water Head Distribution

The water head distribution within the soil describes the compatibility of the soil-geotextile in a qualitative manner. The resolution of water head readings measured by differential pressure transducers (DPTs) was determined to be 0.5mm of water for a range of 0 to 500mm of differential water head. The water head distribution curves were plotted from the two DPTs (see Section 4.1.2) readings to measure the head loss within the soil ($h_{25\text{-}75}$) and across the soil-geotextile interface ($h_{0\text{-}25}$), as well as the miniature pressure transducer to measure the head loss at the bottom of geotextile. The head loss measured by miniature pressure transducer was treated as zero since it was installed below the geotextile, at the outlet value of triaxial cell (see Figure 4.2). The figures of variations of mean static and cyclic head differences within the soil and across the soil-geotextile interface with time, which were measured by the DPTs, are given in Appendix C. The mean cyclic head differences were calculated by taking the average of top peak and bottom peak of water head. This can be illustrated with the help of Figure 5.2 which shows the

head difference within the soil measured by DPT. The dashed grid line shows the time when cyclic load was applied on the test sample. The distance between two dashed grid lines is one second which shows a cyclic load frequency of 1Hz.

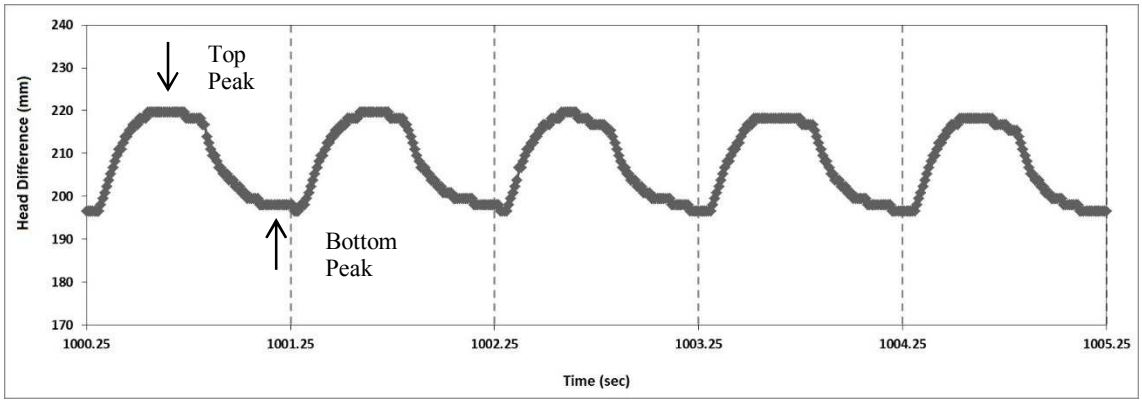


Figure 5.2 Measuring mean cyclic head difference

Figure 5.3 represents few possible scenarios of water head distribution along the sample from the bottom of geotextile. The reference line in all scenarios represents the theoretical head distribution where rate of head loss across soil-geotextile interface ($h_{0\text{-}25}$ per mm) is equal to rate of head loss within soil ($h_{25\text{-}75}$ per mm) for an imposed hydraulic gradient of 5. Scenario 1 represents water head distribution which is as linear as the reference line which indicates no loss in the system, as well as across the soil-geotextile interface and within the parent (base) soil. Scenario 2 represents high flow rate in the system due to which the head losses elsewhere in the system become significant and disproportional to those in the soil and geotextile. Scenario 3 represents equal losses in parent soil and across soil-geotextile interface. Scenario 4 represents less head loss across soil geotextile interface due to loss of fines near geotextile. Scenario 5 represents less head loss within the parent soil which suggests migration of fines from the base soil towards the soil-geotextile interface. Scenario 6 represents low flow rates where the head losses in the system are less significant. More head loss can be observed near the soil-geotextile interface which suggests fine particles accumulation near the geotextile.

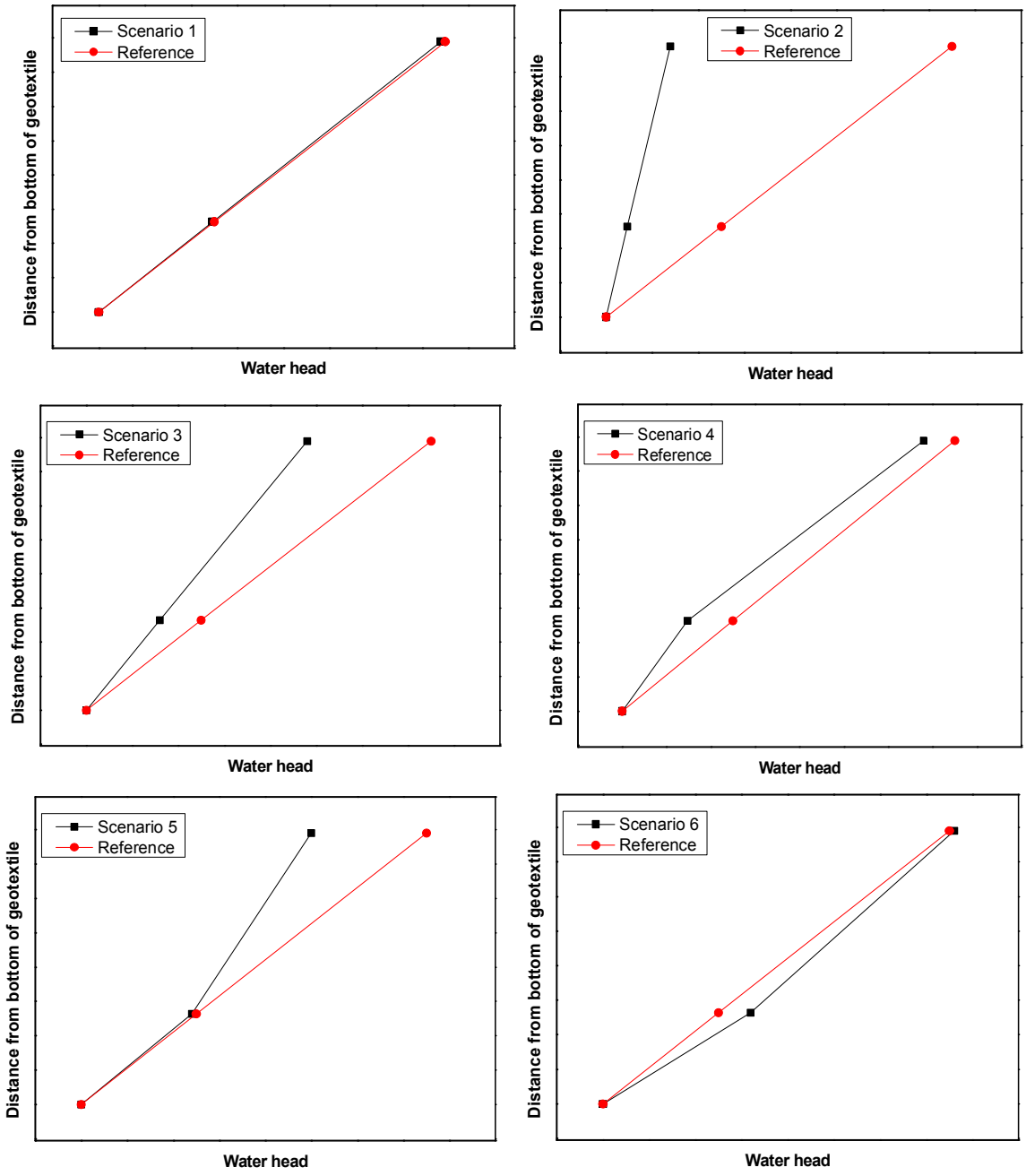
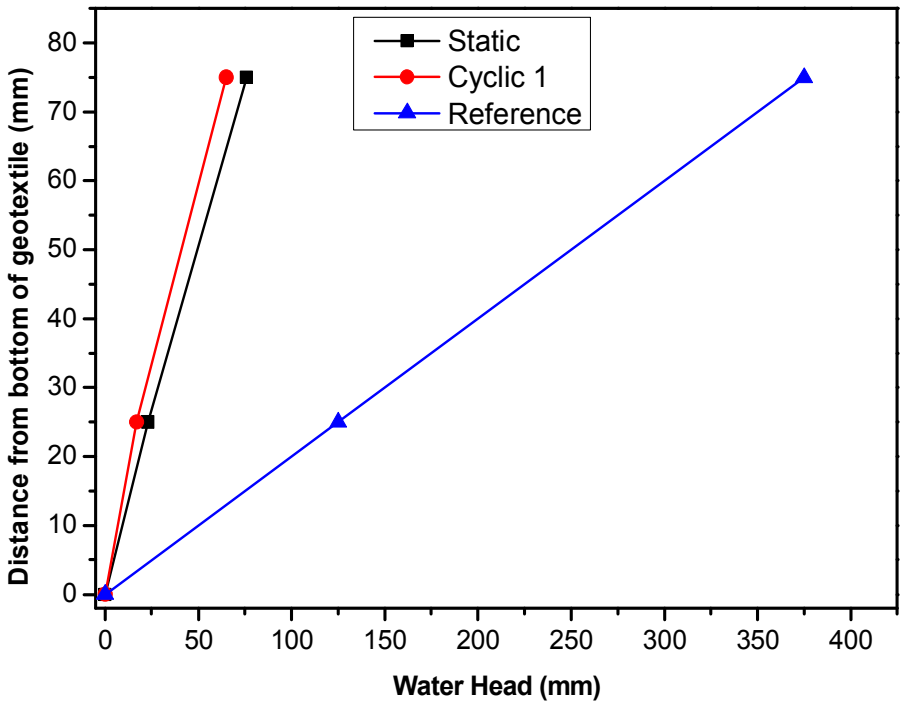


Figure 5.3 Summary of water head distribution responses

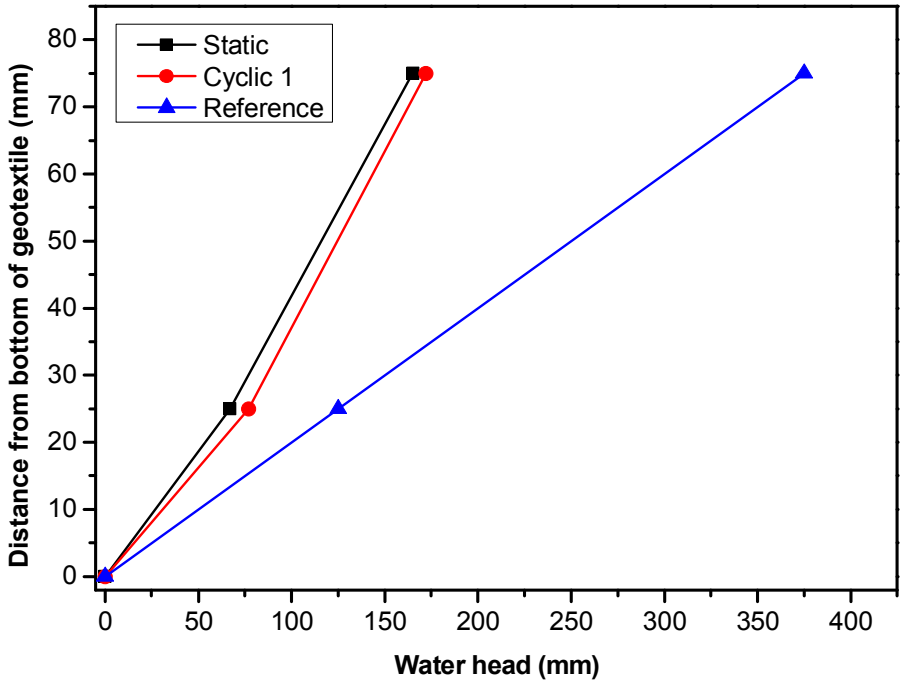
The water head distribution of medium sand with NW8, NW20 and ST170 geotextiles is shown in Figure 5.4a, 5.4b and 5.4c respectively. It can be seen from Figure 5.4 that the magnitude of head losses for medium sand with different geotextile samples is too low for both static unidirectional and cyclic stages as compared to reference or theoretical head loss. The head loss pattern is similar to scenario 2 in Figure 5.3 which shows flow induced head losses in the system.

Figure 5.4a shows that, for NW8 and medium sand sample, the $h_{0\text{-}25}$ per mm is slightly lower than $h_{25\text{-}75}$ per mm, suggesting soil-geotextile interface is more permeable than the soil itself. The water head distribution at the end of cyclic stage is nearly the same as for static stage. The cyclic loading resulted in a slight more decrease in $h_{0\text{-}25}$ per mm than $h_{25\text{-}75}$ per mm which suggests washing of soil particles through the geotextile filter. In contrast, the water head distribution of NW20 and medium sand, for both static and cyclic stages, showed $h_{0\text{-}25}$ per mm to be more as compared to the $h_{25\text{-}75}$ value (Figure 5.4b). The $h_{0\text{-}25}$ per mm increased with cycling loading as compared to the $h_{25\text{-}75}$ per mm rate, implying that the soil-geotextile zone is less permeable than the soil itself.

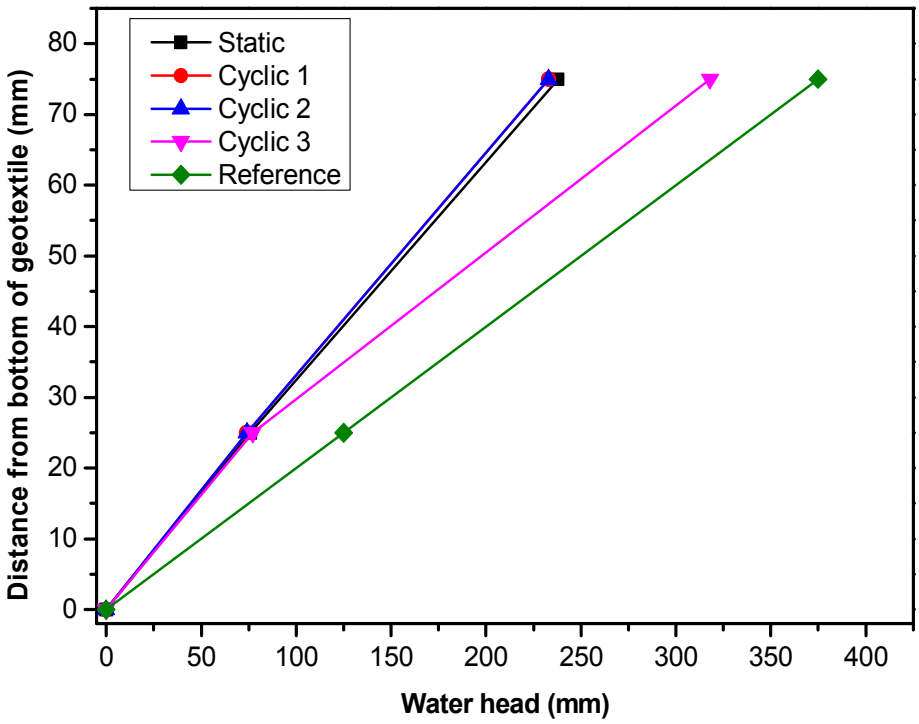
ST170 and medium sand were tested for static and three stages of cyclic loading (Figure 5.4c). The water head distribution is linear across the soil-geotextile interface and within the base soil for static and Cyclic 1 and Cyclic 2 stages which implies a similar permeability within the soil and across the geotextile. However, the $h_{0\text{-}75}$ increased for Cyclic 3 stage when the cyclic deviator stress was increased from 30 to 60 kPa. This increase in $h_{25\text{-}75}$ with Cyclic 3 stage is discussed in Section 7.2.2.



(a) NW8 and medium sand



(b) NW20 and medium sand



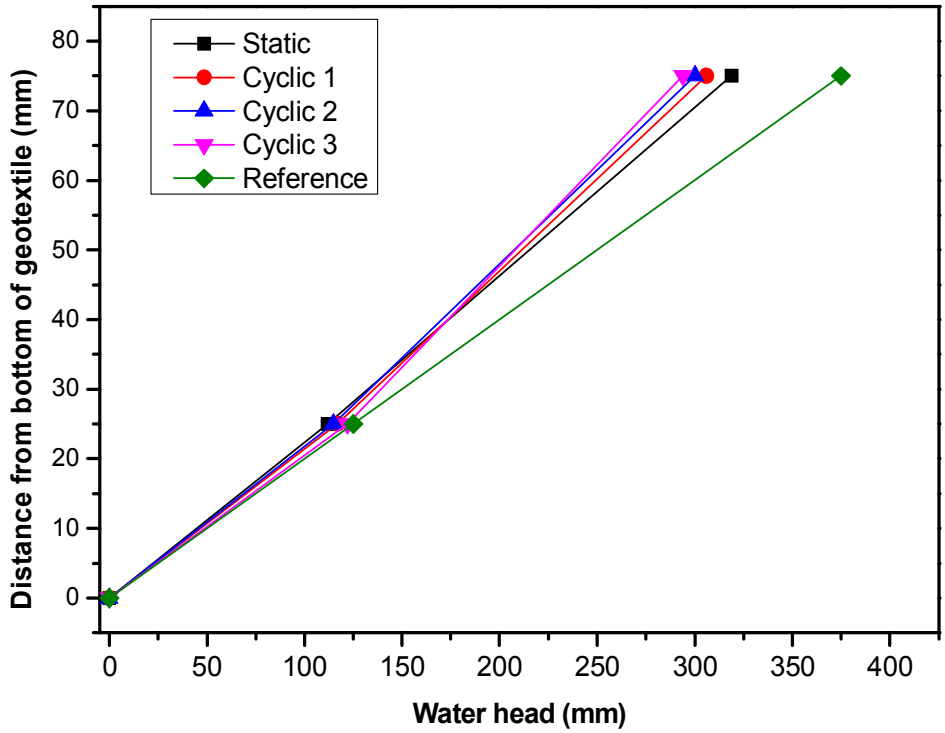
(c) ST170 and medium sand

Figure 5.4 Water head distribution of medium sand with different geotextiles

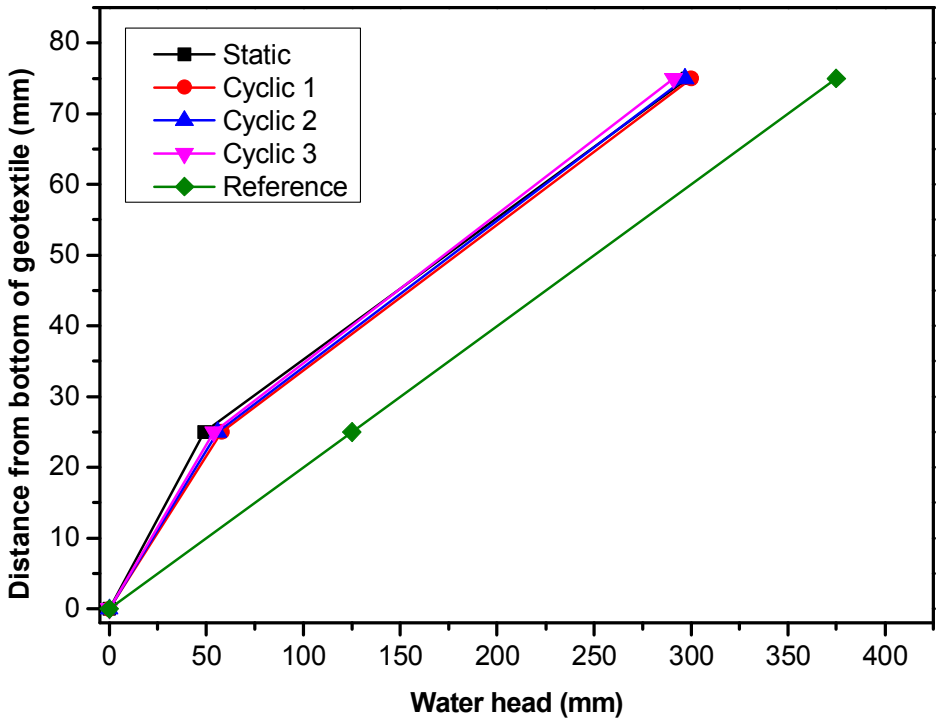
Figure 5.5 shows the water head distribution in fine sand with geotextile samples NW20 and NW8. The $h_{0\text{-}75}$ along both samples is in the range of 250-300mm for static and three stages of cyclic loading. The head losses $h_{0\text{-}25}$ and $h_{25\text{-}75}$ across fine sand and NW20 are linear for static and cyclic stages which is similar to scenario 3. Figure 5.5b shows that $h_{0\text{-}25}$ is too low for the NW8 and fine sand sample as compared to $h_{25\text{-}75}$. The water head distribution remained the same for static and all stages of cyclic loading. The decreased $h_{0\text{-}25}$ for NW8 and fine sand sample as compared to NW20 may be attributed to the more open pores of the NW8 geotextile sample.

The water head distribution in 90% sand 10% PFA mix with NW20 and NW8 geotextiles is shown in Figure 5.6. The water head distribution is similar to scenario 6 (Figure 5.3) which shows the decrease in flow rate with increase of fine content. The $h_{0\text{-}25}$ was found to be quite high for both geotextile samples. The higher $h_{0\text{-}25}$ for the 90% sand 10% PFA

mix with NW20 and NW8 geotextiles, as compared to values with medium sand and fine sand, can be explained by particles retained by the geotextiles.

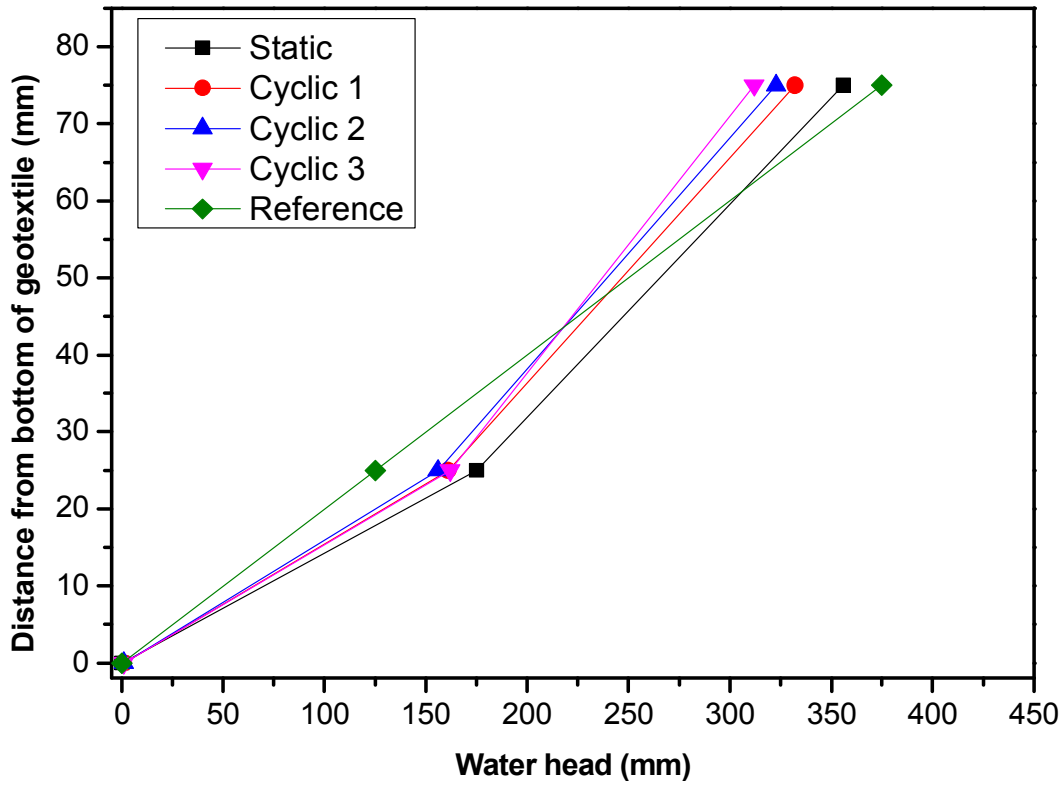


(a) NW20 and Fine Sand

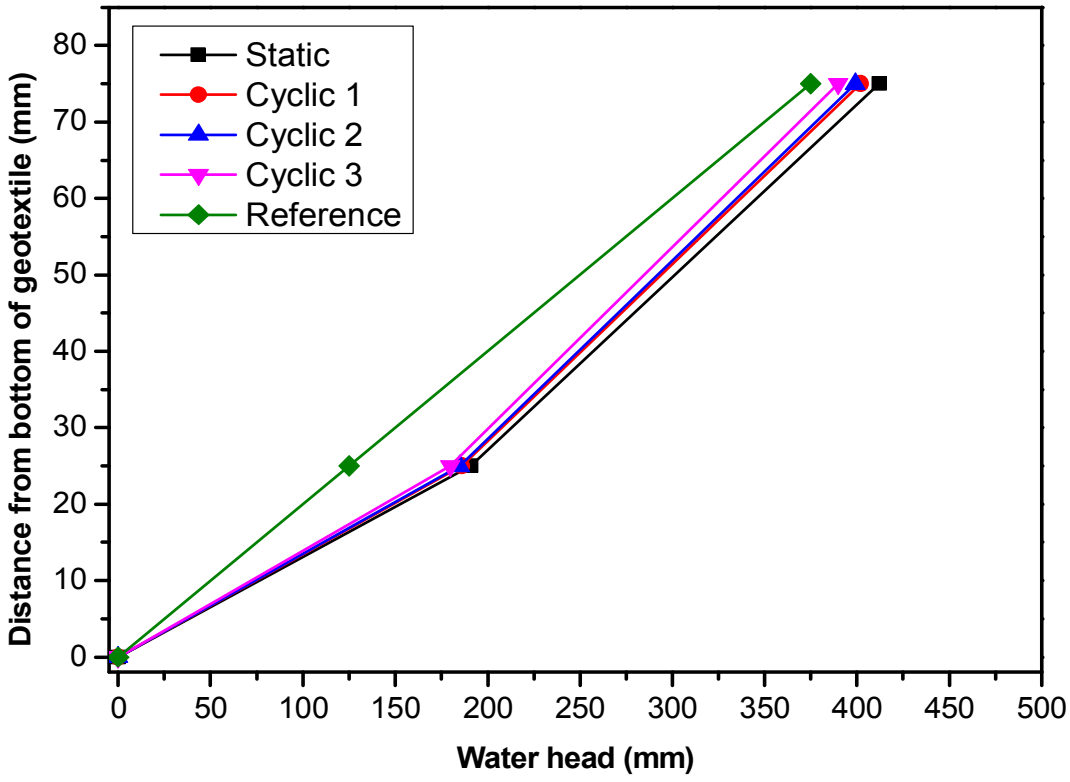


(b) NW8 and Fine Sand

Figure 5.5 Water head distribution of fine sand with NW20 and NW8 geotextiles



(a) NW20 and 90% sand 10% PFA



(b) NW8 and 90% sand 10% PFA

Figure 5.6 Water head distribution of 90% sand 10% PFA mix with NW20 and NW8 geotextiles

5.3.2. Gradient Ratio

Although the water head distribution of all narrow graded soils are explained in the previous section, the filtration performance of soil-geotextile interfaces is usually assessed in terms of Gradient Ratio (GR). As mentioned in Section 2.10.1, a GR is the ratio of hydraulic gradient in the soil-geotextile composite to the hydraulic gradient within the parent soil. A GR of less than 1 indicates that there is an increase in permeability immediately above the geotextile due to loss of some soil, while GR more than 1 shows some clogging within or above geotextile. A continuous decrease in GR value shows piping while continuous increase in value shows clogging.

The variation of GR with time for static unidirectional condition and variation of GR with No. of cycles for cyclic loading are provided in Appendix C. The static and cyclic GR values of narrow graded soils are shown in the Table 5.1. The soil particle sizes D_{85}, D_{50}, D_{30} and D_{15} values are commonly used in filter design criteria (see Section 2.9). The D_{15} index size is usually used in clogging criteria. Therefore, O_{90}/d_{85}, O_{90}/d_{50}, O_{90}/d_{30} and O_{90}/d_{15} are included for reference in Table 5.1. For all tests, no continuous increase or decrease in GR values were observed for static as well as cyclic stages (Appendix C).

Table 5.1 shows that there is not much difference in GR values at the end of static stage and cyclic stages. However, the GR value for ST170 and medium sand at the end of Cyclic 3 stage changed considerably from the GR value at the end of Cyclic 2 stage which is due to more head loss in the soil rather than across the soil geotextile interface (see Figure 5.4). This behaviour can be explained later in terms of decrease in soil permeability during Cyclic 3 stage (see Table 5.2).

Table 5.1 Narrow graded soils: GR values

Geotextile	Soil	O_{90}/d_{85}	O_{90}/d_{50}	O_{90}/d_{30}	O_{90}/d_{15}	GR (End of Static Stage)	GR (End of Cyclic Stages)		
							Cyclic 1	Cyclic 2	Cyclic 3
NW8	Medium Sand	0.29	0.48	0.63	0.80	0.83	0.69	-	-
NW20	Medium Sand	0.17	0.28	0.37	0.28	1.27	1.51	-	-
ST170	Medium Sand	0.17	0.28	0.37	0.47	0.90	0.89	0.9	0.61
NW20	Fine Sand	0.36	0.41	0.50	0.82	1.00	1.15	1.15	1.31
NW8	Fine Sand	0.62	0.71	0.86	1.41	0.38	0.46	0.45	0.43
NW20	90% Sand 10% PFA	0.18	0.30	0.41	0.61	1.79	1.73	1.72	1.97
NW8	90% Sand 10% PFA	0.30	0.52	0.71	1.04	1.66	1.65	1.65	1.65

5.3.3. Permeability

The coefficient of permeability values of the soil-geotextile sample (k_{sys}), within the soil (k_s), and across soil-geotextile interface (k_{sg}) are reported in Table 5.2. The coefficient of permeability values were calculated using Darcy's law. Based on the flow rate and average particle diameter, the Darcy's law was found valid for test samples (see Equation 2.2). Permeability of the system was calculated from the volumetric flow rate and hydraulic gradient applied across the sample. The permeability values of soil and across soil-geotextile interface were calculated from system flow rate, and the head loss that occurred within soil sample and across soil-geotextile interface respectively. It is important to measure the permeability of soil-geotextile system (k_{sys}) since the flow rate of soil-geotextile decreases as the geotextile gets clogged and increases with loss of finer fraction. For each soil type, the narrow range of k_s during the static stage indicates the homogeneity of test samples.

For the medium sand with NW8 and ST170 test samples, the k_{sg} was found to be more than k_s which means the soil-geotextile interface is more permeable than the parent soil and no clogging/ blinding has occurred in the geotextile zone. Table 5.2 shows nearly constant values of k_{sys}, k_{soil} and k_{sg} for respective static and cyclic stages. The greatest change was observed for ST170 and medium sand sample where during Cyclic 3 stage, a reduction in k_{soil} value occurred. This is due to accumulation of fines inside the soil zone (25-40mm), as shown later in Table 5.5.

In the fine sand test series, the k_{sg} of NW20 and fine sand is less than k_s which suggests clogging/blinding of geotextile sample. The k_{sg} of NW8 and fine sand suggests soil-geotextile interface more permeable than the parent soil. The permeability values for 90% sand 10% PFA mix with both geotextile samples suggests clogging/blinding of

geotextiles. Changes in permeability of 90% sand 10% PFA samples are less pronounced than with the medium sand and fine sand samples. The permeability values remained nearly constant for static and cyclic stages. The deduced values of permeability are appropriate as similar values for narrow graded soils were measured by Shan et al. (2001).

Table 5.2 Narrow graded soils: Coefficient of permeability values (x 10^{-5} m/s)

Geotextile	**Soil**	**k**	**Static**	**Cyclic**		
				Cyclic 1	**Cyclic 2**	**Cyclic 3**
NW8	Medium Sand	k_{sys}	3.40	3.80	-	-
		k_s	4.29	4.16	-	-
		k_{sg}	5.14	5.20	-	-
NW20	Medium Sand	k_{sys}	3.60	3.72	-	-
		k_s	3.85	4.07	-	-
		k_{sg}	3.03	2.72	-	-
ST170	Medium Sand	k_{sys}	3.49	3.51	3.11	2.28
		k_s	3.33	3.41	3.01	2.05
		k_{sg}	3.78	3.81	3.36	3.33
NW20	Fine Sand	k_{sys}	0.67	0.71	0.74	0.83
		k_s	0.67	0.83	0.84	1.11
		k_{sg}	0.63	0.69	0.71	0.81
NW8	Fine Sand	k_{sys}	0.76	0.74	0.75	0.74
		k_s	0.64	0.65	0.66	0.66
		k_{sg}	1.70	1.40	1.47	1.51
NW20	90% Sand 10% PFA	k_{sys}	0.25	0.24	0.25	0.31
		k_s	0.30	0.29	0.30	0.38
		k_{sg}	0.16	0.17	0.17	0.20
NW8	90% Sand 10% PFA	k_{sys}	0.22	0.23	0.23	0.24
		k_s	0.26	0.27	0.27	0.29
		k_{sg}	0.16	0.17	0.17	0.18

5.3.4. Post-Test Procedure

5.3.4.1. Mass of Particles Washed Out

The mass of soil particles passed through geotextile samples was collected at the end of each test (Table 5.3). The cumulative mass per unit amount of soil collected in all tests for narrow graded soils was less than 500 g/m^2. For reference, 100 g/m^2 represent just 0.2g of particles.

It can be seen from the Table 5.3 that, for the three narrow graded soil samples, the mass of particles collected was highest for medium sand, followed by fine sand and 90% sand 10% PFA. For geotextiles NW20 and ST170, which have the same O_{90} opening size, almost the same amount of soil particles was collected. For each soil type, the amount of soil particles collected increased with increasing the O_{90}/d_{85}. Figure 5.7 shows a plot between mass collected and O_{90}/d_{30}. It can be seen from the figure that there is not a well-defined relationship between the mass of particles passed and the O_{90}/d_{30} ratio.

Table 5.3 Narrow graded soils: Mass of particles collected after each test

Geotextile	Soil	O_{90}/d_{85}	O_{90}/d_{50}	O_{90}/d_{30}	O_{90}/d_{15}	Mass of Soil Particles Collected g/m^2
NW8	Medium Sand	0.29	0.48	0.63	0.80	311
NW20	Medium Sand	0.17	0.28	0.37	0.47	180
ST170	Medium Sand	0.17	0.28	0.37	0.47	189
NW20	Fine Sand	0.36	0.41	0.50	0.82	154
NW8	Fine Sand	0.62	0.71	0.86	1.41	215
NW20	90% Sand 10% PFA	0.18	0.30	0.41	0.61	143
NW8	90% Sand 10% PFA	0.30	0.52	0.71	1.04	171

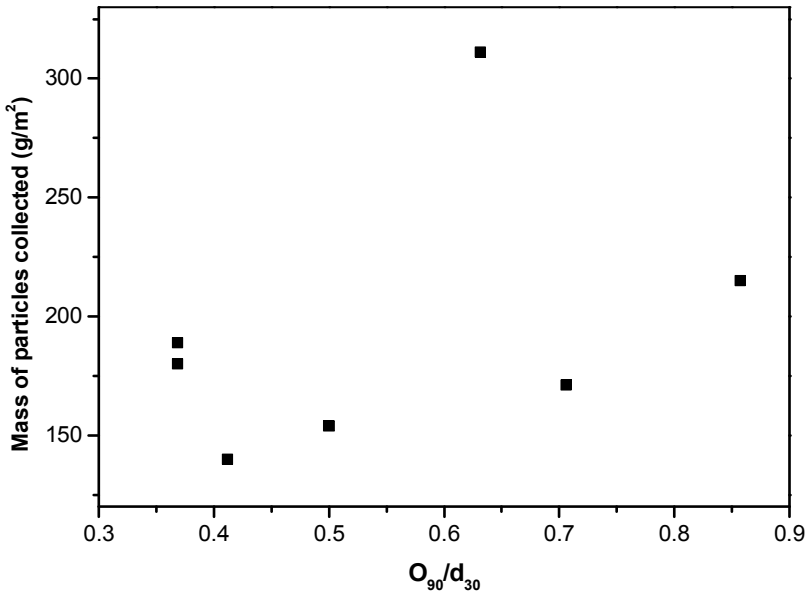


Figure 5.7 Relationship between O_{90}/d_{30} and mass collected for narrow graded soils

5.3.4.2. Gradation of Particles Washed Out

Selected samples of soil particles washed out through the geotextile were taken to a Nikon microscope for particle size analysis (see Section 4.2.6.2). The d_{90} of soil particles passed, defined as d_{90p}, was measured. It can be seen from Table 5.4 that, d_{90p} was highest for medium sand, followed by 90% sand 10% PFA mix and fine sand. For the same soil sample, the d_{90p} increased with increasing O_{90} of the geotextile.

Table 5.4 Narrow graded soils: d_{90p} of washed out particles

Geotextile	Soil	O_{90} (µm)	d_{90p} (µm)
NW8	Medium Sand	120	35
NW20	Medium Sand	70	31
ST170	Medium Sand	70	30
NW20	Fine Sand	70	15
NW8	Fine Sand	120	18
NW20	90% Sand 10% PFA	70	20
NW8	90% Sand 10% PFA	120	25

5.3.4.3. Pre and Post Test Gradation

The comparisons of post-test gradations with the pre-test gradation provide valuable information regarding the change in soil gradation near the geotextile, as well as in the soil itself. The three possible scenarios of pre and post-test gradations are shown in the Figure 5.8. All the pre and post-test gradations of narrow graded soils are provided in Appendix D.

Figure 5.8 shows scenario 1, where there the post-test gradation curve lies on top of pre-test gradation curve. It means the mass of soil particle passed through geotextile shares the same grading as parent soil indicating that there is neither effective filtering nor piping (see Section 2.4) behaviour. Scenario 2 represents post-test gradation where the D_{50}, D_{30} and D_{15} after test increases due to loss of fine particles (<63 µm) and some of the matrix i.e. 63 to greater than 200 µm indicating a lack of filtering by the soil-geotextile system. Scenario 3 represents post-test gradation moved to the left of pre-test gradation which indicates an increase in the finer portion of the soil particles, retained at the soil-geotextile interface suggesting instability and loss of coarse particles from the soil either into or through the geotextile. The gradation curve for scenario 3 result in decrease in D_{50}, D_{30}, and D_{15} particle sizes.

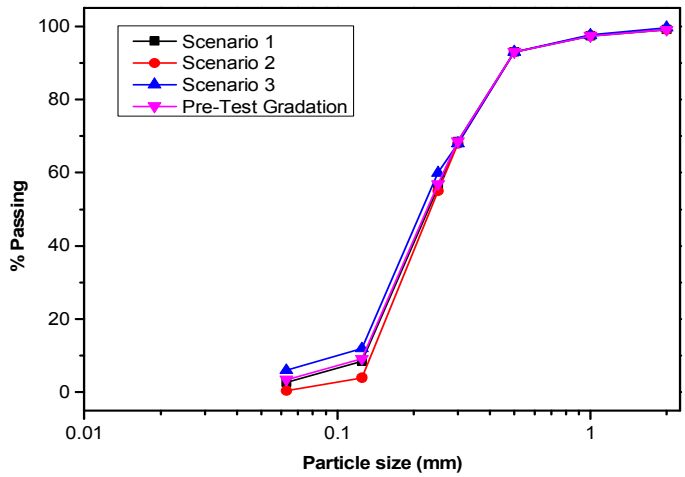


Figure 5.8 Possible scenarios of post-test gradations

Based on the scenarios described in Fig 5.8, the pre and post-test gradations of narrow graded soils are summarized in terms of D_{85}, D_{50}, D_{30} and D_{15} (see Table 5.5). For medium sand tests with NW8 geotextiles, no obvious change in post-gradation of soil was observed for soil samples in the soil-geotextile interface (0-8mm) and within the soil (25-40mm). Results followed scenario 1. However, for NW20 geotextile, the post-test gradation showed a decrease in D_{15} for 0-8mm (Scenario 3), showing an increase in fine content which were stopped by the geotextile sample. The post-test gradation of medium sand for ST170 sample showed a slight decrease in D_{15} for 25-40mm soil layer. This shows an increase in finer content of soil which suggests possibility of particles migrating from top layer into the 25-40mm soil layer.

Fine Sand showed different post-test soil gradations for NW20 and NW8 geotextile samples. For the NW20 sample, the post-test gradation showed no change in D_{85}, D_{50} and D_{30}. However, a decrease in D_{15} was observed for the soil gradation in the 0-8mm zone which suggests that fine particles were stopped by the geotextile. For NW8 sample, post-gradation only showed slight increase in D_{15} in 0-8mm zone, suggesting washing of some fines through the geotextile which is presumably attributed to the more open pore size of NW8.

The post-gradation of 90% sand 10% PFA at the soil-geotextile interface and within the soil were observed similar for NW20 and NW8 samples. A decrease in D_{15} occurred in 0-8mm for both geotextile samples which is believed to be due to the retention of fines by the geotextile.

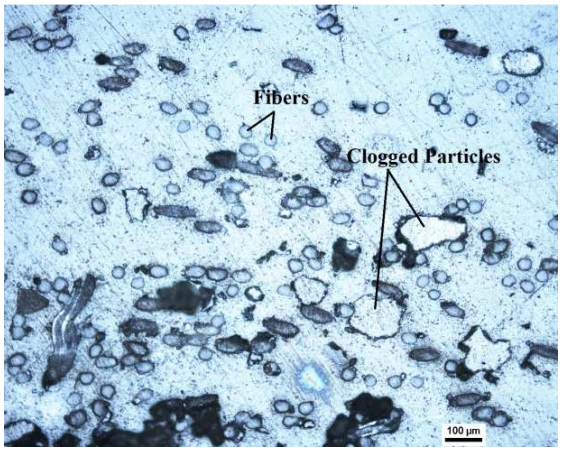
Table 5.5 Narrow graded soils: Summary of pre and post-test gradation

Geotextile	Mass of particles collected (g/m^2)	D_{85}		D_{50}		D_{30}		D_{15}	
		0-8 mm	25-40 mm	0-8 mm	0-8 mm	0-8 mm	25-40 mm	0-8 mm	25-40 mm
Medium Sand		**0.420**		**0.230**		**0.190**		**0.150**	
NW8	311	0.420	0.420	0.230	0.230	0.190	0.190	0.150	0.150
NW20	180	0.420	0.420	0.230	0.230	0.190	0.190	0.140	0.150
ST170	189	0.420	0.420	0.230	0.230	0.190	0.190	0.150	0.145
Fine Sand		**0.195**		**0.170**		**0.140**		**0.085**	
NW20	154	0.195	0.195	0.170	0.170	0.140	0.140	0.080	0.085
NW8	215	0.195	0.195	0.170	0.170	0.145	0.140	0.090	0.085
90% Sand 10% PFA		**0.400**		**0.230**		**0.170**		**0.115**	
NW20	143	0.400	0.400	0.230	0.230	0.170	0.170	0.070	0.115
NW8	171	0.400	0.400	0.230	0.230	0.170	0.170	0.075	0.115

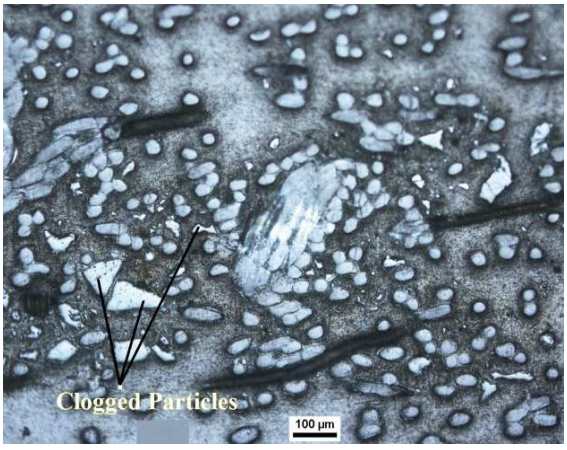
5.3.4.4. Microscopic Images of Geotextile Samples

Images of geotextile samples after each test were taken to observe the clogging condition in geotextiles. The method to take microscopic images of a cross-section of the geotextile was explained in Section 4.2.6. Moreover, the clogging condition in geotextiles were supported by computing the partial clogging values according to the method suggested by Palmeira and Gardoni (2000). The partial clogging 'λ' can be defined as the ratio between mass of soil retained within geotextile and fiber mass in a partially clogged geotextile. The partial clogging values of geotextiles are given in Table 5.6. A smaller partial clogging value suggests that less particles are clogged inside the geotextile. Although there is no limit defined for the partial clogging values by Palmeira and Gardoni (2000), however, they suggested λ from 0.3 to as high as 11 should be expected in laboratory and field tests.

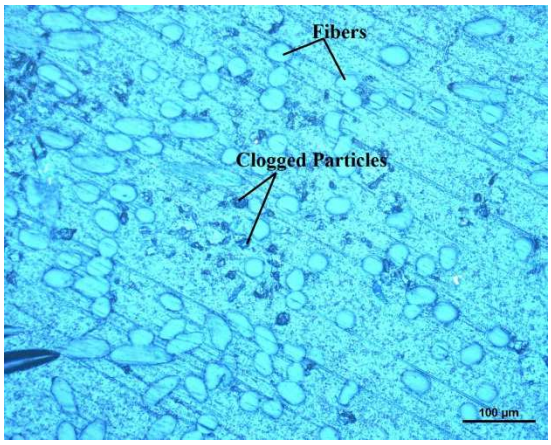
Figure 5.9 shows the microscopic images of geotextile samples tested with medium sand. The geotextile fibers are rounded (sometimes appearing elongated in shape when cut longitudinally) while soil particles are irregular in shape. Particles were observed to be clogged in the middle or middle lower section of geotextile samples where fibers are more closely spaced. NW8 sample showed very few clogged particles which were found to be relatively large in size. This is attributed to the large characteristic opening size of NW8, allowing smaller particles to pass through while retaining bigger particles. NW20 and ST170 showed more clogging sites than NW8, however, no serious clogging was observed. Also, the clogged particles in NW20 and ST170 were relatively smaller in size as compared to those trapped in NW8 due to the smaller opening size of both geotextile samples. The partial clogging of geotextile with medium sand shows large value with NW8 than with NW20 and ST170 which might be attributed to the bigger particles retained inside NW8 geotextile.



(a) NW8



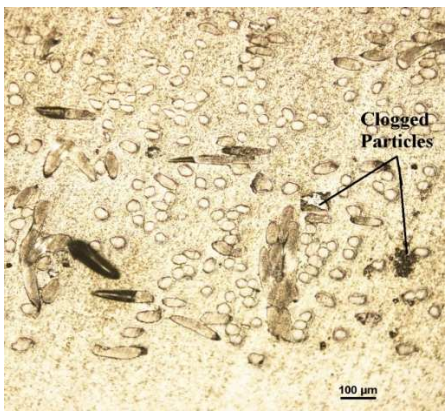
(b) NW20



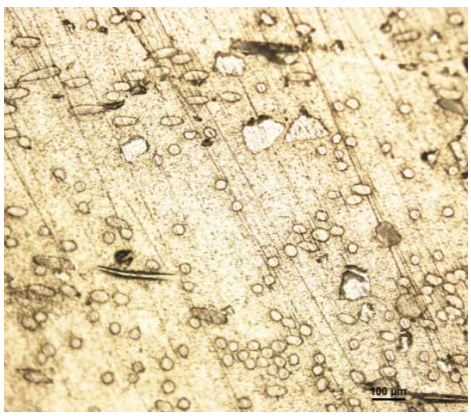
(c) ST170

Figure 5.9 Microscopic images of geotextile samples after filtration test with medium sand

NW20 and NW8 samples with fine sand showed very few clogged particles, as shown in Figure 5.10. Again, the partial clogging value was found to be comparatively large for NW8 as compared to NW20, showing more particles clogged inside NW8. The geotextile samples with 90% sand 10% PFA showed more clogging than with medium sand and fine sand (Figure 5.11). The clogged particles are small which is due to more fine content in the 90% sand 10% PFA soil. Overall, the microscopic images and partial clogging values suggests that no serious clogging of geotextile samples was observed with narrow graded test samples.

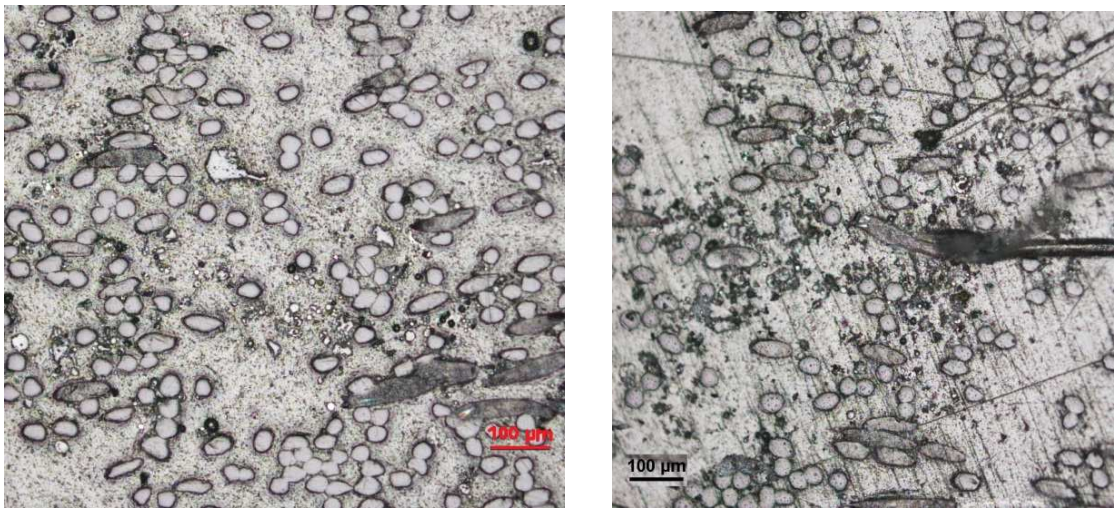


(a) NW20 sample



(b) NW8 sample

Figure 5.10 Microscopic images of geotextile samples after filtration test with fine sand



(a) NW20 sample (b) NW8 sample

Figure 5.11 Microscopic images of geotextile samples after filtration test with 90% sand 10% PFA

Table 5.6 Narrow graded soils: Partial clogging of geotextiles

Geotextile	Soil Type	Mass/Area (Geotextile) (g/m^2)	Mass of Soil Retained Inside Geotextile (g/m^2)	Partial Clogging 'λ'
NW8	Medium Sand	120	128	1.07
NW20	Medium Sand	250	140	0.56
ST170	Medium Sand	237	188	0.79
NW20	Fine Sand	250	96	0.38
NW8	Fine Sand	120	160	1.33
NW20	90% Sand 10% PFA	250	137	0.55
NW8	90% Sand 10% PFA	120	133	1.11

5.4. Filtration Behaviour of Broadly Graded Soils

A total of thirteen filtration tests were performed using broadly-graded soils with four different geotextiles to assess the filtration behaviour under static and dynamic conditions. The objective was to evaluate the design criteria for soil retention with respect to clogging and piping potential of the system. The soil-geotextile combinations as well as their O_{90}/d_{85} ratios are given in Table 5.7. Eleven tests were performed for one stage of cyclic

loading i.e. Cyclic 1 stage, while two tests were performed for two additional cyclic stages (i.e. Cyclic 2 and Cyclic 3). Therefore, the plan was to perform the filtration tests for Cyclic 1 stages for broadly-graded soils since most of these soils were considered internally unstable according to the geometric criteria (see Table 3.6). The filtration test results for static and cyclic stages are discussed in the sections below.

5.4.1. Water Head Distribution

During the filtration test program for broadly-graded soils, only one 85% sand 15% PFA sample was tested with NW20 geotextile. The soil-geotextile sample was tested under one static stage and three stages of cyclic loading. The water head distribution across the 85% sand 15% PFA sample is shown in Figure 5.12. The distribution of water head from bottom of geotextile to 75mm higher in the sample is nearly linear at the end of static stage which shows that sample is internally stable at the end of static stage. The water head distribution at the end of static stage followed scenario 3 which shows equal losses in soil and across soil-geotextile interface. The water head distribution at the end of cyclic stages followed scenario 4 which shows fine loss near geotextile.

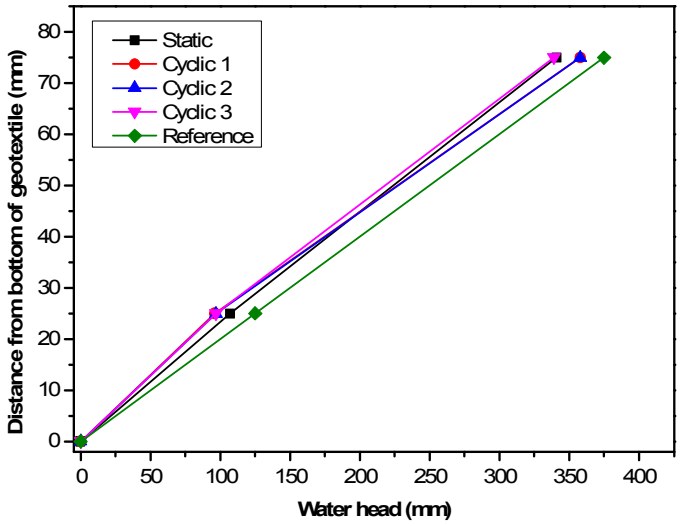


Figure 5.12 Water head distribution of 85% sand 15% PFA with NW20 geotextile

Figure 5.13 shows summary of rate of head loss across soil-geotextile interface and within soil for the 80% sand 20% PFA soil. The $h_{0\text{-}25}$ per mm value was found to be more than $h_{25\text{-}75}$ per mm value for all three geotextile samples, implying that soil-geotextile zone is less permeable than the parent soil, presumably due to clogging/blinding of geotextile samples. No effect of cyclic loading was observed on the rate of head losses, indicating no migration of fine particles within the voids of coarse particles.

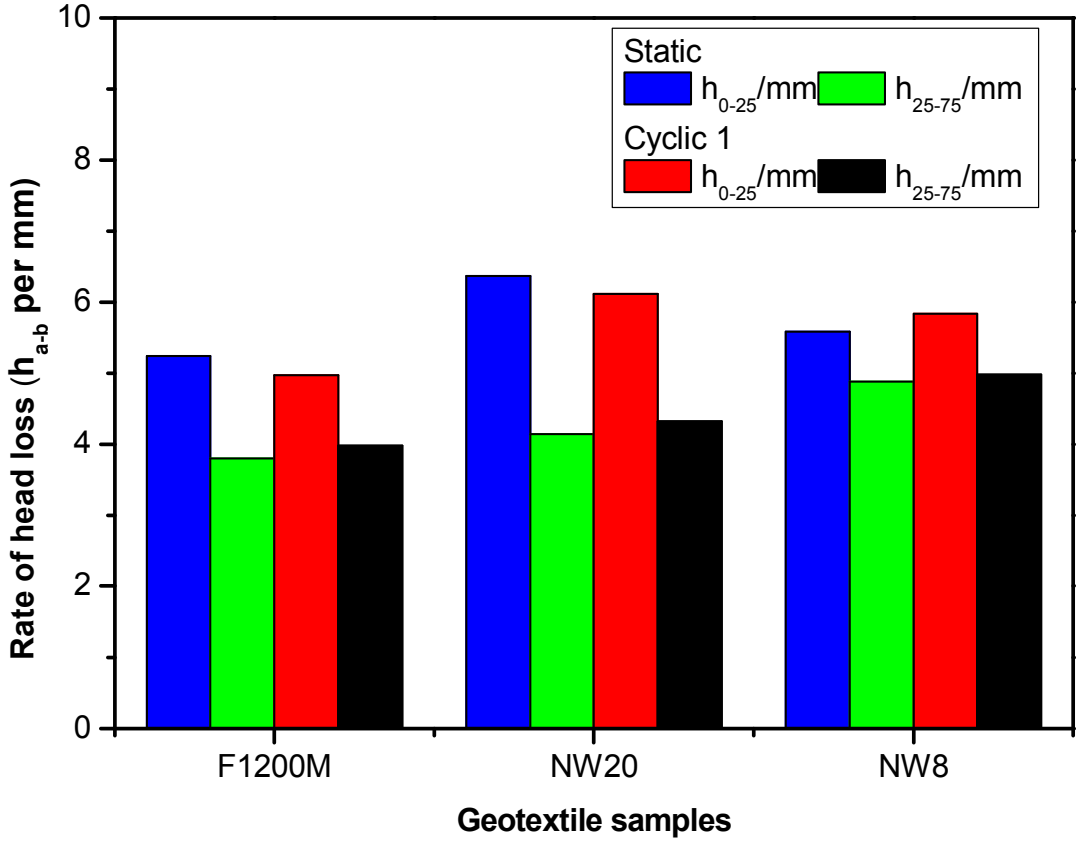


Figure 5.13 80% Sand 20% PFA: Rate of head loss across soil-geotextile interface and within soil

The water head distribution of 70% sand 30% PFA is shown in Figure 5.14. As previously discussed in Section 3.3.3, the gap-graded soil has a gap-width of 2.77. The rate of head loss across the soil-geotextile interface was nearly the same as within parent soil for static and cyclic stages which shows the internal stability of the test sample.

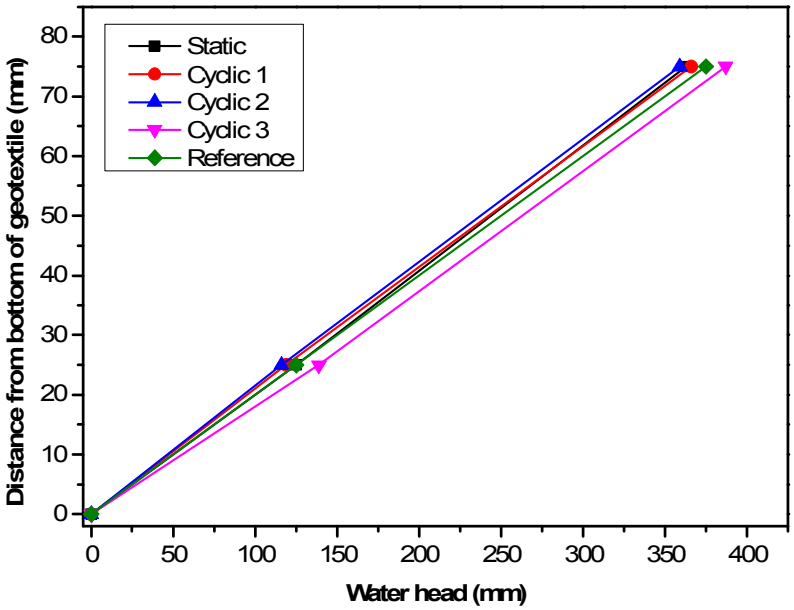


Figure 5.14 Water head distribution of 70% sand 30% PFA with NW20 geotextile

The $h_{0\text{-}25}$ per mm and $h_{25\text{-}75}$ per mm for 60% sand 40% PFA sample with four different geotextiles is shown in Figure 5.15. For all test samples, the $h_{0\text{-}25}$ per mm value is less than $h_{25\text{-}75}$ per mm rate, implying that the soil-geotextile interface is more permeable than the parent soil. The $h_{0\text{-}25}$ per mm rate for test samples decreased with cyclic loading, indicating washing of fine particles through geotextiles. The effect of cyclic loading can be observed on the $h_{25\text{-}75}$ per mm rate, indicating the migration of fines within base soil layers due to the internal instability of soil samples.

The $h_{0\text{-}25}$ per mm rate for 40% sand 60% PF was found more than the rate of $h_{25\text{-}75}$ per mm during the static stage, implying that soil-geotextile zone less permeable than parent soil, suggesting blinding/ clogging (Figure 5.16). The head loss in the soil increased during the cyclic loading, more than the head loss associated with the applied gradient which indicates accumulation of fines inside the base soil due to the internal instability of soil.

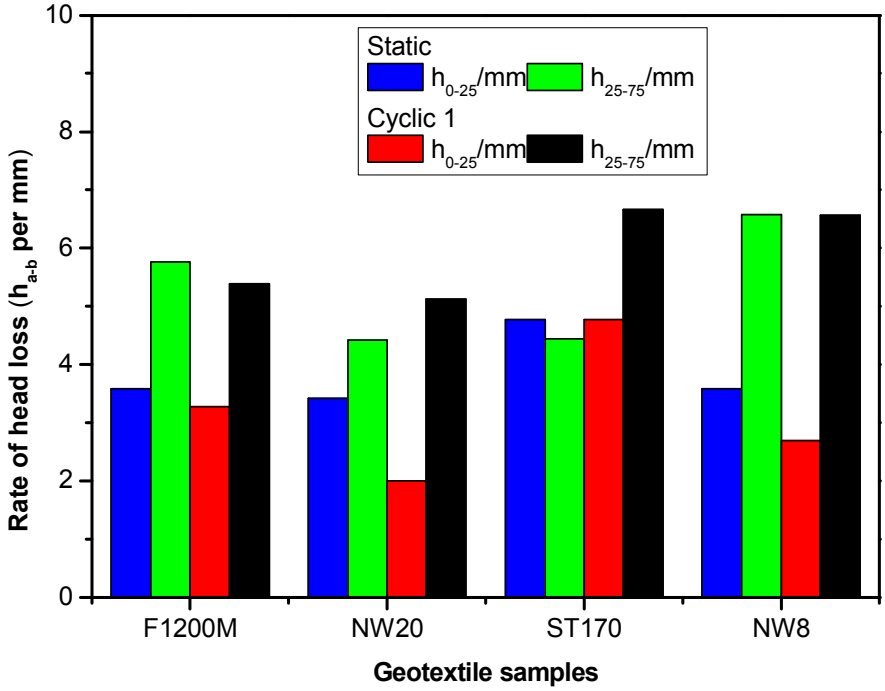


Figure 5.15 60% Sand 40% PFA: Rate of head loss across soil-geotextile interface and within soil

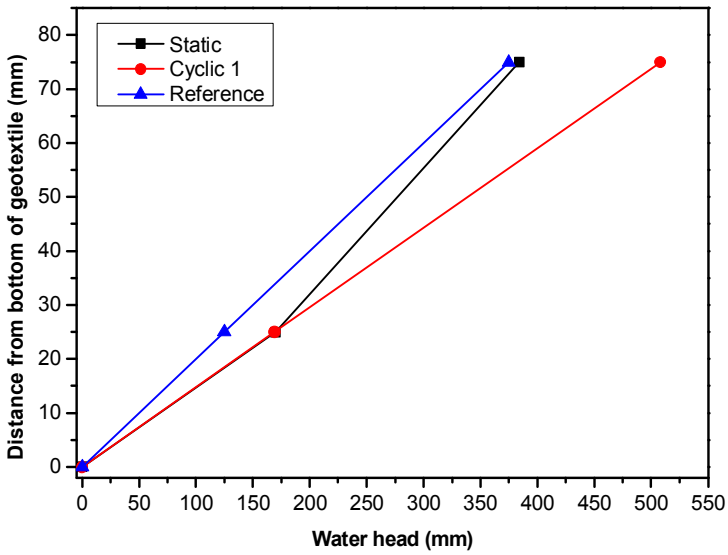


Figure 5.16 Water head distribution of 40% sand 60% PFA with NW20 geotextile

Figure 5.17 shows the rate of head losses of PFA with three geotextile samples. The h_{0-25} per mm value for F1200M and ST170 was less than h_{25-75} per mm rate. The change in h_{0-25} and h_{25-75} per mm rate under cyclic loading shows the internal instability of PFA.

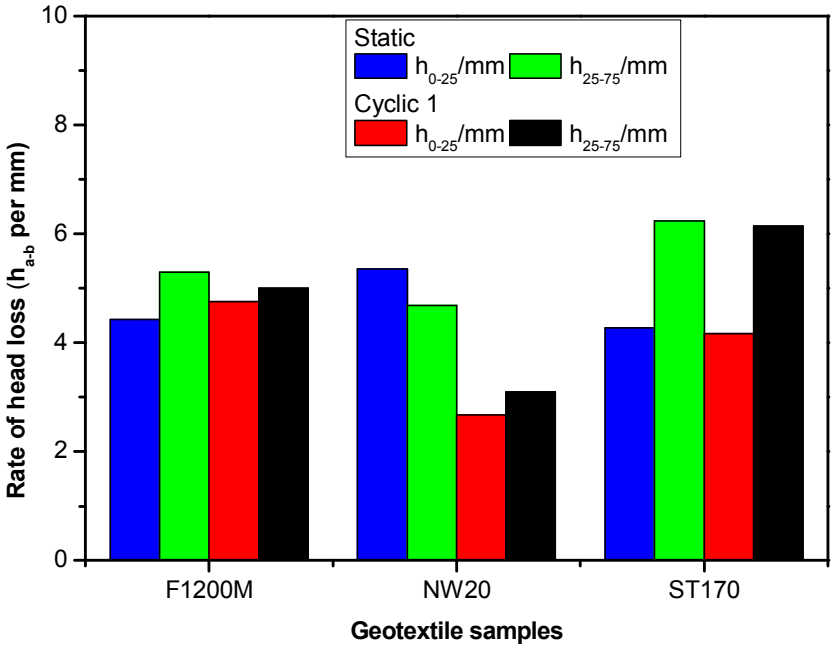


Figure 5.17 PFA: Rate of head loss across soil-geotextile interface and within soil

5.4.2. Gradient Ratio

The GR values for broadly-graded soils at the end of static and cyclic stages are shown in the Table 5.7. The GR plots for static and cyclic stages are given in Appendix C. None of the test showed a GR greater than 3, a limit set by the US Army Corps of Engineers (1977) for excessive clogging.

The last column in Table 5.7 shows the difference in GR values between cyclic stage/stages and static stage. The highest difference in GR values was observed for 40% sand 60% PFA mix, as well as 60% sand 40% PFA with NW20 and ST170 samples. This phenomenon will be explained later in Section 7.3.2 in terms of internal instability of soils. One PFA sample showed a GR difference of 0.28 which indicate washing of fines through the geotextile. The 80% sand 20% PFA mix test samples showed a GR value more than 1 for static and cyclic stages which shows clogging/ blinding of geotextiles (will be discussed later in Section 7.3.2).

Table 5.7 Broadly-graded soils: GR values

Geotextile	**Soil**	**O_{90}/d_{85}**	**O_{90}/d_{50}**	**O_{90}/d_{30}**	**O_{90}/d_{15}**	**GR**	**GR**			**D_{GR} =**
						(Static Stage)	**Cyclic1**	**Cyclic2**	**Cyclic3**	**GR_{static}- $GR_{cyclic)}$**
NW20	85% Sand 15% PFA	0.18	0.32	0.44	1.27	0.85	0.68	0.69	0.74	0.11
F1200M	80% Sand 20% PFA	0.16	0.29	0.40	2.00	1.38	1.25	-	-	0.13
NW20	80% Sand 20% PFA	0.18	0.33	0.47	2.33	1.54	1.41	-	-	0.13
NW8	80% Sand 20% PFA	0.32	0.57	0.80	4.00	1.14	1.13	-	-	0.02
F1200M	70% Sand 30% PFA	0.13	0.20	0.23	4.00	0.80	0.73	0.72	0.85	0.05
F1200M	60% Sand 40% PFA	0.18	0.38	1.76	7.50	0.62	0.61	-	-	0.01
ST170	60% Sand 40% PFA	0.21	0.44	2.06	8.75	1.08	0.73	-	-	0.35
NW20	60% Sand 40% PFA	0.21	0.44	2.06	8.75	0.77	0.40	-	-	0.37
NW8	60% Sand 40% PFA	0.35	0.75	3.53	15.00	0.54	0.52	-	-	0.02
NW20	40% Sand 60% PFA	0.25	1.35	5.00	14.00	1.47	0.87	-	-	0.60
F1200M	PFA	0.95	4.00	10.00	60.00	0.83	0.95	-	-	0.12
NW20	PFA	1.11	4.67	11.67	70.00	1.08	0.80	-	-	0.28
ST170	PFA	1.11	4.67	11.67	70.00	0.66	0.65	-	-	0.01

5.4.3. Permeability

The densification of test samples tends to decrease the permeability, loss of the finer fraction tends to increase the permeability. The coefficient of permeability values for broadly-graded test samples are shown in Tables 5.8, 5.9, 5.10, 5.11 and 5.12. Table 5.8 shows the permeability values of 80% sand 20% PFA test samples with F1200M, NW20 and NW8 geotextiles. The k_{sg} values of all three test samples were less than k_s and k_{sys} during static and cyclic stages, indicating clogging/blocking of geotextiles. The magnitude of difference is not significant as the GR values are less than 3 (see Table 5.7), a limit set by US Army Corps of Engineers (1977).

Table 5.8 Permeability values (x 10^{-7} m/s) for 80% Sand 20% PFA samples

Geotextile	Soil	k	Static	Cyclic 1
F1200M	80% Sand 20% PFA	k_{sys}	5.56	6.18
		k_s	6.60	7.08
		k_{sg}	4.79	5.67
NW20	80% Sand 20% PFA	k_{sys}	5.69	5.88
		k_s	6.46	6.50
		k_{sg}	4.20	4.58
NW8	80% Sand 20% PFA	k_{sys}	7.11	7.27
		k_s	7.28	7.43
		k_{sg}	6.37	6.59

Table 5.9 shows the permeability values of 60% sand 40% PFA soil with four geotextile samples. The permeability values were computed to be smaller than those for the 80% sand 20% PFA test samples due to increase in fines (PFA). The permeability values decreased with cyclic loading, signifying the migration of fine particles within soil layers.

The soil near the geotextile was found to be more permeable which implies local erosion/ local piping. These soils in terms of piping will be discussed later in Section 7.3.2.

Table 5.9 Permeability values (x 10^{-7} m/s) for 60% Sand 40% PFA samples

Geotextile	Soil	k	Static	Cyclic 1
F1200M	60% Sand 20% PFA	k_{sys}	1.22	0.51
		k_s	1.15	1.11
		k_{sg}	1.85	1.88
ST170	60% Sand 20% PFA	k_{sys}	3.28	1.20
		k_s	3.33	1.11
		k_{sg}	3.10	1.55
NW20	60% Sand 20% PFA	k_{sys}	1.18	0.36
		k_s	1.09	0.31
		k_{sg}	1.53	0.80
NW8	60% Sand 20% PFA	k_{sys}	2.40	1.82
		k_s	2.13	1.63
		k_{sg}	4.23	3.94

The coefficients of permeability values for PFA test samples were computed to be smaller than other soil test samples, as shown in Table 5.10. The k_{sg} values were higher than k_s for all PFA test samples which indicate erosion of soil near the geotextile interface.

Table 5.10 Permeability values (x 10^{-7} m/s) for PFA samples

Geotextile	Soil	k	Static	Cyclic 1
F1200M	PFA	k_{sys}	1.59	2.42
		k_s	1.53	2.39
		k_{sg}	1.83	2.52
NW20	PFA	k_{sys}	0.86	0.71
		k_s	0.88	0.68
		k_{sg}	0.82	0.85
ST170	PFA	k_{sys}	0.76	0.92
		k_s	0.70	0.87
		k_{sg}	1.06	1.28

Table 5.11 shows the permeability values of all broadly-graded test samples with NW20 to show how soil type affect results on one geotextile. The k_{sg} value was more than k_s for 85% sand 15% PFA and remained unaffected under the cyclic stages. This will be discussed later in terms of bridging network (Section 7.3.2). The k_{sg} value was less than k_s for only 80% sand 20% PFA mix sample which suggest clogging/blinding behaviour. The k_{sg} for NW20 and three fine soils (60% sand 40% PFA, 40% sand 60% PFA, and PFA) was observed to be larger than k_s. These soils in terms of piping will be discussed later in Section 7.3.2. The test samples showed a tendency from stable to piping with increase in geotextile characteristic opening size to soil index size ratio.

Table 5.11 Permeability values (x 10^{-7} m/s) of test samples with NW20

Geotextile	Soil	k	Static	Cyclic 1	Cyclic 2	Cyclic 3
NW20	85% Sand 15% PFA	k_{sys}	8.59	8.07	8.85	9.08
		k_s	8.26	7.37	7.88	8.5
		k_{sg}	9.76	10.9	11.5	11.5
NW20	80% Sand 20% PFA	k_{sys}	5.69	5.88	-	-
		k_s	6.46	6.50	-	-
		k_{sg}	4.20	4.58	-	-
NW20	60% Sand 40% PFA	k_{sys}	1.09	0.32	-	-
		k_s	1.09	0.31	-	-
		k_{sg}	1.53	0.80	-	-
NW20	40% Sand 60% PFA	k_{sys}	1.60	0.93	-	-
		k_s	1.8	0.91	-	-
		k_{sg}	1.18	0.99	-	-
NW20	PFA	k_{sys}	0.82	0.42	-	-
		k_s	0.88	0.68	-	-
		k_{sg}	0.82	0.85	-	-

The permeability values show that the soil-geotextile interface for gap-graded soil is more permeable than the base soil at the end of static and cyclic stages which suggest erosion of fines near the geotextile. The filtration behaviour of 70% sand 30% PFA in terms of GR and permeability will be discussed later in Section 7.3.2.

Table 5.12 Permeability values (x 10^{-5} m/s) for 70% sand 30% PFA sample

Geotextile	**Soil**	**k**	**Static**	**Cyclic**		
				Cyclic 1	**Cyclic 2**	**Cyclic 3**
F1200M	70% Sand 30% PFA (Gap-graded)	k_{sys}	2.59	1.81	2.76	2.66
		k_s	2.60	1.78	2.71	2.65
		k_{sg}	3.26	2.43	3.74	3.12

5.4.4. Post Test Procedure

5.4.4.1. Mass of Particles Washed Out

The mass of soil particles washed out and collected at the end of each test is shown in Table 5.13. Except one test, the cumulative mass per unit amount of soil collected in all tests was less than 500 g/m^2. The amount of particles collected was least for 85% sand 15% PFA, followed by 70% sand 30% PFA. These both samples behaved stable, as discussed in Section 5.3.1. Both samples had a linear water head distribution. . The 60% sand 40% PFA samples showed more particles collected than the 80% sand 20% PFA test samples. The largest amount of particles collected was for the 60% sand 40% PFA mix with NW8 geotextile. The PFA test samples showed less than 500 g/m^2 with all geotextile

samples. Figure 5.18 shows that not a well-defined relationship exists between the O_{90}/d_{30} ratio and mass of particles collected.

Table 5.13 Broadly-graded soils: Mass of soil particles collected after each test

Geotextile	**Soil**	**O_{90}/d_{85}**	**O_{90}/d_{50}**	**O_{90}/d_{30}**	**O_{90}/d_{15}**	**Mass of Soil Particles Collected (g/m^2)**
NW20	85% Sand 15% PFA	0.18	0.32	0.44	1.27	125
F1200M	80% Sand 20% PFA	0.16	0.29	0.40	2.00	259
NW20	80% Sand 20% PFA	0.18	0.33	0.47	2.33	290
NW8	80% Sand 20% PFA	0.32	0.57	0.80	4.00	310
F1200M	70% Sand 30% PFA	0.13	0.20	0.23	4.00	143
F1200M	60% Sand 40% PFA	0.18	0.38	1.76	7.50	300
NW20	60% Sand 40% PFA	0.21	0.44	2.06	8.75	480
ST170	60% Sand 40% PFA	0.21	0.44	2.06	8.75	370
NW8	60% Sand 40% PFA	0.35	0.75	3.53	15.00	2707
NW20	40% Sand 60% PFA	0.25	1.35	5.00	14.00	275
F1200M	PFA	1.11	4.00	10.00	60.00	392
NW20	PFA	0.95	4.67	11.67	70.00	450
ST170	PFA	1.11	4.67	11.67	70.00	410

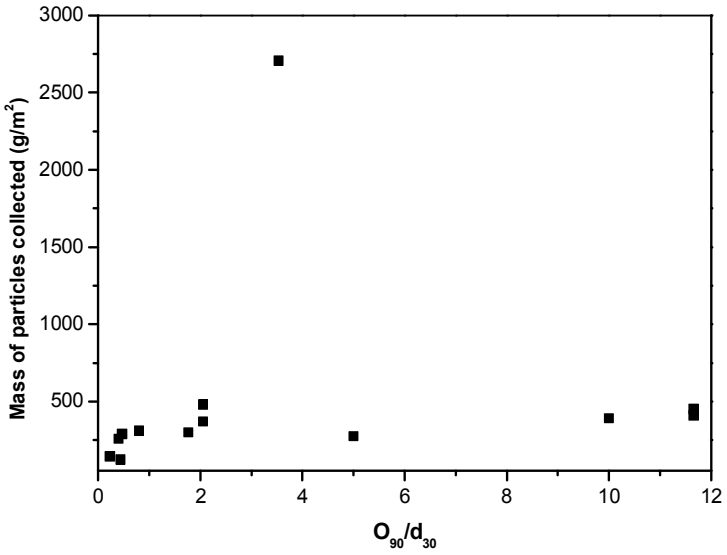


Figure 5.18 Relationship between O_{90}/d_{30} and mass collected for broadly-graded soils

5.4.4.2. Gradation of Particles Washed Out

The gradation of soil particles washed out, d_{90p}, is given in Table 5.14. The d_{90p} is much lower than the O_{90} of geotextile samples. The highest d_{90p} was computed for the 60% sand 40% PFA samples. The lowest d_{90p} was computed for PFA samples. For every soil sample, the d_{90p} increased with increasing O_{90}. The effect of d_{90p} on the filtration performance is explained in Chapter 7 (Section 7.3.1).

Table 5.14 Broadly-graded soils: d_{90p} of washed out particles

Geotextile	O_{90} µm	Soil Type	d_{90p} µm
NW20	70	85% Sand 15% PFA	25
F1200M	60	80%Sand 20%PFA	15
NW20	70	80%Sand 20%PFA	17
NW8	120	80%Sand 20%PFA	22
F1200M	60	70% Sand 30%PFA (Gap graded)	16
F1200M	60	60%Sand 40%PFA	11
NW20	70	60%Sand 40%PFA	34

Geotextile	O_{90} µm	Soil Type	d_{90p} µm
ST170	70	60%Sand 40%PFA	27
NW8	120	60%Sand 40%PFA	35
NW20	70	40%Sand 60%PFA	16
NW20	70	PFA	17
ST170	70	PFA	15
F1200M	60	PFA	13

5.4.4.3. Pre and Post-Test Gradation

The pre- and post-test gradations of the broadly-graded soils are given in Appendix D. The gradations are summarized in terms of D_{85}, D_{50}, D_{30} and D_{15} in Table 5.15. For the 85% sand 15% PFA with NW8 test sample, no obvious change in post-gradation of soil was observed for soil samples in the soil-geotextile interface (0-8mm) and within soil (25-40mm) region. The gap-graded test sample showed a slight increase in D_{15} for the 0-8mm zone which suggests washing of fines through geotextile sample. The 40% sand 60% PFA sample showed a slight increase in D_{15} for both 0-8mm and 25-40mm which shows washing of soil particles through geotextile sample.

The post-test gradation test samples with 80% sand 20% PFA showed a slight decrease in D_{15} for both 0-8mm and 25-40mm, except with the NW20 geotextile sample for which the pre- and post-gradations remained the same. On the other hand, the 60% sand 40% PFA samples showed a change in D_{15} as well as D_{30}. The post-test gradation of 60% sand with NW20 resulted in a large decrease in D_{30} and D_{15}. The other test samples showed higher values of D_{30} and D_{15} for 0-8mm zone which indicated washing of soil particles through geotextile samples.

The post-test gradations of test samples with PFA showed a variation in D_{50}, D_{30} and D_{15}. All the test samples showed an increase in post-test D_{50}, D_{30} and D_{15} values for the 0-8mm zone which is due to the washing of PFA particles into or through the geotextile samples.

Table 5.15 Broadly-graded soils: Summary of pre and post-test gradation

Geotextile	**D_{85}**		**D_{50}**		**D_{30}**		**D_{15}**	
	0-8 mm	**25-40 mm**	**0-8 mm**	**25-40 mm**	**0-8 mm**	**25-40 mm**	**0-8 mm**	**25-40 mm**
85% Sand 15% PFA	**0.400**		**0.220**		**0.160**		**0.055**	
NW20	0.400	0.400	0.220	0.220	0.160	0.160	0.055	0.030
80% Sand 20% PFA	**0.380**		**0.210**		**0.150**		**0.030**	
F1200M	0.380	0.380	0.210	0.210	0.130	0.150	0.020	0.020
NW8	0.380	0.380	0.210	0.210	0.150	0.150	0.030	0.035
NW20	0.380	0.380	0.210	0.210	0.150	0.150	0.025	0.025
70% Sand 30% PFA	**0.470**		**0.300**		**0.260**		**0.015**	
NW20	0.470	0.470	0.300	0.300	0.260	0.260	0.022	0.012
60% Sand 40% PFA	**0.340**		**0.160**		**0.034**		**0.008**	
F1200M	0.340	0.340	0.160	0.160	0.060	0.018	0.015	0.006
NW20	0.340	0.340	0.160	0.160	0.015	0.010	0.003	0.001
ST170	0.340	0.340	0.160	0.160	0.040	0.035	0.012	0.008
NW8	0.340	0.340	0.160	0.160	0.090	0.030	0.030	0.009
40% Sand 60% PFA	**0.285**		**0.052**		**0.014**		**0.005**	
NW20	0.285	0.285	0.052	0.052	0.017	0.017	0.006	0.006
PFA	**0.063**		**0.015**		**0.006**		**0.001**	
F1200M	0.063	0.063	0.015	0.010	0.008	0.004	0.003	0.001
NW20	0.063	0.063	0.018	0.008	0.007	0.003	0.003	0.001
ST170	0.063	0.063	0.016	0.016	0.007	0.006	0.003	0.003

5.4.4.4. Microscopic Images of Geotextile Samples

Figure 5.19 shows microscopic image of NW20 geotextile sample after static and cyclic testing with 85% sand 15% PFA soil. A very few clogged particles were observed inside the geotextile sample. The geotextile samples with 80% sand 20% PFA soil showed some more clogged particles (Figure 5.20).

The geotextile samples with 60% sand 40% PFA soil showed more clogging than with 80% sand 20% PFA soil (Figure 5.21). This shows the internal instability of 60% sand 40% PFA mix to loose fine particle through voids of the coarse particles (see Section 5.4.3). This can also be supported by the partial clogging values (Table 5.16). The clogged particles were observed to be fine particles and no coarse particles were observed. The F1200M sample showed less clogging as compared to ST170 and NW8. The clogging sites were mostly at the middle and lower part of the geotextile samples where the fibers are congested. The microscopic images of geotextile samples with PFA did not show serious clogging (Figure 5.22). The partial clogging values showed large partial clogging values for NW20 and ST170 with PFA. The F1200 geotextile with PFA showed less partial clogging which is due to the large mass per unit area of the geotextile.

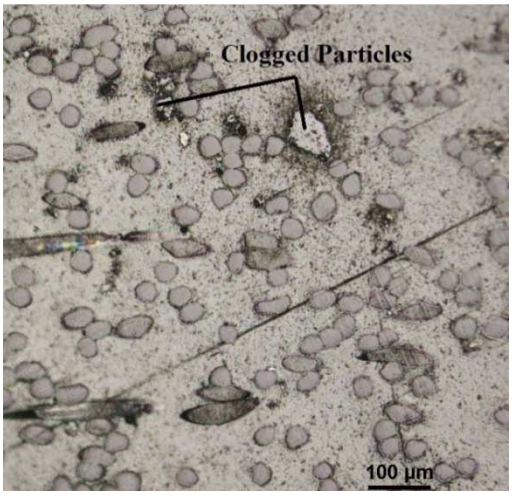
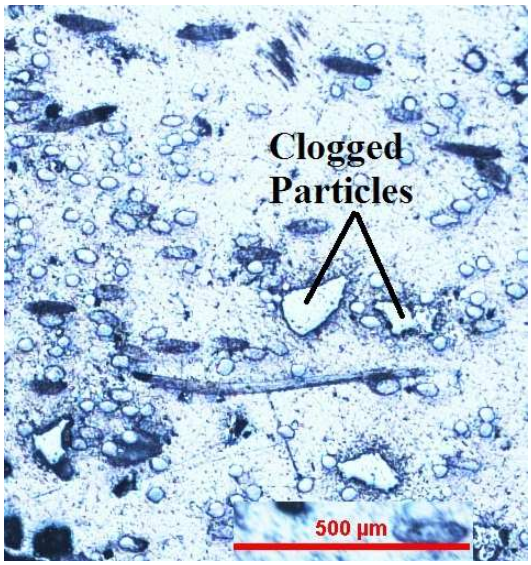
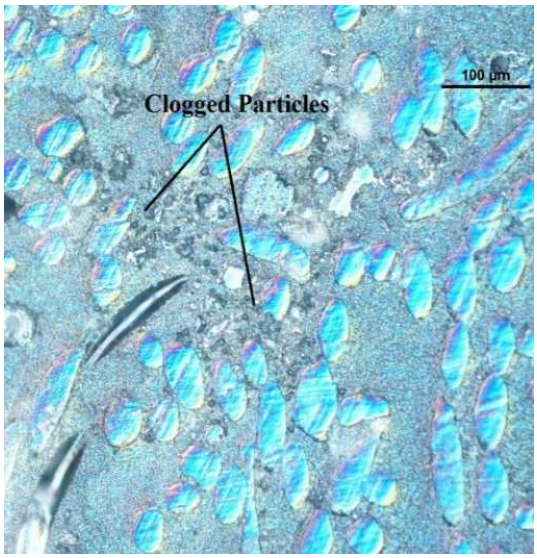


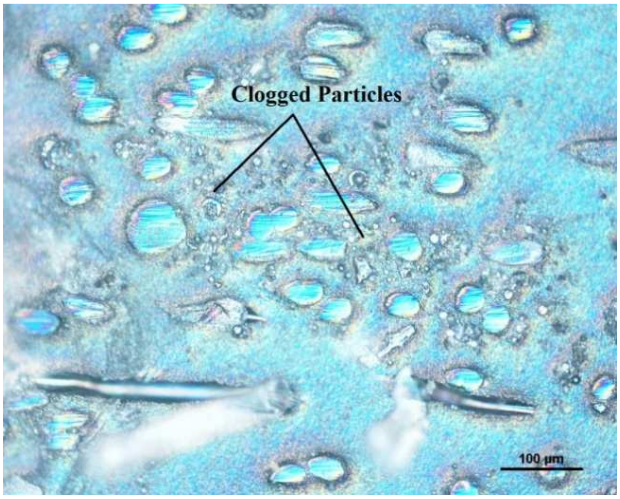
Figure 5.19 Microscopic images of geotextile samples after filtration test with 85% sand 15% PFA mix



(a) NW20

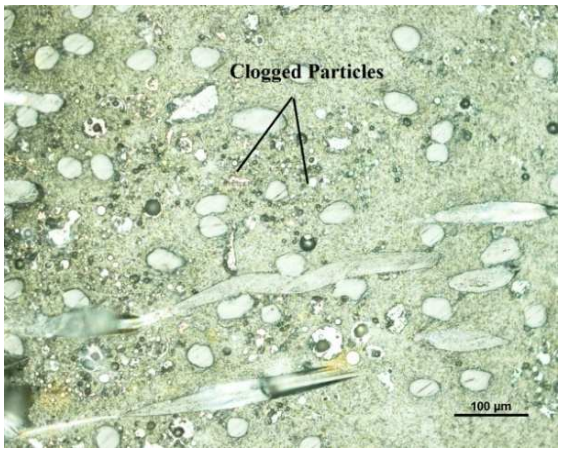


(b) F1200M

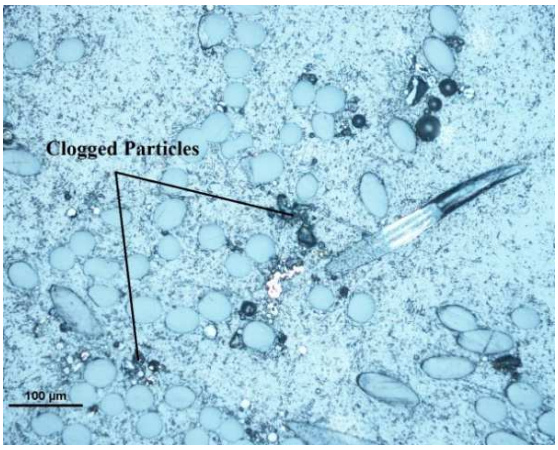


(c) NW8

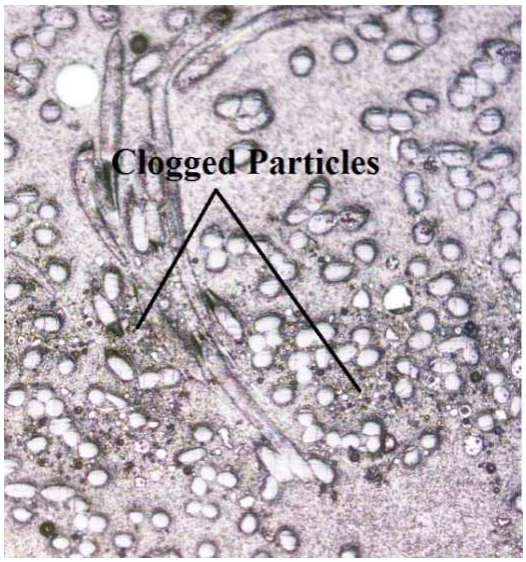
Figure 5.20 Microscopic images of geotextile samples after filtration test with 80% sand 20% PFA



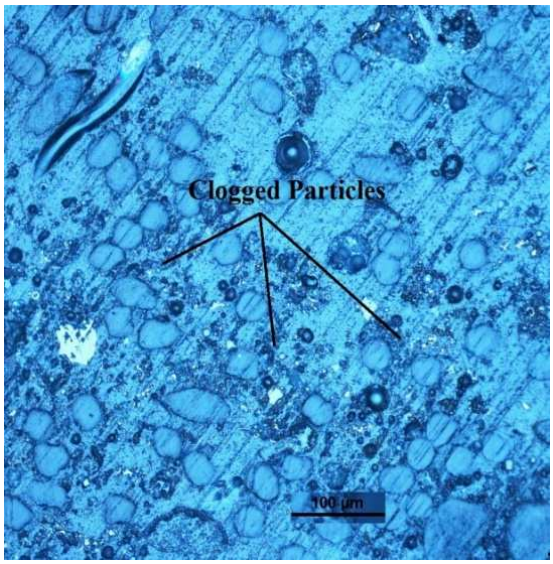
(a) NW20



(b) F1200M

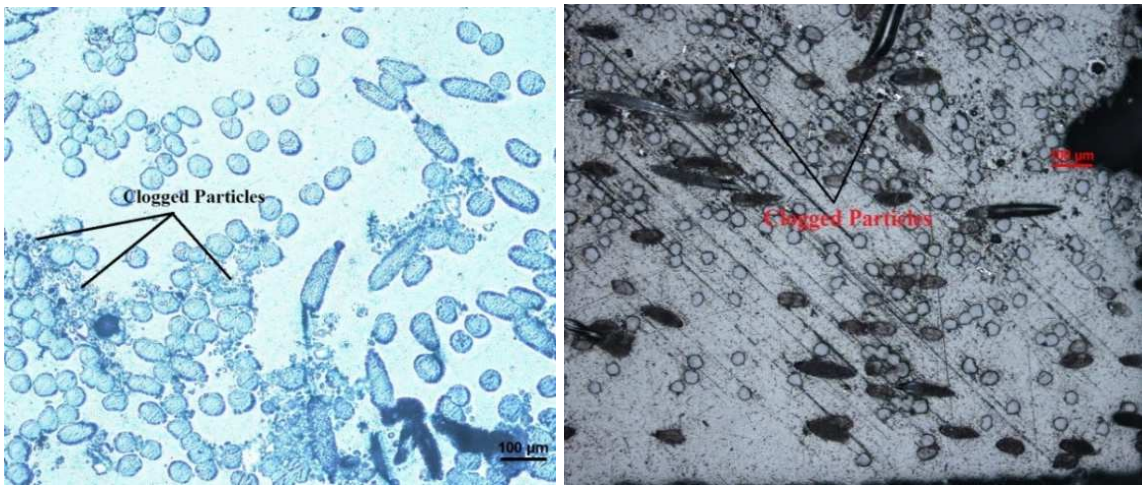


(c) ST170

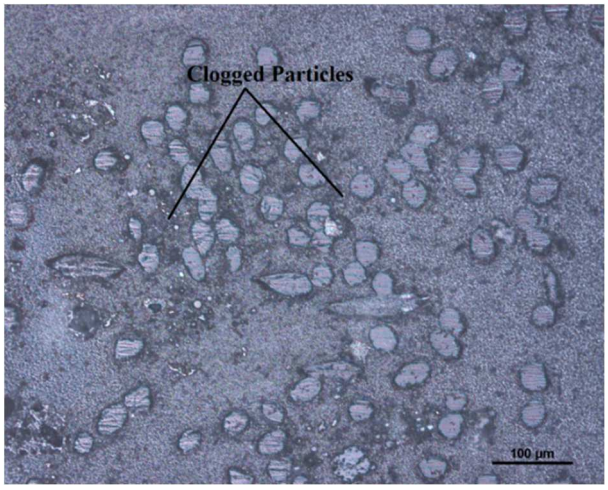


(d) NW8

Figure 5.21 Microscopic images of geotextile samples after filtration test with 60% sand 40% PFA



(a) F1200M (b) NW20



(c) ST170

Figure 5.22 Microscopic images of geotextile samples after filtration test with PFA

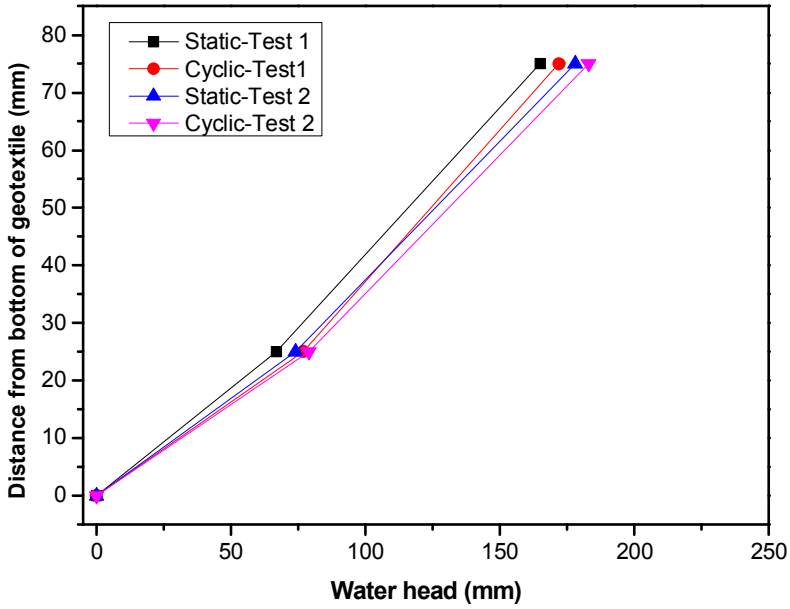
Table 5.16 Broadly-graded soils: Partial clogging of geotextiles

Geotextile	Soil Type	Mass/Area (Geotextile) (g/m^2)	Mass of Soil Retained Inside Geotextile	Partial Clogging 'λ'
NW20	85% Sand 15% PFA	250	78	0.31
F1200M	80%Sand 20%PFA	1200	360	0.30
NW20	80%Sand 20%PFA	250	220	0.88
NW8	80%Sand 20%PFA	120	120	1.00
F1200M	70% Sand 30%PFA	1200	888	1.33
F1200M	60%Sand 40%PFA	1200	425	0.35
NW20	60%Sand 40%PFA	250	188	0.75
ST170	60%Sand 40%PFA	237	241	1.02
NW8	60%Sand 40%PFA	120	187	1.56
NW20	40%Sand 60%PFA	250	327	1.31
NW20	PFA	250	385	1.54
ST170	PFA	237	425	1.79
F1200M	PFA	1200	800	0.67

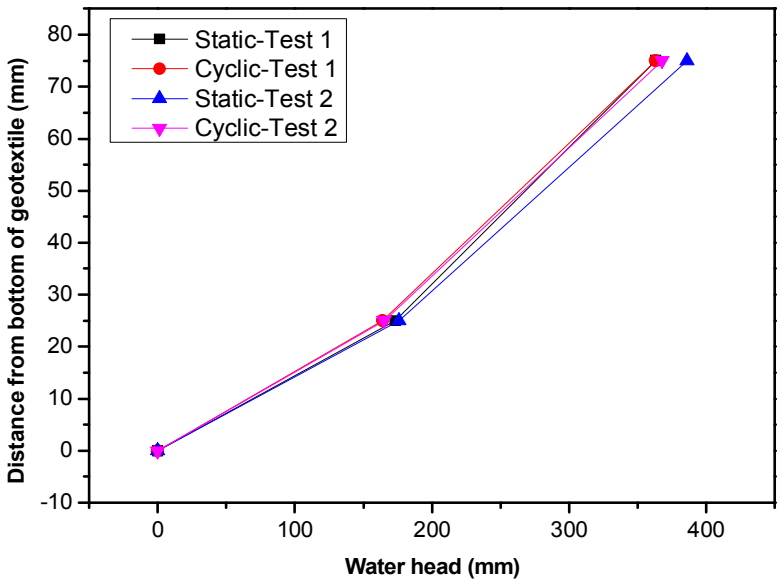
5.5. Test Repeatability

To assess the experimental repeatability and to check whether the test results are reliable with respect to sample preparation and quality of data, two sets of duplicate tests were performed. Two tests were performed on medium sand with NW20 geotextile; while other two tests were performed using 80% sand 20% PFA with F1200M. The repeatability of the performance tests is discussed below, with reference to GR values, permeability and mass of passing through particles.

The water head distribution of medium sand with NW20 (Figure 5.23a) and the 80% sand 20% PFA with F1200M (Figure 5.23b) is shown below. The water head distribution is almost similar for both set of tests, showing that the tests are repeatable.



(a) Medium Sand and NW20



(b) 80% sand 20% PFA and F1200M

Figure 5.23 Repeatability Tests: Water head distribution

It is evident from the results shown in Table 5.17 that the GR, the k_{sys}, and the mass of particles collected were all in good agreement, showing that the dynamic gradient ratio test is repeatable and the results are reliable.

Table 5.17 Repeatability Tests

Geotextile	**Soil**	**Mass of particles collected (g/m^2)**	**GR**		**k_{sys} (m/s)**	
			Static	**Cyclic 1**	**Static**	**Cyclic 1**
NW20	Medium Sand	220	1.27	1.51	3.60 ($x10^{-5}$)	3.72 ($x10^{-5}$)
NW20	Medium Sand	234	1.35	1.40	3.71 ($x10^{-5}$)	3.73 ($x10^{-5}$)
F1200M	80% Sand 20% PFA	259	1.38	1.25	5.56 ($x10^{-7}$)	6.18 ($x10^{-7}$)
F1200M	80% Sand 20% PFA	236	1.27	1.22	5.93 ($x10^{-7}$)	6.02 ($x10^{-7}$)

5.6. Test without Geotextile

To see whether geotextile samples are effective in retaining soil particles, one test was performed without a geotextile sample in the modified gradient ratio test apparatus. The soil sample was placed on a cuspated core which had pore openings of 2mm. The water head distribution of the test is shown in Figure 5.24. It can be seen from the water head distribution that the rate of head loss across soil-base interface is more than the rate of head loss within the soil. The Cyclic 1 stage was run just for 3000 cycles due to continuous decrease in head loss across the soil-base interface.

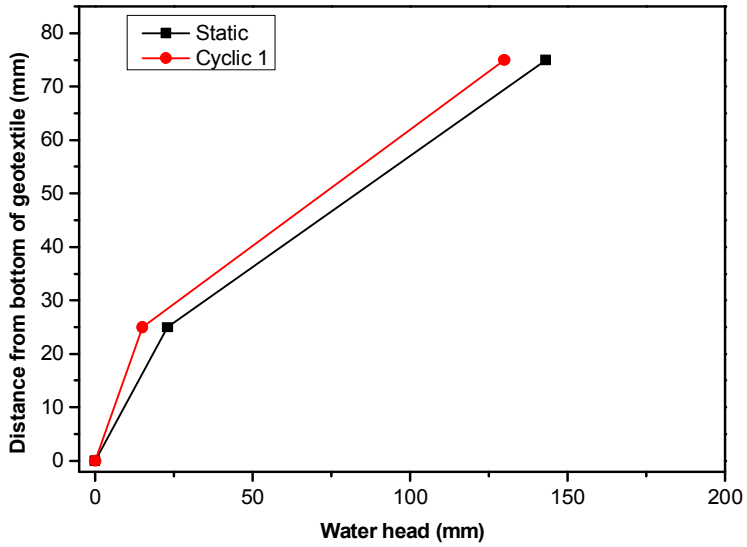


Figure 5.24 Test without geotextile: Water head distribution

It is evident from the results shown in Table 5.18 that the GR value is quite a lot less than the GR values with geotextile samples (see Table 5.1). The amount of soil particles collected was 2315 g/m^2 which suggest that geotextile samples used were effective in retaining the soil particles. The pore size 'O_c' in Table 5.18 shows the opening sizes of cuspated core.

Table 5.18 Test without geotextile

Soil	**O_c/d_{85}**	**Mass of particles collected**	**GR**	
			Static	**Cyclic 1**
Medium Sand	4.77	2315	0.38	0.26

5.7. Summary

Twenty tests were performed under the static and cyclic GR test program for different soil/ geotextile combinations; seven tests for narrow graded soils and thirteen tests for broadly-graded soils. Two tests were performed to assess the experimental repeatability

of the modified GR apparatus. One test was performed without geotextile to observe the effectiveness of geotextile samples in retaining soil particles.

The narrow graded soils did not show any continuous increase or decrease in GR values for static and cyclic stages. One broadly-graded sample lost more particles than all the other samples. Except two 60% sand 40% PFA test samples, the broadly-graded soil behaved stable in terms of GR during the static stage. One 60% sand 40% PFA sample and one PFA test sample showed a continuous decrease in cyclic GR.

Inspection of repeatability tests for narrow and broadly-graded soils showed that the modified gradient ratio test is repeatable and reliable. One filtration test without a geotextile sample showed that geotextiles are effective in retaining soil particles.

Chapter 6

Evaluating Pore Sizes of Non-Woven Geotextiles

6.1. Introduction

Geotextile filter design criteria are based on the ratios of geotextile pore sizes to soil grain sizes. The retention criterion is usually designed on the basis of Apparent Opening Size (AOS) of a geotextile which is determined by ASTM method (ASTM D4751)**.** Carroll (1983) indicated that, although AOS may provide satisfactory results in terms of retention and permeability, it doesn't give an idea about the clogging potential of geotextiles. AOS retains the larger soil particles but the finer particles may clog the filter. This fact is also explained by Christopher and Holtz. (1985) who suggested that clogging of a geotextile will not occur if the majority of geotextile pore openings are large enough to allow the smaller soil particles to pass through. They provided a criterion on the basis of a minimum pore size that would allow fine particles to pass through the filter while retaining the larger soil particles.

Giroud (1996) indicated that it is the constriction size which affects the filtration performance of geotextiles. Constriction size (throat size) is the minimum pore size of a pore channel. Every pore channel has one constriction size which may be located at any depth in the pore channel. A soil particle must be smaller than the constriction size

in a filtration path in order to pass through the filter. Fischer et al. (1990) developed filter design criteria on the basis of constriction pore size distribution of non-woven geotextiles.

Currently, there are many techniques available to find the pore size distribution (PSD) of geotextiles. A thorough discussion of each of these methods along with the advantages and disadvantages is described in Section 2.7.1. The two commonly used techniques to find PSD of geotextiles are dry sieving and bubble point test. Dry sieving is commonly used by geosynthetic manufacturers because there is an ASTM standard (ASTM D4751) available to carry out this test. However, due to several problems associated with this method, this method may not give accurate results. Dry sieving finds the near-largest opening size of geotextile but it cannot find the constriction sizes of pore channels in geotextiles. On the other hand, bubble point finds the constriction sizes of pores indirectly by using the Washburn equation (Washburn, 1921) which assumes pores to be cylindrical. However, the measured air flow rates depend on pore opening area instead of its size.

Image analysis is an alternative method to find the pore sizes and constriction sizes of geotextiles. Image analysis measures the actual distance between geotextile fibers (Bhatia et al., 1993). The two-dimensional (2-D) pore structure of woven geotextile makes image analysis suitable for finding its PSD. However, image analysis requires three-dimensional (3-D) information for non-woven geotextiles in order to find the PSD because of the fiber's arrangement is in all directions. The principle of stereology shows that the 3-D structure of materials can be studied from 2-D sections from thin foils (Underwood, 1979). If a limited number of test planes are cut parallel and uniformly distributed, then the area of test planes give the volume of the specimen (Kuo & Frost, 1996). Using the principle of stereology, Serra (1982) showed that 2-D section images cut parallel could give

information about the 3-D structure of a material. This concept was used by Aydilek et al. (2005) who developed an image based probabilistic model 'CONS' to measure the constriction sizes of non-woven geotextiles. Planar and cross-sectional thin sections of geotextile specimens were prepared according to the procedures used for preparing thin sections of soil and rock. The images of thin sections were captured using an optical light microscope to obtain the 3-D structure of non-woven geotextiles. Pore sizes in each cross-sectional image were determined using the image processing software IMAQ. A probabilistic description of pore channels in geotextiles was constructed using Markov chain process and constriction sizes were measured. The CONS method takes into account the randomness of fibers in non-woven geotextiles but its disadvantage is tedious specimen preparation procedure. Moreover, the procedure to prepare the thin sections of specimens is destructive (ASTM-D18, 1970; Marr & Fairhurst, 1999). There is still a need for development of a non-destructive approach to measure the actual pore sizes along the entire thickness of non-woven geotextiles than current available techniques.

6.2. Scope of the Chapter

This chapter focusses on evaluating the pore sizes of four non-woven geotextile specimens with different PSD techniques. The chapter introduces a bubble analysis technique to find the 2-D PSD of geotextile specimens. Also, a new method to determine the 3-D constriction sizes of non-woven geotextiles from X-ray CT images is introduced. The digital image concept and image processing methods for the 2-D image analysis and 3-D constriction size measurement of geotextile specimens is explained in this chapter. The chapter also seeks to explain the clogging mechanism of two clogged geotextile specimens, NW20 and ST170 clogged with pulverized fuel ash (PFA), by visualizing the different 3-D cross-sections of X-Ray CT images. Finally, the chapter compares the 3-D

constriction sizes C_{95} and C_{90} with the pore sizes measured from 2-D image analysis, mercury intrusion porosimetry, manufacturer's reported O_{90} values, and pore sizes calculated from theoretical equations. The difference in pore sizes from different methods are explained in detail and conclusions drawn.

6.3. Image Analysis Technique

Image analysis is considered to be a reliable method to measure the PSD of geotextiles. Image analysis involves obtaining useful information from images by means of digital image processing techniques. The different steps in digital image analysis techniques are image acquisition, image processing and image analysis.

The first step in image analysis is image acquisition. Image acquisition in image processing is the action of extracting an image from some source, usually a hardware-based source. Digital cameras, electron microscopes, scanners, video cameras and X-ray CT are the common sources to capture images. It is always the first stage because, without an image, no processing is possible.

The second stage in image analysis is image processing. Image processing is a sequence of processes applied on a single image or a set of images, with the aim of accomplishing some purpose. Image processing is necessary to suppress unwanted information, extract necessary elements, or improve image data by enhancing the image features which are important for further processing. Image processing consists of algorithms mostly performed by means of computers and suitable software. Application of different image processing algorithms depends on the specific job. (Wojnar, 1998).

The last step in digital image analysis techniques is image analysis itself which transforms the image data to produce some information representing a description or a decision. The

information can then be processed statistically or used to generate graphs and to be interpreted.

6.4. Two-Dimensional PSD

Image analysis has been previously used to measure the 2-D PSD of non-woven geotextiles from cross-sectional images (Elsharief and Lovell, 1996, Bhatia and Smith, 1996). The 2-D analysis is performed either on a 2-D projection of the whole stack, or by analysing all the slices one by one. In this study, image analysis was performed on individual slices. The purpose of finding the 2-D PSD of non-woven geotextiles was to compare the 2-D PSD with the pore sizes measured from other techniques.

A new approach has been developed to find the 2-D pore size distribution of non-woven geotextile specimens from cross-sectional images. Microscopic images of geotextile samples were taken and analysed using freely available ImageJ software. The two-dimensional bubble analysis is a simple and reliable approach which works by analysing, one by one, images in a stack of 2-D images. For each type of geotextile, the method provides an accurate estimate of the different pore sizes by fitting circles into the pore zones of geotextiles. The main stages for 2-D image analysis are presented in Figure 6.1. Detailed explanations of these stages are discussed in the following sections.

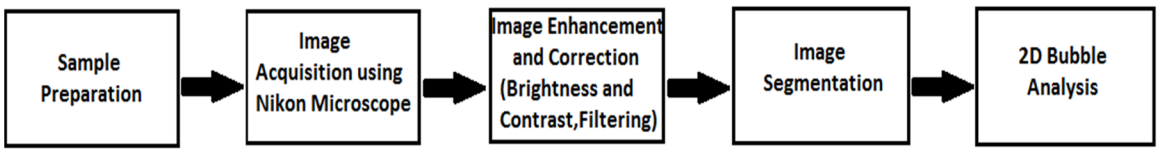


Figure 6.1 Different stages to measure 2-D PSD of geotextiles

6.4.1. Sample Preparation

Scanning Electron Microscopy (SEM) photographs were used in the past (Praprahan, 1989) to find the PSD of geotextiles by using an image analyser. Elsharief and Lovell

(1996) attempted to measure the PSD of geotextiles from SEM photographs but the depth and shading effects in SEM photographs made it difficult to find the surface pore sizes.

In this study, efforts were first made to use SEM images to find the planar pores at different depths into the geotextiles. The scattered electron method was used to find the different pore sizes from SEM images. The images were capable of showing only the top fibers and it was too difficult to find the pore sizes through the depth of geotextile specimen (Figure 6.2). It was necessary to see the fiber's distribution throughout the thickness of filter to find the constriction sizes which are responsible for filter clogging. Another approach called Back Scattered Electron (BSE) method was used in the SEM machine and SEM images of geotextile sample were taken at different depths (Figure 6.3). The solid (coloured) fibers show the fibers at the given depth while the dark fibers show the fibers above the given depth. It is difficult to find the pore sizes when images are taken at greater depths because it becomes difficult to differentiate between solid and dark fibers. Therefore, this method was considered unsuitable for determining the PSD of geotextile specimens.

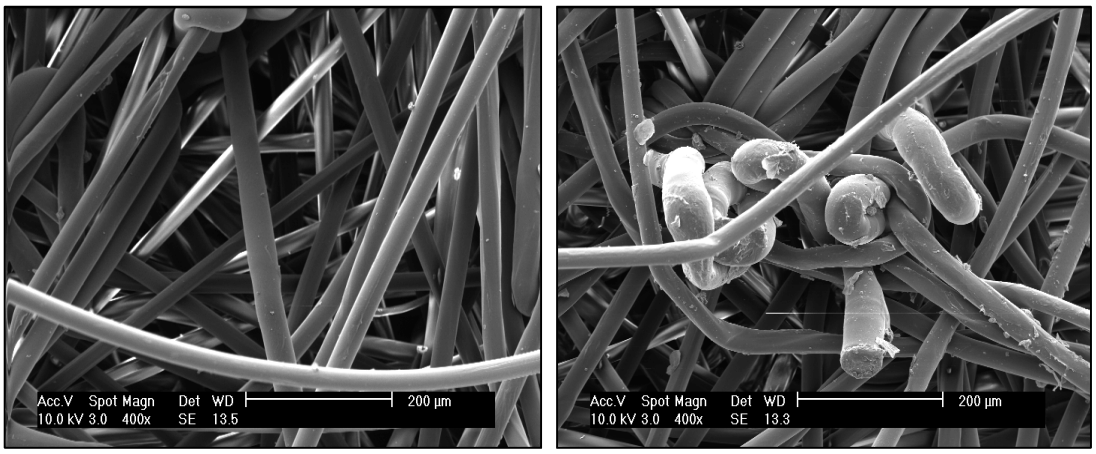
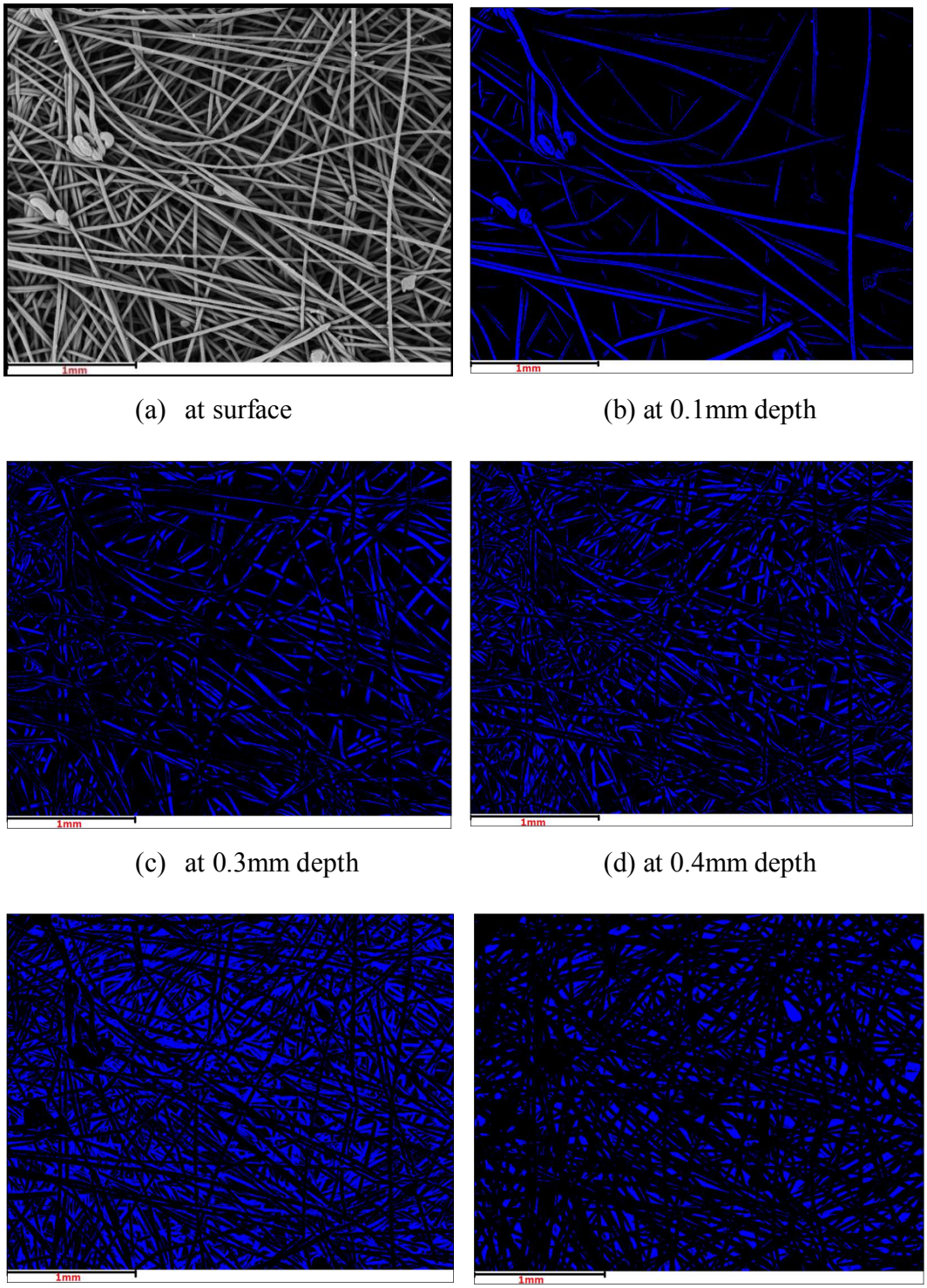


Figure 6.2 SEM Images of geotextile specimen using scattered electron method



(a) at surface (b) at 0.1mm depth

(c) at 0.3mm depth (d) at 0.4mm depth

(e) at 0.5mm depth (f) at 0.8mm depth

Figure 6.3 SEM images of NW8 geotextile specimen (1.2mm thickness) at different depths using back scattered method

The next step was to find a method which is more suitable for studying the internal structure of geotextiles. Also, it was necessary to measure the pore size variations along

the depth of geotextiles. To achieve this objective, the procedure used for preparing thin sections of soil and rock was considered more suitable for preparing geotextile specimens. The same procedure was followed as for clogged geotextile specimens, as explained in Section 4.2.6. Preparation steps involved epoxy-resin impregnation, grinding and polishing. Vertical sections of impregnated geotextile specimens were prepared. The same process of grinding and polishing were performed again and again on the same specimen to take images at 50µm spacing of depth through the geotextile's height.

6.4.2. Image Acquisition

Image acquisition is the most important step because it is always necessary to get a good quality image. High quality images of the cross-section of impregnated geotextile specimens were taken using a light microscope Nikon LV100ND (Figure 6.4). The cross-sectional image consists of rounded fibers and elongated fibers, depending on whether fibers were cut laterally or longitudinally. A detailed procedure of the image acquisition using a light microscope was given in the Section 4.2.6. Microscopic images were taken at 50µm spacing through the geotextile's height by repeating the grinding, polishing and image acquisition steps.

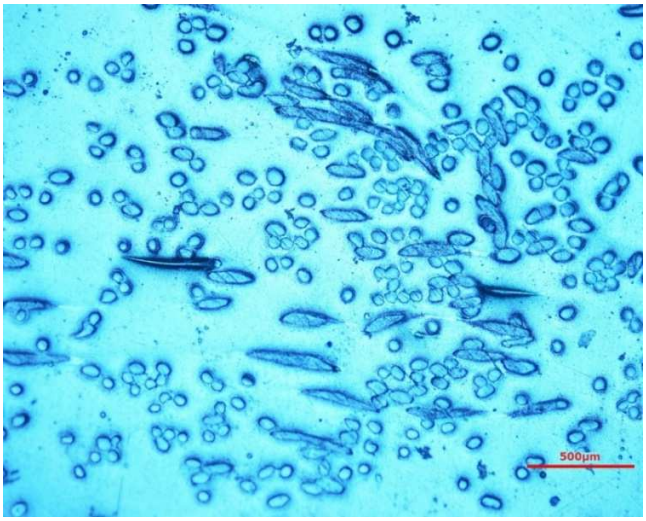


Figure 6.4 Microscopic image of geotextile specimen using Nikon microscope

6.4.3. Image Enhancement and Correction

The next step after image acquisition is image enhancement and correction using ImageJ. This stage is the key to obtaining good quality images in order to get better segmentation results. Two simple functions; brightness and contrast, and filtering were applied to grey images to increase the image enhancement. No geometric transformation was applied to the images as there was no need to change image size, image rotation or scaling. Images were converted to 8-bit grey before applying image processing techniques. 8-bit images have 0-256 grey levels which are sufficient for most applications. In this representation 0 denotes a black pixel while 256 represent a white pixel.

6.4.3.1. Brightness and Contrast

Brightness and contrast functions are helpful in visualization of images. Since brightness and contrast might cause data loss, a normalization function was used which is a modification of brightness and contrast. Normalization was applied to all images to get the same brightness and contrast for all images. Figure 6.5 shows a geotextile specimen image before and after applying normalization.

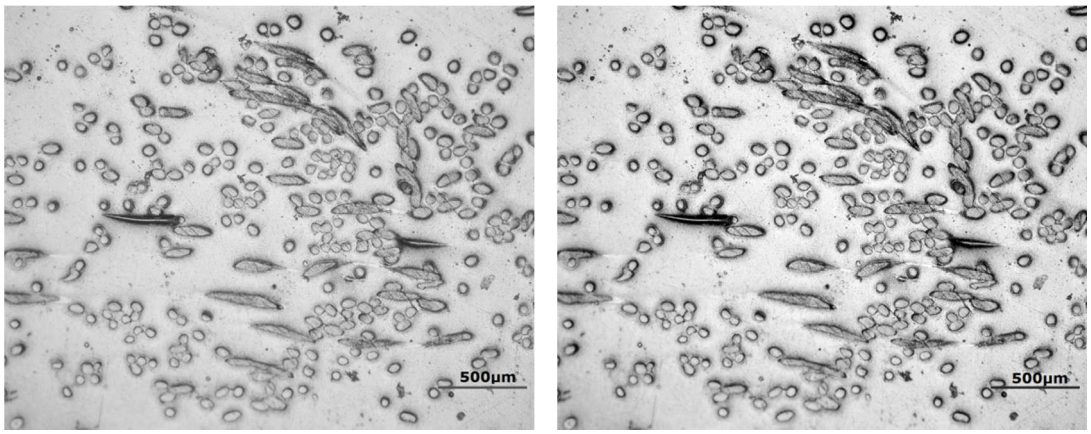


Figure 6.5 8-bit grey image before (left) and after (right) normalization

6.4.3.2. Filtering

Filtering reduces the noise in images which may be due to scratches left after grinding in impregnated specimen. Although there are many types of filters, the two simplest filters were applied to the normalized image i.e. smoothing filter and median filter (Figure 6.6). Smoothing filter works well for less noisy images while median filter is recommended for heavily noisy images. Since the normalized image illustrated is not too noisy, both filters work well to reduce the noise. The median filter was found to give smoother images as compared to the smoothing filter. The median filter replaces the value of each pixel in the image with the median of the neighbouring pixel values. The resulting image after median filter is a smoothed grey scale image with clear distinction between geotextile fibers and pores. The median filter was applied to all the images in the 2-D analysis.

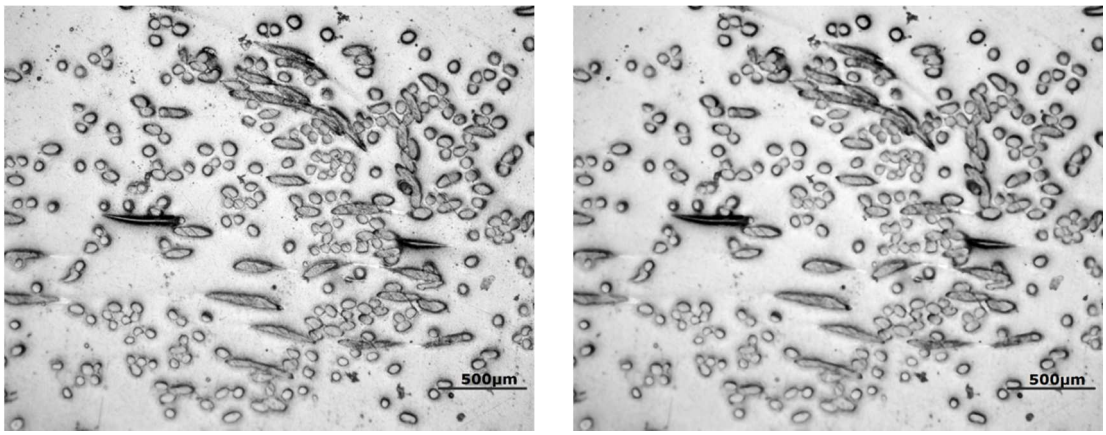
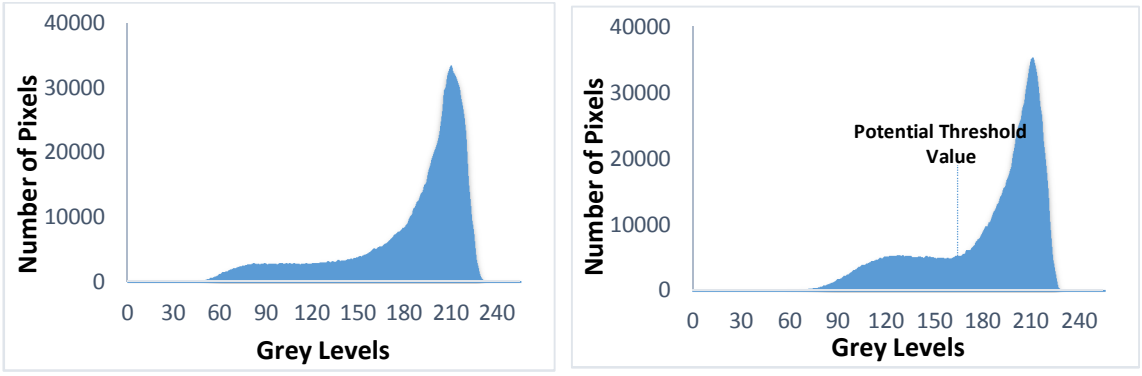


Figure 6.6 8-bit grey image after smoothing filter (left) and median filter (right)

6.4.4. Image Segmentation

Image segmentation subdivides an image into regions or categories and extracts object of interest from the background. Thresholding is the simplest and most common method to achieve segmentation. A proper thresholding results in better segmentation of an image (Sonka et al., 2014). Thresholding converts a grey level image into a binary image. Binary images use less memory and allow features of the image to be more readily detected.

Pixels with grey levels below the threshold value will be classified as black and pixels with grey levels above the threshold will evaluate as white. One way of getting a suitable threshold value is to visually examine the separated region and reasonably estimate the threshold value. However, this is not the best method as it depends on human judgement which may result in errors and inconsistencies. The common method of selecting a threshold value is to analyse the histogram of grey level pixels. It is easy to get a suitable threshold value for images having a bimodal (two distinct peaks) histogram. A typical image based histogram of the grey levels is shown in Figure 6.7. It can be seen from Figure 6.7 (a) that the image histogram has one peak instead of two peaks i.e. one peak for fibers while other parts represent the background (pores). This unimodal histogram means that the contrast intensity between the background and fibers is low. It is necessary to find the point of discontinuity or valley in the histogram because it represents the boundary between the zones. One approach used for finding this boundary is to apply a Gaussian filter (Tsai, 1995). A Gaussian filter reduces the variation in pixels grey level which results in a smooth histogram for each class distribution. Figure 6.7(b) shows that after applying Gaussian filter, there is a discontinuity or a valley at the point of intersection of two overlapping distributions. That point of intersection was selected as the potential threshold value. The grey scale image was converted to a binary image after applying the threshold value, as shown in Figure 6.8.



(a) (b)

Figure 6.7 Image histograms before (a) and after (b) Gaussian filter

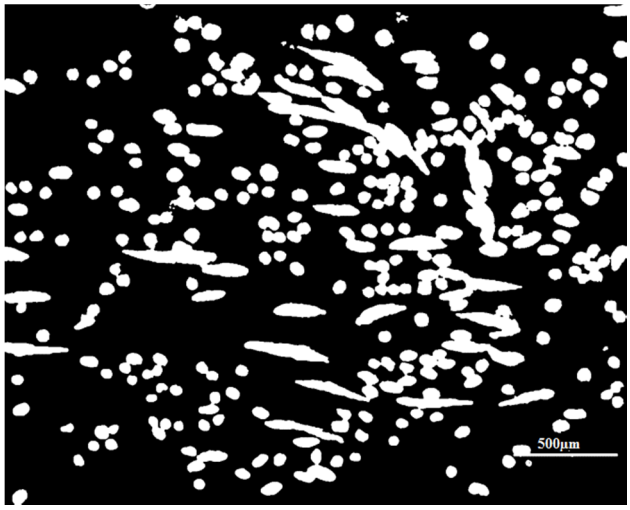


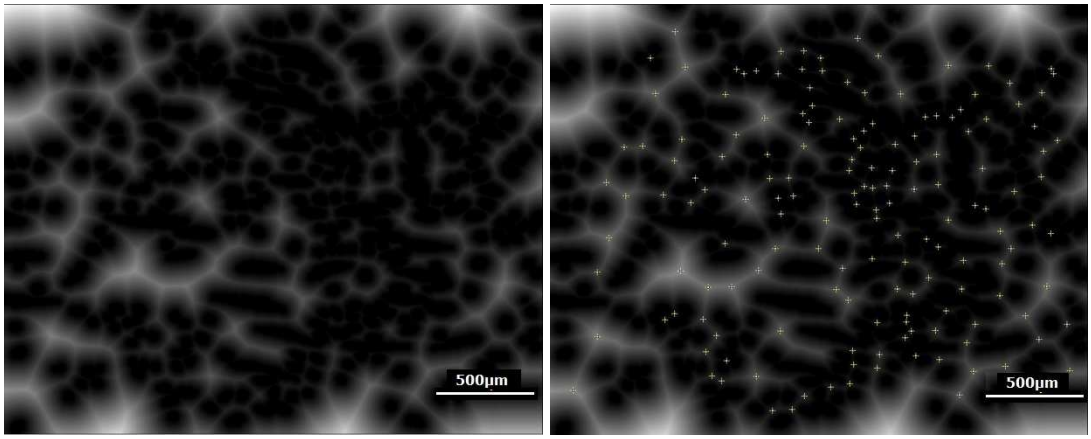
Figure 6.8 Binary image of cross-sectional image after thresholding

6.4.5. Bubble Analysis

The last stage in 2-D image analysis was to characterize the pore sizes by using the bubble analysis technique on the binary images. This technique was proposed by Münster and Fabry (2013) to find the PSD of biopolymer networks. The technique works by finding non-overlapping circles (bubbles) of maximum diameter that can be fitted into the pore zones and which cover the maximum area. The pore sizes can be taken as the diameter of the bubbles in the different zones of the image. The procedure is repeated for all slices in the stack and the 2-D PSD measured.

Bubble analysis is a fast and two-step algorithm which can be performed using ImageJ. Firstly, the binary image was transformed with the Euclidean distance map (EDM) algorithm, using the Distance Map command in ImageJ. EDM assigns each pore pixel the Euclidean distance to the nearest fiber pixel. The Euclidean distance is calculated as the square root of the sum of horizontal and vertical distances from pore pixels to the nearest fiber pixels. The EDM transformation results in a grey scale image rather than black and white, as shown in Figure 6.9. The EDM value at any pore pixel suggests the radius of the largest circle centered at that pore pixel without overlapping any fibers. The second

stage was to find the local maxima of the EDM (Find Maxima command in ImageJ). A local maximum in 2-D is a pixel whose eight neighbours have smaller values. This means that a bubble centered at a local maximum will have a larger radius than a bubble centered at any of the neighbouring pixels, without overlapping any of the surrounding fibers. Therefore, EDM values at the local maxima are the centroids of all possible 2-D bubbles. Local maxima at the edges of image were discarded to avoid boundary effects. Analysis were run on the EDM transformed images with local maxima to measure the diameters of bubbles or pores. The cumulative PSD was obtained based on the summation of pore sizes smaller than a certain pore size divided by the total summation of pore sizes. Finally, the average cumulative PSD was measured for the stack of images for each geotextile specimen.



(a) Euclidean Distance Map (EDM) (b) EDM with local maxima (yellow cross)

Figure 6.9 Bubble analysis of binary image in two steps; the black shades are fibers and white shades show pore spaces

6.4.6. Results

The 2-D PSD for various geotextile specimens measured from bubble analysis is shown in the Figure 6.10. The pore sizes of different geotextiles are in agreement with Giroud (1996) that the pore sizes along the pore channels decrease with increasing thicknesses of geotextiles. F1200M geotextile (8mm thick), having more thickness than other

geotextiles, has smaller pore sizes as compared to other geotextile specimens. The pore sizes of geotextiles increases with decreasing thickness, except for ST170. ST170 is a needle punched geotextile in which there are more chances of encountering elongated fibers in the images, as compared to NW20 geotextile. These elongated fibers are very closely spaced in some cases which results in measuring smaller pore sizes. This is the reason that ST170 has smaller pore sizes than NW20, although, the thickness of ST170 is less than NW20.

The pore sizes measured from 2-D images are not necessarily constriction sizes because the pore channel can be cut at any location. The 2-D PSD is rather image specific which depends on the location of measurement. The 2-D PSD is more useful for woven geotextiles because the pore sizes are uniform throughout the thickness. However, it is less suitable for measuring the PSD of non-woven geotextiles because of the significance of the tortuosity of the pore channels.

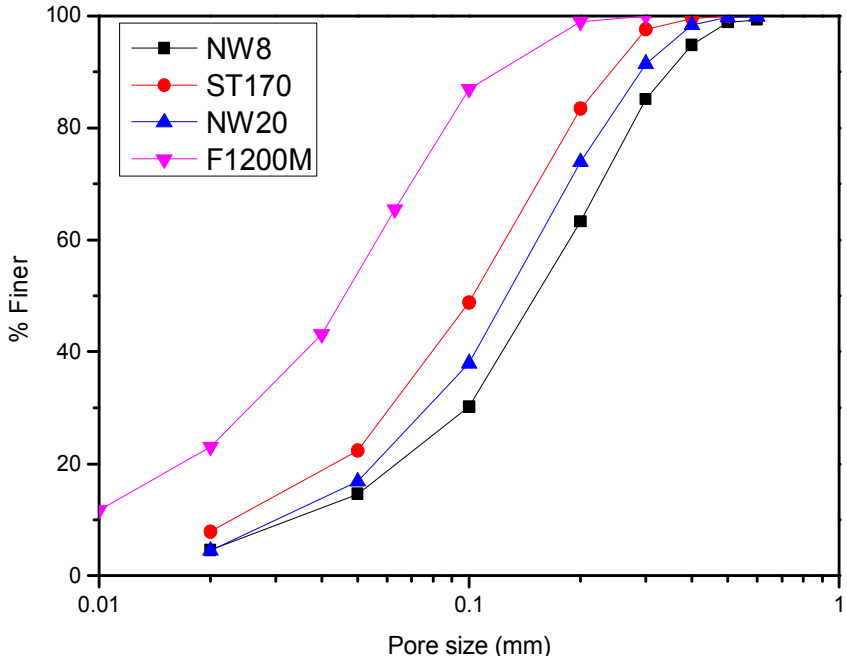


Figure 6.10 Two-dimensional PSD of different geotextiles from cross-sectional images

6.5. Three-Dimensional Constriction Size Measurement

The filtration behaviour of geotextile filters is not affected by the shape of pore channel; rather it is the least dimension or constriction of the pore channel which influences the filtration behaviour of geotextiles (Kenney et al., 1985). As discussed in the previous section, 2-D images cannot provide the true constriction sizes of non-woven geotextiles. Therefore, a new method was developed to find the 3-D constriction sizes of geotextiles. The method consists of three main stages; image acquisition from X-ray CT, processing the images using Avizo Fire software to get locations and equivalent diameters of different pores, and developing a program in MATLAB to plot pores and find the constriction sizes along pore channels. On a trial basis, X-ray images were obtained for two geotextile specimens i.e. NW20 and ST170. Both geotextiles have the same opening size reported by the manufacturer i.e. 70µm based on wet sieving method. Wet sieving only finds the largest pore opening and does not give an idea about the complete PSD. It was important to obtain the complete 3-D PSD of NW20 and ST170 and compare with each other to see if the two geotextiles will behave similarly or differently as filter material. The detailed explanation of the methodology is given in the next sections.

6.5.1. Image Acquisition

X-ray CT is a non-destructive 3-D imaging technique to visualize accurately the internal structure of solid objects by producing a series of slice images of the scanned object. X-ray CT scanning consists of an X-ray source and a detector. The technique uses the ability of X-rays from a source to pass through a rotating object from different angles and collect the X-rays at a detector. After scanning, two-dimensional slice images of the object are obtained using image reconstruction algorithms. These slice images can be stacked to generate a 3-D volume of the scanned object using computer software.

In this test program, an advanced X-Ray machine XRADIA Versa XRM-500 microscope was used for image acquisition of geotextiles. The XRM-500 X-ray machine provides non-destructive imaging of samples with little or no sample preparation. The X-ray machine is capable of accommodating large samples without loss of resolution. Specimen sizes of 10x10mm were taken as representative of the geotextiles. A spatial resolution of 0.089 pixels/µm (11.26 pixel size) provided clear features of geotextile specimens (see Figure 6.11). The 2-D X-Ray images of NW20 and ST170 are given in the Figure 6.12.

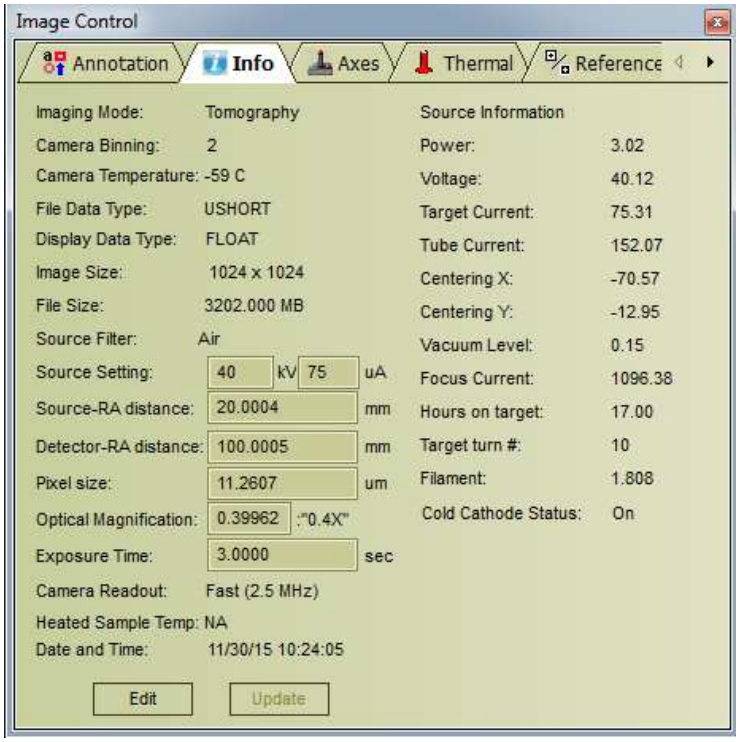


Figure 6.11 Image control information for X-ray image acquisition

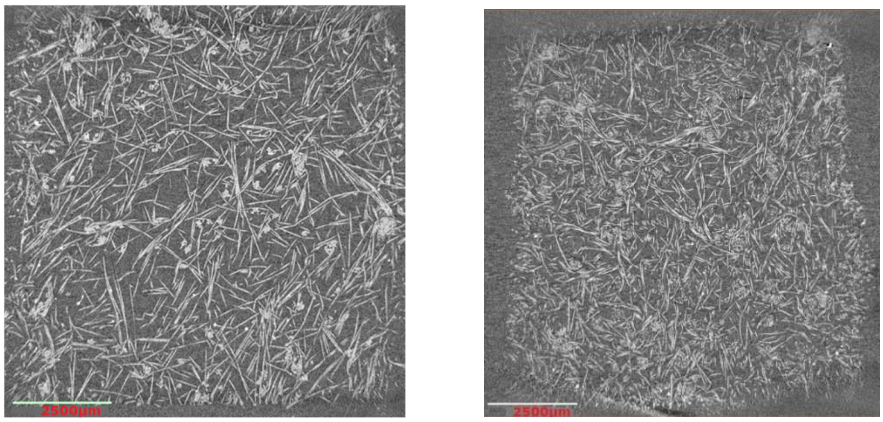
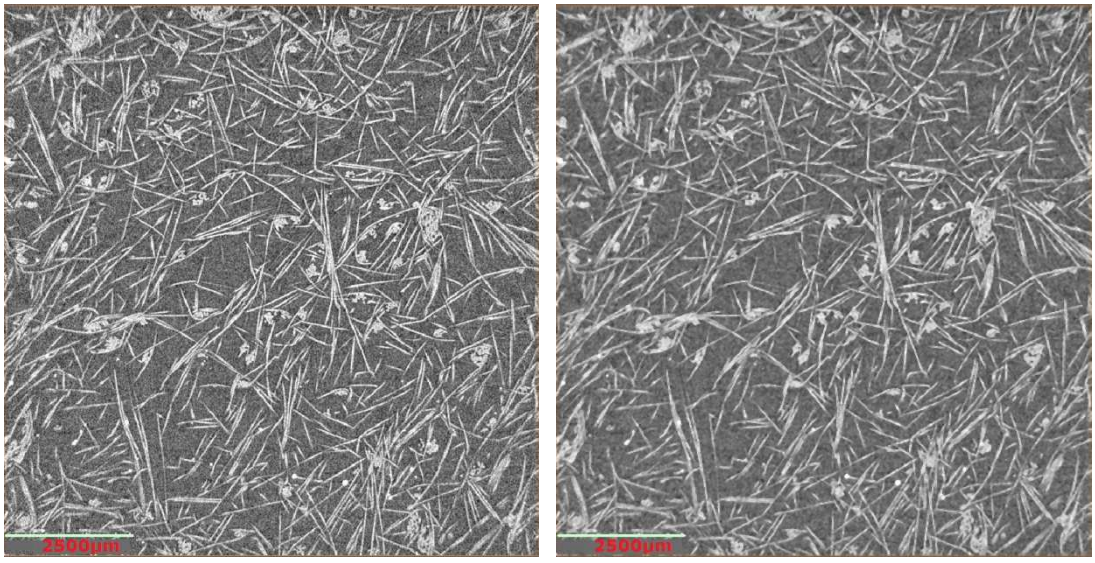


Figure 6.12 2-D slice images of NW20 (left) and ST170 (right)

6.5.2. Image Processing

Avizo Fire software was used to stack the 2-D slice images of geotextile specimens to generate a 3-D volume rendering of specimens. Avizo Fire is 3-D analysis software to process 3-D imaging data in materials science, geosciences or engineering applications. The grey scale stack images were transformed to binary images and eventual pores identified and labelled. The labelled images will be used to find pores properties i.e. pores location and their equivalent diameter. These pore properties will be used to carry out further analysis in Matlab since Avizo cannot find the constriction sizes of pore channels.

The first step was to import the 2-D grey scale images into Avizo Fire. As shown from the Figure 6.12, the boundaries of the image represent the sample holder instead of the geotextile specimen. A sub-volume was extracted from the original volume of 2-D stacked images to carry out further image processing, as shown in the Figure 6.13 (a). The median filter was applied to the stack of 2-D grey images to reduce noise in the images (Figure 6.13b).



(a) Extracted Sub-volume (b) Median filter applied

Figure 6.13 Grey images of NW20 (a) before and (b) after Median filter

The next stage was image segmentation by transforming the grey level images into binary images by thresholding. Image segmentation can be achieved by applying interactive thresholding option in Avizo. It was important to apply an adequate threshold value to the grey level images. Once again, as for the 2-D analysis, the image histogram of grey level images was found to unimodal, as shown in the Figure 6.14. Therefore the Gaussian filter was used to find a discontinuity or a valley between two distributions, by reducing the variation in the pixels. However, this time no discontinuity nor valley was observed in the histogram.

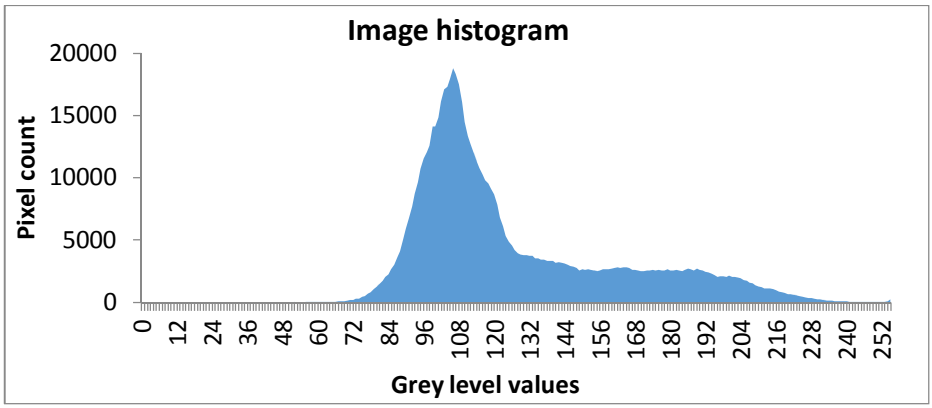


Figure 6.14 Image histogram of NW20 geotextile

There are various techniques available for selecting automatic threshold values for unimodal histograms. Some of these methods include the Kapur method, the iterative method, and also by calculating threshold values manually. The Kapur method (Kapur et al., 1985) is a popular entropy based thresholding technique for image segmentation. This technique was used to find the optimal threshold values for the grey images of NW20 and ST170 geotextile specimens. Kapur's method works by evaluating the 2-D entropies of the distribution of each threshold pair and a threshold value is selected at the point for which maximum distribution of background and object class entropies are obtained.

Let f_1, f_2, f_3, ... , f_n be the observed grey level frequencies and h_1, h_2, h_3, ... , h_n be the probability distribution of grey levels in the image. The probability distributions of object and background classes can be derived from this distribution. One probability distribution is defined for discreet values 1 to t and the other one for values t+1 to n. The two distributions are given by;

$$D_1 = \frac{h_1}{h_t}, \frac{h_2}{h_t}, \frac{h_3}{h_t}, \ldots, \frac{h_t}{h_t} \tag{6.1}$$

$$D_2 = \frac{h_{t+1}}{1-h_t}, \frac{h_{t+2}}{1-h_t}, \frac{h_{t+3}}{1-h_t}, \ldots, \frac{h_n}{1-h_t} \tag{6.2}$$

$$\text{Where } h_k = \frac{f_k}{N} \sum_{k=1}^{n} f_k = N \quad k = 1, 2, 3, \ldots, n$$

The entropies for the two probability distributions can be calculated as;

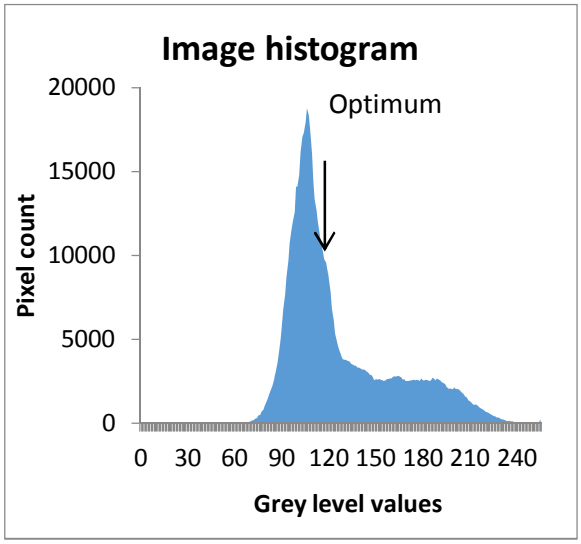
$$H(D_1) = -\sum_{k=1}^{t} \frac{h_k}{h_t} \ln \frac{h_k}{h_t} \tag{6.3}$$

$$H(D_2) = -\sum_{k=t+1}^{n} \frac{h_k}{1-h_t} \ln \frac{h_k}{1-h_t} \tag{6.4}$$

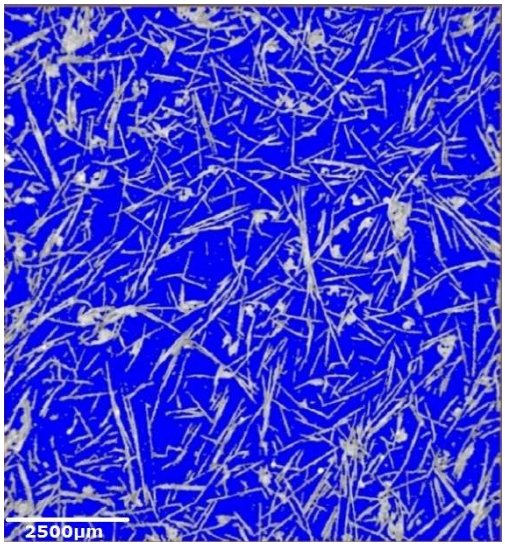
The sum of two entropies $\gamma(t)$ is calculated from equation 6.3 and 6.4:

$$\gamma(t) = H(D_1) + H(D_2) \tag{6.5}$$

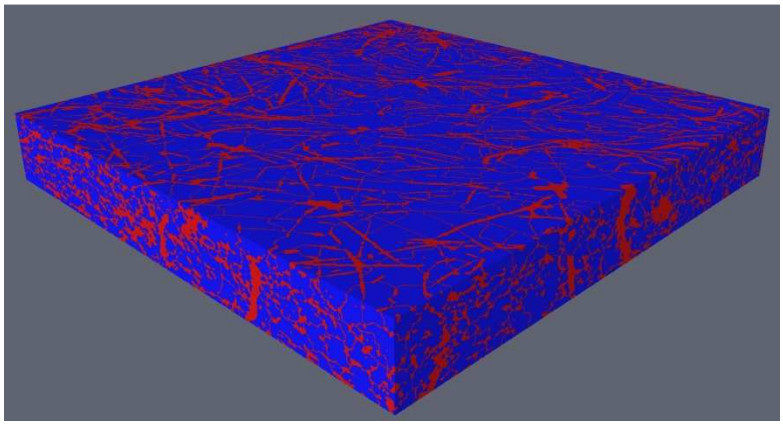
Kapur's method chooses threshold value T for which maximum value of $\gamma(t)$ is obtained. The optimum T value calculated for NW20 is shown in Figure 6.15 (a). This value was applied to the 3-D volume rendering of NW20 and ST170 by using the interactive thresholding option in Avizo. Binary images then showed geotextile fibers clearly separated from the background, as shown in the Figure 6.15 (b).



(a) Kapur's method to find T value



(b) NW20 specimen after applying T value



(c) Reconstruction of 3-D CT images after applying T value

Figure 6.15 Image segmentation by finding the optimum threshold value

The last step in image processing was to find the centroids and equivalent diameter of individual pores in the 3-D volume rendering of binary images. Before carrying out the final stage, it was necessary to separate the pores since Avizo considers different pores connected with each other as a single pore. The separation of pores was achieved with the separate objects command in Avizo which is a combination of watershed, distance transformation, and numerical reconstruction algorithms. The separate object command accurately removes small areas of contact between pores. Finally, the pore parameters i.e. centroid and equivalent spherical diameter of all the pores, were measured using the Label Analysis option in Avizo. Equivalent spherical diameter of irregular shaped material is

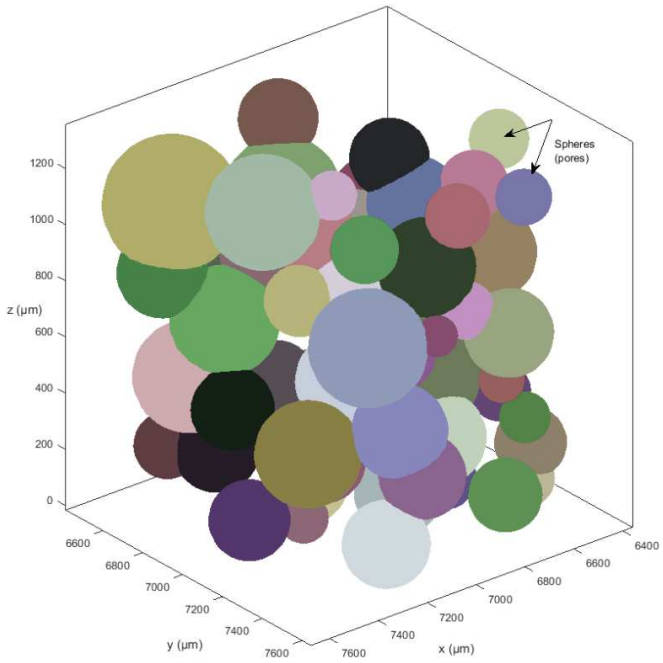
the diameter of a sphere of equivalent volume. The equivalent diameter has been frequently used in the literature for 3-D pore structural description (Cnudde et al., 2011; Van Dalen & Koster, 2012). Avizo measures the centroids of equivalent diameter of pores on the basis of x, y and z voxel (smallest volume element in 3-D space) sizes. These pore parameters were measured and recorded for both NW20 and ST170 geotextile specimens.

6.5.3. Plotting Pores in Matlab

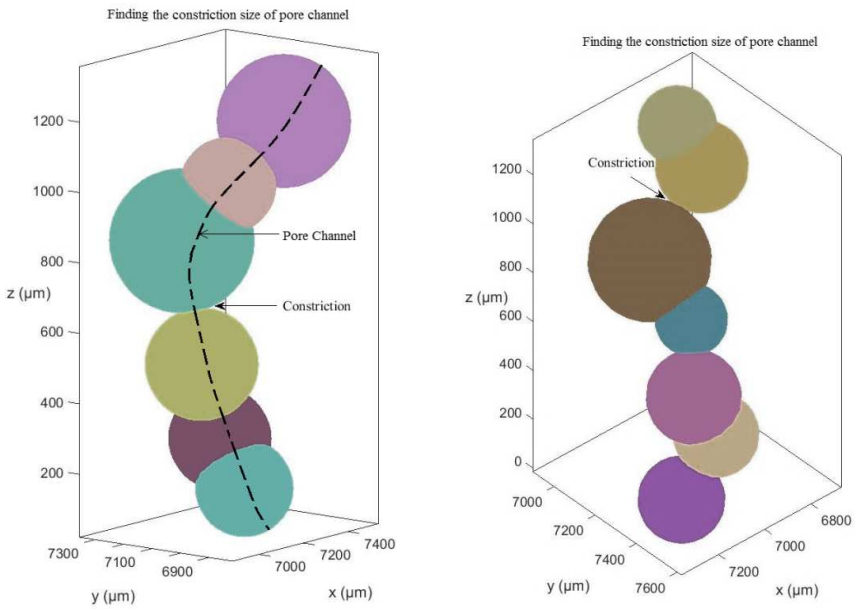
The last step in the 3-D constriction size measurement was to plot the equivalent spherical diameters in Matlab. To achieve this, a code to plot spheres was written in Matlab R2015b. Firstly, the pore parameters saved in an Excel sheet were imported into Matlab. The code was run to plot spheres (pores) at the measured centroids in 3-D space. Figure 6.16(a) shows spheres plotted in Matlab for a small section of NW20 geotextile. Pore channels are formed by overlapping spheres through the entire thickness (z-axis) of geotextile. A symmetric matrix was calculated to find the spheres which are overlapping with each other. Spheres were determined to be overlapping with each other if the sum of the radii of the spheres is greater than the distance between spheres. The overlapping matrix gives a value of 1 for overlapping spheres and 0 for non-overlapping spheres. There are some pores which have a dead end and are not involved in any pore channel. These pores terminate at some point along the z-axis in XYZ space, without overlapping with other pores further down. Boundary conditions were applied to delete the dead end pores so that only those spheres which are involved in pore channels that cross the entire geotextile thickness are plotted. The spheres forming different pore channels were identified from the overlapping matrix.

For better visualization of the pore channels in Figure 6.16(a), two pore channels are plotted separately in Figure 6.16(b). The point where there is minimum sphere-sphere

intersection along the pore channel is the constriction size. This constriction size can be located at any depth along the pore channel.



(a) Plotting spheres (pores) in Matlab



(b) Finding the constriction size along each pore channel

Figure 6.16 3-D plotting of spheres (pores) in Matlab

The sphere-sphere intersection mechanism is shown in the Figure 6.17. Suppose two spheres are located along x-axis centered at (0,0,0) and (d,0,0), having radii R and r respectively. The intersection of two spheres is a circle having a radius "a" whose plane is perpendicular to the line joining the centers of two spheres.

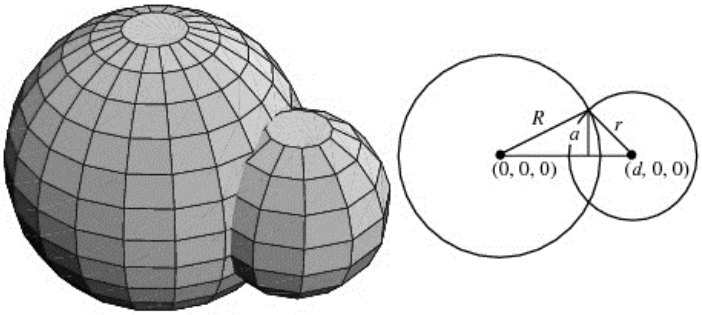


Figure 6.17 Sphere-sphere intersection (Weisstein, 2007)

The radius of the circle can be calculated using the equation proposed by Weisstein (Weisstein, 2007):

$$A = \frac{1}{2d}\sqrt{4d^2R^2 - (d^2 - r^2 + R^2)^2} \qquad (6.6)$$

Eq. 6.6 was written in Matlab to find the radii of the circles at the spherical surfaces intersection. The diameter or throat sizes were measured from the radii for all overlapping spheres along pore channels. The minimum throat size measured along each pore channel was taken as the constriction size of pore channel. The entire constriction size distributions were measured for the two geotextile specimens. The brief steps to find the 3-D constriction sizes of geotextile specimens is shown in Figure 6.18.

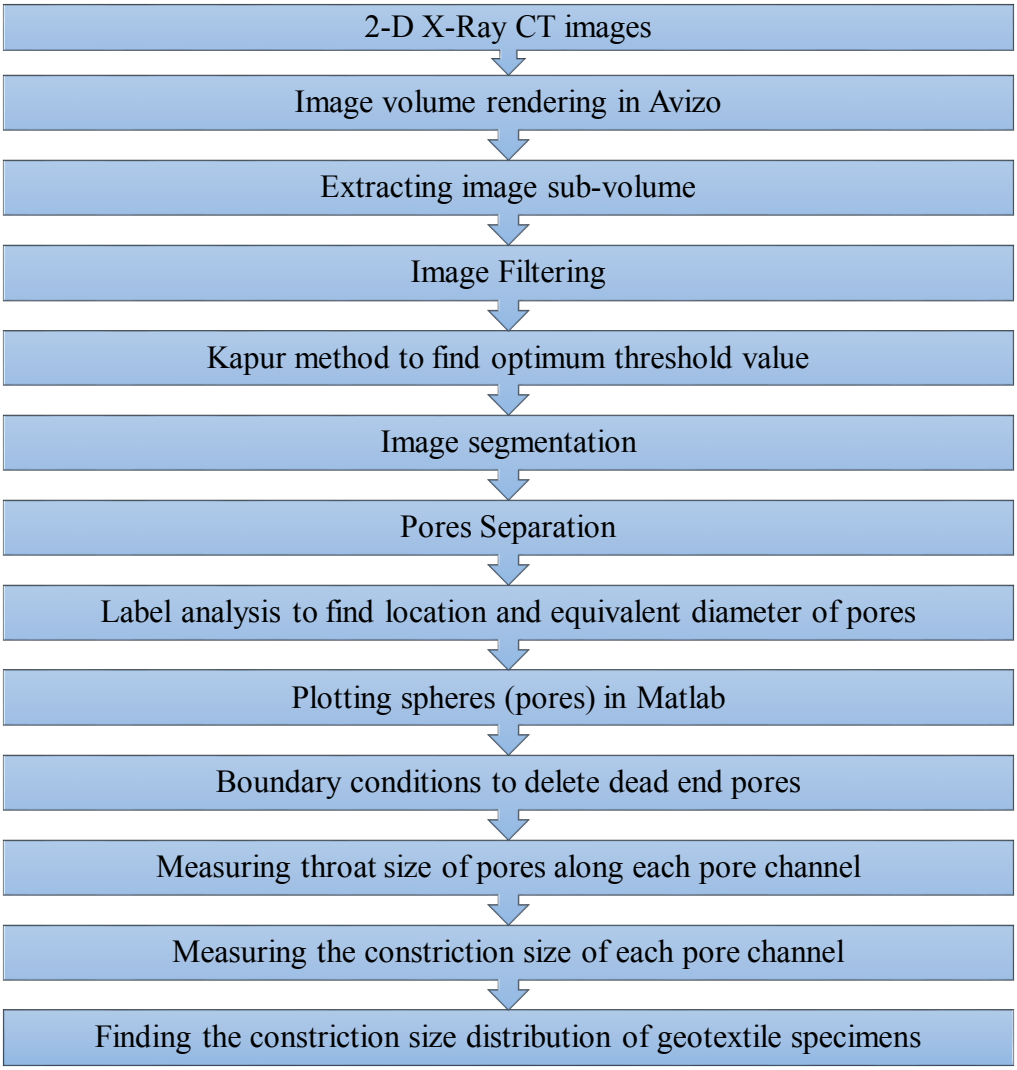


Figure 6.18 Flowchart of the detailed steps to find 3-D constriction size distribution of geotextiles

6.5.4. Results

The 3-D constriction size distribution of geotextile specimens NW20 and ST170 is plotted in the Figure 6.19. The constriction size for which 95% of the pores are smaller (referred as C_{95}), was found to be 145µm and 140µm for NW20 and ST170 specimens respectively. It can be seen from the PSD that, despite C_{95} values being nearly similar for both NW20 and ST170 specimens, the PSD is different for both specimens. The difference in the PSD for both geotextile specimens were found to be more for smaller constriction sizes. This

means that the PSD is not necessarily the same for geotextiles having the same large pore size.

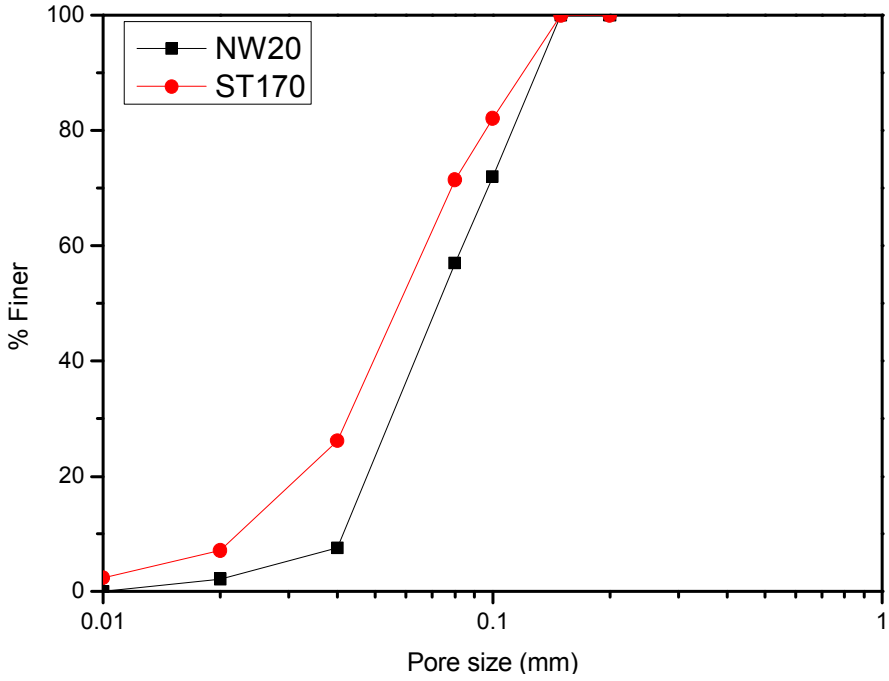
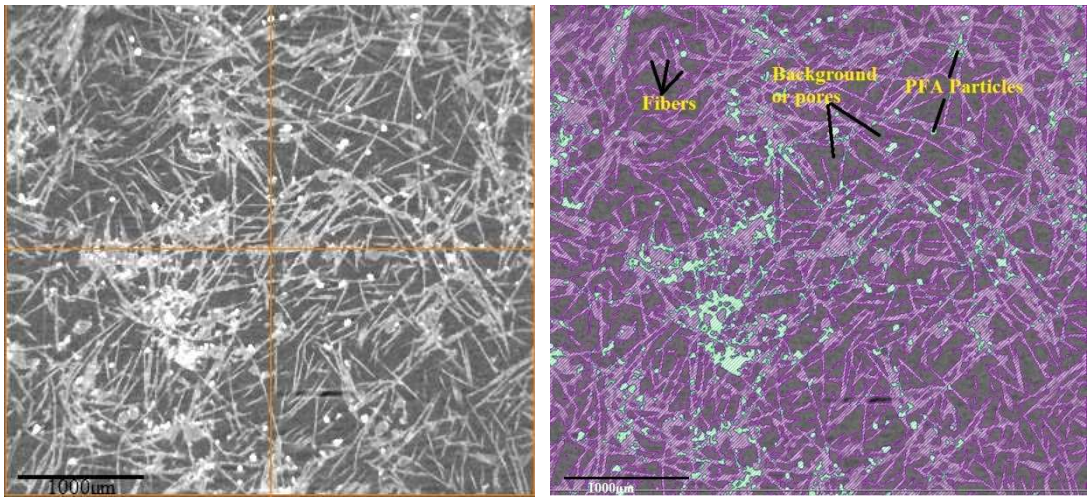


Figure 6.19 Constriction size distributions of NW20 and ST170 specimens

Most filter design criteria are based on the basis AOS or O_{95} of geotextiles which provides satisfactory results in term of retention of soil. However, the clogging potential of geotextiles should be designed on the basis of smaller pore sizes because the smaller pore sizes are responsible for passing fine particles (Carroll, 1983, Christopher & Holtz, 1985).

Gradient ratio tests were performed by testing NW20 and ST170 specimens with PFA (see Section 5.4). PFA is a fine material for which 85% particles are smaller than 63µm (Figure 3.1). As the C_{95} values of both geotextile specimens were quite a lot larger than the PFA d_{85} size, it was important to observe how both geotextiles perform in terms of clogging. X-ray CT images of geotextile specimens NW20 and ST170, after the gradient ratio test with PFA, were taken. The X-ray images were visualized in Avizo to see the clogged PFA particles inside the geotextile samples (Figure 6.20). The grey level images

were segmented by creating label fields for every phase i.e. PFA, fibers and background. It can be seen from the Figure 6.20 that soil particles are clearly differentiated from fibers and background by assigning threshold values to different phases.

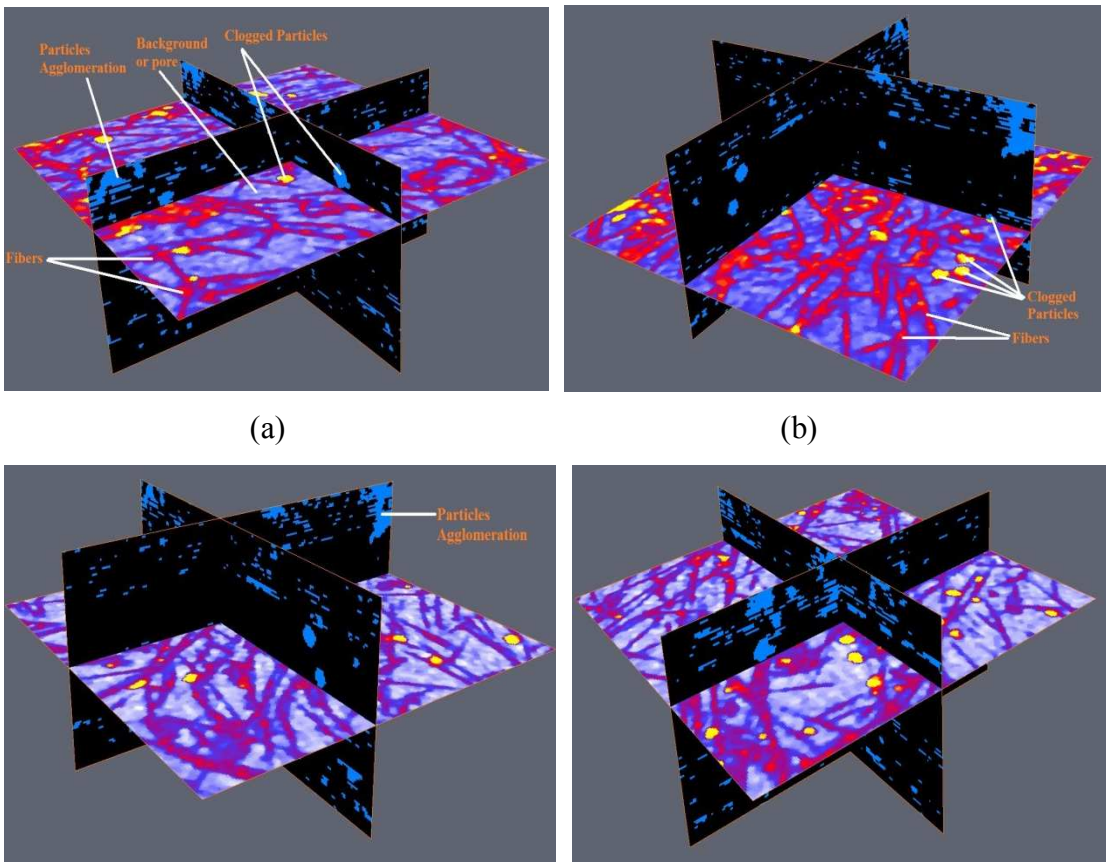


(a) (b)

Figure 6.20 X-ray image of NW20 clogged with PFA (a) before and (b) after segmentation

The X-ray image in Figure 6.20 is a planar image taken at the middle of the geotextile specimen. Although PFA particles can be clearly distinguished in the planar image, it does not give an idea about the location of these particles inside the pore channels. The orthoslice option in Avizo was found to be the best way to identify the location of clogged particles. Three orthoslices of the segmented images were selected in the xy (transverse), xz (frontal) and yz (sagittal) directions, respectively (see Figure 6.21). The locations of clogged particles were searched by navigating through orthoslices. It can be seen from Figure 6.21 that PFA particles are stopped by the fibers. Most of the particles are stopped at locations where the fibers are highly congested. The PFA particles are not necessarily clogged at the top of the geotextile specimen, rather the clogging depends on the smallest void or constriction come across by particles along the pore channel. Also, particle agglomerations can be observed in Figure 6.21. If a particle comes across a constriction

smaller than its size, it will be stopped by the constriction and the trapped particle will stop the other particles coming through the same pore channel which results in particle agglomeration.



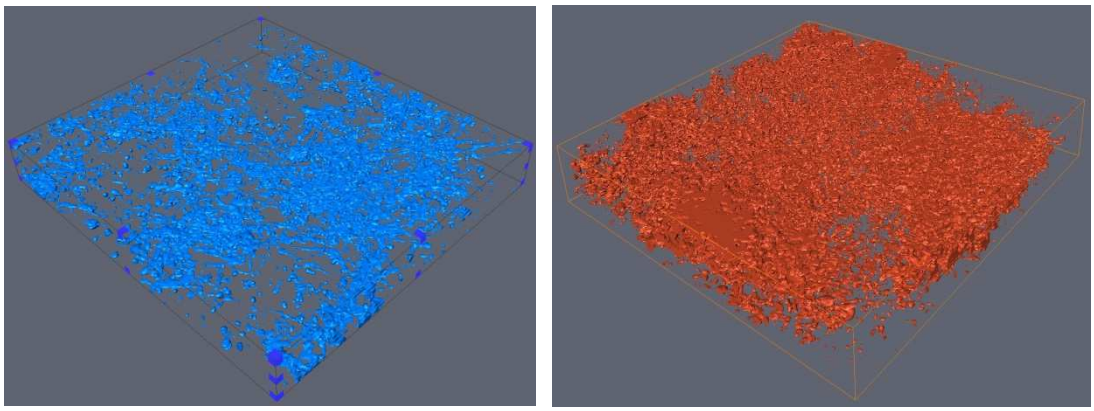
(a) (b)

(c) (d)

Figure 6.21 Orthoslices of NW20 images in xy, xz, and yz directions to observe clogging

It has already been discussed that the PSD of NW20 and ST170 were different from each other, despite having the same C_{95} values. It was interesting to see the amount of particles clogged inside each geotextile. By deleting label fields for fibers and background, 3-D volume of clogged particles inside NW20 and ST170 were created (see Figure 6.22). It can be seen from Figure 6.22 that the amount of clogged particles inside ST170 was found to be more than NW20. Although both geotextile specimens were tested for filtration with

PFA under the same conditions, but the clogged soil was found to be different. This might be attributed to the different PSD of both geotextile specimens.



(a) Clogged particles inside NW20 (b) Clogged particles inside ST170

Figure 6.22 PFA particles clogged inside NW20 and ST170 geotextiles specimens

6.6. Theoretical Constriction Size Measurement

Theoretical constriction sizes of geotextile specimens were measured using equations proposed by Giroud (1996) and Faure et al. (1990). Giroud (1996) indicated that the number of constrictions is directly related to the thickness of geotextiles. The theoretical equation developed by Giroud depends on thickness, porosity and diameter of fiber of non-woven geotextile:

$$\frac{O_f}{d_f}=\frac{1}{\sqrt{1\text{-}n}}\text{-}1+\frac{10nd_f}{(1\text{-}n)t_{GT}} \tag{6.7}$$

where O_f is the opening size, d_f is fiber diameter, n is porosity and t_{GT} is thickness of geotextile. A detailed explanation of this equation is provided by Giroud (1996). The porosity, n, of the geotextiles was calculated using Wayne and Koerner (1993) equation:

$$n=1-\frac{u_g}{\rho t_{GT}} \tag{6.8}$$

where u_g is the mass per unit area of geotextile and ρ is the fiber density.

Faure et al. (1990) proposed a theoretical equation on the basis of the Poissonian polyhedra method. Epoxy-impregnated non-woven geotextile specimens were sliced and the three-dimensional structure of geotextiles was modelled by random staking of elementary longitudinal planes (i.e. parallel to the plane of sheet). The thickness of each elementary plane in a stack was equal to the fiber diameter, d_f. Pores were considered to be cylindrical conduits having diameter d and the axes of pores were perpendicular to the longitudinal planes having depth equal to d_f. The probability that a particle of diameter d passing through the elementary planes of a non-woven geotextile is given by;

$$P(d)=1-\left(\frac{2+\gamma(d+d_f)}{2+\gamma d_f}\right)^{2N} . e^{-\gamma N d} \qquad (6.9)$$

where $\gamma=\frac{4}{\pi}\frac{(1-n)}{d_f}$; $N=\frac{t_{GT}}{d_f}$

γ is specific length which is the total length of straight lines per unit area and N is the number of slices in the geotextile.

6.6.1. Results

The Giroud (1996) and Faure et al. (1990) equations were used to measure the constriction sizes of all four geotextiles. Figure 6.23 compares the theoretical constriction sizes computed for all geotextile specimens. The constriction sizes are comparable for NW20, ST170 and NW8 geotextiles. The constriction sizes C_{95} were found to be 20-30% higher for Giroud (1996) compared to Faure et al. (1990) for NW20, ST170 and NW8 geotextiles. However, the Faure et al. (1990) equation gave quite a lot smaller values for F1200M compared to Giroud (1996) where Giroud (1996) gave a C_{95} value 154% more than Faure et al. (1990). This difference is attributable to an assumption in the Faure et al. (1990) approach that constriction size tends to approach zero if the geotextile thickness is

relatively high. F1200M has a thickness of 8mm as compared to other geotextile specimens whose thicknesses range between 1 to 2mm. The Faure et al. (1990) equation is not recommended for geotextile having large thickness because of this assumption. Overall, the Giroud (1996) equation is a clear and detailed technique to provide constriction size of geotextiles of various thicknesses as compared to the Faure et al. (1990) equation.

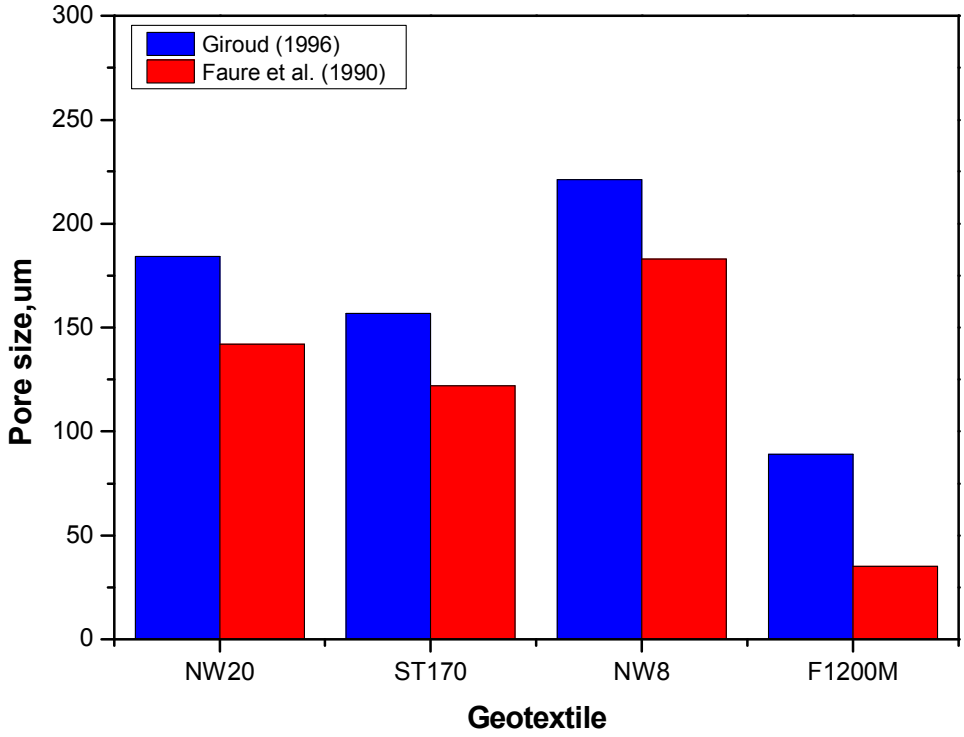


Figure 6.23 Comparison of constriction sizes C_{95} from theoretical equations

6.7. Merury Intrusion Porosimetry

The MIP method for finding the pore sizes of geotextiles is already a standard test procedure (ASTM D 4404) for determination of pore volume and pore volume distribution of soil and rock materials. The detailed procedure of the test method can be found in Prapaharan et al. (1989) and Elsharief and Lovell (1996). The advantages and disadvantages of the test technique was described in Section 2.7.1.1. The MIP technique

was used to find the PSD of NW20, ST170 and NW8 geotextile specimens using Micromeritics Autopore IV 9500 at the University of Nottingham.

6.7.1. Results

The absolute pressure readings obtained from the MIP test were converted to apparent intruded pore diameters using the Washburn equation. The Washburn equation assumes pores to be cylindrical. The pore volume distributions of the geotextile specimens were determined by plotting pore diameter versus the cumulative percentage of pore volume smaller than pore diameter, on an arithmetic scale. Figure 6.24 shows the volumetric pore size distribution of NW20, ST170 and NW8 specimens. The percentage of pores smaller than a particular pore size can be calculated from the graphs.

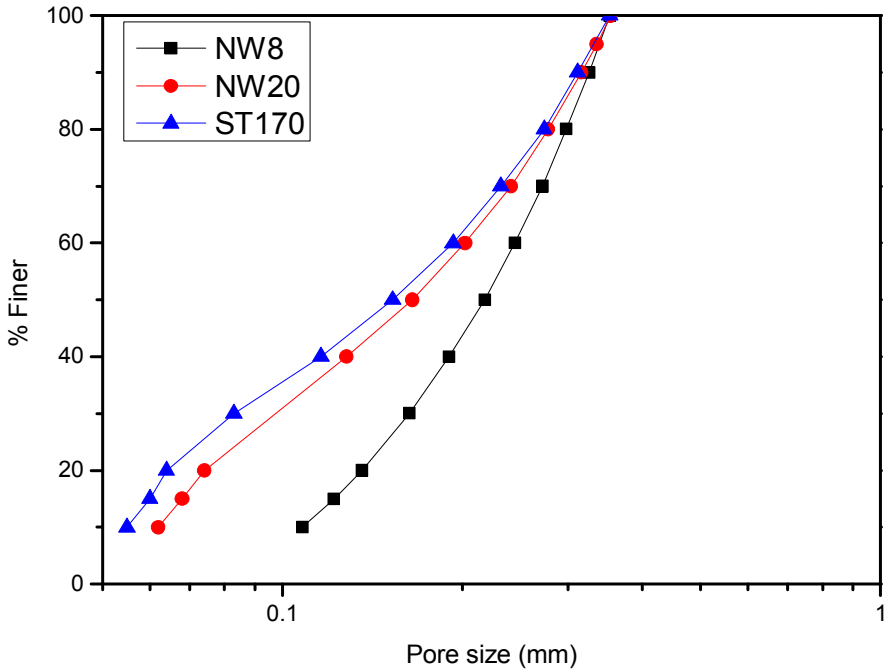


Figure 6.24 Comparison of PSD measured from MIP technique

It can be seen from the graphs that the large pore size O_{95} and O_{90} values are in the range of 0.3 to 0.350 mm for all three geotextile specimens. The PSD of geotextile specimens were found to be different for smaller pore sizes. The O_{50} values were found to be

0.165mm, 0.153mm and 0.218mm for NW20, ST170 and NW8 respectively. The PSD values of NW20 and ST170 fell within a narrow range as compared to the NW8 specimen.

6.8. Comparison of Pore Sizes from Different Techniques

In the previous sections, the results of measuring pore sizes of four geotextile specimens by different techniques have been presented. The characteristic opening size 'O_{90}' values of geotextile specimens were provided by the manufacturers on the basis of the wet sieving method. Figure 6.25 shows the comparison of O_{95} and C_{95} measured by these different techniques. As discussed in Section 2.7.1, the pore opening size of a geotextile depends on the testing technique. Therefore, a comparison is made here to outline the difference between the different pore opening sizes. The Figure 6.25 shows that O_{95} measured from 2-D image analysis and MIP was found to be higher than the C_{95} measured from 3-D constriction size method and theoretical equations. The reason for the higher O_{95} values of geotextile specimens from 2-D image analysis and MIP is that pore sizes are a function of pore spaces and pore volume respectively, rather than measuring the constriction sizes of pore channels. The pore sizes measured by MIP are based on the percentage of pore volume occupied by each pore size, including the dead end pores.

A good comparison was found between the C_{95} values measured from 3-D constriction size and the theoretical equations. Faure et al (1990) gave smaller C_{95} values compared to the Giroud (1996) equation because of the assumption that constriction size approaches zero for geotextiles having high thicknesses. That is the reason that Faure et al. (1990) approach gave much smaller C_{95} values for F1200M (8mm thickness) geotextile compared to the Giroud (1996) equation. Due to limitations of the Faure et al. (1990) approach, the 3-D constriction size and Giroud (1996) equation were found to be appropriate methods for finding the C_{95} values of geotextiles.

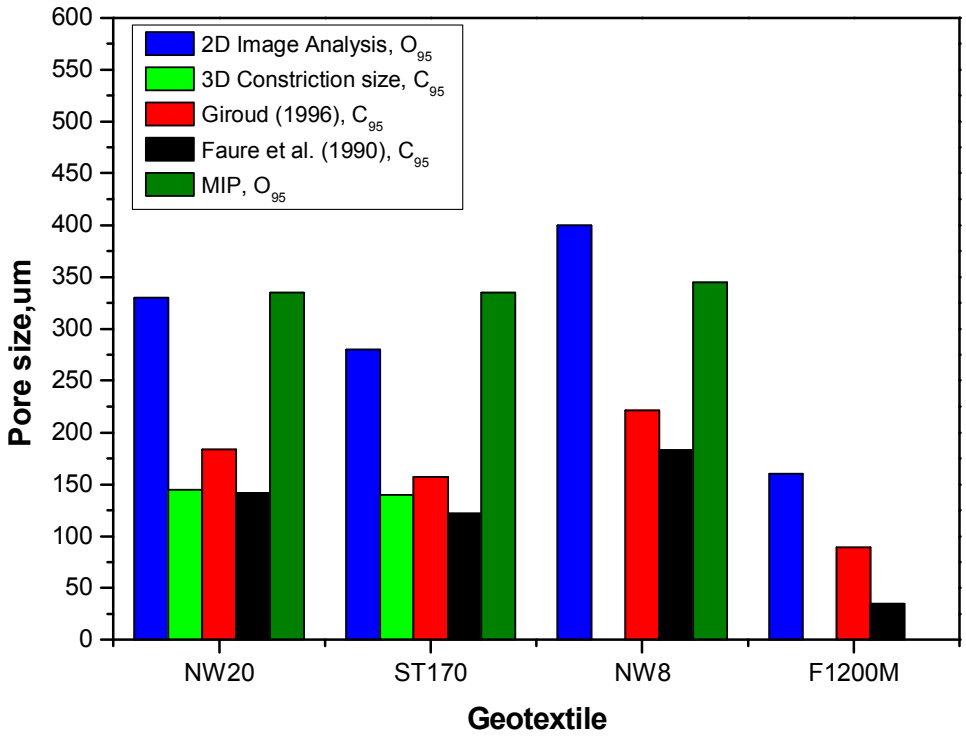


Figure 6.25 Comparison of O_{95} and C_{95} measured from different techniques

The constriction sizes C_{90} measured from 3-D constriction size were compared against the manufacturer's reported O_{90} values which are based on the wet sieving technique (see Figure 6.26). For comparison, O_{90} values from the 2-D image analysis and the MIP technique are also plotted. It was not possible to plot the C_{90} values from the Giroud (1996) equation because that equation only measures the C_{95} value of geotextiles. Like O_{95} values, the O_{90} values measured from the 2-D image analysis and the MIP were found to be much higher than the C_{90} values from the 3-D constriction approach. The characteristic opening size, O_{90}, measured from wet sieving (see Section 2.7.1.1) was found to be the smallest for both geotextile specimens. Although pore sizes obtained from wet sieving depend on pore channel constriction size, sieving is a random process because a particle may encounter a constriction smaller than its diameter and vice versa (Fischer et al., 1996). Wet sieving does not give an idea of how easily a particle passed through the constriction. Also, particle agglomerations inside the geotextiles is a big problem with wet sieving which results in fine particles unable to pass through geotextiles because these fine

particles are stopped by the agglomerate (Bhatia et al., 1996b). These problems associated with the wet sieving lead to somewhat arbitrary results and thus the pore size measured cannot be considered to be a true size. It is obvious that if the fine particles passing through geotextiles during wet sieving are stopped by the agglomerate, it will result in smaller pore sizes being identified by the test than are the actual sizes. This is the reason that the O_{90} of geotextiles was found to be smaller than the C_{90}. The wet sieving method does not account for the soil particles trapped inside the dead end pores during sieving. As already shown in Figure 6.16(a) there are dead end pores inside the geotextiles which are not part of pore channels. These dead end pores were removed during the 3-D constriction size technique. Although wet sieving is the current European standard method for determination of the characteristic opening size of geotextile filters (BS EN ISO 12956:2010), the limitations of the wet sieving method need to be considered during filter design.

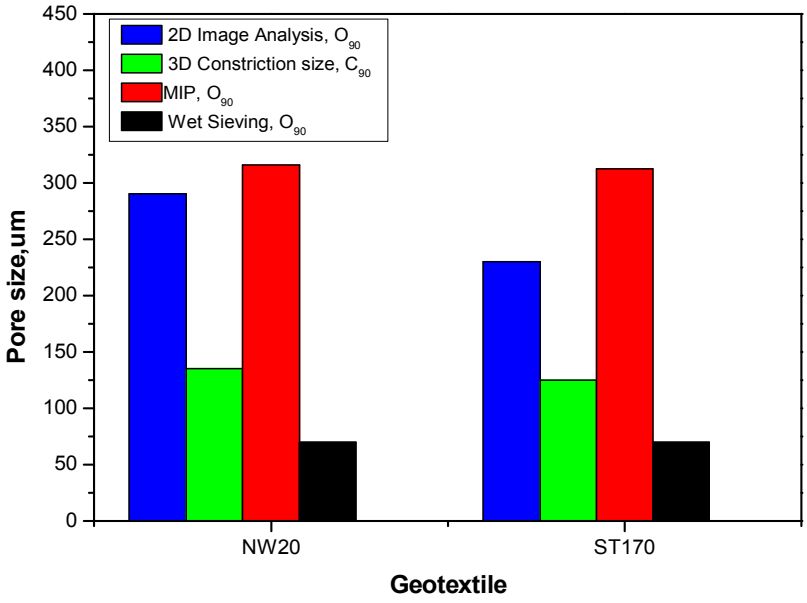


Figure 6.26 Comparison of O_{90} and C_{90} measured from different techniques

6.9. Summary and Conclusions

Image analysis has been used in the past by various researchers to find the 2-D PSD of non-woven geotextiles. In this study, a new method, bubble analysis, was used to determine the 2-D PSD of four non-woven geotextile specimens from the cross-sectional images. Previous studies have shown that it is the constriction size of geotextiles which controls the filtration behaviour. There is still a need for a standard method to find the constriction size of geotextile filters. In this study, a new method was suggested for finding the constriction sizes of two geotextile specimens, NW20 and ST170. The 3-D constriction size method measures more realistically the three-dimensional constriction sizes from X-ray CT images. Pore sizes of geotextile specimens were also calculated from MIP as well as theoretical equations i.e. the Giroud (1996) and Faure et al. (1990) equations. O_{90} values on the basis of wet sieving techniques were provided by the manufacturers. The pore sizes measured from all these methods were compared against each other and the following conclusion can be drawn:

1) The pore size O_{95} measured from 2-D image analysis and MIP was found to be much higher than C_{95} calculated from the 3-D constriction size method and theoretical equations. This difference is due to the fact that O_{95} measured from 2-D image analysis and MIP is a function of pore space and pore volume respectively, instead of measuring the constriction sizes of pore channels.
2) A good correlation was found for the C_{95} values measured from the newly suggest 3-D constriction size method and theoretical pore equations, although the Faure et al. (1990) approach is limited to geotextiles having small thicknesses.

3) The O_{90} values based on wet sieving method, were found to be significantly less than the C_{90} values measured from the 3-D constriction size method. This high difference in the values is due to the disadvantages associated with the wet sieving method.
4) The 3-D constriction size method measured the same C_{95} values for NW20 and ST170 but the PSD was found to be different for both specimens. It shows that geotextiles having the same largest pore size do not, necessarily, have the same pore size distribution.
5) The visualization of X-ray CT images of clogged NW20 and ST170 specimens showed that clogging of particles does not necessarily occur at the top pores of geotextile specimens. Particles were seen to be clogged at the sites where fibers were highly congested.
6) The 3-D constriction size method provides the complete PSD of geotextile specimens. The PSD measured will be useful to quantify the clogging potentials of geotextiles, since it is the constriction size of geotextiles which controls the filtration behaviour. The effect of geotextile PSD on the filtration performance will be discussed later in Section 7.4.

Chapter 7

Discussion

7.1. Introduction

As described in Chapter 5, in the dynamic GR test program the sample was subjected to static and cyclic loading conditions. Static conditions were applied by imposing unidirectional flow under an applied external gradient of 5 (see Section 4.2.4). The static stage was followed by cyclic stage imposed with the help of the INSTRON machine. A few filtration tests were performed for two additional cyclic stages to observe the effect of increase in frequency and increase in deviator stress on the filtration performance of soil/geotextile interfaces.

In this chapter the test results present in Chapter 5 are discussed and interpreted with reference to previous related studies. This chapter addresses the overall performance of internally stable/ unstable soils and the soil/geotextile compatibility. The effect of PSD (see Section 6.8) on the filtration performance of soil/geotextile interfaces is also addressed in this chapter. Finally, a designed criterion is suggested for internally unstable soils and, compared with the existing filter design criteria.

7.2. Filtration Behaviour of Narrow Graded Soils

As discussed in Section 3.4, soils with $C_u < 6$ were identified as internally stable by at least two of the three geometric stability criteria i.e. the Kézdi (1979), Kenney and Lau

(1985) and Burenkova (1993) criteria. That is why the filtration behaviour of narrow and broadly graded soils is discussed separately in this Chapter.

7.2.1. Gradation of Particles Passed

Table 5.3 shows that the mass of particles collected at the end of filtration test was less than the limit of 2500 g/m^2 recommended for significant piping by Lafleur et al (1989). However, his recommendations were based on long term flow conditions. The filtration tests in this research were only performed for 5000-10000 cycles depending on the stability of GR and permeability values. As previously mentioned in the literature review (Section 2.5.1), Kenney and Lau (1985) suggested amount of fine particles in uniformly graded soils should be at most 30% finer by weight. Therefore, it was important to compare the gradations of soil particles washed out through geotextiles with the original gradation of soil samples to find out whether the gradation of washed out particles constitutes the primary (coarse fraction) or secondary structure (fine fraction) of base soil.

Table 7.1 shows comparison between d_{90} of particles (termed here as d_{90p}) washed out with the base soil original gradation. The % finer by weight of original sample having same size as d_{90p} is termed as % original grading (Table 7.1) and this term is used later in this chapter. The stability analysis of soil gradations by the Kezdi (1979) as well as the Kenney and Lau (1985) criteria is given in the Table 3.5. The 90% sand 10% PFA soil which was evaluated as internally unstable by the Kezdi (1979) criterion showed d_{90p} with both geotextiles as 6 to 8 % original grading. This was predicted as 5 to 12 % finer by weight of original sample by the Kezdi (1979) criterion. The medium sand which has a C_u of 1.9 showed the largest d_{90p} as compared to other soil samples. This was expected as soil with $C_u < 2$ is usually considered as one fraction regarding filtration criteria by U.S. FHWA (Holz et al., 1998), suggesting a more stringent retention criterion. Overall, the %

original grading for all test samples is less than 30 which suggests that the washed out particles through geotextiles is part of secondary structure instead of primary structure of base soils.

Table 7.1 Comparison of d_{90p} and original sample for narrow graded soils

Geotextile	**Soil**	**O_{90} µm**	**d_{90p} µm**	**% original grading**	**Kezdi (1979)**		**Kenney and Lau (1985)**	
					% finer by weight at $(D_{15}/d_{85})_{max}$	% finer by weight showing D_{15}/d_{85} >4	% finer by weight at $(H/F)_{min}$	% finer by weight showing H/F <1
NW8	Medium Sand	120	35	<4	5	-	30	-
NW20	Medium Sand	70	31	<4	5	-	30	-
ST170	Medium Sand	70	30	<4	5	-	30	-
NW20	Fine Sand	70	15	<8	10	-	2.3	-
NW8	Fine Sand	120	18	< 8	10	-	2.3	-
NW20	90% Sand 10% PFA	70	20	6	5	5-12	4.5	-
NW8	90% Sand 10% PFA	120	25	8	5	5-12	4.5	-

7.2.2. Influence of Flow Regime

Although it is believed that a natural bridging network is able to develop at the soil-geotextile interface under static unidirectional conditions, however, it may or may not develop under cyclic flow conditions (see Section 2.8.3.2). To observe this effect, static unidirectional flow was followed by cyclic stages to observe the filtration mechanism at soil-geotextile interfaces.

For filtration tests with medium sand, the GR values did not show much difference at the end of static stage and Cyclic 1 stage (see Table 5.1). The medium sand with NW8 and ST170 showed a GR value less than 1 while NW20 showed a GR value more than 1. The test sample with ST170 showed a sudden drop in GR value from 0.89 to 0.61 when Cyclic 3 stage was applied. As mentioned in Section 5.3.1, this was due to more head loss within soil than across the soil-geotextile interface (Appendix C). The post-test gradation (see Table 5.5) shows that there was a slight increase in D_{15} for 25-40 mm layer which resulted in increase in $h_{25\text{-}75}$ after applying Cyclic 3 stage. The increase in fine content might be, presumably, attributed to migration of fines from the upper soil in the 25-40mm soil layer due to densification due to increase in deviator stress. As discussed in Section 4.4, the deformation of test samples was not measured. The densification of base soil might have occurred due to deformation of test sample. However, it did not affect the GR value significantly (Table 7.2). The permeability values (see Table 5.2) shows that there was a more drop in k_s as compared to k_{sg}. This suggests that the soil-geotextile interface was less affected by increase in deviator stress.

The permeability data shows that, for medium sand with NW8 and ST170 geotextiles, the k_{sg} was more than k_s for NW8 and ST170 during static stage and remained unaffected during Cyclic 1 stage. The test sample with ST170 however showed a decrease in k_s and k_{sg} during Cyclic 2 stage which suggests that the increase in frequency is not allowing the pore water pressure to dissipate fully. The fact that k_{sg} is more than k_s during static and cyclic stages suggests a porous soil skeleton behind the geotextile interface, and hence the flow rate at the soil-geotextile interface is more than the flow rate within the soil. This result is supported by wash-out of some fine materials near the geotextile (Appendix D). The low GR values indicate lower hydraulic gradients and, therefore, lower seepage forces ($F_{seepage} = i\gamma_w$) at the soil-geotextile interface. The permeability data for NW20 and

medium sand showed k_{sg} less than k_s for static stage. The Cyclic 1 stage resulted in a decrease in k_{sg}. The microscopic images of geotextile samples after filtration tests (see Figure 5.9) showed very few clogged particles inside the geotextiles. This suggests that a layer with low permeability was formed upstream of geotextile. This is supported by accumulation of some fine particles where the post-test gradation showed a slight decrease in D_{15} for soil above geotextile. Also, the partial clogging values were found less for NW20 as compared to NW8 and ST170 geotextiles (Table 5.6). This shows blinding mechanism (filter cake) may have occurred due to coarse particles retained by geotextile, which in turn intercepted fines migrating from the soil. The decrease in k_{sg} with cyclic loading shows further fine particles movement towards the low permeability layer. This is in consistence with Chang and Nieh (1996) that, for clean sands which have less fines, a blinding layer is expected instead of clogging inside fabrics.

The test samples with fine sand showed very little difference in GR values at end of static and cyclic stages. The microscopic images of geotextile samples after filtration tests (see Figure 5.10) showed very few clogged particles inside the geotextiles. The k_{sg} for test sample with NW20 was less than k_s for static and cyclic stages which suggests less permeable layer (blinding layer) at the soil-geotextile interface. No effect of cyclic stages was observed on k_{sg} values. The probability of a blinding layer having formed is supported by a decrease in D_{15} for 0-8mm layer as well as low geotextile partial clogging value (Table 5.6). The k_s remained stabilized for static and Cyclic 1 and Cyclic 2 stages, however, a slight increase in k_s was observed during Cyclic 3 stage. The increase in k_s might be attributed to loss of fines in the base soil layer. The post-test gradation showed a slight increase in D_{15} for 25-40mm, showing migration of few fine particles from the base soil. GR value of test sample with NW8 shows a more permeable layer at soil-geotextile interface as compared to base soil. This might be attributed to the large pore

size of NW8 geotextile. The permeability value shows that k_{sg} was more than k_s for static and cyclic stages. Also, the post-test gradation showed an increase in D_{15} for the 0-8mm layer above geotextile. The k_{sg} value decreased when Cyclic 1 stage was applied and remained constant thereafter which suggests migration of fine particles towards geotextile interface under cyclic loading.

The test samples with 90% sand 10% PFA, like fine sand test samples, did not show much variation in GR at the end of static and Cyclic 1 and Cyclic 2 stages. The test sample with NW20, however, showed a slight increase in GR with Cyclic 3 stage. This behaviour was found to be similar as was observed for fine sand with NW20. The increase in GR was due to decrease in head loss within the soil instead of increase in head loss across soil-geotextile interface (see Figure 5.6) which shows the migration of fines in the base soil. Although the post-test gradation did not show any change in soil gradation in 25-40mm, the fines migration presumably occurred in the soil above the 25-40mm zone. The $k_{sg,}$ for filtration tests with both geotextile samples, was found to be less than k_s for static and cyclic stages. The k_{sg} value remained constant for static and cyclic stages. The microscopic images of geotextile samples after filtration tests (see Figure 5.9) showed very few clogged particles inside the geotextiles. The post-test gradation showed decrease in D_{15} for the 0-8mm layer above geotextiles which suggests the increase in GR was due to a blinding layer formed at the soil-geotextile interface.

No significant effect of cyclic stages was found on the filtration behaviour of soil-geotextile interfaces. For the filtration tests with narrow graded soils, three test samples evidenced formation of a bridging network, and four test samples showed blinding of the geotextile. The blinding mechanism shows the internal instability of soils. The blinding mechanism occurs when the filter opening size is less than the loose soil particles

diameter. The narrow graded soils were evaluated as internally stable by at least two of the three geometric criteria (Table 3.6). It is attributed to the higher hydraulic gradient which resulted in internal instability of soils by migration of loose fine particles towards the geotextiles. It is believed that this blinding layer was formed during the static stage since no significant effect of cyclic loading was observed on the soil-geotextile interface permeability.

7.2.3. Clogging Ratios

As mentioned in Section 5.3.2, the GR values were calculated from the water head distribution within the soil and across the soil-geotextile interface. The filtration performance of soil-geotextile interface is generally assessed in terms of GR. The k_s and k_{sg} are indirectly related to GR since these values are computed from the head loss within the soil and across-soil geotextile interface respectively (see Section 2.10.1). Although GR values are a good indicator of assessing the overall filtration performance of soil-geotextile behaviour, however, it does not give clear idea about whether the increase in GR occurred due to more head loss within the soil or head loss across the soil-geotextile interface. For example, Table 7.2 shows a GR value of 0.61 for medium sand and ST170 test sample at the end of Cyclic 3 stage which suggests a decrease in rate of head loss across soil-geotextile interface. However, as mentioned in Section 7.2.2, this decrease was due to increase of head loss within the soil. Therefore, the best practice is to observe the filtration performance of soil-geotextile in terms of hydraulic conductivity as well as GR together.

No continuous increase or decrease in GR was observed during the static and cyclic stages (Appendix C). For the static and three cyclic stages applied, the change in GR after each successive stage was more obvious for Cyclic 1 stage but it was not significant. The GR

plot shows that this change occurred during the first 500 cycles. No significant effect of increase in frequency (Cyclic 2 stage) and increase in deviator stress (Cyclic 3 stage) was observed on GR values for all test samples.

Fischer (1994) indicated that GR values may not truly reflect the filtration behaviour of soil/geotextile combinations due to small soil-geotextile zone in the GR apparatus. Another ratio, called permeability ratio (KR), has been used by different researchers (Aydilek & Edil, 2002; Emin Kutay & Aydilek, 2005) to investigate filtration tests with silty sand and fine material. The permeability ratio is given by:

$$KR = k_s/k_{sys}$$

A KR value greater than 1 indicates clogging of geotextile due to reduction in system permeability. The KR values for the filtration tests are plotted next to GR values in Table 7.2. The KR value is greater than 1 for most of the test samples. The medium sand with NW8 test sample which showed bridging network formation and increase in hydraulic conductivity at the soil-geotextile interface, a KR value more than 1 was computed. The main reason is that, for soils having high permeability, the hydraulic behaviour of the filtration system is dominated by soil unless clogging or piping occurs. This can be seen from Table 5.2 where k_s values have a direct effect on k_{sys} values, however, this effect decreased for soils having less k_s. On the other hand, the GR value is a good measure for assessing the filtration performance for soils having high permeability which is recommended by ASTM-D5101 (2012) and Holtz et al. (2008)

.

Table 7.2 GR and KR values for narrow graded soils

Geotextile	Soil	O_{90}/d_{85}	O_{90}/d_{50}	O_{90}/d_{15}	End of Static Stage		End of Cyclic Stages					
							Cyclic 1		Cyclic 2		Cyclic 3	
					GR	KR	GR	KR	GR	KR	GR	KR
NW20	Medium Sand	0.17	0.28	0.28	1.27	1.07	1.51	1.09	-	-	-	-
ST170	Medium Sand	0.17	0.28	0.47	0.90	0.95	0.89	0.97	0.9	0.97	0.61	0.90
NW20	90% Sand 10% PFA	0.18	0.30	0.61	1.79	1.18	1.73	1.21	1.72	1.20	1.97	1.22
NW8	Medium Sand	0.29	0.48	0.80	0.83	1.30	0.69	1.11	-	-	-	-
NW20	Fine Sand	0.36	0.41	0.82	1.06	1.00	1.15	1.17	1.15	1.14	1.31	1.34
NW8	90% Sand 10% PFA	0.30	0.52	1.04	1.66	1.18	1.65	1.17	1.65	1.17	1.65	1.21
NW8	Fine Sand	0.62	0.71	1.41	0.38	0.85	0.46	0.87	0.45	0.88	0.43	0.89

7.3. Filtration Behaviour of Broadly Graded Soils

The broadly-graded soils were mostly evaluated as internally unstable by the geometric criteria. In order to evaluate the filtration performance of soil-geotextile interfaces for internally unstable soils, the results in Section 5.4 are discussed in this section.

7.3.1. Gradation of Particles Passed

Except one test, the mass of particles collected at the end of filtration test was less than the limit of 2500 g/m^2 recommended for significant piping by Lafleur et al. (1989). As explained in Section 7.2.1, his recommendations were based on long term flow conditions. The Kenney and Lau (1985) method suggests amount of fine particles in broadly-graded soils at most 20%. However, fine particles at 30% by mass passing has been recommended by Hameiri (2000) and Moffat (2005). Therefore, the piping here is suggested as the test samples for which d_{90p} is equal to the 30% of the original sample gradation.

The d_{90p} of passing soils was less than the O_{90} of geotextile samples. As suggested by Giroud (2010) and Fischer et al. (1990), the soil particles will not pass easily through openings of filters if the soil is in a dense state. As the soil samples were compacted during the testing program, the d_{90p} was expected to be much smaller than the opening size of geotextiles. From comparison of d_{90p} with the original gradation, it can be seen that the Kezdi (1979) and Kenney and Lau (1985) criteria predicted well the potential instability of broadly-graded samples (Table 7.3). The % original gradation values show that washed out particles for 85% sand 15% PFA, 80% sand 20% PFA, and 70% sand 30% PFA were part of the secondary structure of soil instead of primary structure. The secondary structure provides stability to the primary structure and its loss results in the internal instability of primary structure (Yadeti et al., 2013). The 60% sand 40% PFA, 40% sand 60% PFA, and

PFA mixes lost more than 30% original gradation which indicates loss of the primary structure of soils.

Table 7.3 Comparison of d_{90p} and original sample for broadly-graded soils

Geotextile	**Soil**	**O_{90} µm**	**d_{90p} µm**	**% original gradation**	**Kezdi (1979)**		**Kenney and Lau (1985)**	
					% finer by weight at $(D_{15}/d_{85})_{max}$	% finer by weight showing D_{15}/d_{85} >4	% finer by weight at $(H/F)_{min}$	% finer by weight showing H/F <1
NW20	85% Sand 15% PFA	70	25	11	5	5-15	10	5-11
F1200M	80%Sand 20%PFA	60	15	11	5	5-20	15	7-18
NW20	80%Sand 20%PFA	70	17	12	5	5-20	15	7-18
NW8	80%Sand 20%PFA	120	22	13	5	5-20	15	7-18
F1200M	70% Sand 30%PFA	60	16	15	5	5-30	25	10-26
F1200M	60%Sand 40%PFA	60	11	18	10	10-30	30	15-30
NW20	60%Sand 40%PFA	70	35	30	10	10-30	30	15-30
ST170	60%Sand 40%PFA	70	27	27	10	10-30	30	15-30
NW8	60%Sand 40%PFA	120	40	32	10	10-30	30	15-30
NW20	40%Sand 60%PFA	70	16	31	10	15-17	30	20-30
NW20	PFA	70	17	50	12	12-19	15	10-17
ST170	PFA	70	15	47	12	12-19	15	10-17
F1200M	PFA	60	13	45	12	12-19	15	10-17

7.3.2. Influence of Flow Regime

The water head distribution curves of broadly-graded samples show that most of the test samples showed internal instability (Section 5.4.1). The internal instability of soil particles results in segregation of particles which, therefore, results in a non-linear water head distribution as well as modifying the permeability properties.

The linear water head distribution of the 85% sand 15% PFA mix sample at the end of static and cyclic stages showed the internal stability of soil (Figure 5.12). No continuous increase or decrease in GR was observed (Appendix C). The post-test gradation showed no change in the gradation of soil near the geotextile interface. This suggests stable filtration behaviour at the soil-geotextile interface for this soil/ geotextile combination.

The water head distribution curves of all three test samples with 80% sand 20% PFA showed internal instability of test samples (Figure 5.13). The GR values did not show much difference at the end of static stage and Cyclic 1 stage (see Table 5.7). The permeability values show that soil-geotextile layer is less permeable than the base soil for the 80% sand 20% PFA mix with three geotextile samples (Table 5.8). The permeability plots show that k_{sg} for the 80% sand 20% PFA mix samples decreased during the start of static stage and then stabilized afterwards; suggesting the soil-geotextile interface reached equilibrium (Appendix C). The soil-geotextile interface permeability for test samples with F1200M and NW8 became stable after 2000 cycles. The test sample with NW20 sample showed a slow response in terms of k_{sg} stability. This may suggest continuous movement of fine particles towards the filter interface. The microscopic images of geotextile samples after filtration tests (see Figure 5.20) showed very few clogged particles inside the geotextiles which is supported by the partial clogging 'λ' values (Table 5.16). The post-test gradation showed a decrease in D_{15} of soil sample near the filter interface for F1200M

and NW20 samples which indicate blinding layer formation. However, no decrease in D_{15} near the filter interface occurred for NW8. This suggests that the larger O_{90} value of NW8 resulted in stable filtration behaviour at soil-geotextile interface instead of blinding.

The linear water head distribution of 70% sand 30% PFA mix (gap-graded) with F1200M for static and cyclic stages revealed the internal stability of test sample (Fig 5.14). No significant changes in GR value at the end of static stage and end of cyclic stages was observed. For all test samples with F1200M geotextile, the highest partial clogging value was observed for the gap-graded soil. Although the partial clogging value is not high, however, it indicates that the deficiency of a certain size range of particles make it easy for the smaller particles to move freely through the coarse particles filters (i.e. a lack of constriction). The post-test gradation shows an increase in D_{15} of soil sample near the filter interface which indicates washing out of fine particles.

The water head distribution of the 60% sand 40% PFA mix samples showed internal instability within the base soil as well as across the soil-geotextile interface at the end of cyclic stage (Figure 5.15). A GR less than one was obtained for all test samples during static and cyclic stages which indicate the soil-geotextile interface being less permeable than the base soil. The permeability values shows large difference in k_s values at the end of static and cyclic stages for NW20 and ST170 test samples which shows that the internal instability of base soil increased under cyclic loading (Table 5.9). The post-test gradation shows that particles were washed out near the filter interface for all test samples. As shown in Table 7.3, the % original grading was more than 30 for NW20 and NW8 geotextiles which indicate that the particles washed out were part of the primary fabric of the base soil. The % original grading was as less as 18 for F1200M. This shows that the pore sizes of F1200M were smaller enough to stop migration of the primary fabric of soil. The pore

water pressure at the soil-geotextile interface dissipated during the first 1000 cycles of cyclic loading for 60% sand 40% PFA mix samples (Appendix C). This effect was less prominent for test sample with NW8 since the test was already showing a continuous decrease in GR (erosion of fines) during the static stage. It is believed that this was due to the largest opening size of NW8 as compared to other geotextile samples. The decrease in GR for the 60% sand 40% PFA mix with NW8 was observed at higher rate during the cyclic stage which suggests particle loss, presumably, increased with cyclic loading. The GR value decreased significantly for the NW20 sample during the 2000-3000 cycles of cyclic loading, however, this decrease in GR was due to increase in head loss within the base soil which shows soil instability under cyclic loading.

The 40% sand 60% PFA mix with NW20 remained stable under static stage. The GR value decreased during the cyclic stage. As shown in Figure 5.16, the head loss in the sample was more than the head loss associated with the applied gradient. As the applied deviator stress was only 30kPa and the increase in head loss in base soil (25-75mm) occurred after 2000 cycles, it is presumably caused by the migration of soils from top layer into the 25-75mm base soil layer under dynamic loading rather than the deformation of test sample. It resulted in a decrease of GR after 2000 cycles. The % original gradation is more than 30 which shows primary structure of soil washed through geotextile (Table 7.3).

A GR less than one was obtained for PFA test samples with F1200M and ST170 and a GR value more than 1 for NW20 sample at the end of static stage. An effect of cyclic loading was observed on GR during the first 1000 cycles for all test samples, which resulted in a GR less than 1 for PFA with NW20. The % original gradation indicates that the particles passed are part of the primary fabric of soil. This is supported by the post-

test gradation where an increase in D_{50} occurred for the soil near the geotextile particles. The partial clogging values show that test samples with PFA showed more clogging as compared to other filtration tests. This possibly shows that some of the particles which were piping through the geotextile samples retained inside the filters.

7.3.3. Clogging Ratios

The broadly-graded soils did not show a GR more than 3, a limit set for clogging by U.S Army Corps of Engineers (1977) (see Table 5.7). As discussed in Section 7.2.3, it is suggested to use permeability ratio 'KR' along with GR to assess the filtration performance of soil-geotextile interfaces in terms of hydraulic conductivity. Figure 7.1 shows GR and KR versus O_{90}/d_{30} for broadly-graded samples. The grain size 'd_{30}' has been used since this grain diameter has been recommended by Lafleur (1999) to retain the finer part of base soil grain size distribution.

It can be seen from Figure 7.1 that, for all broadly-graded filtration tests, a good correlation can be found between KR and O_{90}/d_{30}. The KR value decreased with increasing the O_{90}/d_{30}, suggesting the hydraulic conductivity of the system increased with decreasing the particle sizes. The GR for 80% sand 20% PFA mix with NW8 showed a GR value of 1.13. The KR for the same soil-geotextile interface was measured as 1. Therefore, this soil will be considered as internally stable during the design criteria. The GR for 85% sand 15% PFA and 70% sand 30% PFA mixes showed a GR less than 1. This behaviour is already explained in Section 7.3.2 where they were evaluated as internally stable. The same test samples showed KR values nearly equal to one which suggests the hydraulic conductivity of soil-geotextile interface is same as base soil and the arrangements are stable. Apart from these two samples, the GR and KR showed a similar correlation with O_{90}/d_{30}. It shows that both GR and KR values provide valuable information about the

filtration performance of geotextiles. However, the formation of a bridging network and blinding layer, as well as the internal stability of the soil should be further investigated by performing post-gradient ratio test sieve analysis.

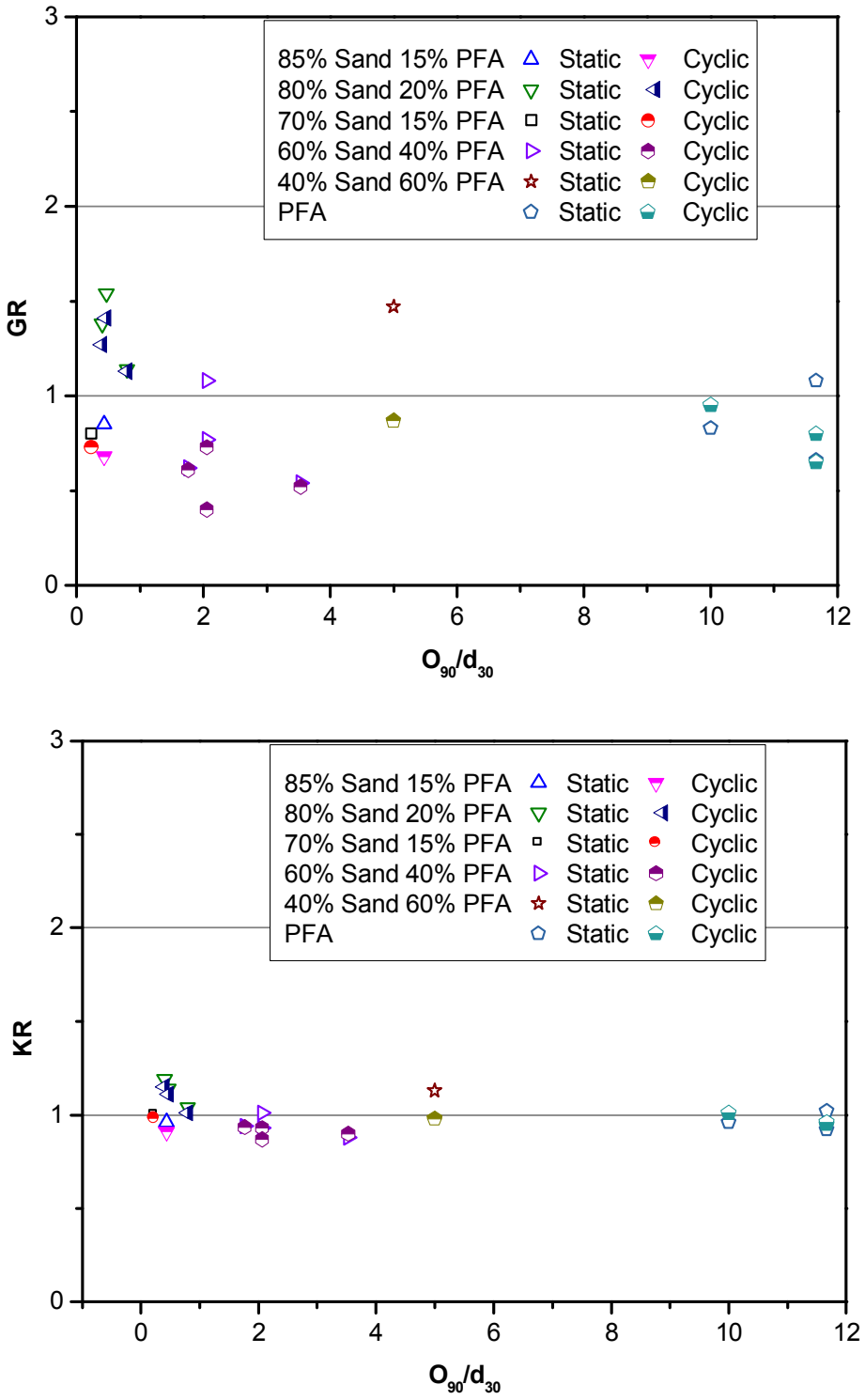


Figure 7.1 GR and KR values for broadly-graded soils

7.4. Effect of Geotextile PSD on Filtration Performance

As discussed in Section 2.7.1.1, although the wet sieving method to measure O_{90} of geotextile specimens is currently the European Standard (EN ISO 12956), there are several problems associated with this method. Nevertheless, many researchers have recommended O_{90} for retention of soil particles (Table 2.6). The wet sieving method measures the largest opening size instead of measuring the complete pore size distribution (PSD). To observe the effect of geotextile PSD on filtration performance of soil-geotextile interface, a new method '3-D constriction size' was suggested to measure the complete PSD of geotextiles (Section 6.5). The new method is able to measure the constriction sizes by finding the minimum throat of pore channels. The PSDs of two geotextile samples, NW20 and ST170, were measured using this method. Both geotextile specimens have the same O_{90} value (70μm) but different PSD (Figure 6.19).The results of six filtration tests with NW20 and ST170 geotextiles are summarized in Table 7.4. Three constriction pore sizes of geotextile samples i.e. C_{95}, C_{50} and C_{15} are used in the pore size to grain size ratios. The opening size O_{50} has been suggested by C.F.G.G. (1986) and Christopher and Holtz (1985). The Table shows that both geotextile samples have same O_{90}/d_{30} ratio but different filtration performance. The variation of C_{95}/d_{30} is less as compared to C_{50}/d_{30} and C_{15}/d_{15}. It shows that both geotextiles have very similar largest opening sizes but the smaller pore sizes are in different proportions different from each other. The retention of both geotextile specimens is explained in terms of C_{50}/d_{30}.

For the filtration tests with medium sand, both geotextile samples performed well in terms of retention of soil. The amount of soil particles passed, partial clogging level, and d_{90p} of both geotextile samples were similar. NW20 geotextile showed blinding with medium

sand as compared to ST170 where a stable soil-geotextile interface was observed (Section 7.2.1).

For the 60% sand 40% PFA mix, a different filtration response was observed with both geotextile samples. The amount of soil passed was measured to be more for NW20 sample. The partial clogging level shows more clogged particles inside ST170. Although ST170 geotextile has less thickness than NW20, the higher partial clogging level is believed to be due to the smaller C_{50}/d_{30} ratio of ST170. The d_{90p} of 60% Sand 40% PFA was measured smaller for ST170. As discussed in Section 7.3.1, the d_{90p} of ST170 indicated that the secondary fabric of original gradation has been transmitted whereas for the NW20 sample, the d_{90p} indicated that that washed out particles were part of primary fabric, indicating piping. The 60% sand 40% PFA mix showed higher GR values at the end of static and cyclic stages for ST170. The behaviour of both test samples in terms of GR and permeability is already explained in Section 7.3.2.

The PFA test series, which had a larger C_{50}/d_{30} ratio, reveals a slight difference between the two geotextile samples in terms of GR. The d_{90p} of both geotextile samples is higher which shows that the washed out particles constitute the primary fabric of soil in both cases. The smaller pore sizes of ST170 retained more fines inside as compared to NW20, as shown by the partial clogging level values. This is also supported by the X-ray CT images of both clogged geotextiles with PFA (see Figure 6.22). The amount of clogged particles inside ST170 sample was visually observed to be more than within the NW20.

The results of this comparison, therefore, indicate that the filtration behaviour of soil-geotextile samples can be assessed more precisely in terms of different pore sizes. A similar characteristic opening size of two geotextiles does not necessarily mean the same PSD, it is this that can lead to different filtration responses of geotextile samples.

Table 7.4 Summary of filtration tests for NW20 and ST170 geotextile samples

Geotextile	Soil	$\frac{O_{90}}{d_{30}}$	$\frac{C_{95}}{d_{30}}$	$\frac{C_{50}}{d_{30}}$	$\frac{C_{15}}{d_{15}}$	GR		KR		Soil Washed Out (g/m^2)	Soil Retained in Geotextile (g/m^2)	Partial Clogging Level 'λ'	d_{90p}	% Original gradation	Filtration Result
						Static	Cyclic1	Static	Cyclic1						
ST170	Medium Sand	0.37	0.74	0.31	0.19	0.9	0.89	0.95	0.97	189	188	0.80	30	<4	NB/NP
NW20	Medium Sand	0.37	0.76	0.38	0.31	1.27	1.51	1.07	1.09	180	140	0.56	31	<4	B
ST170	60% Sand 40% PFA	2.06	4.12	1.74	3.63	1.08	0.73	1.01	0.93	370	241	1.02	27	27	NB/NP
NW20	60% Sand 40% PFA	2.06	4.26	2.10	5.88	0.77	0.4	0.93	0.87	480	188	0.75	35	30	P
ST170	PFA	11.67	23.35	9.80	29.00	0.66	0.65	0.92	0.95	450	425	1.80	15	47	P
NW20	PFA	11.67	24.15	12.00	47.00	1.08	0.8	1.02	0.96	410	385	1.54	17	50	P

B-Blinding; NB-No blinding; NP-No piping; P-Piping

7.5. Soil/Geotextile Compatibility

As previously discussed in Section 7.2.2, the filtration test with narrow graded soils showed no piping. Few samples showed blinding behaviour which will be discussed in Section 7.5.2. The filtration tests of broadly graded soils showed mixed behaviour in terms of blinding and piping. The results for narrow and broadly-graded soils are summarized in Appendix E.

The idea of a filtration test with narrow graded soil was to assess the filtration performance of internally stable soils. Four out of seven filtration tests for narrow graded soils showed blinding behaviour which shows internal instability of soil (see Section 7.2.2). The internal instability of narrow-graded soils may be attributed to the high hydraulic gradient applied to the test samples. The broadly graded soils showed internal instability in terms of blinding, as well as migration of particles within the soil and wash out through geotextiles (see Section 7.3.2).

The soil-geotextile compatibility is observed in terms of piping and clogging/blinding in the following sections. The filtration design criteria are based on relationships between geotextile characteristic opening size and base soil. The indicative grain size is usually d_{85}, d_{50} or d_{30}. The permeability criteria requires a permeability of geotextile more than 10 times that of soil for critical applications (Carroll, 1983; Christopher & Holtz, 1985). The permeability values of geotextile samples are given in Table 3.1. The permeability of three geotextile samples (NW20, ST170, and NW8) is more than 250 times the permeability of medium sand (Table 3.2) which has higher permeability than other soils samples. The permeability of F1200M samples is 50 times more than the permeability of sand. Therefore, the permeability criteria will not be evaluated for the test samples.

7.5.1. Piping

The retention criteria of geotextile requires little washed out of finer particles near the geotextile in order to develop a bridging network upstream of geotextile. The piping of soil may result in migration of finer particles as well as coarse particles from the soil matrix (Moffat, 2005). The undesirable piping limit through geotextiles has been set at 2500 g/m^2 (Lafleur et al. 1989) . This amount of soil piping may be too large an amount of base soil migrating into the downstream drain (Lafleur, 1999). However, their suggestions were based on long term filtration tests which were performed for 3000 to 8000 minutes for the static stage. The total duration of filtration tests (static and cyclic stages) in the current test program was not more than 300 minutes. Nonetheless, the filtration tests were performed under confined conditions and the soil samples were compacted. There is a possibility of less mass of particles passing through geotextile openings if the soil sample is in dense state (Giroud, 2010). That is the probable reason that except one test, the rest of filtration tests showed mass of particles washed out less than 500 g/m^2 (Table 5.3 and 5.13). Different soils can lose different masses before the filter equilibrium is reached, and the loss of soil particles may affect the soil skeleton's stability dependant on the grain size distribution (Cazzuffi et al., 1999). The consideration of 2500 g/m^2 cannot be viewed as a limitation (Hawley, 2001). The short-term tests undertaken in the present study also helps to explain, for the filtration test without geotextile, for which O_c/d_{85} was as large as 4.77, why only 2315 g/m^2 of soil mass was collected (see Table 5.18). Kenney and Lau (1985) suggested amount of mobile finer fraction at most 20% of the total mass for widely graded soils. Internally unstable soils are usually broadly-graded soils which have a potential of erosion of finer particles, which leave the coarser fraction less effective in protecting the core materials from erosion (Wan and Fell, 2008). The transport of finer fraction of soil affects the stability of coarser

fraction as well (Yideti et al., 2013). Moffat (2005) and Hameiri (2000) reported the 20% limit as conservative and suggested 30% of total mass as considerable portion of finer fraction for widely graded soils, therefore, considering 30% as piping limit. The limit state of piping occurs when the primary fabric of base soil move through the geotextile filter by the hydraulic flow (Moraci and Mandaglio, 2008). Therefore, the piping limit is better defined as a gradation of particle passed constituting less than 30% of the original soil gradation.

Figure 7.2 shows mass of particles collected and % original gradation (% finer by weight of original sample having same size as d_{90p}) versus O_{90}/d_{85} and O_{90}/d_{30}. It can be seen that the mass of particles that passed through geotextiles gradually increased with increasing the O_{90}/d_{85} and O_{90}/d_{30} ratios. Except one test sample (60% sand 40% PFA with NW8 geotextile) which showed mass of particles passed through geotextiles equal to 2707 g/m^2, the rest of test samples showed mass collected below 500 g/m^2. As discussed in the earlier paragraph, the mass of particles collected cannot be taken as a piping limit. The piping limit depends on the retention of the primary fabric (coarse fraction) of soil. The % original gradation showed a well-defined relationship with O_{90}/d_{30} as compared to O_{90}/d_{85}. A better fit to the % original gradation is obtained for O_{90}/d_{30} ratio which suggests that a retention criteria based on O_{90}/d_{30} is preferable. The soil index size d_{85} does not give information about the smaller particles if the soil is not smoothly graded. The smaller particles need to be retained to satisfy the retention criteria for geotextile. As shown in Figure 3.1 and Figure 3.4, all soils are concave upward graded except medium sand and fine sand which are uniformly graded. It can be seen from figure 7.2 that the % original gradation increased with increasing the O_{90}/d_{30}. Although a geotextile is not expected to retain all the soil particles, however, the retention criterion on the basis of O_{90}/d_{30} make sure that lowest size of the primary fabric is retained. Most of the filter design criteria take

into account the d_{85} of the base soil which usually satisfies the retention criterion for narrow graded soils as these soils are mostly internally stable (Lafleur, 1999). The Lafleur (1999) criterion recommends the use of smaller grain diameters in filter design to avoid erosion of the primary fabric of concave upward soils which are usually internally unstable. A similar approach has also been suggested by Moraci et al. (2011) who suggested critical diameter for suffusion instead of d_{85} or d_{50} for retention of internally unstable soils. The critical diameter of suffusion can be defined as the diameter of soil at which maximum instability of soil is expected. The critical diameter of suffusion is chosen in correspondence $(H/F)_{min}$ (H, mass fraction between particle diameter D and 4D; F, mass fraction of particles smaller than D) in Kenney and Lau (1985) method (see Appendix A).

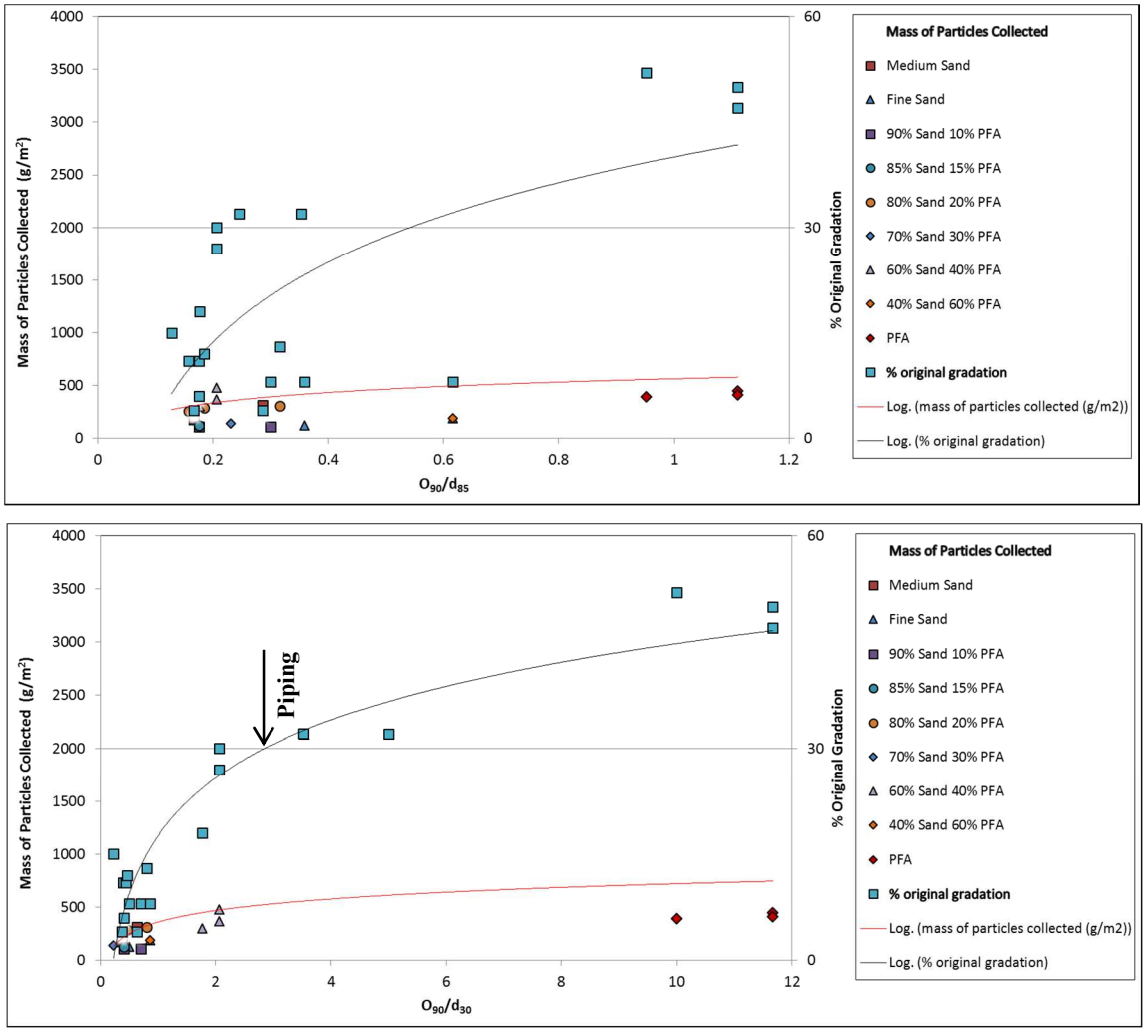


Figure 7.2 Retention criteria on basis of O_{90}

It can be seen from Fig 7.2 that the line of best fit shows % original gradation more than 30 at a O_{90}/d_{30} ratio of 2.9 which indicate the wash out of coarse fraction of soil through geotextiles. Thus the retention criterion on the basis of O_{90}/d_{30} to limit piping is suggested at a ratio of 2.9.

Two geotextile samples, NW20 and ST170, which have the same O_{90}/d_{30} ratio, showed different behaviour with same test samples (Table 7.4). As explained in Section 7.4, this difference in behaviour was attributed to the difference in PSD of both geotextiles. All filtration tests with NW20 and ST170 are plotted versus C_{50}/d_{30} (Figure 7.3).The constriction sizes for both geotextiles were measured by a new method which is explained in Section 6.5. The median constriction size C_{50} is used in the plot since the two geotextiles have similar large constriction sizes but different median constriction sizes (Figure 6.19). The C_{50} can be considered as a more meaningful size with which soil fines may interact. It can be seen from Figure 7.3 that the mass of particles as well as % original gradation increased with increasing C_{50}/d_{30} for both geotextile samples. For the 60% sand 40% PFA mix, the NW20 sample lost % original gradation more than 30 which indicates piping while the ST170 sample showed a % original gradation less than 30 which indicates that that the coarse fraction of soil was retained. This difference in behaviour cannot be explained by the O_{90} pore opening size. The retention criterion on the basis of C_{50}/d_{30} to limit piping is suggested at 2.5.

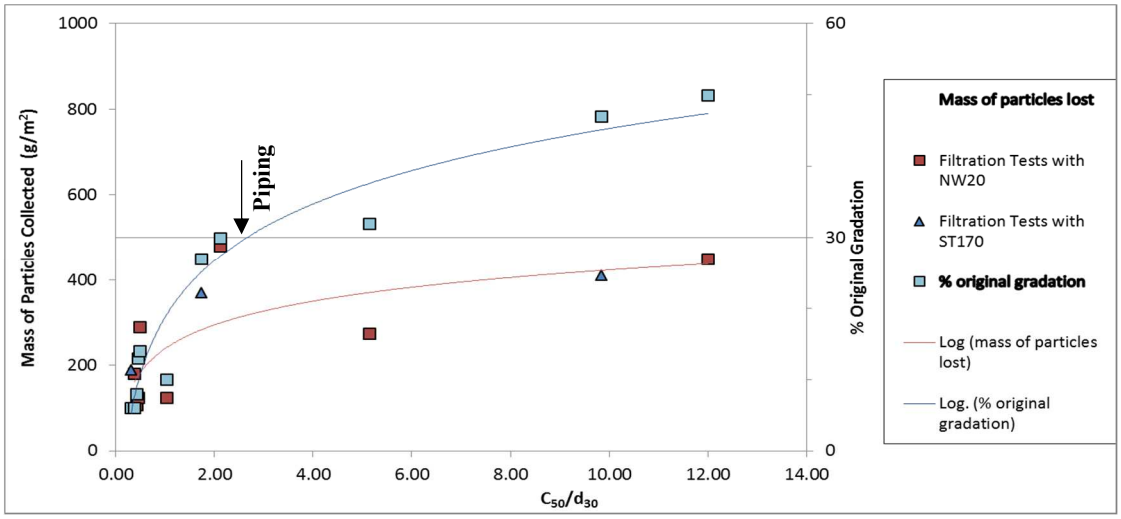


Figure 7.3 Retention criteria on basis of C_{50}

The filtration results are compared with the existing filtration design criteria which are representative of those most widely used in practice (Table 7.5). These criteria are for unsteady flow conditions. Two more criteria i.e. Lafleur (1999) and Moraci et al. (2012), although for steady state conditions, are also compared with the current filtration results since these criteria are based on minimum grain size and critical suffusion diameter (D_c), respectively. In Table 7.5, the relationship between geotextile characteristic opening size and base soil is evaluated using an interaction ratio (IR):

$$IR=\frac{O_i}{C \times d_i} \tag{7.1}$$

Where O_i is the characteristic opening size of geotextile, C is constant, and d is the indicative grain size (d_{85}, d_{50}, d_{30} or d_c).

The criteria in Table 7.5 use either Apparent Opening Size (AOS) or Filtration Opening Size (FOS) of geotextiles. The differences in the characteristic opening sizes (AOS, O_{90}, and FOS) are attributed to the different methods used to measure these pore sizes (Section 2.7.1.1). Bhatia et al. (1996) found that, for non-woven geotextiles, the O_{90} of geotextile

samples is 60-70% of AOS while O_{90} is nearly equal to FOS in most of the cases. Using this relation, O_{90} will be taken as 65% of AOS, and will be considered equal to FOS.

Table 7.5 The interaction ration (IR) for widely used retention criteria in practice

Author	**IR**	**Comments**	**Flow Condition**
Holtz et al. (1997)	$O_{95}/(0.5d_{85})$	Internally Stable Soils	Unsteady
Heerten (1982)	O_{90}/d_{50}	Granular soils	Unsteady
Lafleur (1999)	FOS/d_{85}	Granular soils ($C_u < 6$)	Steady
	$FOS/(5d_{30})$	Granular soils ($C_u > 6$ & concave upward)	
Moraci et al. (2012)	$FOS/(3D_c)$	Granular soils ($C_u > 6$)	Steady

Figure 7.4 illustrates the Holtz et al. (1997) criterion for all the dynamic filtration tests. Although the Holtz et al. (1997) criterion is suggested for internally stable soils, it is compared here with the new piping criteria. The Holtz et al. (1997) criterion is not supported by any systematic mechanics-based study of soil-geotextile behaviour in dynamic, cyclic or pulsating flow. According to the Holtz et al. (1997) criterion, a soil will be susceptible to piping if it shows an IR greater than 1.

Figure 7.4 shows two different trends. Trend 1 shows narrow graded soils and three broadly graded soils i.e. 85% sand 15% PFA mix, 80% sand 20% PFA mix, and 70% sand 30% PFA mix. The soil gradations between d_{85} and d_{30} for these soils are linearly graded. The trend 2 shows the broadly graded soils for which the gradation between d_{85} and d_{30} is non-linear. Since IR which is based on d_{85} soil index size is plotted against O_{90}/d_{30}, it

shows different trends for both gradations. It can be seen from figure that Holtz et al. (1997) criterion suggests fine sand is susceptible to piping. The filtration tests with narrow graded soils showed that fine sand was retained by the geotextile samples (Section 7.2.2). The criterion tends to be more conservative for narrow graded soils which is in agreement with Srikongsri et al. (2011) and Hameiri (2000). Also, the criterion suggests that the 80% sand 20% PFA mix with NW8 may be susceptible to piping, although the filtration test showed a GR slightly more than 1 and % original gradation value of 13 which shows that the finer portion of the original gradation lost was less. This might be due to the fact that the criterion emphasizes the need for contact between geotextile and the soil which results in a more conservative design.

The criterion seems to be less conservative for broadly-graded soils. The probable reason is that the Holtz et al. (1997) criterion is valid only for internally stable soils which are mostly narrow graded soils. Also, the internal instability of soils were enhanced by dynamic loading which resulted in increase of washing out of soil through geotextiles (Section 7.3.2). This shows that the use of Holtz et al. (1997) criterion ($O_{90}/d_{85} < 0.5$) under dynamic loading with broadly-graded soils bears the risk of piping. The criterion is based on d_{85} size which does not give idea about smaller gradation sizes if the gradation curves are not smooth.

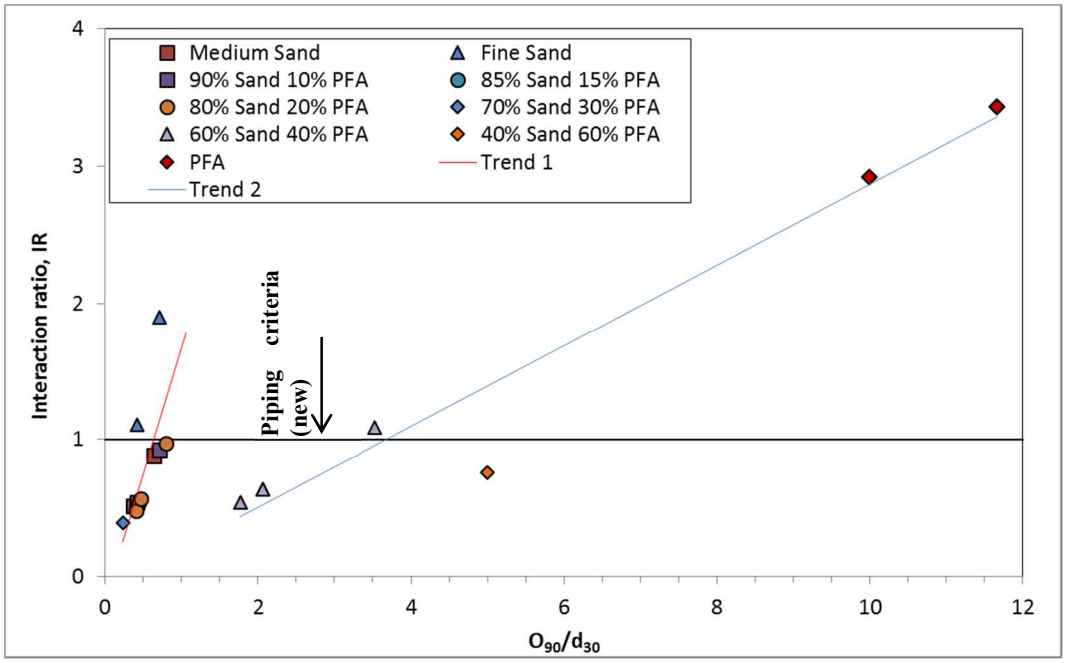


Figure 7.4 The interaction ratio based on Holtz et al. (1997) criterion with current test results

The Heerten (1982) criterion is based on grain size d_{50} (Table 7.5). The interaction ratio on the basis of O_{90}/d_{50} (Fig 7.5) also shows two trends. The Trend 1 for Heerten (1982) criterion was found less conservative as compared to the Holtz et al. (1997) criterion. The Heerten (1982) criterion is less conservative with broadly-graded soils (Trend 2). The d_{50} grain size do not represent the lower end of the primary fabric of soil which increase the risk of piping for broadly-graded soils.

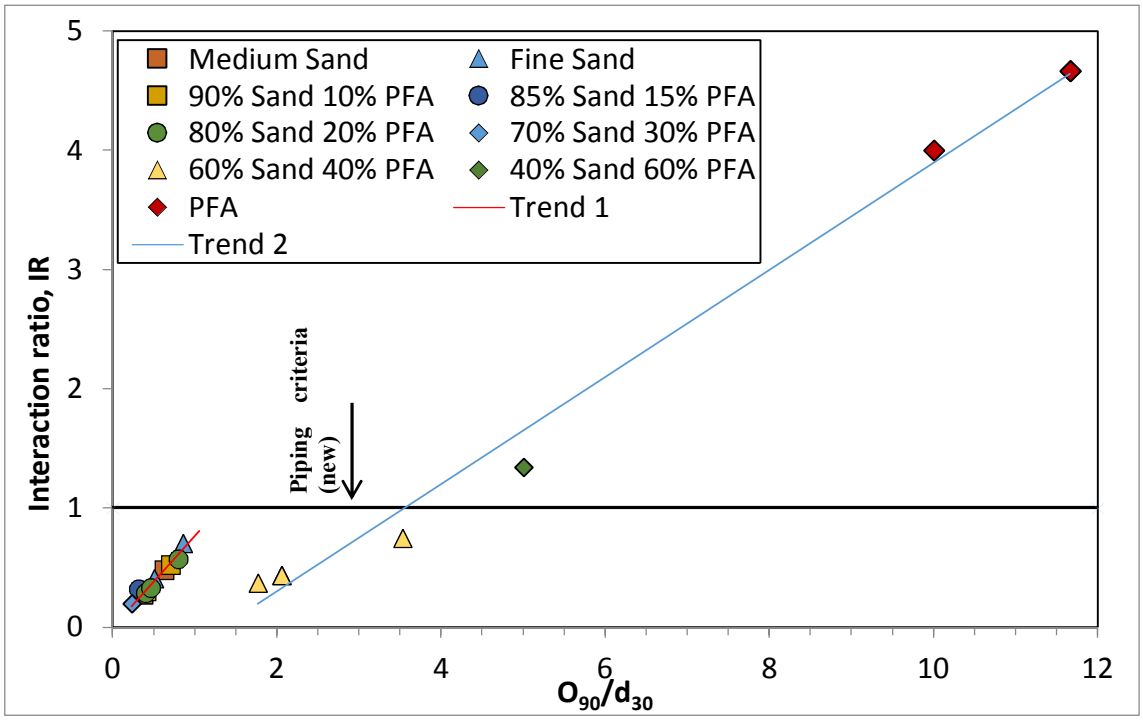
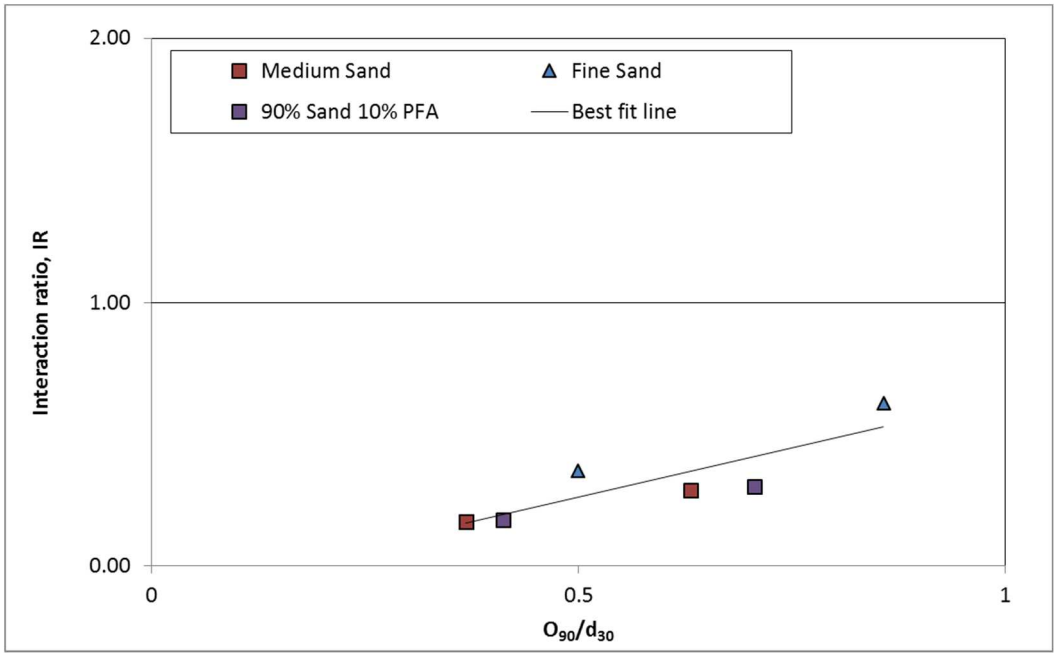
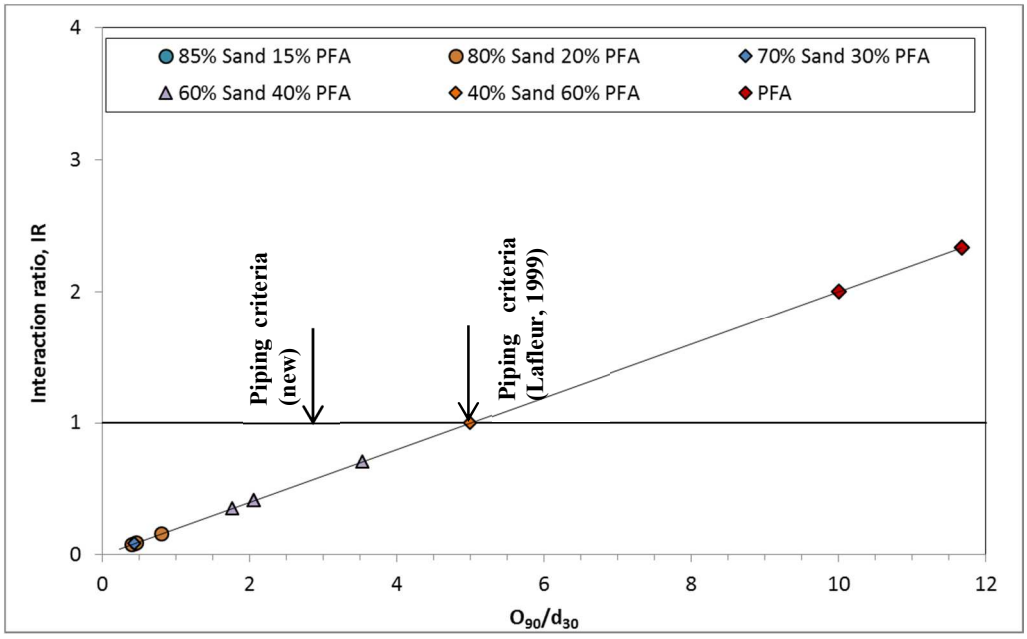


Figure 7.5 The interaction ratio based on Heerten (1982) criterion with current test results

Lafleur (1999) identified the potential risk of piping with broadly-graded soils and, therefore, suggested retention criteria for narrow and broadly-graded soils separately (Table 7.5). The proposed criteria are based on steady state flow conditions. The Lafleur (1999) criterion for steady flow conditions predicts well the retention behaviour of narrow-graded soils for unsteady flow conditions (Figure 7.6). The criterion is less conservative for broadly-graded soils. As discussed in Section 7.3.2, the dynamic loading appeared to increase the migration of soil within the base soil and through geotextiles for broadly-graded soils. The increase in instability was observed more for 60% sand 40% PFA, 40% sand 60% PFA, and PFA mixes in terms of water head distribution, and migration of soil within base soil and particles that washed out through geotextiles. Therefore, the Lafleur (1999) criterion for steady state flow conditions is less conservative for dynamic conditions.



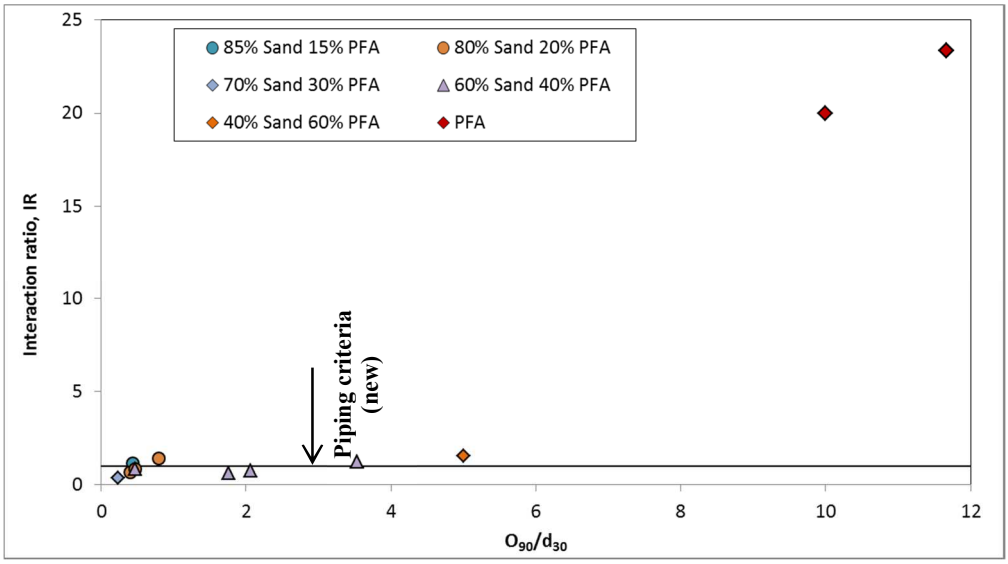
(a) Retention criterion for narrow graded soils



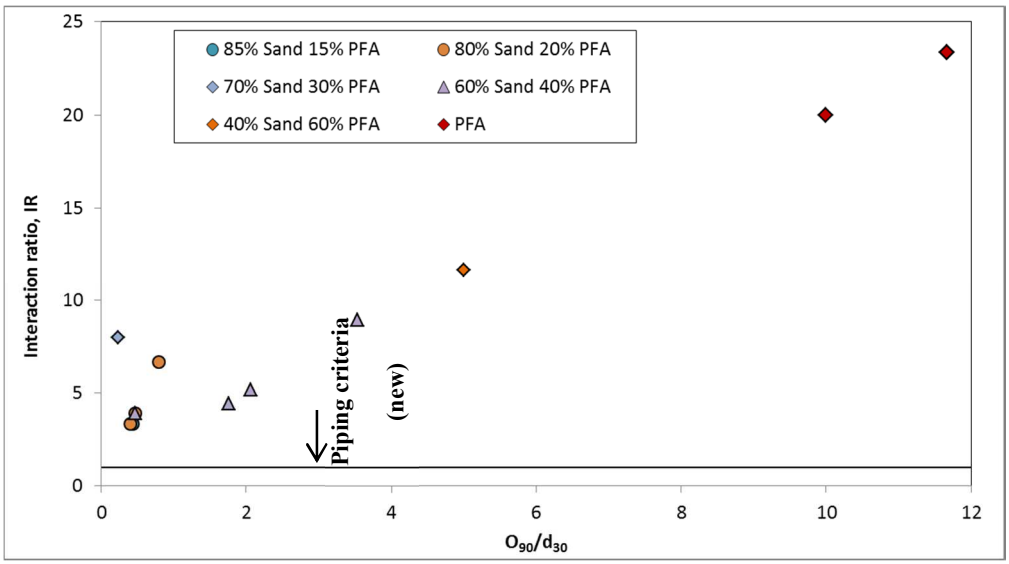
(b) Retention criterion for broadly-graded soils

Figure 7.6 The interaction ratio based on Lafleur (1999) criterion with current test results

Moraci et al. (2012) recommended retention criterion on the base of critical suffusion diameter (D_c) since it indicates the highest potential of migration of fines through the primary fabric of soil. Figure 7.7 shows IR on the basis of D_c measured by the Kenney and Lau (1985) (Figure 7.7a) and Kezdi (1979) method (Figure 7.7b). The D_c is chosen in correspondence $(H/F)_{min}$ (H, mass fraction between particle diameter D and 4D; F, mass fraction of particles smaller than D) in Kenney and Lau (1985) method, and (D_{15c}/D_{85f}) in the Kezdi (1979) method. The Fig 7.7a shows that the Moraci et al. (2012) retention criterion, although suggested for steady flow conditions, predicted well the response of many filtration tests. Although the D_c used in Moraci et al. (2012) criterion is calculated on the basis of a theoretical model 'SimulFiltr', however, the Kenney and Lau (1985) method predicts well the values of D_c (Moraci et al., 2011). The two test samples i.e. 80% sand 20% PFA with NW8, and 85% sand 15% PFA with NW20, were predicted as susceptible to piping by the Moraci et al. (2011) criterion, although these samples behaved stable during the filtration process (Appendix E). The reason is that the D_c values measured by the Kenney and Lau (1985) method for these soil samples were too small which corresponded to less than 15% finer of soil gradations and, therefore, higher IR's were computed ($IR = O_{90}/3D_c$). One test sample (60% sand 40% PFA mix with NW20) which showed piping was predicted non-susceptible to piping by the criterion. The criterion needs to be more conservative for the dynamic flow conditions to stop piping of particles. On the other hand, the IR calculated on the basis of D_c measured by the Kezdi (1979) method showed all filtration tests susceptible to piping. The Kezdi (1979) criterion, unlike the Kenney and Lau (1985) criterion, does not take into account the relative density of soils and is more conservative for finer fraction of soil gradation less than 15%. (Moraci et al., 2011).



(a) D_c based on Kenney and Lau (1985) method



(b) D_c based on Kezdi (1979) method

Figure 7.7 The interaction ratio based on Moraci et al. (2012) criterion with current test results

7.5.2. Clogging/ Blinding

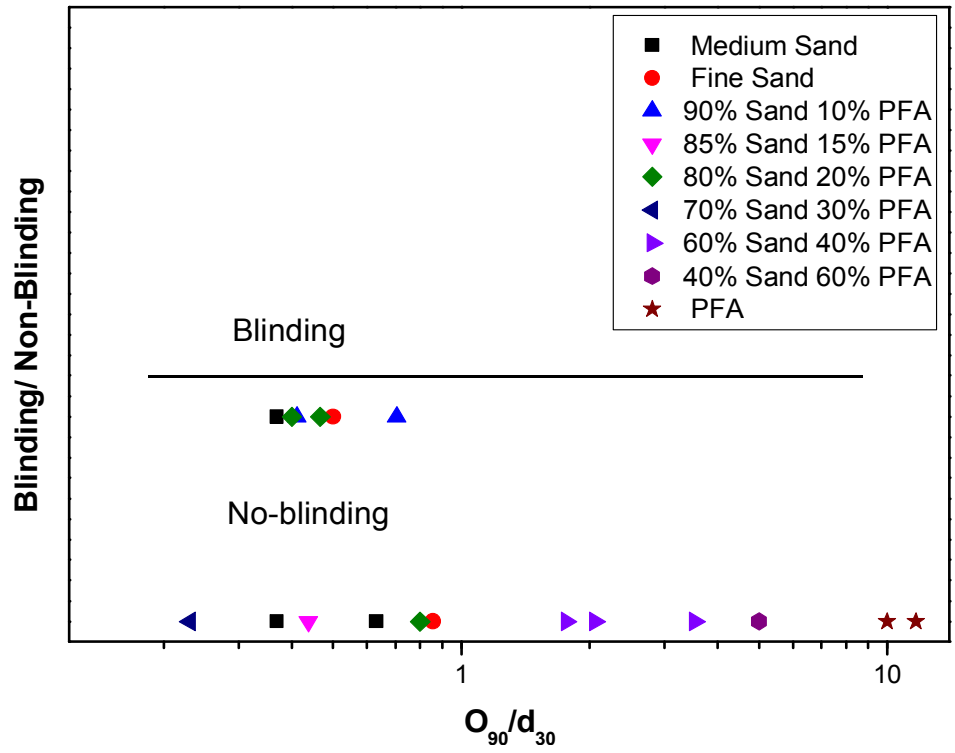
The tendency toward blinding was observed through GR values, permeability at the soil-geotextile interface, and the post-test gradation of soil near the geotextile interface. None of the tests showed a GR value more than the limit of 3 set by the U.S. Army Corps of Engineers (1977) for clogging of filters which means no serious clogging has occurred in

the soil-geotextile zone (Appendix E). This is supported by the microscopic observation of geotextile samples after filtration tests (Section 5.3.4.4 & Section 5.4.4.4).

The results show that four geotextile samples with narrow graded soils and two samples with broadly-graded soils showed blinding which resulted in a decrease in soil-geotextile permeability and a GR value more than 1. This blinding layer is believed to have been formed during the static stage since no significant effect of cyclic loading was observed on the soil-geotextile permeability. The permeability of the soil-geotextile interface was slightly less than the permeability of the base soil (Table 5.2 and Table 5.8) which shows that no severe blinding occurred. The GR for test samples which showed blinding showed a slight increase during the cyclic loading for narrow graded soils, while a slight decrease in GR occurred for broadly graded soils (Appendix E). Cazzuffi et al. (1999) observed no blinding of geotextile samples for smaller geotextile opening to grain size ratios, although his findings were based on change of flow directions which resulted in removing the particles from the geotextile interface (accumulated during downward flow) by an upward flow direction. The test condition during the present testing program was dynamic unidirectional which is a typical of traffic load.

Not much literature is available regarding the blinding criteria for geotextile filters. A similar design criterion is used for blinding and clogging since both mechanisms result in stopping of fine particles and increase the pore water pressure. The blinding criterion recommends the characteristic opening size of geotextiles to be large enough to permit the washing out of soil particles near the geotextile interface. There is no suggested criteria for clogging/blinding limits for dynamic flow conditions. There are few criteria available for static flow conditions which are based on characteristic opening size of geotextiles to smaller soil index sizes (d_{15} or d_{30}) (see Table 2.8). The use of a large pore size of

geotextile is recommended for clogging criterion to stop particles trapping inside the geotextiles (Koerner, 2012, Lafleur, 1999). Some researchers define the clogging limit in terms of porosity of geotextiles. If a geotextile has more porosity, it will not allow the accumulation of fines inside the filter. The filtration tests in terms of blinding and non-blinding versus O_{90}/d_{30} and O_{90}/d_{15} are summarized in Figure 7.8. It can be seen that blinding results all fall below the threshold value of 0.8 for O_{90}/d_{30} and 2.33 for O_{90}/d_{15} values respectively, although this is also true of some non-blinding behaviour. A stable bridging network was observed for test samples which did not show blinding for smaller O_{90}/d_{30} and O_{90}/d_{15} values. The blinding layer during the testing program was observed for two uniformly graded soils and four concave upward gradation soils. It is not easy to define the blinding limit on the basis of O_{90}/d_{15} ratio since the O_{90}/d_{15} ratios between 2.33 and 4 are missing (Figure 7.8). However, the blinding limit is clearly defined for O_{90}/d_{30} values. The blinding behaviour of geotextiles could be explained in terms of the grain index size d_{30} to be consistent with the observations of Kenney and Lau (1985), Lafleur (1999), Hameiri (2000) and Moffat (2005). Koerner (2012) recommended minimum migration of fines for internally unstable soil so that the stability of base soil is not affected. It can be seen from Figure 7.2 that the % original gradation is less than 10% for most of the test samples for a O_{90}/d_{30} ratio below 0.8. The blinding criterion for filtration tests is nearly similar to Lafleur (1999) criterion under static unidirectional flow which recommends O_{90}/d_{30} ratio more than one to avoid blinding limit state. The Lafleur (1999) criterion is for concave upward soil gradation and is conservative (Hameiri, 2000).



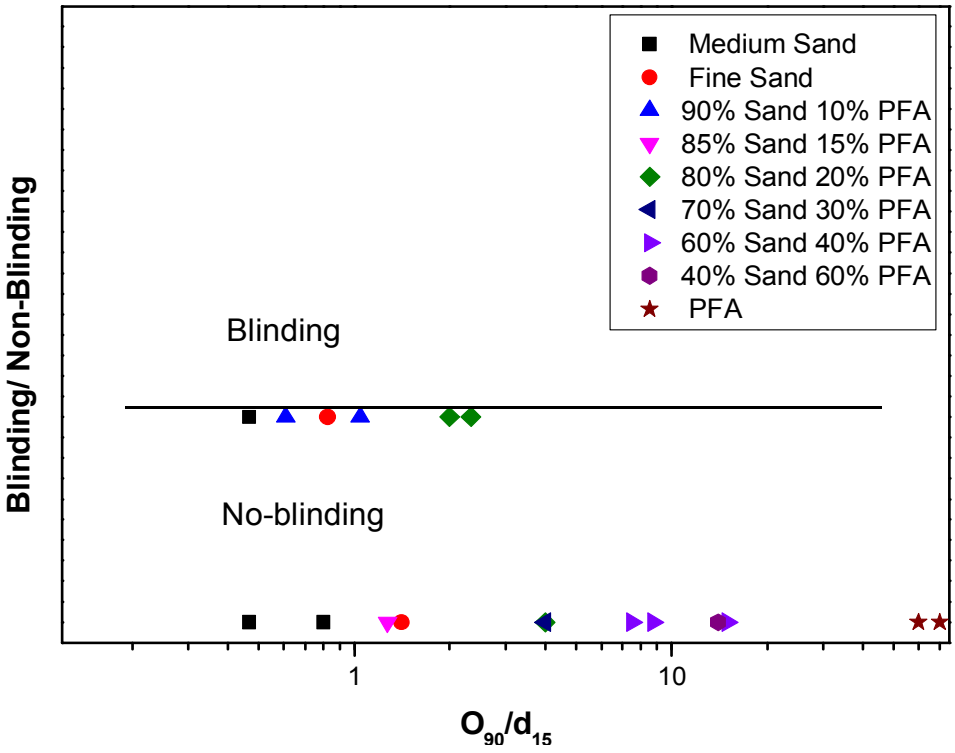


Figure 7.8 Summary of filtration tests in terms of blinding/ non-blinding

7.6. Summary of Suggested Criteria

It is possible to define piping and blinding limit states on the basis of O_{90} opening size. The O_{90} opening size was found to be the controlling factor on the filtration behaviour of soil-geotextile composite systems. The d_{85} and d_{50} index sizes do not give any idea about the smaller particle sizes for concave upward soils. However, the d_{30} soil index size was found to be more representative in terms of retaining the lower end of the coarse fraction of soil. As described in Section 7.4, the two geotextile samples which had similar O_{90} and C_{95} showed different filtration behaviour. This behaviour was better explained in terms of median constriction size C_{50}.

The design criteria suggested here is based on the ability of geotextile to retain the primary structure of soil fabric, while allowing a limited amount of the finer fraction to pass through geotextiles to avoid clogging/blinding of filters. The design criteria take into account the gradation of base soil and geotextile characteristic opening size, the density of soil, and confined conditions.

7.6.1. Piping

As shown in Figure 7.3, the piping limit was defined on the basis of % original gradation. Therefore, the design criteria on the basis of characteristic opening size of geotextile 'O_{90}' to retain the primary structure of soil is suggested as:

$$O_{90} < 2.9 d_{30} \qquad (7.2)$$

The retention capability of C_{50} constriction size is shown in Figure 7.3. Although the plot does not show many points due to unavailability of constriction sizes of other two geotextile samples, however, it can be seen that retention of base soil was achieved for

C_{50}/d_{30} ratio less than 2.5. Apply Equation 7.3 against piping on the basis of geotextile constriction size C_{50}.

$$C_{50} < 2.5d_{30} \quad (7.3)$$

7.6.2. Clogging/Blinding

As discussed in Section 7.5.3, no clogging of geotextile samples occurred. Blinding of samples occurred during the static stage. Apply Equation 7.4 against blinding if the soil is internally unstable.

$$O_{90} > 0.8d_{30} \quad (7.4)$$

7.7. Critical Review of Suggested Criteria

The soil-geotextile filtration mechanism is a complex process which depends on the physical compatibility between geotextile filter and the soil to be retained. Although there is no universal solution where a unique geotextile is compatible with all soil types or broad range of soils, however, it is possible to assess the filtration compatibility of geotextiles with soil types defined by parameters such as particle size distribution and state of compaction (Lee and Bourdeau, 2006). Geotextiles have been used as a separator and filter materials for several decades. Little literature is available that evaluates the dynamic filtration of geotextile with soils in highways and railroads (Section 2.8.3.1).The filter criteria (Section 7.6) is suggested on the basis of limited experimental work. Specific soil and geotextile materials were used in the dynamic filtration test program (see Chapter 3). The soil materials used in experimental program were prepared to be narrow graded (internally stable) and broadly-graded (internally unstable). In internally unstable soils, there is a risk of fine particles passing through the geotextiles due to fine particles ability to move within the voids of the primary fabric of soil (see Section 2.5). The geotextile

samples were selected due to their frequent use as filters for applications such as pavement edge drains, reservoirs and dams, and under revetments.

The experimental work was carried out by using the test apparatus described in Chapter 4. The test equipment was found to be advantageous over other test equipment used for filtration compatibility of soil-geotextile interface (see Table 2.10). All the filtration tests were performed under unidirectional dynamic flow conditions. Such conditions exists underneath highways and railroads as a result of traffic. The soil samples were compacted in the test apparatus to simulate field conditions. The in-situ deviator stresses were applied on the test samples which were calculated by using KENLAYER, a pavement design/ analysis software (see Figure 4.13).

The filter retention criteria (Section 7.6.1) was suggested to make sure that geotextiles stop the coarse fraction (primary fabric) of soil, while allowing the fines (secondary structure) to pass through geotextile (see Section 7.6.1). Moffat (2005) and Hameiri (2000) suggested finer fraction at most 30% of total mass for narrow graded and widely graded soils. Therefore, the retention criteria was suggested on the basis of d_{30} soil index size so that the coarse fraction of the soil is retained. The first suggested retention criterion is based on characteristic opening size O_{90} and d_{30} index size (Equation 7.2). The O_{90} pore size is measured from wet sieving technique which is the current European Standard for measuring the characteristic opening size of geotextiles (see Section 2.7.1.1). The retention criterion was compared with the existing filtration design criteria (see Section 7.6.1). The Holtz et al. (1997) criterion, which is based on d_{85} index size, was found to be more conservative for narrow graded soils (Figure 7.4). However, the criterion was found to be less conservative for broadly-graded soils which were evaluated as internally unstable by the geometric criteria (see Table 3.6). This is due to the fact that the Holtz et

al. (1997) criterion is based on d_{85} soil index size which, unlike narrow graded soils, does not give idea about the smaller gradation sizes for broadly-graded soils. A filter design criterion on the basis of d_{85} index size may not stop the smaller gradation sizes of broadly-graded soils. The erosion of primary fabric of soil through geotextiles may result in significant changes in volume inside the soil and/ or failure of the structure (see Section 2.4). The Heerten (1982) criterion which is based on d_{50} index soil, like Holtz et al. (1997) criterion, was found more conservative for narrow graded soils and less conservative for broadly-graded soils (Figure 7.5). Therefore, the retention criteria on the basis of d_{30} index size is more appropriate in terms of retaining the primary fabric of soil.

Another retention criterion (Equation 7.3) was suggested on the basis of median constriction size C_{50} and d_{30} index size to stop erosion of the primary fabric of soil. The median constriction sizes of geotextile samples were measured from a new suggested method '3-D constriction size method' (see Section 6.5). As discussed in Section 7.4, the filtration behaviour of geotextiles can be assessed more precisely in terms of different pore sizes. The retention criterion suggested on the basis of C_{50} takes the median pore size of the geotextile which is a more meaningful size in terms of interaction with soil fines. The suggested retention criterion could not be compared with the existing design criteria as the existing design criteria are based on the large pore sizes of geotextiles (see Table 2.6). The value of each pore size depends on the method to find these pore sizes (see Section 2.7.1.1).

The clogging/ blinding criterion is suggested on the basis of characteristic opening size O_{90} and d_{30} index size (Equation 7.3). The use of d_{30} index size for clogging/ blinding is recommended by Lafleur (1999) and Hameiri (2000). The clogging/ blinding criterion was found nearly similar to Lafleur (1999) and Hameiri (2000) criteria (Table 2.8).

The suggested filter criteria are suitable for geotextile filters underneath highways which are used as a separator to stop mixing of sub-grade particles with base-soil, and as a filter around pavement edge drains to stop erosion of subgrade soils into the drainage aggregate. The validity of the suggested criteria for bi-directional cyclic flow conditions, which exists in coastal structures, should be investigated. The change of flow directions in bi-directional cyclic flow conditions tends to destabilize the bridging network formed at the filter interface which results in erosion of particles near the interface (Giroud, 1982).

Chapter 8

Conclusions and Recommendations

Filter design criteria to meet the retention requirement are well established for steady state flow conditions. However, the filtration compatibility of soil-geotextile interface is challenging when dynamic conditions are applied. It becomes more severe when the surrounding soil is internally unstable. Therefore, the research study had two main aims. The first aim was to investigate the filtration behaviour of soil-geotextile interface with internally stable/ unstable soils under dynamic conditions. The second aim was to develop an appropriate filter design criteria which takes into account the internal instability of soils.

8.1. Conclusions

The main body of work and conclusions are summarised as follows:

8.1.1. Dynamic GR Apparatus

The filtration compatibility of soil-geotextile combinations were systematically investigated in laboratory by designing and developing a flexible wall gradient ratio test apparatus (see Section 4.1). The apparatus is capable of saturating the soil and has complete control over stresses. The apparatus can be used to perform filtration tests for fine grained soils since it is possible to saturate fine grained soils in a flexible wall membrane. Moreover, the accuracy of pore pressure measurement was improved by using

electronic pressure transducers instead of piezometers which have issues such as air trapped inside the tubings (see Section 4.1.2).

8.1.2. Test Procedure

The filtration tests were performed under an external hydraulic gradient of five (see Section 4.2.4). In terms of high gradients and full saturation of samples, the testing conditions can be considered more severe than most field conditions in terms of particle migration. The filtration test results obtained using flexible wall GR apparatus for different soil-geotextile combinations are believed to be realistic enough to define a filtration design criteria. The dynamic effect caused by moving traffic near to the roadway edge resulting in cyclic loading of the subgrade near the filter were induced in the laboratory.

8.1.3. A New Method to Find the PSD of Geotextiles

A new method '3-D constriction size method' was suggested to measure more realistically the 3-D pore size distribution (PSD) of geotextiles from X-ray CT images and image processing technique (see Section 6.5). The method is able to find the minimum pore size (constriction) of each pore channel. Moreover, a quick method to find the 2-D pore size distribution (PSD) of geotextiles was developed using image analysis. The 3-D PSD of geotextiles was compared with the 2-D PSD, volumetric PSD measured from mercury intrusion porosimetry (MIP), O_{90} values of geotextiles provided by the manufacturers which is based on wet sieving technique, and pore sizes measured from theoretical equations i.e. Giroud (1996) and Faure et al. (1990). The pore sizes measured from 2-D image analysis and MIP were measured higher due to the fact that O_{95} measured from 2-D image analysis and MIP is a function of pore space and pore volume respectively, instead of measuring the constriction sizes of pore channels. The O_{90} values based on the

wet sieving method, were found to be significantly less than the C_{90} values measured from the 3-D constriction size method. This high difference in the values may be due to the disadvantages associated with the wet sieving method. A good correlation was found for the C_{95} values measured from 3-D constriction size method and from theoretical pore equations. This suggests that the ability of the 3-D constriction size method to find the PSD creates the potential for filter design criteria on the basis of PSD. The two geotextiles NW20 and ST170, which have the same O_{90} values, showed similar large pore sizes C_{95} but different PSDs. This suggests a difference in filtration performance of geotextiles as suggested by Elton et al. (2007) and Fischer et al. (1990).

8.1.4. Dynamic Filtration Tests

The soil-geotextile filtration mechanism is a complex process. Its successful application depends on retention of soil particles by the geotextile while allowing the fines near the geotextile interface to wash through geotextiles. Therefore, it is important to consider the characteristics of soil at the site, and the range of available geotextile products. There is no universal design criteria which recommends a unique geotextile filter suitable for a broad range of soils. But it is possible to assess the filtration compatibility of geotextiles having known physical properties with soil types that are defined by parameters such as particle size distribution.

The test results (Section 5.2) showed that head losses in the system increased with increasing flow rate, which is due to energy losses associated with flow. The gradient ratios and permeability values (see Chapter 5) allowed identification of the different filtration mechanisms. However, the bridging network and blinding layer was better investigated by performing post-test gradations of soil above geotextile. Since the GR values do not differentiate between blinding and clogging mechanism, it is better to

understand the clogging mechanism with the help of microscopic images of geotextiles after the test and by measuring partial clogging level values. Another ratio, permeability ratio was used to assess the filtration behaviour of soil-geotextile interfaces in terms of permeability of soil and soil-geotextile system. The GR was found to be a good measure for assessing the filtration behaviour of soils having high permeability. For soils having low permeability, the filtration performance of soil-geotextile composite can be assessed in terms of both GR and KR. The gradation of particles washed out through geotextiles were smaller than the characteristic opening size of geotextiles for all test samples. This is attributed to the restricted mobility of soils due to dense state of soils and the confining stresses.

In general, the Kenney and Lau (1985) and the Kezdi (1979) criteria predicted well the internal stability/ instability of soils. The Kenney and Lau (1985) method was found more precise in terms of describing the portion of soil gradation which might show erosion. The Kezdi's (1979) criterion was found to be more conservative in terms of finding the critical diameter for suffusion. Two soil samples which were evaluated as internally stable by the Burenkova's (1993) criterion showed internal instability. One of the most interesting findings from the testing program is the influence of different index sizes of soils on filtration performance. The index size d_{30} was found to be more representative in terms of controlling the filtration behaviour as compared to d_{85}. This is due to the fact that most of the gradations were concave upward which are internally unstable (see Figure 3.4). For such gradations the index size d_{85} does not give idea about the smaller particles in the gradation and, therefore, does not guarantee the retention of particles below d_{85}.

One of the findings from this study was the influence of hydraulic gradient on the internal stability of soils. A blinding layer was observed for smaller O_{90}/d_{30} ratios for both

internally stable and unstable soils that was determined to have formed during the static stage. Since the blinding mechanism is a consequence of internal instability of a soil, it implies that a high hydraulic gradient has the ability to initiate the internal instability of a soil which results in the migration of fines towards the geotextile.

Another finding from this study was the influence of dynamic loading on the filtration performance of soil-geotextile combinations. No significant effect of dynamic loading was observed on test samples having smaller O_{90}/d_{30} ratios. The smaller opening size of geotextiles did not allow particles to pass through geotextiles. The instability of test samples, which had a higher percent finer by weight of original gradation that was expected to migrate within the soil voids, was enhanced by dynamic loading. That is, there was a migration of particles within the base soil and there was washing out of particles through geotextiles. The dynamic loading resulted in the migration of primary structure as well as secondary structure of soil gradations through the geotextiles (see Section 7.3). It concluded that the dynamic loading has the ability to influence the filtration behaviour at the soil-geotextile interface. No significant effect of increase in frequency and deviator stress on the filtration performance was observed. This suggests that dynamic conditions under low vertical stress have more influence on the internal instability of soils as compared to high vertical stress.

The geotextile characteristic opening size was found to be the most controlling factor on the filtration behaviour as compared to other geotextile properties (manufacturing style and thickness). Although thermally bonded geotextiles are considered problematic due to their smoother surface which favours blinding of soil at the geotextile surface, however, the blinding mechanism was also observed with both needle-punched as well as needle-punched with thermally-bonded geotextiles. The F1200M geotextile having much larger

thickness did not show much partial clogging level which suggests the particles were either retained at the surface of this geotextile or were smaller than the pore sizes and, hence, washed out. However, a good relationship was observed between O_{90}/d_{30} in terms of mass of particles washed out and piping (see Figure 7.2). It is concluded that the filtration design criteria should be on the basis of the pore size of the geotextiles as compared to other geotextile properties, which is also suggested by most of the researchers. Moreover, the NW20 and ST170 geotextiles having the same large openings but different PSD resulted in different filtration behaviour. This shows the need for a more accurate design criteria on the basis of PSD instead of on the basis of a single pore size.

8.1.5. Filter Design Criteria

It is not expected that geotextiles will retain all the solid particles. However, it should stop piping of the primary structure of soil which is the load carrying structure. Therefore, consideration of 2500 g/m^2 mass of particles washed out cannot be viewed as a limitation. The piping limit should better be defined as the gradation of particle passed that constitute less than 30% of the original soil gradation which constitutes the finer portion (secondary structure) of soil. The blinding mechanism should be stopped by allowing fines near the geotextiles to wash out. A design criterion was suggested as a piping limit on the basis of O_{90}/d_{30} which takes into account the combined effect of vertical stress, maximum hydraulic gradient, as well as the soil internal instability (see Section 7.6). Another criterion for limiting piping is on the basis of C_{50}/d_{30} which takes the median pore size of the geotextile as a more meaningful size with which soil fines may interact. Moreover, a criterion to stop blinding has also been suggested on the basis of O_{90}/d_{30}.

8.2. Recommendations for Future Research

The following recommendations are made for further research:

- The filtration tests have been performed by simulating field conditions. The filter criteria is suggested on the basis of limited laboratory data. It is recommended to perform more laboratory tests to further investigate the validity of the suggested criteria.
- The filter design criteria suggested in this research were derived for non-woven geotextile. It is recommended to extend the criteria to woven geotextiles. This can be done by following the research methodology performed in this research.
- To further investigate the effect of different dynamic conditions on the filtration performance of soil-geotextile interface, further testing should be done by using different hydraulic gradients, vertical stresses, soil gradations.
- As seen in Chapter 6, a new method was suggested to find the PSD of geotextiles. Due to limitation of the image analysis software, the pore shapes were assumed as spherical. Since the non-woven geotextiles have random pore shapes, it is recommended to use an image analysis software which can find random pore sizes of geotextiles to get a more realistic PSD.
- The 3-D constriction size method should be performed for more geotextiles and filtration tests should be performed with the same geotextiles to develop a more accurate filter design criteria.
- The geotextile manufacturing is a very rapidly developing and innovative industry. It is possible that new geotextile products will be developed in the near future which may have better filtration performances as compared to the currently

available geotextiles. It will be necessary to perform filtration tests with these geotextiles once they become available.

References

Acar, Yalcin B, Hamidon, Abu-bakr, Field, Stephen D, & Scott, Lisa. (1985). The effect of organic fluids on hydraulic conductivity of compacted kaolinite *Hydraulic barriers in soil and rock*: ASTM International.

Adel, H. D., Bakker, K. J., & Breteler, M. K. (1988). *Internal stability of minestone.* Proceedings of international symposium of modelling soil–water-structure interaction. Balkema, Rotterdam, pp. 225-231.

Allen, David L, & Fleckenstein, John. (1991). Evaluation and Performance of Geocomposite Edge Drains in Kentucky. *Transportation Research Record*(1329), pp.49-56.

Alobaidi, I., & Hoare, D. J. (1996). The development of pore water pressure at the subgrade-subbase interface of a highway pavement and its effect on pumping of fines. *Geotextiles and Geomembranes,* Vol. 14(2), pp.111-135. DOI: 10.1016/0266-1144(96)84940-5

ASTM-D18. (1970). Special Procedures for Testing Soil and Rock for Engineering Purposes: Fifth Edition *ASTM International*.

ASTM-D698. (2012). Standard Test Methods for Laboratory Compaction Characteristics of Soil Using Standard Effort (12 400 ft-lbf/ft3 (600 kN-m/m3)) *ASTM International*. West Conshohocken, PA.

ASTM-D2488. (2009). Standard practice for description and identification of soils (visual-manual procedure) *ASTM International*. West Conshohocken, PA, 2009.

ASTM-D4404. (2010). Standard Test Method for Determination of Pore Volume and Pore Volume Distribution of Soil and Rock by Mercury Intrusion Porosimetry *ASTM International*. West Conshohocken, PA.

ASTM-D4491. (2009). Standard test methods for water permeability of geotextiles by permittivity *ASTM International*. West Conshohocken, PA.

ASTM-D4751. (2016). Standard Test Methods for Determining Apparent Opening Size of a Geotextile *ASTM International*. West Conshohocken, PA.

ASTM-D5101. (2012). Standard Test Method for Measuring the Filtration Compatibility of Soil-Geotextile Systems *ASTM International*. West Conshohocken, PA.

ASTM-F316-11. (2011). Standard Test Methods for Pore Size Characteristics of Membrane Filters by Bubble Point and Mean Flow Pore Test *ASTM International*. West Conshohocken, PA.

ASTM. D6767-11 *Standard Test Method for Pore Size Characteristics of Geotextiles by Capillary Flow Test*. West Conshohocken, PA.

Aydilek, A. H. (2004). *Geotextile Pore Structure Characterization Using Image Analysis.* 4th International Conference on Filters and Drainage in Geotechnical and Environmental Engineering. GeoFilter 2004,

Aydilek, A., Hondt, D., & Holtz, R. (2006). Comparative Evaluation of Geotextile Pore Sizes Using Bubble Point Test and Image Analysis. *Geotechnical Testing Journal,* Vol. 30(3), pp.173-181. DOI: 10.1520/GTJ100663

Aydilek, A.H., & Edil, T.B. (2002). Filtration Performance of Woven Geotextiles With Wastewater Treatment Sludge. *Geosynthetics International,* Vol. 9(1), pp.41-69. DOI: 10.1680/gein.9.0210

Aydilek, AH. (2006). A semi-analytical methodology for development of woven geotextile filter selection criteria. *Geosynthetics International,* Vol. 13(2), pp.59-72. DOI: 10.1680/gein.2006.13.2.59

Aydilek, AH, & Edil, TB. (2003). Long-term filtration performance of nonwoven geotextile-sludge systems. *Geosynthetics International,* Vol. 10(4), pp.110-123. DOI: 10.1680/gein.2003.10.4.110

Aydilek, Ahmet H, Oguz, Seyfullah H, & Edil, Tuncer B. (2005). Constriction size of geotextile filters. *Journal of geotechnical and geoenvironmental engineering,* Vol. 131(1), pp.28-38. DOI: 10.1061/(Asce)1090-0241(2005)131:1(28)

Bell, A. L., McCullough, L. M., & Snaith, M. S. (1982). *An experimental investigation of sub-base protection using geotextiles.* Proceedings of the 2nd International Conference on Geotextiles, Vol. 2, pp. 435-440.

Bell, J. R., & Hicks, R. G. (1980). Evaluation of test methods and use criteria for geotechnical fabrics in highway applications - Interim Report. *No. FHWA-RD-80-021 Intrm Rpt.*

Bendahmane, F., Marot, D., & Alexis, A. (2008). Experimental Parametric Study of Suffusion and Backward Erosion. *Journal of Geotechnical and Geoenvironmental Engineering,* Vol. 134(1), pp.57-67. DOI: 10.1061/(ASCE)1090-0241(2008)134:1(57)

Bergado, DT, Youwai, S, & Maneecharoen, J. (2002). Influence factors on the laboratory testing of geotextiles under controlled environment. *Lowland technology international: the officisl journal of the International Association of Lowland Technology (IALT)/Institute of Lowland Technology, Saga University,* Vol. 4(1), pp.1-12.

Bertram, G. E. (1940). An experimental investigation of protective filters. Vol. 267, pp.21.

Bhatia, S.K., & Huang, Q. (1995). Geotextile Filters for Internally Stable/ Unstable Soils. *Geosynthetic International,* Vol. 2(3), pp.537-565. DOI: 10.1680/gein.2.0022

Bhatia, S.K., & Smith, J.L. (1996). Geotextile Characterization and Pore-Size Distribution: Part II. A Review of Test Methods and Results. *Geosynthetics International,* Vol. 3(2), pp.155-180. DOI: 10.1680/gein.3.0058

Blond, E., & Veermersch, O. (2015). *A Comprehensive Analysis of the Measurement Techniques used to Determine Geotextile Opening Size: AOS, FOS, O90, and 'Bubble Point'*. Geosynthetics 2015, February 15-18, Portland, Oregon,

Brown, SF, Lashine, AKF, & Hyde, AFL. (1975). Repeated load triaxial testing of a silty clay. *Geotechnique,* Vol. 25(1), pp.95-114.

BS-EN-ISO-12956. (2010). Geotextiles and geotextile-related products. Determination of the characteristic opening size. *International Standardization Organization*.

Burenkova, V. V. (1993). *Assessment of Suffusion in Non-Cohesive and Graded Soils.* Proceedings of the 1st International Conference "Geo-Filters, Filters in geotechnical and hydraulic engineering. Balkema, Rotterdam, pp. pp. 357−360.

C.F.G.G. (1986). Recomandations pour l'emploi des géotextiles dans les systemes de drainage et de filtration. Brochure Comitè Francais des Geotextiles. .

Caldas-Vieira, Fernando, & FEUEBORN, HJ. (2013). *Impact of Political Decision on Production and Use of Coal Combustion Products in Europe.* Proceedings of the 2013 World of Coal Ash Conference (WOCA), Lexington KY, April 22, Vol. 25,

Calhoun, C. C. (1972). Development of Design Criteria and Acceptance Specifications for Plastic Fiber Cloths. *DTIC Document*(Technical Report S-72-7), U. S. Army Engineer Waterways Experiment Station, Vicksburg, Mississippi, 105.

CAN/CGSB-148.1. (No. 10 -94 Geotextiles - Filtration Opening Size).

Carroll, R.G. (1983). Geotextile Filter Criteria. *Engineering Fabrics in Transportation Construction*, pp.46-53.

Cazzuffi, Daniele A., Mazzucato, Alberto, Moraci, Nicola, & Tondello, Massimo. (1999). A new test apparatus for the study of geotextiles behaviour as filters in unsteady flow conditions: relevance and use. *Geotextiles and Geomembranes,* Vol. 17(5–6), pp.313-329. DOI: 10.1016/S0266-1144(99)00014-X

CDA. (2007). Geotechnical Considerations for Dam Safety, *Technical Bulletin. Canadian Dam Association*.

Chang, D., & Nieh, Y. (1996). Significance of Gradient Ratio Test for Determining Clogging Potential of Geotextiles. Shoba K. Bhatia and L. David Suits (Ed.), *Recent Developments in Geotextile Filters and Prefabricated Drainage Geocomposites, ASTM International, West Conshohocken, PA* ASTM STP1281, pp. 113-131. DOI: 10.1520/STP15597S

Chang, D. S., & Zhang, L. M. (2013). Extended internal stability criteria for soils under seepage. *Soils and Foundations,* Vol. 53(4), pp.569-583. DOI: 10.1016/j.sandf.2013.06.008

Chang, Dave Ta-Teh, Li, Neng-Hui, Chen, Bor-Ling, & Fu, Hsin-Ming. (2004). Modified Gradient Ratio (GR) Test System with Micro Pore Pressure Transducer Measurement. *岩土工程學報,* Vol. 26(6), pp.832-837.

Chen, Rong-Her, Ho, Chia-Chun, & Chung, Wen-Bin. (2008). The filtration mechanism and micro-observation of soil-geotextile systems under cyclic flows. *Journal of GeoEngineering,* Vol. 3(3), pp.101-112. DOI: 10.6310/jog.2008.3(3).2

Chew, S. H., Zhao, Z. K., Karunaratne, G. P., Tan, S. A., Delmas, Ph., & Loke, K. H. (2000). Revetment Geotextile Filter Subjected to Cyclic Wave Loading *Advances in Transportation and Geoenvironmental Systems Using Geosynthetics*, 162-175. DOI: doi:10.1061/40515(291)11

Christopher, B. R., & Holtz, R. D. (1985). Geotextiles Engineering Manual. (FHWA-TS-86/203), U.S. Federal Highway Administration, 1044.

Christopher, B.R., & Holtz, R.D. (1989). Geotextile construction and design guidelines. *HI-89-050*, Federal Highway Administration, Washington, DC.

Cnudde, Veerle, Boone, Matthieu, Dewanckele, Jan, Dierick, Manuel, Van Hoorebeke, Luc, & Jacobs, Patric. (2011). 3D characterization of sandstone by means of X-ray computed tomography. *Geosphere,* Vol. 7(1), pp.54-61. DOI: 10.1130/GES00563.1

Daniel, David E, Foreman, David E, Trautwein, Stephen J, & Boynton, Stephen S. (1984). Permeability testing with flexible-wall permeameters. pp.113-122. DOI: 10.1520/GTJ10487J

Darcy, Henry. (1856). *Les fontaines publiques de la ville de Dijon: exposition et application*: Victor Dalmont.

Dawson, Andrew. (2008). *Water in road structures: movement, drainage & effects* (Vol. 5): Springer Science & Business Media.

de Graauw, A., van der Meulen, T., & van der Does de Bye, M. (1984). Granular Filters: Design Criteria. *Journal of Waterway, Port, Coastal, and Ocean Engineering,* Vol. 110(1), pp.80-96. DOI: 10.1061/(ASCE)0733-950X(1984)110:1(80)

Dierickx, Willy, & Myles, Bernard. (1996). Wet sieving as a European en-standard for determining the characteristic opening size of geotextiles *Recent Developments in Geotextile Filters and Prefabricated Drainage Geocomposites*: ASTM International.

Elandaloussi, R., Bennabi, A., & Dupla, J. C. (2014). Suffusion study of coarse soils treated with lime *Scour and Erosion*: CRC Press, 137-142. DOI: 10.1201/b17703-17

Elsharief, A., & Lovell, C. (1996). Determination and Comparisons of the Pore Structure of Nonwoven Geotextiles *Recent Developments in Geotextile Filters and Prefabricated Drainage Geocomposites* STP15591S: ASTM International, West Conshohocken, PA, 35-53. DOI: 10.1520/STP15591S

Elsharief, Ahmed M. (2016). Pore Structure and Long Term Performance of non woven geotextile filters.

Elton, D., Hayes, D., & Adanur, S. (2007). Bubblepoint Testing of Geotextiles: Apparatus and Operation. *Geotechnical Testing Journal,* Vol. 30(1), pp.9-16. DOI: 10.1520/GTJ100308

Emin Kutay, M., & Aydilek, A. (2005). Filtration Performance of Two-Layer Geotextile Systems. *ASTM geotechnical testing journal* Vol. 28(1), pp.79-91. DOI: 10.1520/GTJ12580

Engineers, U.S. Army Corps of. (1977). Plastic fiber cloth. *Civil Works Construction Guide Specification No. CE-02215*, Office Chief of Engineers, Washington, 16.

Espinoza-Melendrez, JA, Tamari, S, & Aguilar-Chavez, A. (2005). Simulation of water infiltration below a damage in the pavement surface course. *Ingenieria Hidraulica en Mexico,* Vol. 20(4), pp.77-95.

Fancher, GH, Lewis, JA, & Barnes, KB. (1933). Some physical characteristics of oil sands.[Porosity, permeability, and screen analysis]. *Penn. State Coll., Mineral Ind. Expt. Sta., Bull.,* Vol. 12.

Fannin, R Jonathan, Vaid, Yoginder P, Palmeira, Ennio M, & Shi, Yucheng C. (1996). A modified gradient ratio test device. Shoba K. Bhatia and L David Suit (Ed.), *Recent Developments in Geotextile Filters and Prefabricated Drainage Geocomposites* ASTM STP 128, 100-112.

Fannin, R. J., & Moffat, R. (2006). Observations on internal stability of cohesionless soils. *Géotechnique,* Vol. 56(7), pp.497-500. DOI: 10.1680/geot.2006.56.7.497

Fannin, R. J., Vaid, Y. P., & Shi, Y. C. (1994). A Critical-Evaluation of the Gradient Ratio Test. *Geotechnical Testing Journal,* Vol. 17(1), pp.35-42. DOI: 10.1520/GTJ10070J

Fannin, RJ, & Pishe, Rashmi. (2001). *Testing and specifications for geotextile filters in cyclic flow applications.* Proceedings of the Geosynthetics Conference, Portland, Oregon, USA, pp. 423-435.

Fatahi, Behzad, Khabbaz, Hadi, & Liem Ho, Huu. (2011). Effects of geotextiles on drainage performance of ballasted rail tracks. *Australian Geomechanics,* Vol. 46(4), pp.91-102.

Faure, Y. (1988). Estimation du comportement hydraulique a long terme des geotextiles a partir des essais a court terme. *Durability of Geotextiles,* Vol. 3, pp.222.

Faure, Y, Gourc, JP, Brochier, P, & Rollin, A. (1986). *Soil geotextile interaction in filter systems.* Proceedings of the Third International Conference on Geotextiles, pp. 671-676.

Faure, YH, Gourc, JP, & Gendrin, P. (1990). Structural study of porometry and filtration opening size of geotextiles. I. D. Peggs (Ed.), *Geosynthetics: microstructure and performance* ASTM STP 1076, 102-119. DOI: 10.1520/STP23500S

Faure, Yves-Henri, Ho, Chia Chun, Chen, Rong-Her, Le Lay, Mattieu, & Blaza, Jon. (2010). A wave flume experiment for studying erosion mechanism of revetments using geotextiles. *Geotextiles and Geomembranes,* Vol. 28(4), pp.360-373.

Fayoux, D. (1977). *Filtration hydrodynamique des sols par les textiles.* Colloque Int. sur l'emploi des textiles en geotechnique, Paris, France, April (1977), (in French), Vol. 2, pp. 329-332.

Fetter, CW. (2001). Applied hydrogeology (Vol. 4th Edition): New Jersey.

FHWA, DP. (1992). Drainable Pavement Systems, Participant Notebook Publication FHWA-SA-92-008. *FHWA, United States Department of Transportation, Washington, DC*.

Fischer, G. R. (1994). *The Influence of Fabric Pore Structure on the Behavior of Geotextile Filters.* (PhD Dissertation), University of Washington, Seattle, Washington, USA.

Fischer, G. R., Christopher, B. R., & Holtz, R. D. (1990). *Filter Criteria Based on Pore-Size Distribution.* Proceedings of the Fourth International Conference on Geotextiles, The Hague The Natherlands, Vol. 1, pp. 289-294.

Fischer, Gregory R, & Holtz, Robert D. (1991). Comparative studies of different porometry determination methods for geotextiles by L. Van der Sluys & W. Dierickx. *Geotextiles and Geomembranes,* Vol. 10(4), pp.379-381. DOI: 10.1016/0266-1144(91)90012-L

Fischer, Gregory R, Holtz, Robert D, & Christopher, Barry R. (1996). Evaluating geotextile pore structure. S. Bhatia and L. Suits (Ed.), *Recent developments in geotextile filters and prefabricated drainage geocomposites* ASTM STP 128: ASTM International. DOI: 10.1520/STP15589S

Fischer, Gregory R, Maré, André D, & Holtz, Robert D. (1999). Influence of procedural variables on the gradient ratio test. *ASTM, GTJODJ,* Vol. 22(3), pp.22-31.

Gabr, M. A., & Akram, M. H. . (1996). *Clogging and Piping Criteria for Geotextile Filters for Fly Ash.* Proceedings of the 3rd International Symposium on Environmental Technology, San Diego, California, USA, pp. 836-847.

GEO. (1993). Review of granular and geotextile filters. GEO Publication No. 1/93. Civil Engineering Department, Ho Man Tin, Hong Kong.

Giroud, J. P. (1996). *Granular filters and geotextile filters.* Geofilters '96 Conference, Montreal, 565-680,

Giroud, J.P. (1981). Designing with Geotextiles. Vol. 14(4), pp.257-272.

Giroud, JP. (2010). Development of criteria for geotextile and granular filters. *Proceedings of the 9th International Conference on Geosynthetics, Guaruja, Brazil,* Vol. 2327, pp.4564.

Glynn, DT, & Cochrane, SR. (1987). *The behavior of geotextiles as separating membranes on glacial till subgrades.* Proceedings of the Geosynthetics '87, New Orleans, pp. 26-37.

Gourc, J. P., & Faure, Y. H. (1990). *Soil particle, water and fiber - A fruitful interaction now controlled.* Fourth International Conference on Geotextiles, Geomembranes and Related Products, The Hague, The Natherlands, pp. 949-971,

Haliburton, T. A., & Wood, P. D. . (1982). *Evaluation of U.S. Army Corps of Engineers gradient ratio test for geotextile performance.* 2nd Int. Conf. on Geotextiles, Las Vegas, Nev. , Vol. 1, pp. 97-101.

Hameiri, A. (2000). *Soil / geotextile filtration behavior under dynamic conditions of cyclic flow and vibration.* (PhD Dissertation), The University of British Columbia.

Harney, MD, & Holtz, RD. (2001). *A flexible wall gradient ratio test.* Geosynthetics Conference 2001, pp. 409-422.

Hawley, Rashmi A. (2001). *Filtration performance of geotextiles in cyclic flow conditions : a laboratory study.* (MSc Thesis). Retrieved from https://open.library.ubc.ca/collections/831/items/1.0063728

Hazen, A. (1892). Physical properties of sands and gravels with reference to use in filtration. *Report to the Massachusetts State Board of Health,* Vol. 539.

Head, Kenneth H. (1992). *Manual of soil laboratory testing 1, 1*. London: Pentech Pr.

Heerten, G. (1982). *Dimensioning the filtration properties of geotextiles considering long-term conditions.* Proceedings of the 2nd International Conference on Geotextiles, Las Vegas, USA, pp. 115-120.

Highlands, Keith L, Turgeon, Robert, & Hoffman, Gary L. (1991). Prefabricated Pavement Base Drain. *Transportation Research Record*(1329), pp.42-48.

Hoare, D. J. (1982). *A laboratory study into clay through geotextiles under dynamic loading.* Proceedings of the 2nd International Conference on Geotextiles, Las Vegas, Vol. 2, pp. 423-428.

Hoffman, C.E. (1983). *A Empirical Model for the Design of Fibres Filter Media.* Proc. of the llth Technical Symposium of the Association of Nonwoven Fabrics Industries, Baltimore, pp. 93-105.

Holtz, R. D., Christopher, Barry R., & Berg, Ryan R. (2008). Geosynthetic design & construction guidelines : reference manual. (FHWA NHI-07-092), U.S. Dept. of Transportation, Federal Highway Administration, National Highway Institute, Washington, D.C., 592.

Holtz, R.D., Christopher, B.R., & Berg, R.R. (1997). Geosynthetic Engineering. BiTech Publishers, Vancouver, British Columbia, Canada, 451.

Holz, RD, Christopher, Barry Rodney, & Berg, Ryan R. (1998). Geosynthetic design and construction guidelines. (No. FHWA HI-95-038), U.S. Dept. of Transportation, Federal Highway Administration, National Highway Institute.

Honjo, Y., Haque, M. A., & Tsai, K. A. (1996). *Self-filtration behavior of broadly and gap graded cohesionless soils.* Proceedings of the 2nd International Conference on Geofilters, Montreal, Canada, pp. 227-236.

Hufenus, R., & Schrade, U. (2006). An optimized method to measure the hydraulic conductivity of geosynthetics under load. *Geotextiles and Geomembranes,* Vol. 24(4), pp.243-253. DOI: 10.1016/j.geotexmem.2006.01.005

ICOLD. (1994). Embankment Dams Granular Filters and Drains, Review and Recommendations, *International Commission on Large Dams*.

Indraratna, B., Nguyen, V., & Rujikiatkamjorn, C. (2011). Assessing the Potential of Internal Erosion and Suffusion of Granular Soils. *Journal of Geotechnical and Geoenvironmental Engineering,* Vol. 137(5), pp.550-554. DOI: 10.1061/(ASCE)GT.1943-5606.0000447

Ip, Man, Haque, Asadul, & Bouazza, Abdelmalek. (2012). *Contribution of a geotextile towards the improvement of sub-ballast filtration criteria under cyclic stress pulses.* 11th Australia-New Zealand Conference on Geomechanics Ground Engineering in a Changing World (Stephen Tyson 15 July 2012 to 18 July 2012), pp. 445-450.

Israr, J, Indraratna, B, & Rujikiatkamjorn, C. (2016). Laboratory Investigation of the Seepage Induced Response of Granular Soils Under Static and Cyclic Loading. *Geotechnical Testing Journal,* Vol. 39(5), pp.795-812. DOI: https://doi.org/10.1520/GTJ20150288

Istomina, V. S. (1957). *Filtration Stability of Soils*. Moscow, Leningrad (in Russian).

Kapur, Jagat Narain, Sahoo, Prasanna K, & Wong, Andrew KC. (1985). A new method for gray-level picture thresholding using the entropy of the histogram. *Computer vision, graphics, and image processing,* Vol. 29(3), pp.273-285.

Kayser, Jan, Karl, Fabian, Schürenkamp, David, Schwab, Nora, & Oumeraci, Hocine. (2016). A Test Apparatus for Alternating Flow in Geotechnical Engineering. *Geotechnical Testing Journal,* Vol. 39(5), pp.865-878. DOI: https://doi.org/10.1520/GTJ20150252

Kenney, T. C., & Lau, D. (1985). Internal stability of granular filters. *Canadian Geotechnical Journal,* Vol. 22(2), pp.215-225. DOI: 10.1139/t85-029

Kenney, T.C., & Lau, D. (1986). Internal Stability of Granular Filters: Reply. *Canadian Geotechnical Journal,* Vol. Vol. 23, pp.pp. 420-423.

Kézdi, A. (1979). *Soil physics – selected topics*: Elsevier Science.

Khachan, M. M., Bhatia, S. K., & Smith, J. L. (2012). Retention performance of woven geotextiles subjected to cyclic-flow conditions. *Geosynthetics International,* Vol. 19(3), pp.200-211. DOI: 10.1680/gein.12.00009

Koerner, R. M. (1993). *Designing with geosynthetics* (Fifth edition ed.): Prentice Hall, 2005.

Koerner, R. M., & Koerner, G. R. (2014). On the Need for a Better Test Method Than Dry or Wet Sieving to Obtain the Characteristic Opening Size for Geotextile Filter Design Purposes. *GSI White Paper #31, Geosynthetic Institute*.

Koerner, Robert M. (2012). *Designing with geosynthetics* (Vol. 1): Xlibris Corporation.

Koerner, Robert M, & Ko, FK. (1982). *Laboratory studies on long-term drainage capability of geotextiles.* Proceedings of the Second International Conference on Geotextiles, Vol. 1, pp. 91-96.

Koerner, Robert M, & Koerner, George R. (2015). Lessons learned from geotextile filter failures under challenging field conditions. *Geotextiles and Geomembranes,* Vol. 43(3), pp.272-281.

Koerner, Robert M, Koerner, GR, Fahim, AK, & Wilson-Fahmy, RF. (1994). Long-term performance of geosynthetics in drainage applications. (Project 15-13 FY'90), Transportation Research Board, 60.

Kovács, G. (1981). *Seepage Hydraulics*. Amsterdam: Elsevier Scientific Publishing Company.

Kumar Shukla, Sanjay , & Yin, Jian Hua. (2006). *Fundamentals of Geosynthetic Engineering* (1st Edition ed.). The Netherlands: Taylor & Francis/Balkema.

Kuo, Chun-Yi, & Frost, J David. (1996). Uniformity evaluation of cohesionless specimens using digital image analysis. *Journal of Geotechnical Engineering,* Vol. 122(5), pp.390-396.

Lafleur, J. (1999). Selection of geotextiles to filter broadly graded cohesionless soils. *Geotextiles and Geomembranes,* Vol. 17(5–6), pp.299-312. DOI: 10.1016/S0266-1144(99)00007-2

Lafleur, Jean. (1984). Filter testing of broadly graded cohesionless tills. *Canadian Geotechnical Journal,* Vol. 21(4), pp.634-643. DOI: 10.1139/t84-070

Lafleur, Jean, Mlynarek, Jacek, & Rollin, André L. (1989). Filtration of Broadly Graded Cohesionless Soils. *Journal of Geotechnical Engineering,* Vol. 115(12), pp.1747-1768. DOI: 10.1061/(ASCE)0733-9410(1989)115:12(1747)

Lawson, Chris R. (1982). Filter criteria for geotextiles: relevance and use. *Journal of Geotechnical Engineering Division,* Vol. 108(GT10), pp.1300-1317. DOI: 10.1061/9780784479797.014

Lee, S., & Bourdeau, P. L. (2006). Filter performance and design for highway drains. *FHWA/IN/JTRP-2005/1*, Purdue Univeristy, West Lafayette, Indiana.

Li, Maoxin. (2008). *Seepage induced instability in widely graded soils.* (PhD Dissertation). Retrieved from https://open.library.ubc.ca/collections/24/items/1.0063080

Lindquist, Erik. (1933). *On the flow of water through porous soil.* Premier Congres des grands barrages (Stockholm), pp. 81-101.

Lombard, G., & Rollin, A. L. (1987). Filtration Behaviour Analysis of Thin Heat-Bonded Geotextiles. *Geosynthetics, New Orleans, IFAI, St. Paul, pp.482-492*.

Luettich, S. M. (1993). Geotextile Filter: Designing for the application. Geotechnical Fabrics Report, Vol. 11, No. 1, pp. 70-78.

Madsen, Fritz T, & Mitchell, James K. (1989). Chemical effects on clay hydraulic conductivity and their determination. Peter Baccini (Ed.), *The Landfill: Reactor and Final Storage Swiss Workshop on Land Disposal of Solid Wastes Gerzensee, March 14–17, 1988*. Berlin, Heidelberg: Springer Berlin Heidelberg, pp 201-251. DOI: 10.1007/BFb0011265

Mannsbart, G., & Christopher, B. R. (1997). Long-term performance of nonwoven geotextile filters in five coastal and bank protection projects. *Geotextiles and Geomembranes,* Vol. 15(4–6), pp.207-221. DOI: 10.1016/S0266-1144(97)10003-6

Marr, W Allen, & Fairhurst, Charles. (1999). Nondestructive and Automated Testing for Soil and Rock Properties STP 1350. West Conshohocken, PA: ASTM International, 321. DOI: 10.1520/STP1350-EB

Matziaris, Vasileios, Marshall, Alec M, & Yu, Hai-Sui. (2015). Centrifuge model tests of rainfall-induced landslides *Recent Advances in Modeling Landslides and Debris Flows*: Springer, 73-83.

Miller, Bernard, & Tyomkin, Ilya. (1986). An extended range liquid extrusion method for determining pore size distributions. *Textile Research Journal,* Vol. 56(1), pp.35-40.

Miura, N, Sakai, A, Taesiri, Y, Yamanouchi, T, & Yasuhara, K. (1990). Polymer grid reinforced pavement on soft clay grounds. *Geotextiles and Geomembranes,* Vol. 9(1), pp.99-123.

Mlynarek, J. (1999). Filtration Series: Drawing Conclusions. *Geotechnical Fabrics Report, Vol. 17, No. 2, pp. 24–27.*

Mlynarek, J., Lafleur, J., Rollin, A., & Lombard, G. (1993). Filtration Opening Size of Geotextiles by Hydrodynamic Sieving. *Geotechnical Testing Journal,* Vol. 16(1), pp.61-69.

Moffat, R. (2005). *Experiments on the internal stability of widely graded cohesionless soils* (PhD Disssertation), Retrieved from https://open.library.ubc.ca/cIRcle/collections/831/items/1.0063322 (Original work published 2005).

Moffat, Ricardo, Fannin, R Jonathan, & Garner, Stephen J. (2011). Spatial and temporal progression of internal erosion in cohesionless soil. *Canadian Geotechnical Journal,* Vol. 48(3), pp.399-412. DOI: 10.1139/T10-071

Moraci, N. (2010). *Geotextile filter: Design, characterization and factors affecting clogging and blinding limit states.* Proceeding of the 9th International Conference on Geosynthetics, Theme lecture, At Guarujá, Brazil., Volume: vol.1 pag. 413 - 435.,

Moraci, N., & Mandaglio, M. C. (2008). *The Design of Geotextile Filters for Granular Soils*. Conference Name|, Conference Location|. Type retrieved rom URL, Vol. Volume, pp. Pages.

Moraci, Nicola, Ielo, Domenico, & Mandaglio, Maria Clorinda. (2012). A new theoretical method to evaluate the upper limit of the retention ratio for the design of geotextile filters in contact with broadly granular soils. *Geotextiles and Geomembranes,* Vol. 35, pp.50-60. DOI: 10.1016/j.geotexmem.2012.07.001

Moraci, Nicola, Mandaglio, Maria Clorinda, & Ielo, Domenico. (2011). A new theoretical method to evaluate the internal stability of granular soils. *Canadian Geotechnical Journal,* Vol. 49(1), pp.45-58. DOI: 10.1139/t11-083

Mouw, KAG, Nederlof, KDC, Stuip, J, & Velduijzen van Zanten, R. (1986). *Geotextiles in shore and bottom protection works.* Proceedings of the Third International Conference on Geotextiles, Vienna, Austria, pp. 349-354.

Münster, Stefan, & Fabry, Ben. (2013). A Simplified Implementation of the Bubble Analysis of Biopolymer Network Pores. *Biophysical Journal,* Vol. 104(12), pp.2774–2775. DOI: 10.1016/j.bpj.2013.05.016

Myers, William Scott. (2010). *Dewatering rock crushing fines using geotextile tubes.* (PhD Dissertation), Auburn University.

Narejo, D. B., & Koerner, R. M. (1992). A Dynamic Filtration Test for Geotextile Filters. *Geotextiles and Geomembranes,* Vol. 11(4-6), pp.395-400. DOI: Doi 10.1016/0266-1144(92)90021-2

Narejo, Dhani B. (2003). Opening size recommendations for separation geotextiles used in pavements. *Geotextiles and Geomembranes,* Vol. 21(4), pp.257-264. DOI: 10.1016/S0266-1144(03)00028-1

Nimmo, J.R. (2005). Unsaturated Zone Flow Processes. M.G. Anderson, and Bear, J. (Ed.), *Encyclopedia of Hydrological Sciences: Part 13--Groundwater* 4. Chichester, UK: Wiley, 2299-2322. DOI: 10.1002/0470848944.hsa161,

Nishigata, Tatsuaki, Fannin, R Jonathan, & Vaid, Yoginder P. (2000). Blinding and clogging of a nonwoven geotextile. *Soils and foundations,* Vol. 40(4), pp.121-127.

Ogink, HJM. (1975). *Investigations on the hydraulic characteristics of synthetic fabrics*. Netherlands. Delft Hydraulics Laboratory: WorldCat.

Pak, A., & Zahmatkesh, Z. (2011). Experimental study of geotextile's drainage and filteration propertis under different hydraulic gradients and confining pressures. *International Journal of Civil Engineering,* Vol. 9(2), pp.97-102.

Palmeira, E. M., & Gardoni, M. G. (2000). The Influence of Partial Clogging and Pressure on the Behaviour of Geotextiles in Drainage Systems. *Geosynthetics International,* Vol. 7(4-6), pp.403-431. DOI: 10.1680/gein.7.0178

Palmeira, E. M., & Gardoni, M. G. (2002). Drainage and filtration properties of non-woven geotextiles under confinement using different experimental techniques. *Geotextiles and Geomembranes,* Vol. 20(2), pp.97-115. DOI: 10.1016/S0266-1144(02)00004-3

Palmeira, EM, Gardoni, MG, & Bessa da Luz, DW. (2005). Soil–geotextile filter interaction under high stress levels in the gradient ratio test. *Geosynthetics International,* Vol. 12(4), pp.162-175.

Palmeira, Ennio M, & Tatto, Janaina. (2015). Behaviour of geotextile filters in armoured slopes subjected to the action of waves. *Geotextiles and Geomembranes,* Vol. 43(1), pp.46-55.

Prapaharan, S., Holtz, R. D., & Luna, J. D. (1989). Pore Size Distribution of Nonwoven Geotextiles. *Geotechnical Testing Journal, GTJODG,* Vol. Vol. 12(No. 4), pp.261-268.

Punmia, BC, & Jain, Ashok Kumar. (2005). *Soil mechanics and foundations*: Firewall Media.

Reddi, L., Ming, X., Hajra, M., & Lee, I. (2000). Permeability Reduction of Soil Filters due to Physical Clogging. *Journal of Geotechnical and Geoenvironmental Engineering,* Vol. 126(3), pp.236-246. DOI: 10.1061/(ASCE)1090-0241(2000)126:3(236)

Research, Grand View. (2016). Geotextile Market Analysis By Material (Polypropylene, Polyester, Polyethylene), By Product (Non-Woven, Woven), By Application (Road Construction, Erosion Prevention, Drainage) And Segment Forecasts To 2024. (Report ID: 978-1-68038-023-1), 79. DOI: https://www.grandviewresearch.com/press-release/global-geotextiles-market

Richards, K., & Reddy, K. (2010). True Triaxial Piping Test Apparatus for Evaluation of Piping Potential in Earth Structures. *Geotechnical Testing Journal,* Vol. 33(1), pp.83-95. DOI: https://doi.org/10.1520/GTJ102246

Richards, Kevin S., & Reddy, Krishna R. (2007). Critical appraisal of piping phenomena in earth dams. *Bulletin of Engineering Geology and the Environment,* Vol. 66(4), pp.381-402. DOI: 10.1007/s10064-007-0095-0

Rollin, A. L., & Lombard, G. (1988). Mechanisms Affecting Long-Term Filtration Behavior of Geotextiles. *Geotextiles and Geomembranes,* Vol. 7(1-2), pp.119-145. DOI: 10.1016/0266-1144(88)90021-0

Rose, HE. (1945). An investigation into the laws of flow of fluids through beds of granular materials. *Proceedings of the Institution of Mechanical Engineers,* Vol. 153(1), pp.141-148.

Saathoff, F. , & Kehlhase, S. (1986). *Research at the Franzius-Institut on Geotextile Filters in Hydraulic Engineering.* Proc. of the Fifth Congress Asian and Pacific Regional Division, ADP / IAHR, Seoul, pp. 9-10.

Schober, W, & Teindl, H. (1979). *Filter criteria for geotextiles.* Proceedings of the Seventh European Conference on Soil Mechanics and Foundation Engineering, Vol. 2, pp. 121-129.

Serra, Jean. (1982). *Image analysis and mathematical morphology, v. 1*: Academic press.

Shan, Hsin-Yu, Wang, Wu-Liang, & Chou, Ting-Chang. (2001). Effect of boundary conditions on the hydraulic behavior of geotextile filtration system. *Geotextiles and Geomembranes,* Vol. 19(8), pp.509-527. DOI: 10.1016/S0266-1144(01)00018-8

Sherard, J., & Dunnigan, L. (1989). Critical Filters for Impervious Soils. *Journal of Geotechnical Engineering,* Vol. 115(7), pp.927-947. DOI: 10.1061/(ASCE)0733-9410(1989)115:7(927)

Shi, Yucheng. (1993). *Filtration behaviour of non-woven geotextiles in the gradient ration test.* (MSc Thesis), University of British Columbia.

Shire, T., Sullivan, C. O., & Gaudray, G. (2012). *Comparison of two methods for measurement of soil constriction size distribution.* International Conference on Scour and Erosion, Paris-August 27-31, pp. 249-256.

Skempton, A. W., & Brogan, J. M. (1994). Experiments on piping in sandy gravels. *Géotechnique,* Vol. 44(3), pp.449-460. DOI: 10.1680/geot.1994.44.3.449

Sonka, Milan, Hlavac, Vaclav, & Boyle, Roger. (2014). *Image processing, analysis, and machine vision*: Cengage Learning.

Srikongsri, A, & Fannin, RJ. (2011). *Laboratory evaluation of select retention criteria for cyclic flow conditions.* Geo-Frontiers 2011: Advances in Geotechnical Engineering, March 13-16, 2011, Dallas, Texas, United States, pp. 2055-2064.

Standard, British. (2015). Code of practice for site investigations. *BS,* Vol. 5930, pp.1999.

Take, WA, & Bolton, MD. (2003). Tensiometer saturation and the reliable measurement of soil suction. *Géotechnique,* Vol. 53(2), pp.159-172.

Terzaghi, K. (1939). *Soil mechanics: a new chapter in engineering science*: J. Instn. Civ. Engrs, 12, 106-141.

Thorsteinsson, T. (2013). *Ground Water*. Water science. Lectures. Retrieved from https://notendur.hi.is/~thorstur/teaching/vatna/GROUNDWATER_chapter.PDF

Tomlinson, S. S., & Vaid, Y. P. (2000). Seepage forces and confining pressure effects on piping erosion. *Canadian Geotechnical Journal,* Vol. 37(1), pp.1-13. DOI: 10.1139/Cgj-37-1-1

Tondello, M. (1998). Geotextile filters in unsteady flow conditions. *Italian Geotechnical Journal,* Vol. Vol. 4.

Trani, Laricar Dominic O, & Indraratna, Buddhima. (2010). Assessment of subballast filtration under cyclic loading. *Journal of geotechnical and geoenvironmental engineering,* Vol. 136(11), pp.1519-1528. DOI: 10.1061/(ASCE)GT.1943-5606.0000384

Tsai, Du-Ming. (1995). A fast thresholding selection procedure for multimodal and unimodal histograms. *Pattern Recognition Letters,* Vol. 16(6), pp.653-666. DOI: 10.1016/0167-8655(95)80011-H

Tu, S. K., Bhatia, S. K., & Mlynarek, J. (2002). *Standardization of the Bubble Point Method for the Pore-size Characterization of Woven and Nonwoven Geotextiles.* Proceedings of 7th International conference of Geosynthetics, pp. 1111-1114.

Underwood, EE. (1979). Quantification of microstructures by stereological analysis. *Journal of Histochemistry & Cytochemistry,* Vol. 27(11), pp.1536-1537.

Unnikrishnan, N., Rajagopal, K., & Krishnaswamy, N. R. (2002). Behaviour of reinforced clay under monotonic and cyclic loading. *Geotextiles and Geomembranes,* Vol. 20(2), pp.117-133. DOI: 10.1016/S0266-1144(02)00003-1

USSD. (2011). Materials for Embankment Dams. *Committee on Materials for Embankment Dams, United States Society of Dams, Denver*.

Van Dalen, G, & Koster, MW. (2012). 2D & 3D particle size analysis of micro-CT images. *Unilever Res Dev Netherlands*.

Vermeersch, O., & Mlynarek, J. (1996). Determination of the Pore Size Distribution of Nonwoven Geotextiles by a Modified Flow Porometry Technique. Shoba K. Bhatia & L. David Suits (Ed.), *Recent Developments in Geotextile Filters and Prefabricated Drainage Geocomposites* ASTM STP 1281, pp. 19-34. DOI: 10.1520/STP15590S

Veylon, Guillaume, Stoltz, Guillaume, Mériaux, Patrice, Faure, Yves-Henri, & Touze-Foltz, Nathalie. (2016). Performance of geotextile filters after 18 years' service in drainage trenches. *Geotextiles and Geomembranes,* Vol. 44(4), pp.515-533. DOI: 10.1016/j.geotexmem.2016.02.002

Wan, C., & Fell, R. (2008). Assessing the Potential of Internal Instability and Suffusion in Embankment Dams and Their Foundations. *Journal of Geotechnical and Geoenvironmental Engineering,* Vol. 134(3), pp.401-407. DOI: 10.1061/(ASCE)1090-0241(2008)134:3(401)

Washburn, Edward W. (1921). The dynamics of capillary flow. *Physical review,* Vol. 17(3), pp.273.

Wayne, Mark H, & Koerner, Robert M. (1993). *Correlation between long-term flow testing and current geotextile filtration design practice.* Proceedings of Geosynthetics' 93, Industrial Fabrics Association International, St. Paul, MN, Vol. 11, pp. 501-517.

Weisstein, Eric W. (2007). *Sphere-sphere intersection*. http://mathworld.wolfram.com/Analysis.

Williams, Neil D, & Abouzakhm, Mounir Anwar. (1989). Evaluation of geotextile/soil filtration characteristics using the hydraulic conductivity ratio analysis. *Geotextiles and Geomembranes,* Vol. 8(1), pp.1-26. DOI: 10.1016/0266-1144(89)90008-3

Wojnar, Leszek. (1998). *Image analysis: applications in materials engineering*: Crc Press.

Xiao, M., & Reddi, L. (2000). *Comparison of Fine Particle Clogging in Soil and Geotextile Filters.* Advances in Transportation and Geoenvironmental Systems Using Geosynthetics, Proceedings of Geo-Denver 2000, Colarado, pp. 176-185.

Yideti, Tatek F., Birgisson, Bjorn, Jelagin, Denis, & Guarin, Alvaro. (2013). Packing theory-based framework to evaluate permanent deformation of unbound granular materials. *International Journal of Pavement Engineering,* Vol. 14(3), pp.309-320. DOI: 10.1080/10298436.2012.736620

Ziabari, Mohammad, Mottaghitalab, Vahid, & Haghi, Akbar Khodaparast. (2008). Evaluation of electrospun nanofiber pore structure parameters. *Korean Journal of Chemical Engineering,* Vol. 25(4), pp.923-932. DOI: 10.1007/s11814-008-0151-x

Appendices

Appendix A: Evaluation of Internal Stability of Soils

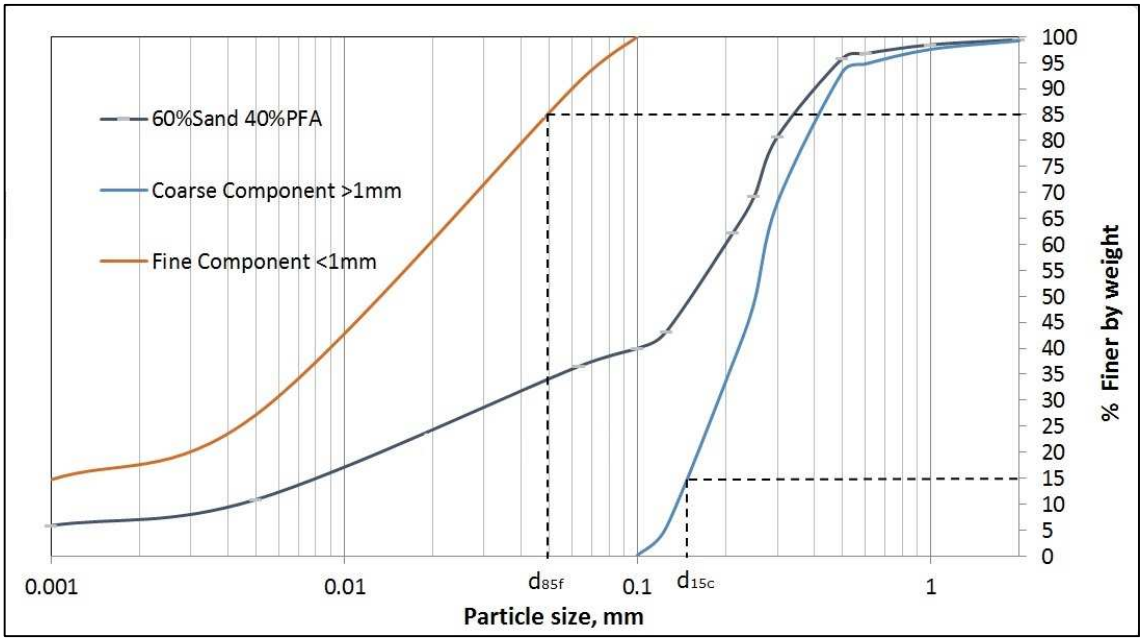
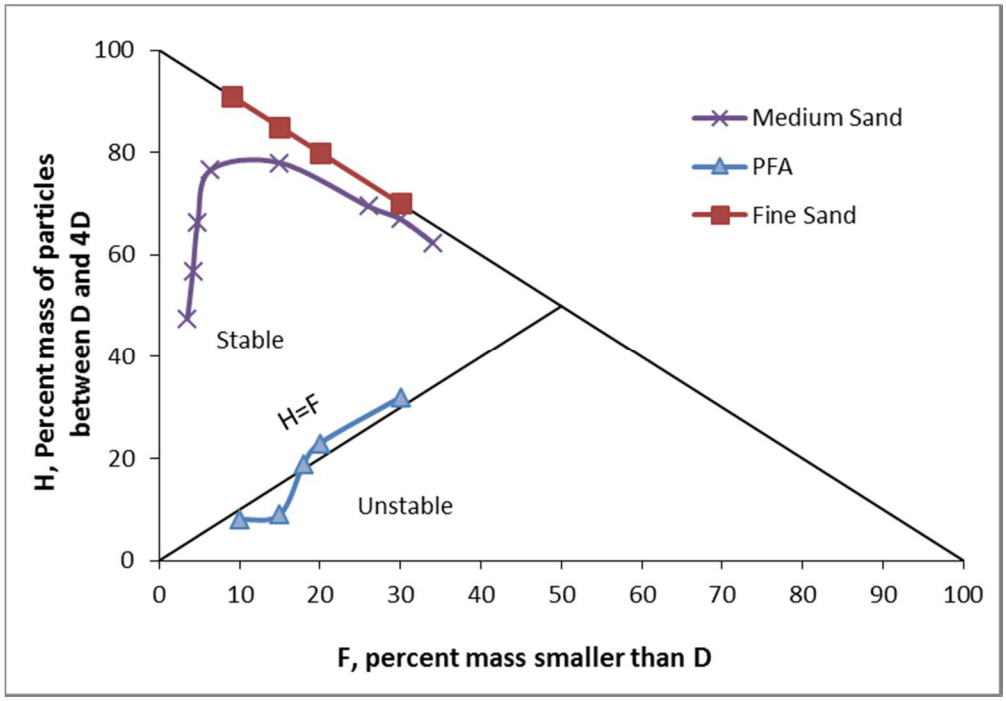
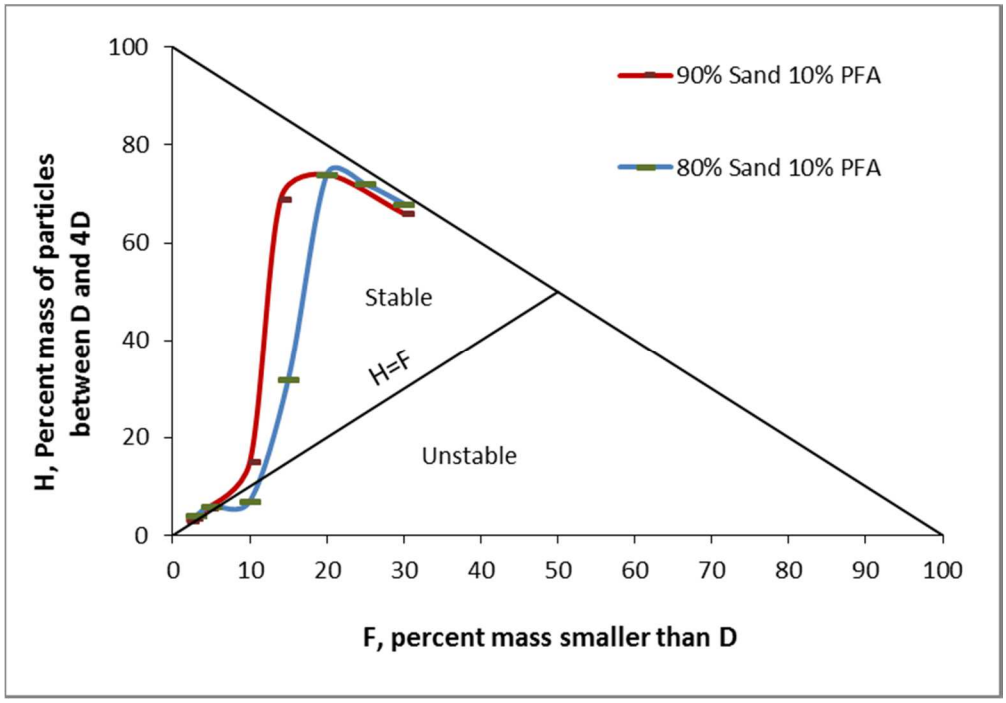


Figure A1 Kezdi's criterion to divide a soil into coarse and fine fractions


100
80
60
40
20
0
0
10
20
30
40
50
60
70
80
90
100
H, Percent mass of particles between D and 4D
F, percent mass smaller than D
Medium Sand
PFA
Fine Sand
Stable
H=F
Unstable


100
80
60
40
20
0
0
10
20
30
40
50
60
70
80
90
100
H, Percent mass of particles between D and 4D
F, percent mass smaller than D
90% Sand 10% PFA
80% Sand 10% PFA
Stable
H=F
Unstable

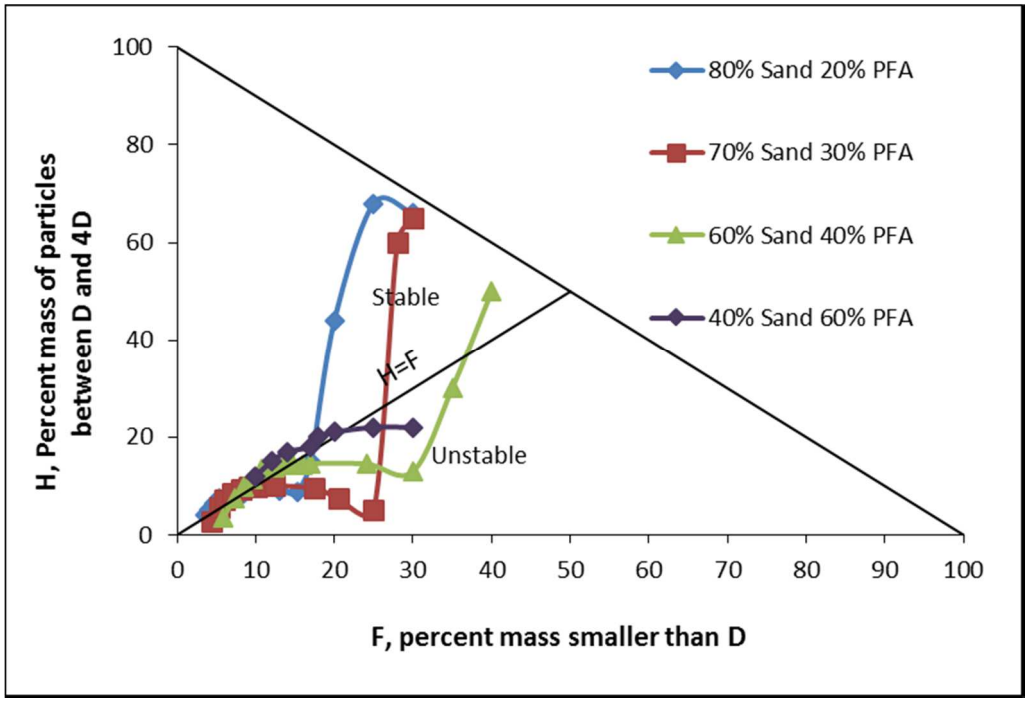


Figure A2 Kenney and Lau's criterion to plot H/F curves

Appendix B: Calibration of pressure transducers

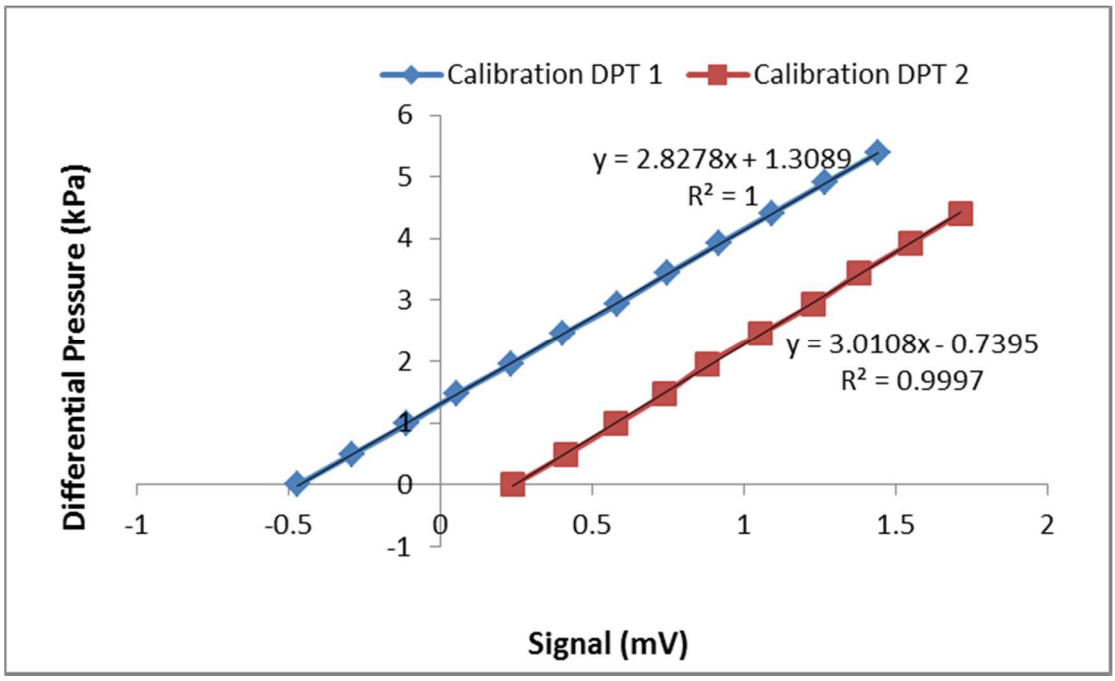


Figure B1 Calibration of differential pressure transducers

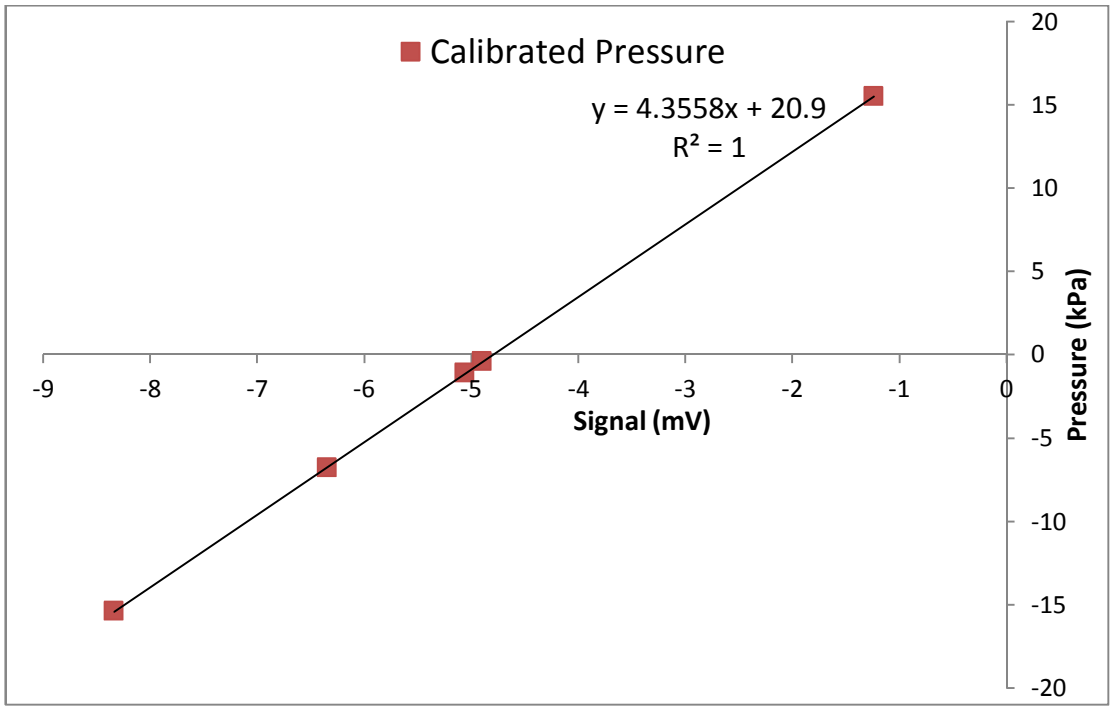


Figure B2 Calibration graph of miniature pore pressure transducer

Appendix C: Test Results

Although the results are mentioned in Chapter 5 in the form of figures and tables, however, some additional figures that may be of interest are presented in Appendix C. The narrow graded test results are presented in section C1 and the broadly graded test results are presented in section C2.

C1: Narrow Graded Soils

Static Stage:

(a) Head losses within the soil and across soil-geotextile interface with time

(b) The variation of GR with time

(e) The variation of permeability with time

Dynamic Stage:

(c) Head losses within the soil and across soil-geotextile interface with No. of cycles

(d) The variation of GR with No. of cycles

(f) The variation of permeability with time

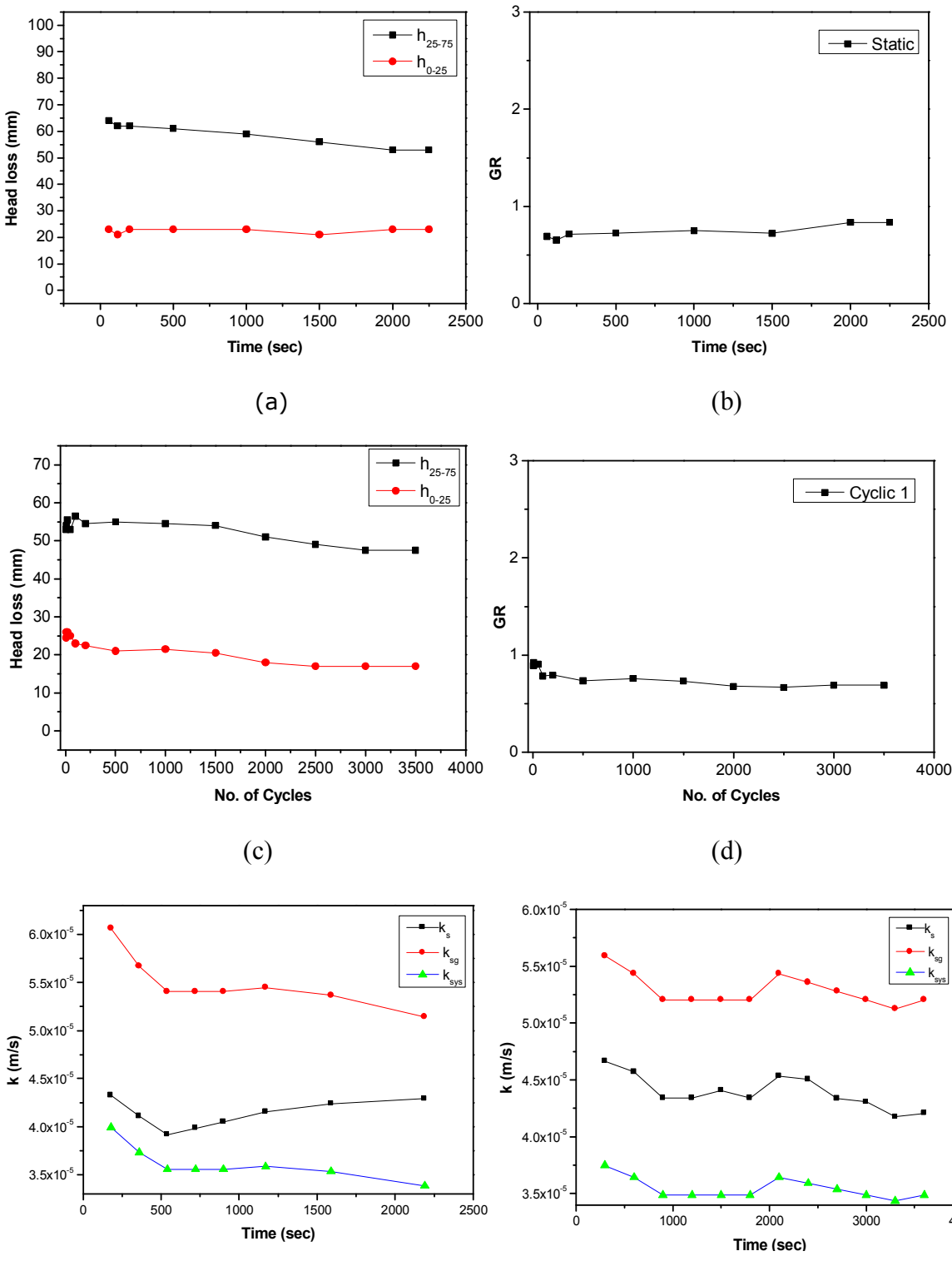


Figure C1.1 NW8 and Medium Sand

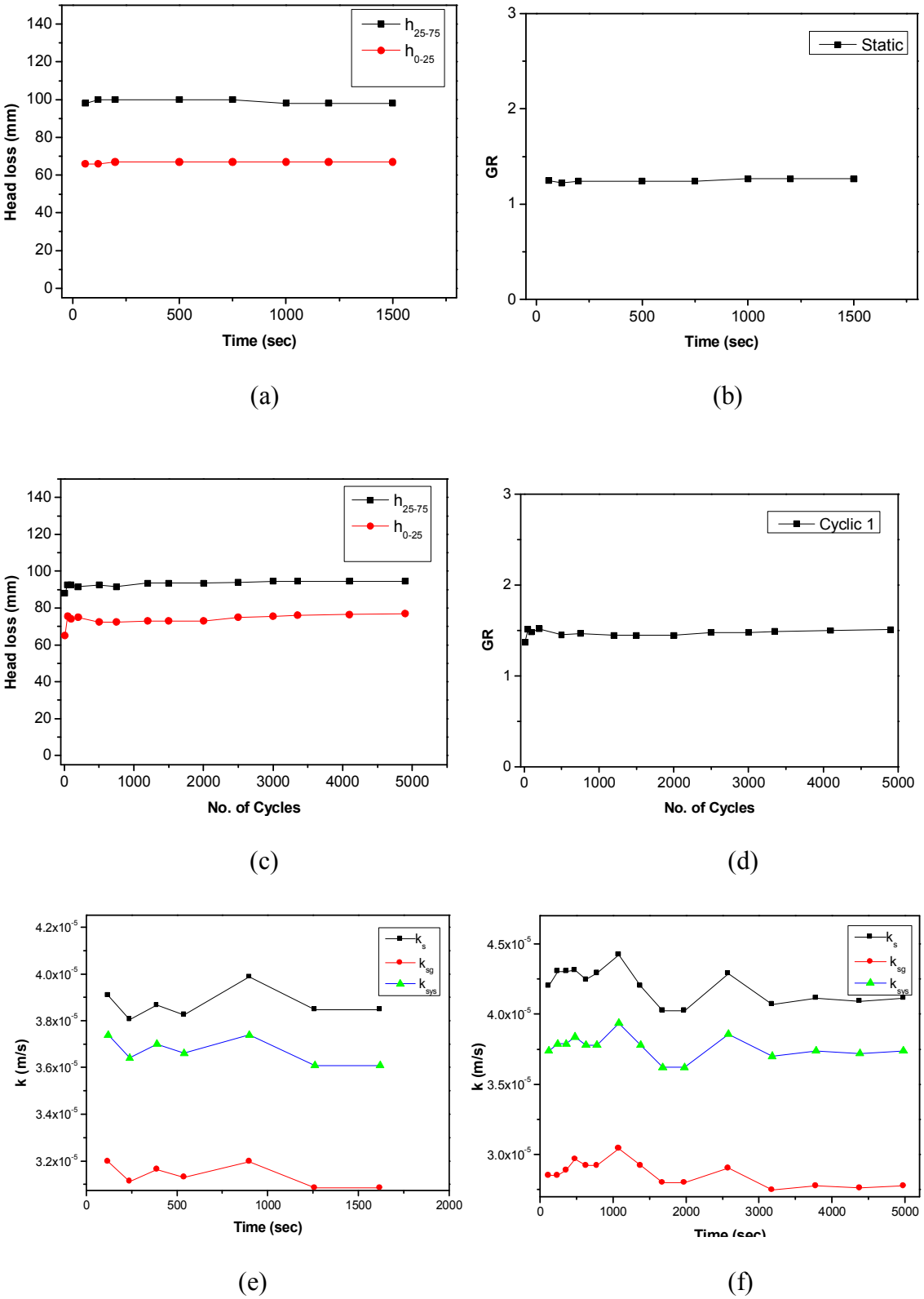


Figure C1.2 NW20 and Medium Sand

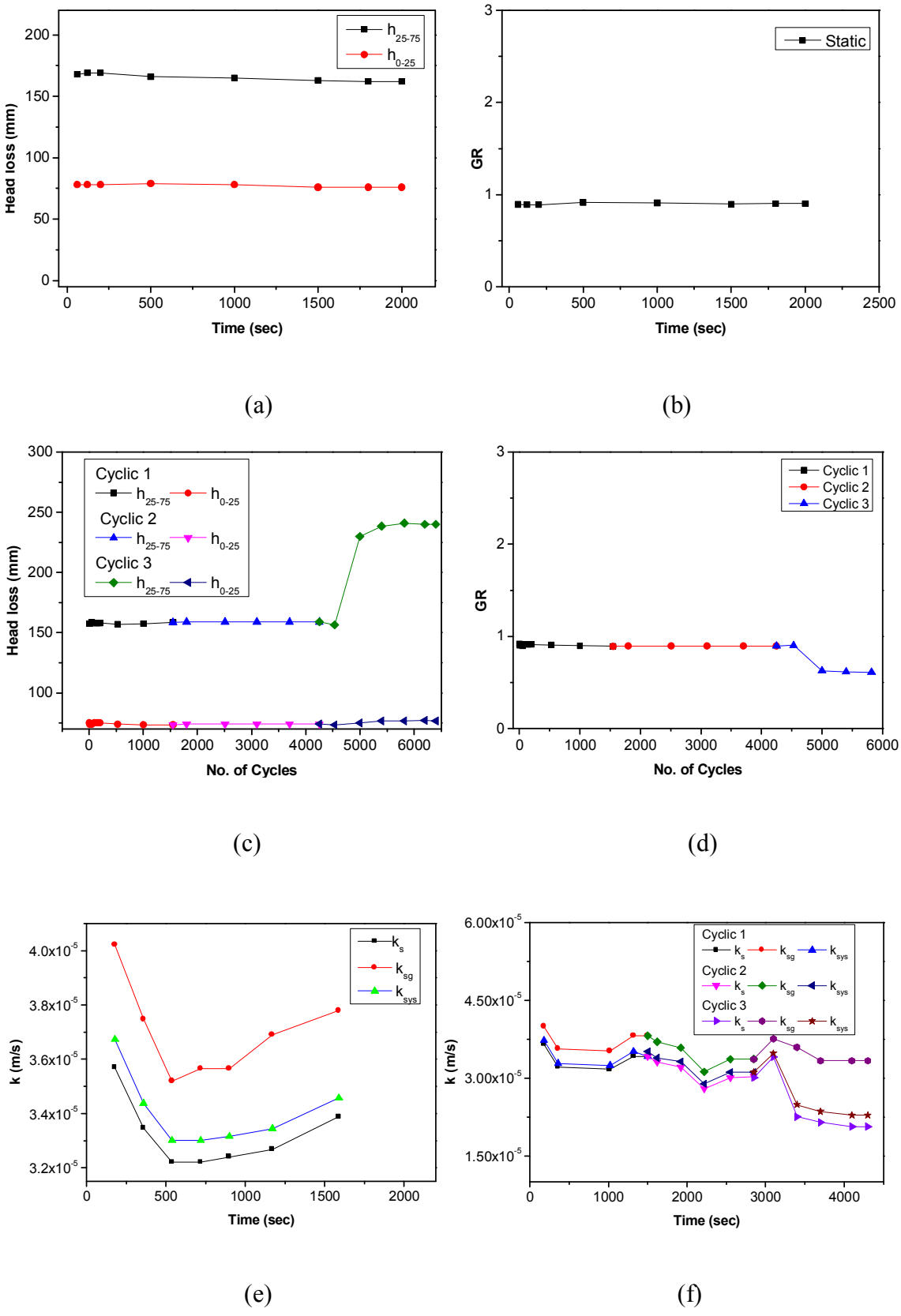


Figure C1.3 ST170 and Medium Sand

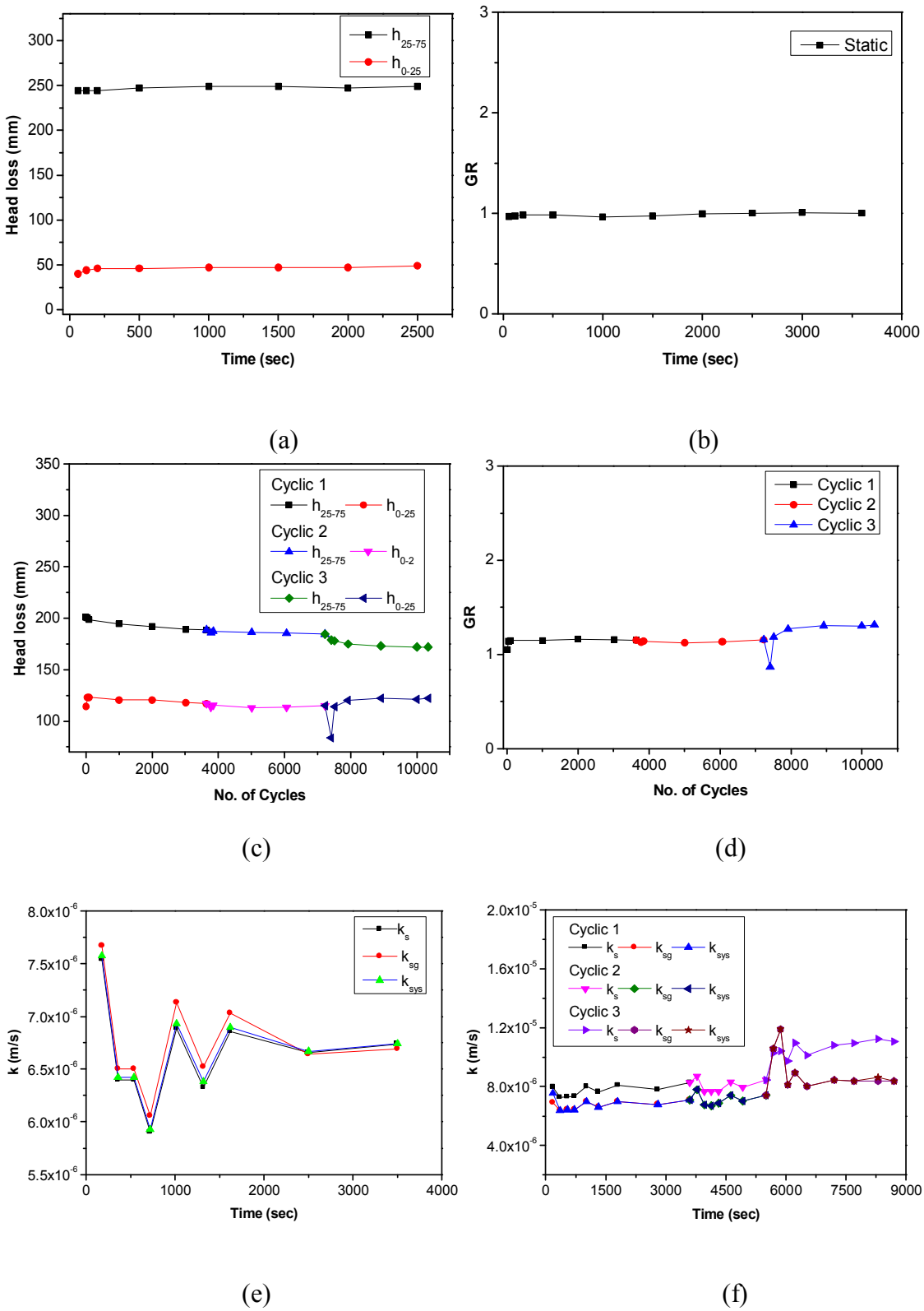
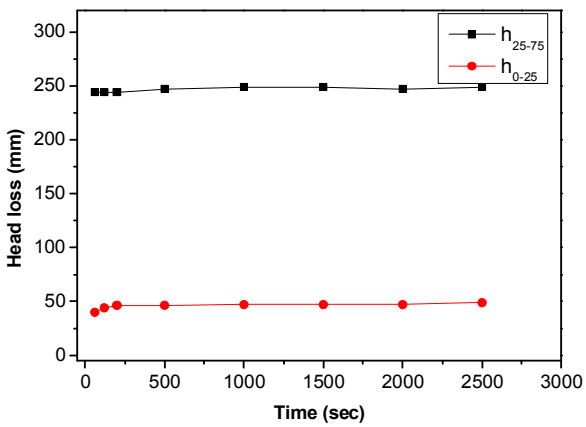
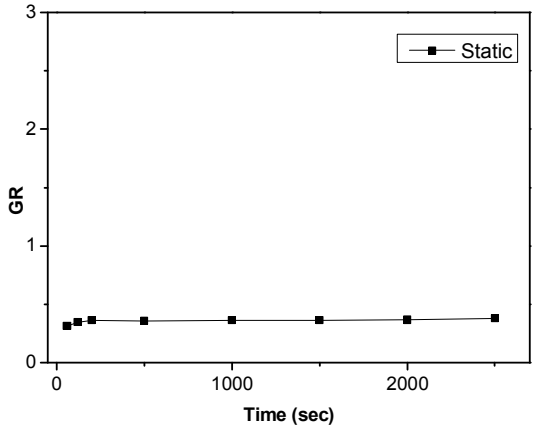


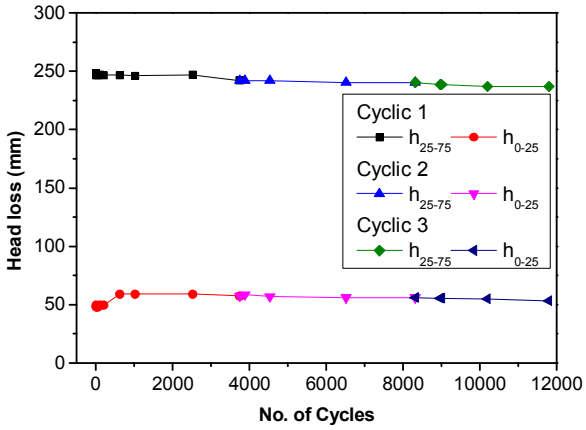
Figure C1.4 NW20 and Fine Sand



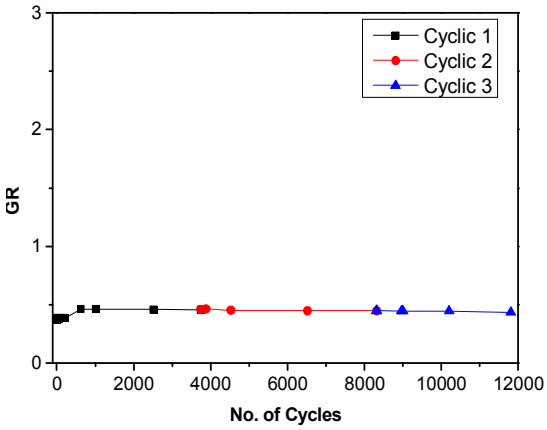
(a)



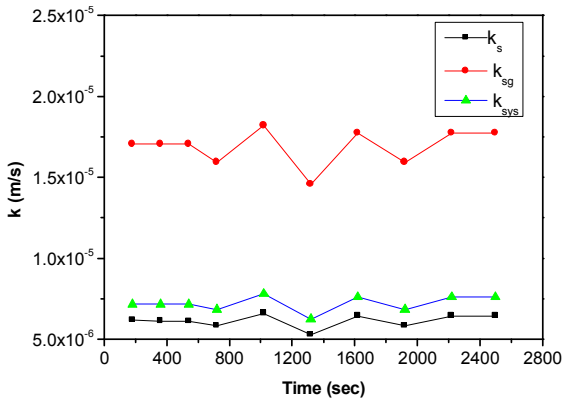
(b)



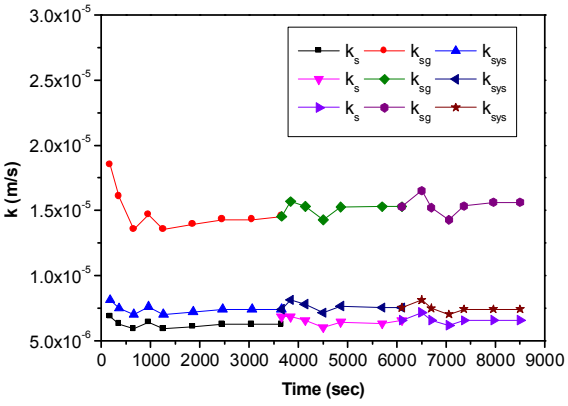
(c)



(d)

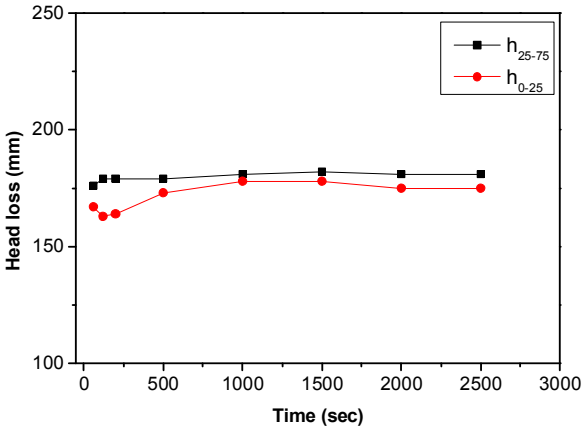


(e)

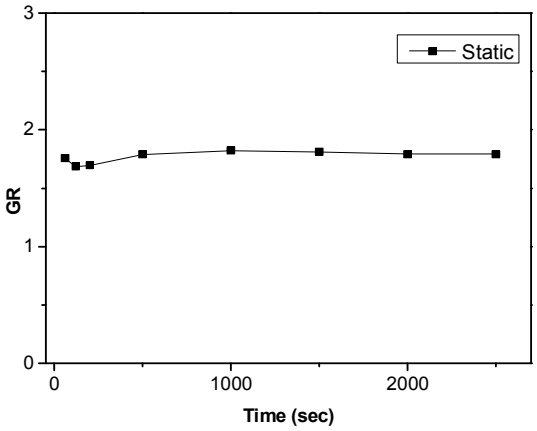


(f)

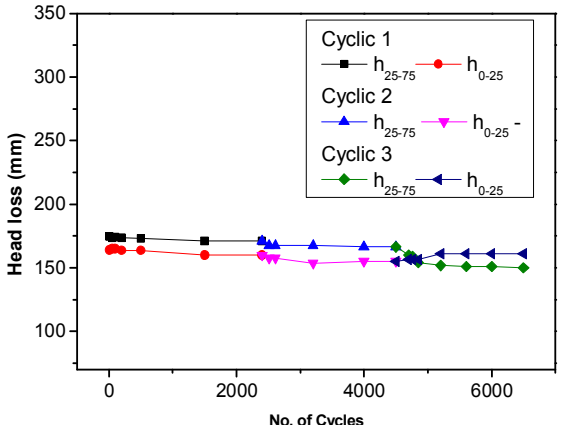
Figure C1.5 NW8 and Fine Sand



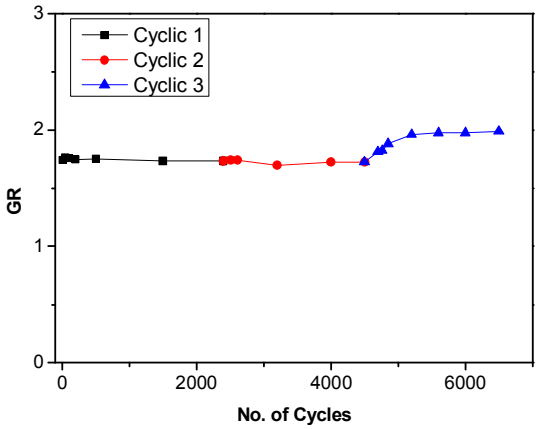
(a)



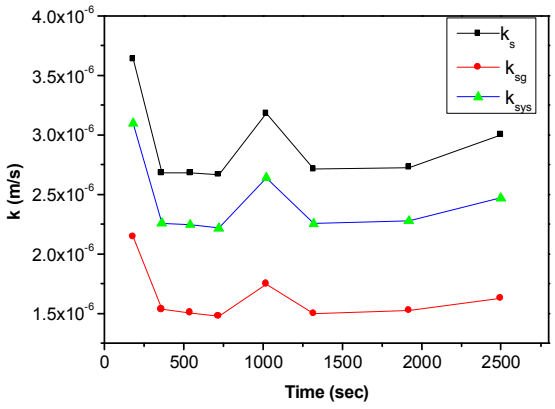
(b)



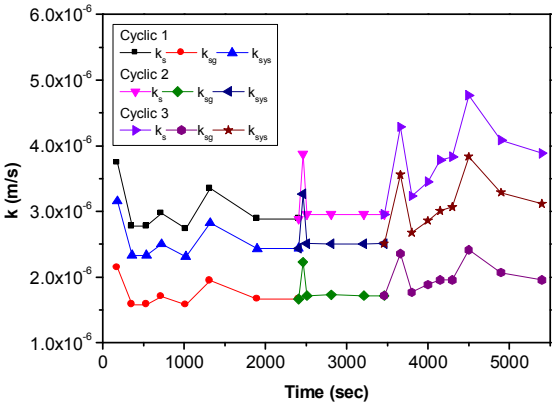
(c)



(d)



(e)



(f)

Figure C1.6 NW20 and 90% sand 10% PFA

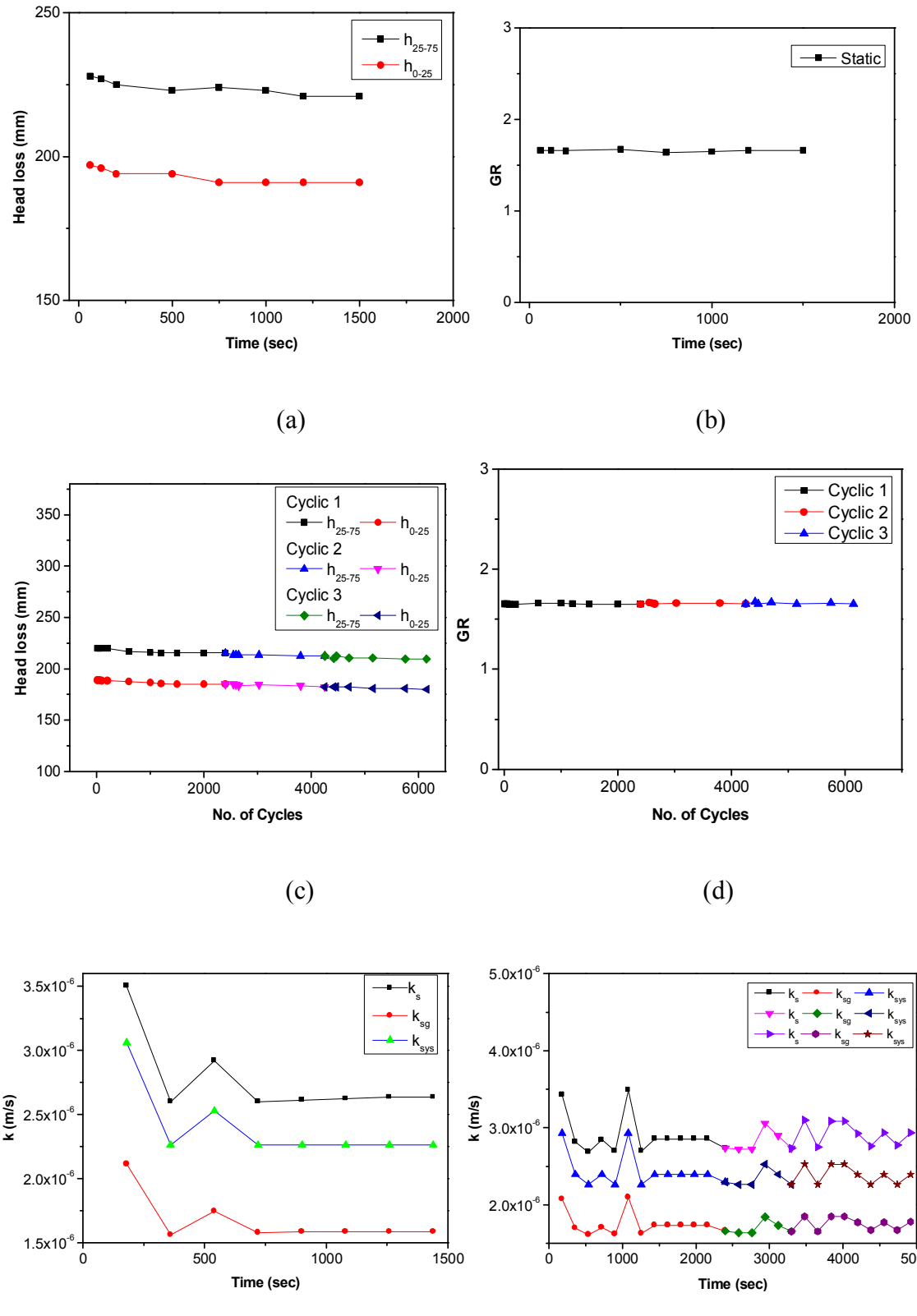


Figure C1.7 NW8 and 90% sand 10% PFA

C2: Broadly-Graded Soils

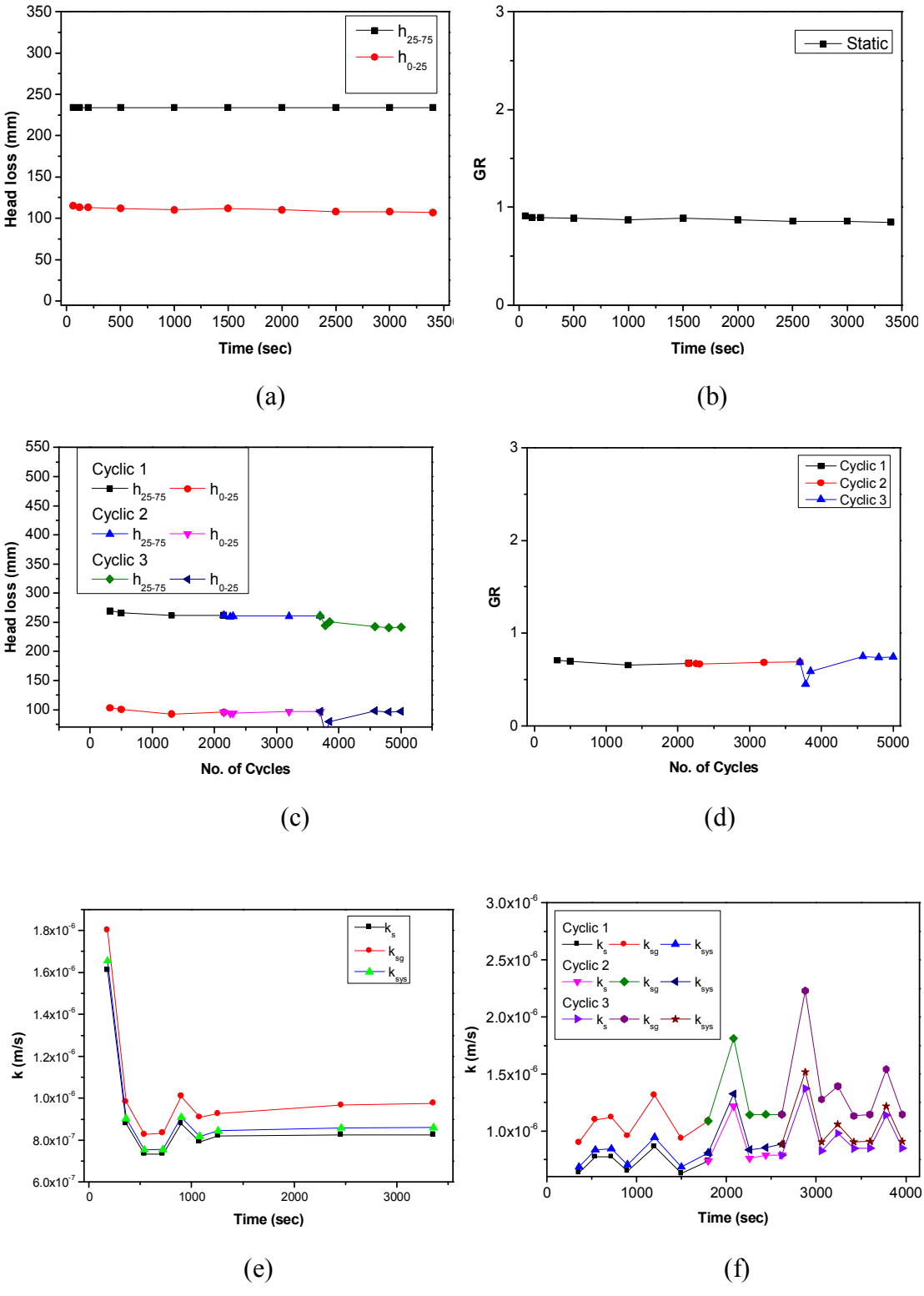
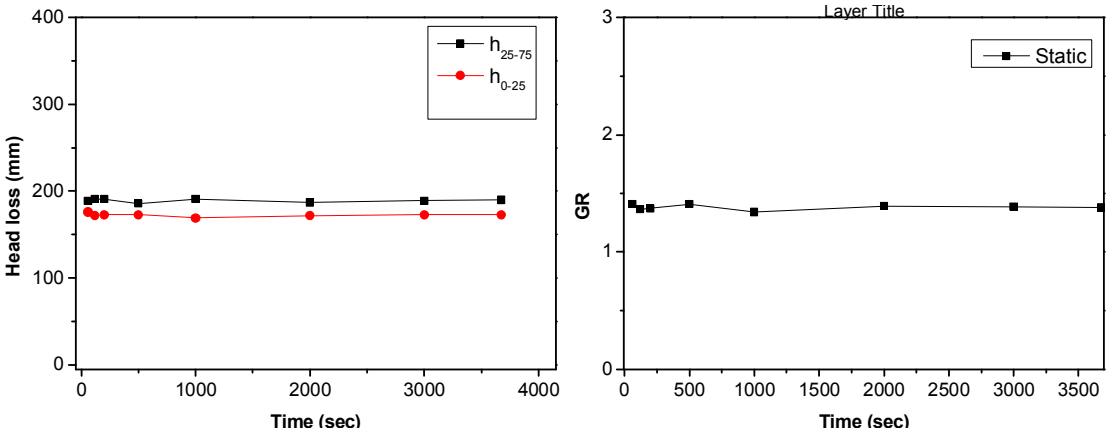
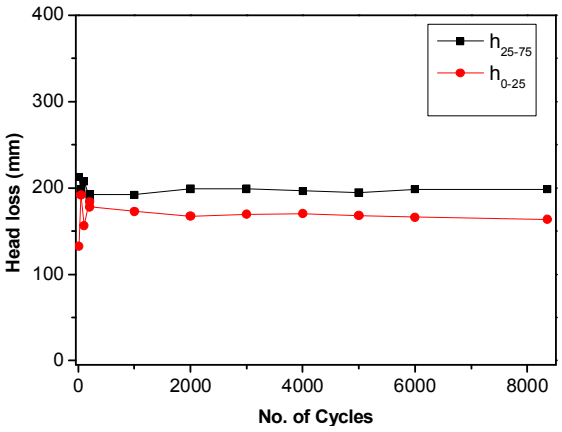


Figure C2.1 NW20 and 85% sand 15% PFA

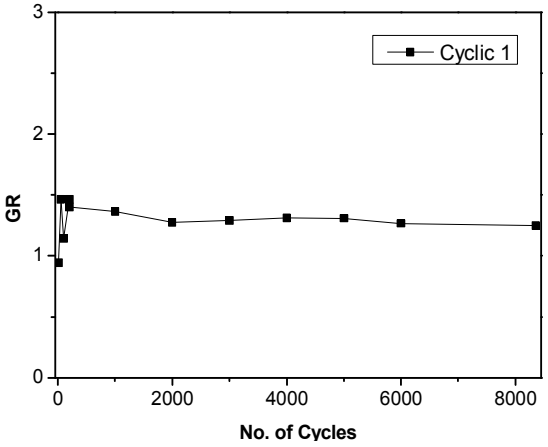


(a)

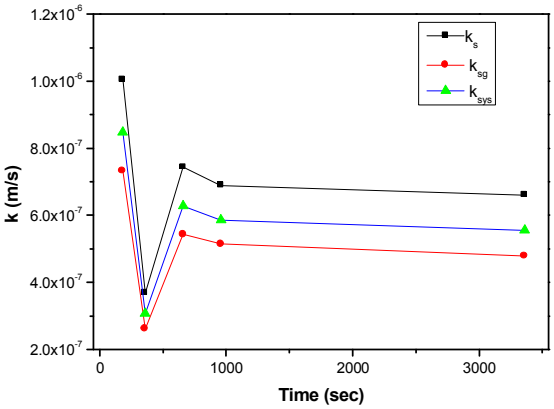
(b)



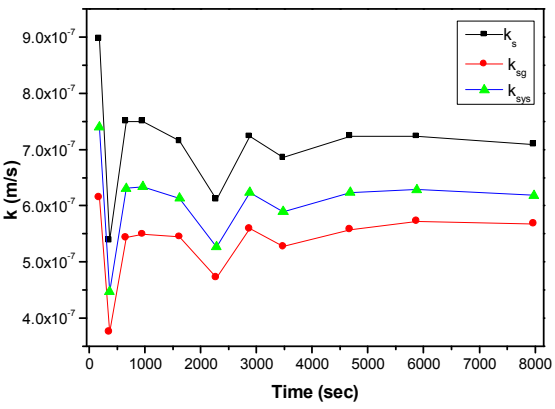
(c)



(d)



(e)



(f)

Figure C2.2 F1200M and 80% sand 20% PFA

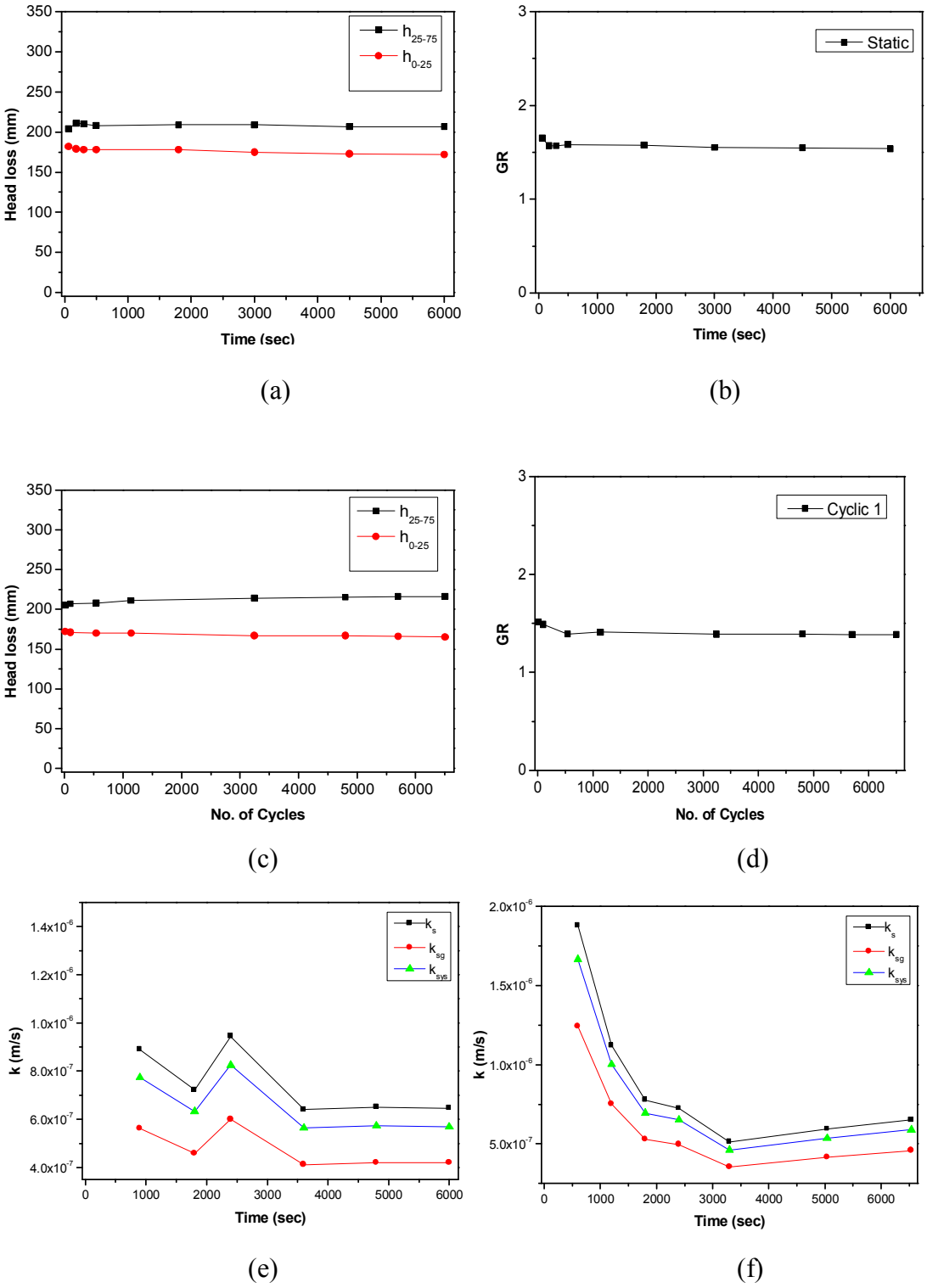


Figure C2.3 NW20 and 80% sand 20% PFA

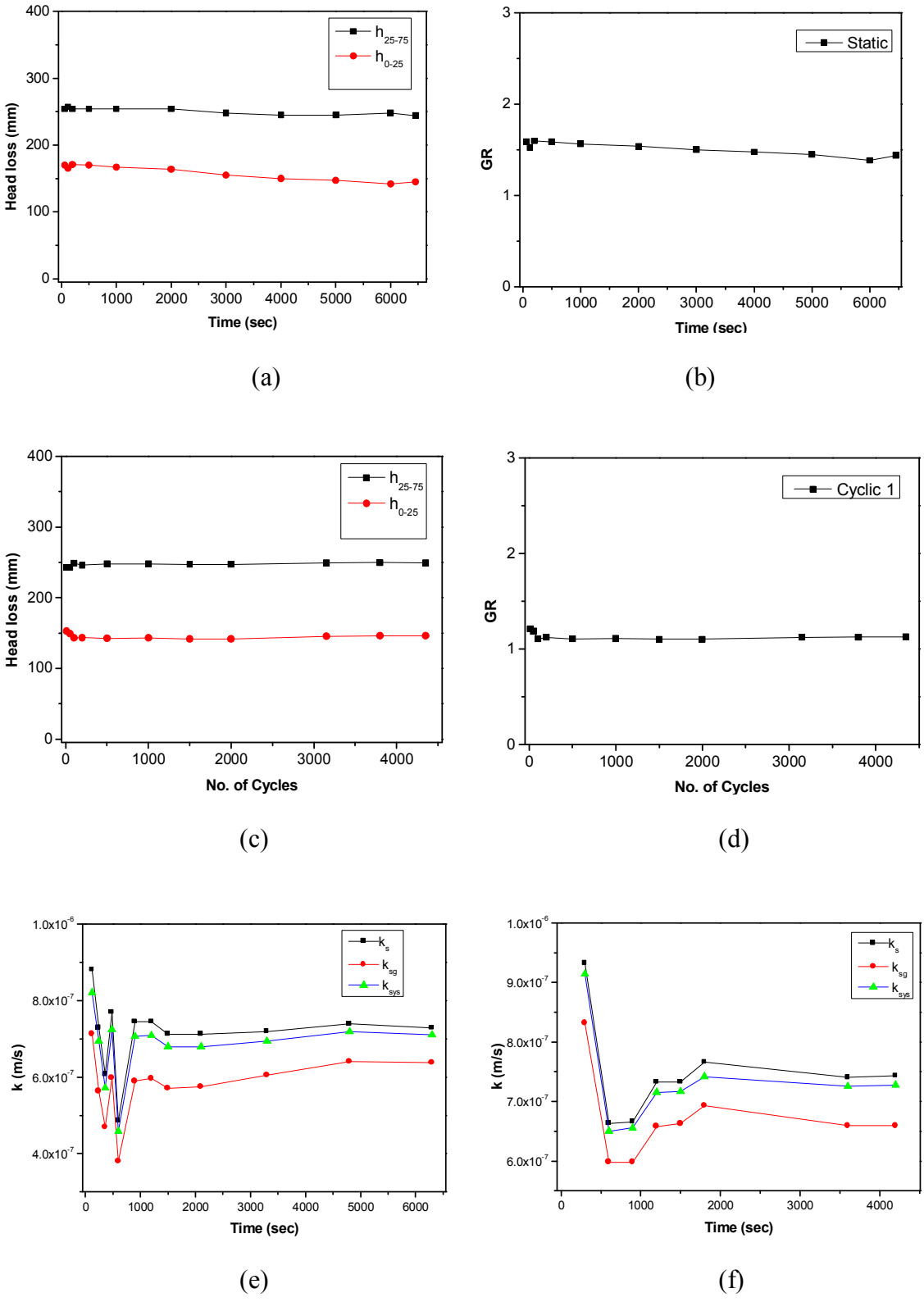


Figure C2.4 NW8 and 80% sand 20% PFA

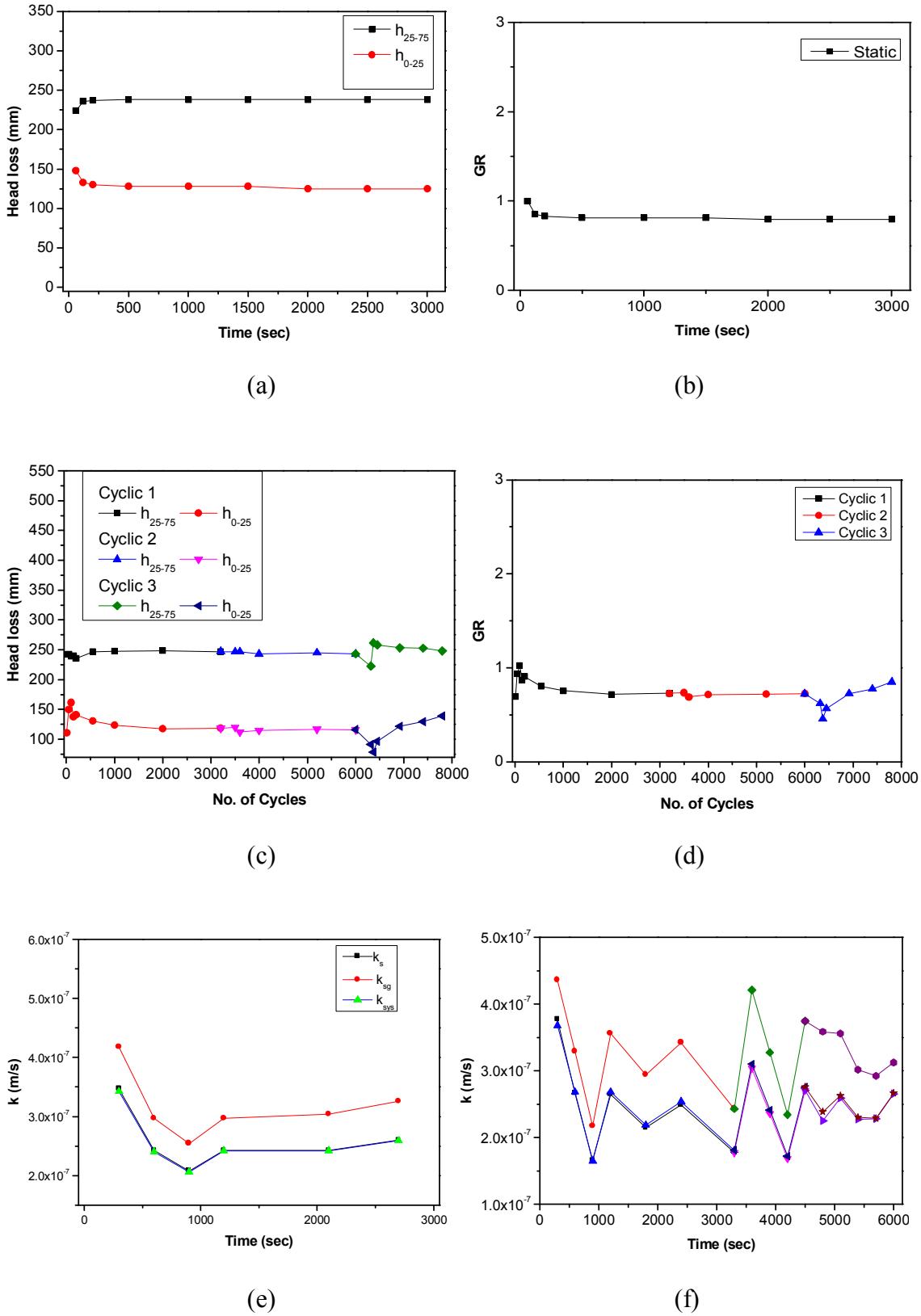


Figure C2.5 F1200M and 70% sand 30% PFA

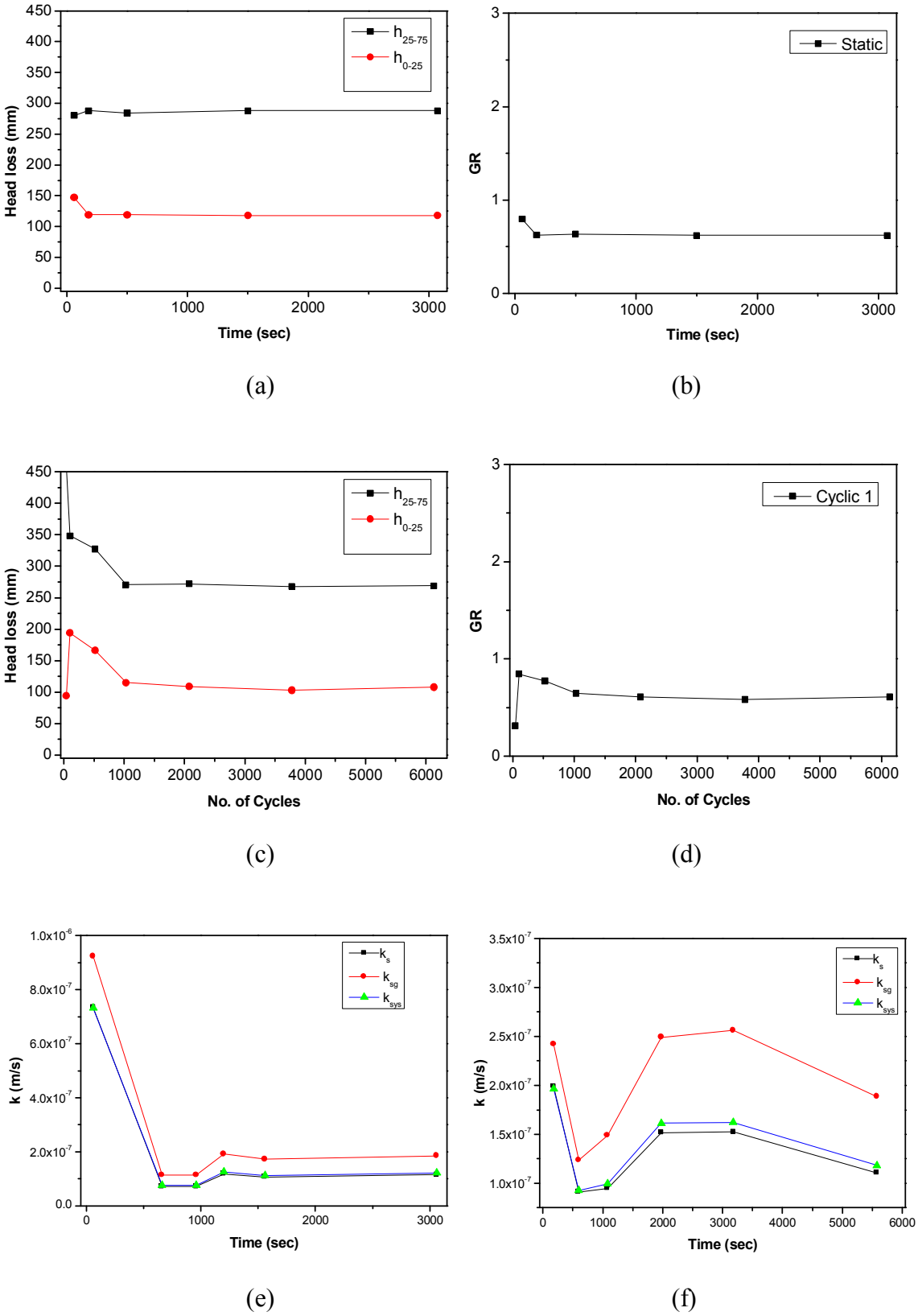


Figure C2.6 F1200M and 60% sand 40% PFA

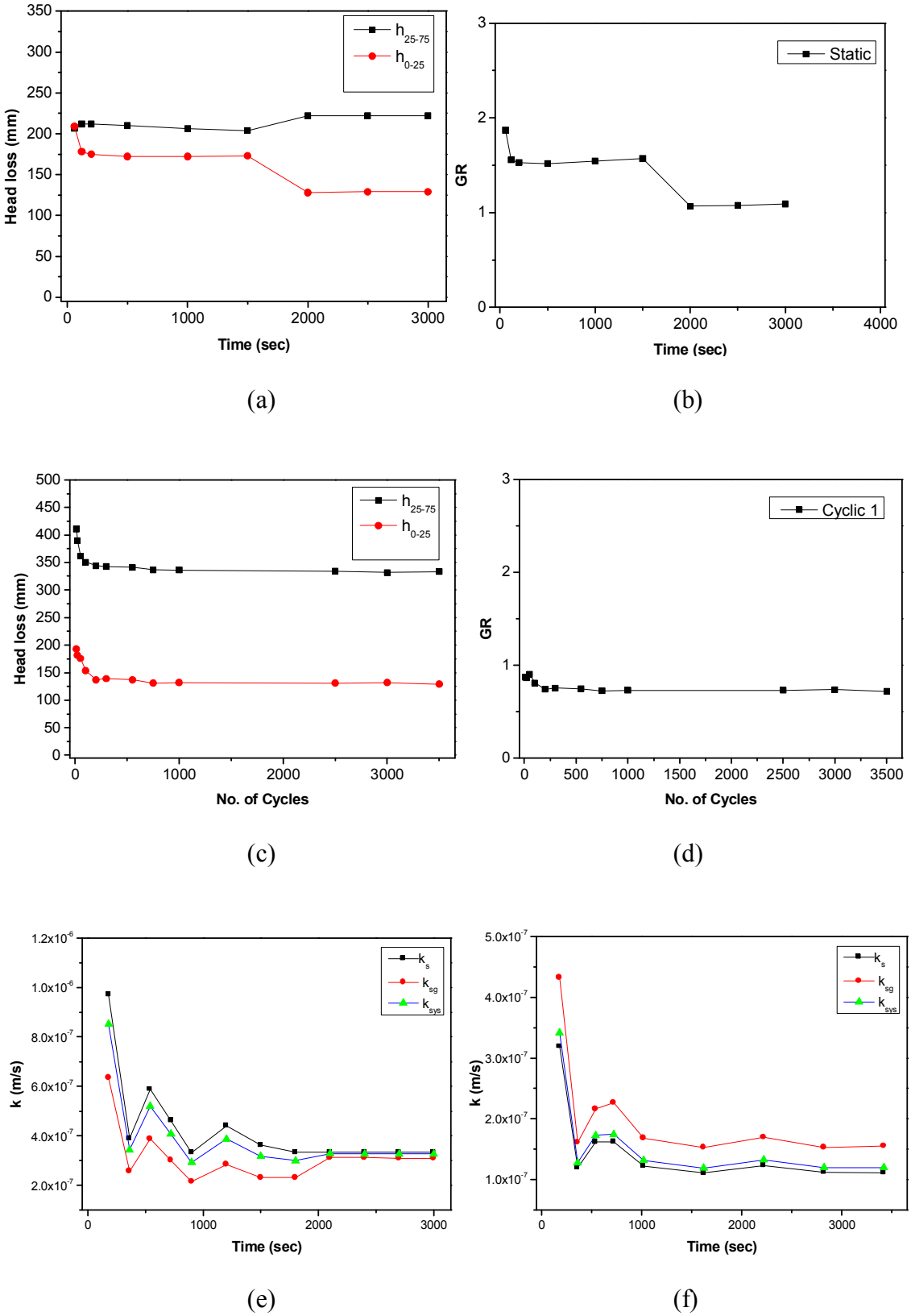


Figure C2.7 ST170 and 60% sand 40% PFA

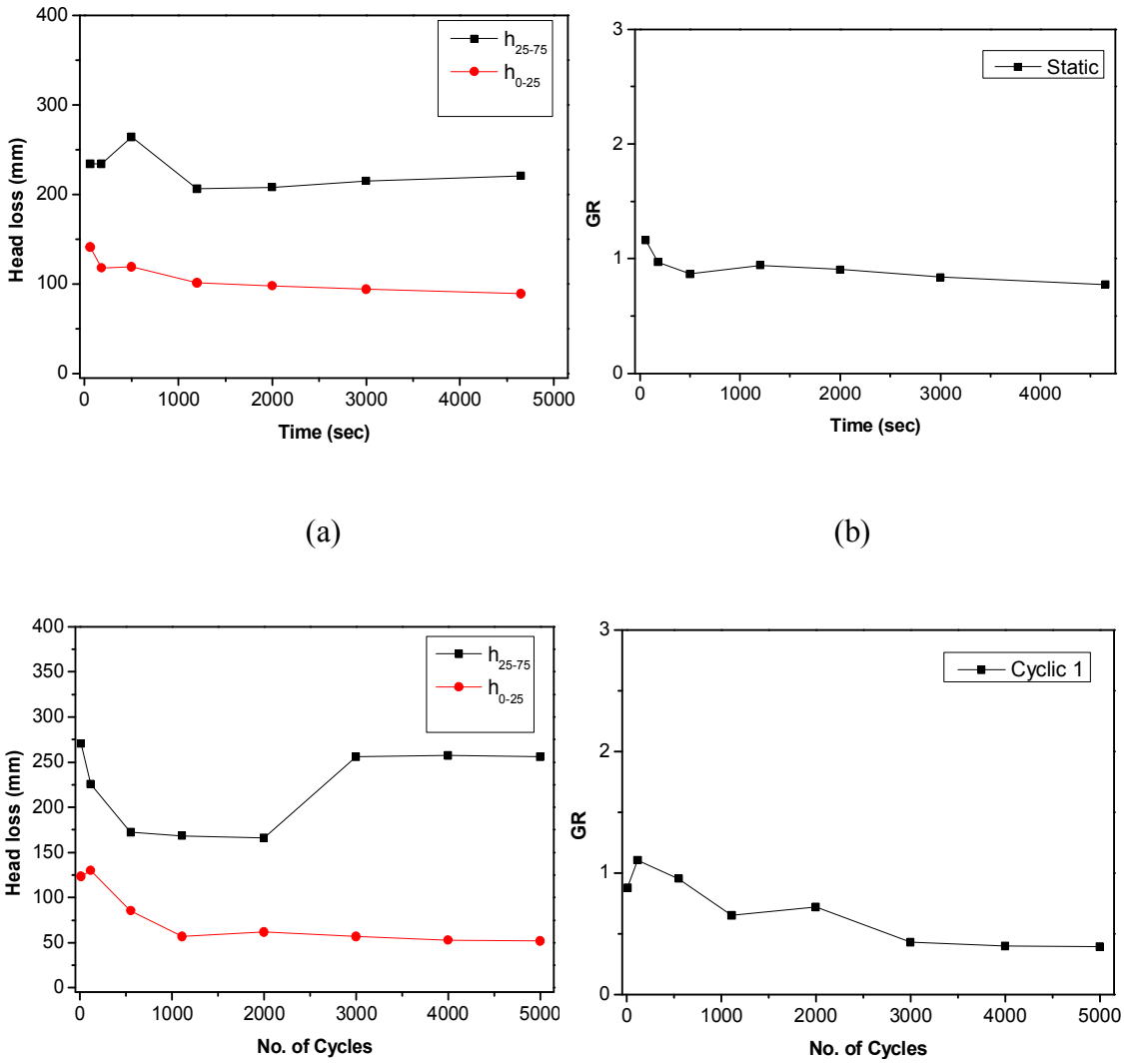


Figure C2.8 NW20 and 60% sand 40% PFA

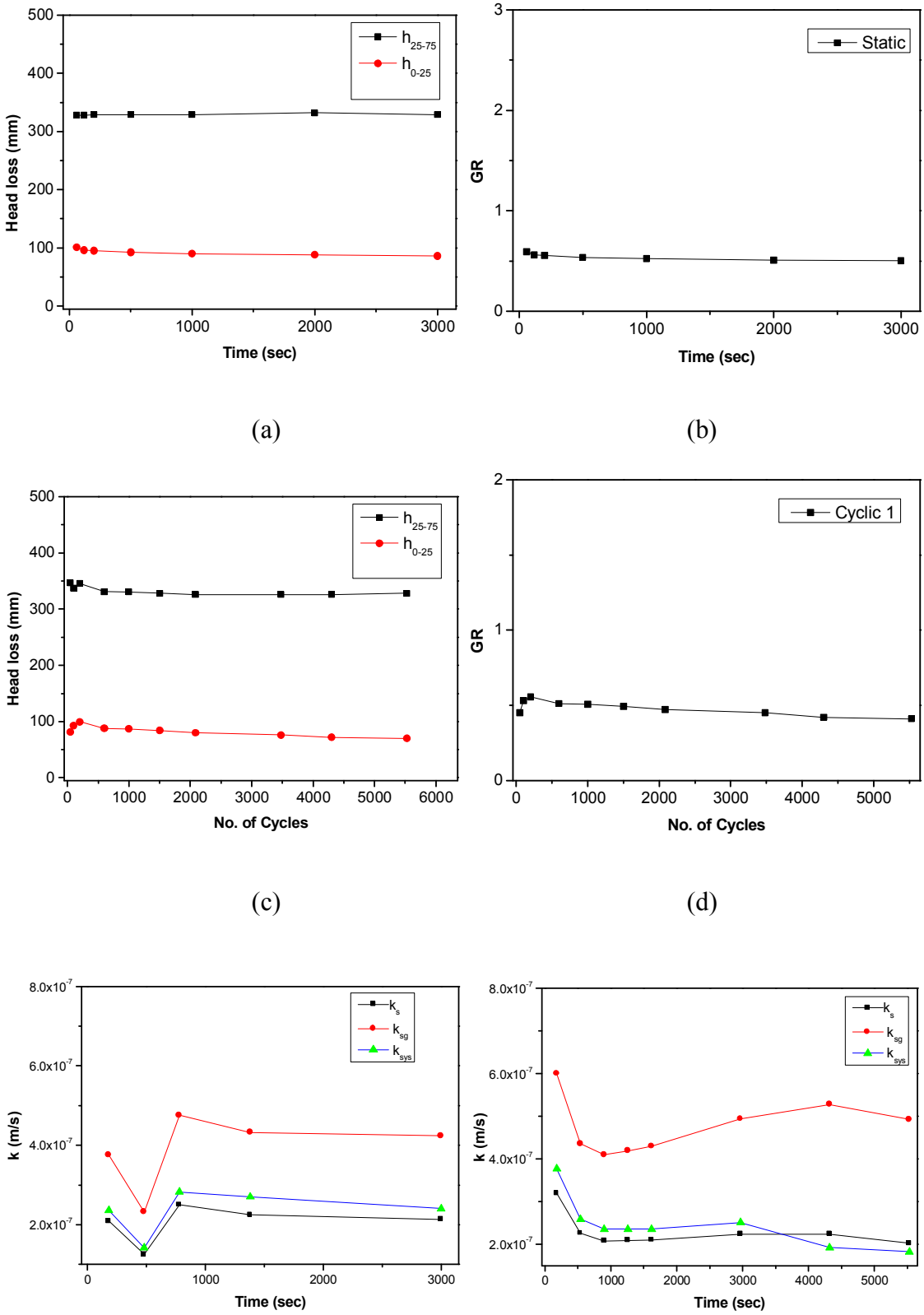
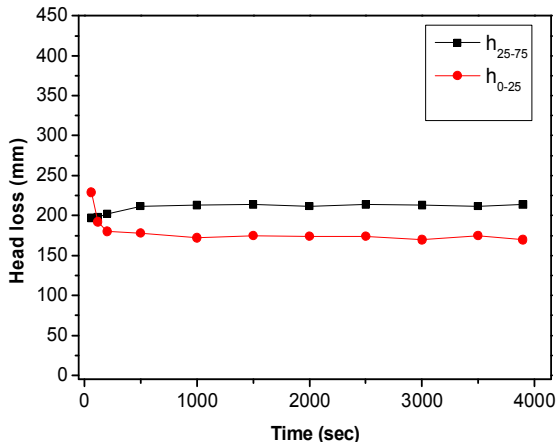
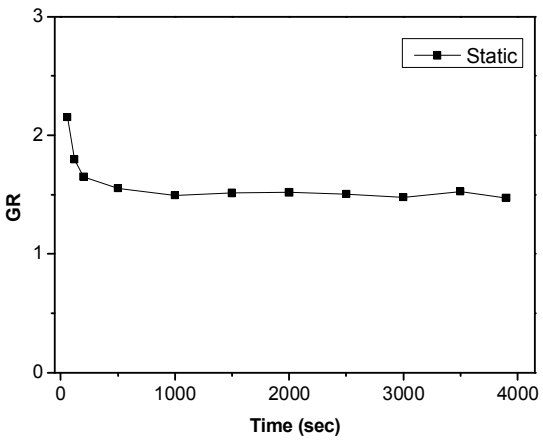


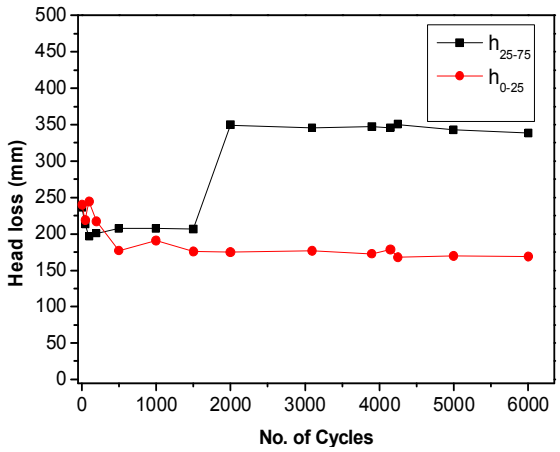
Figure C2.9 NW8 and 60% sand 40% PFA



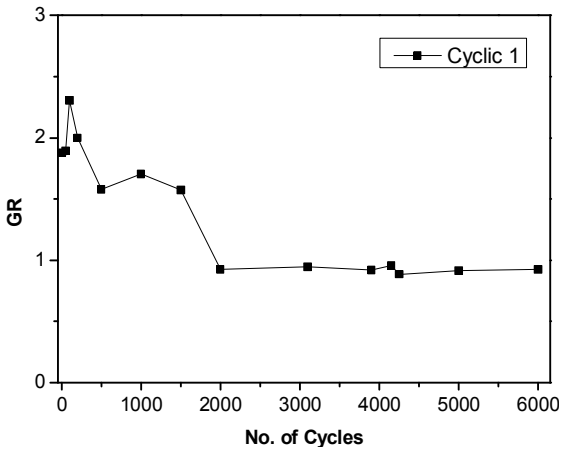
(a)



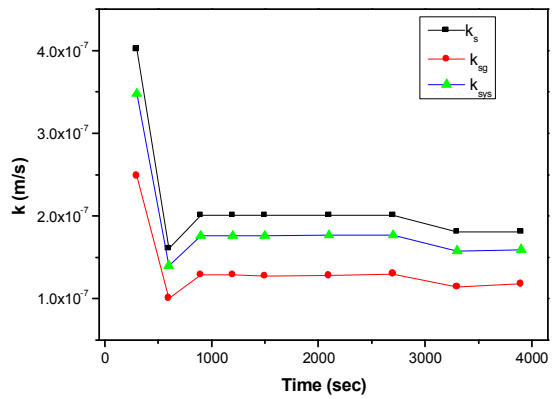
(b)



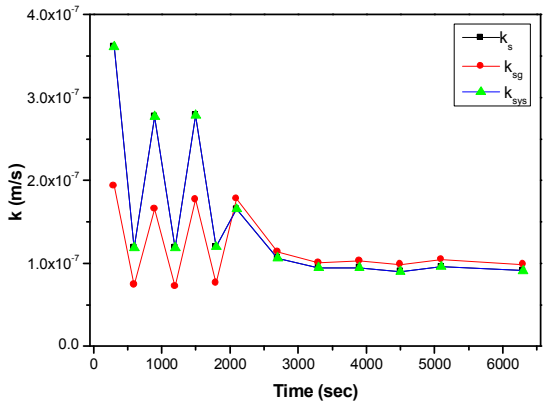
(c)



(d)



(e)



(f)

Figure C2.10 NW20 and 40% sand 60% PFA

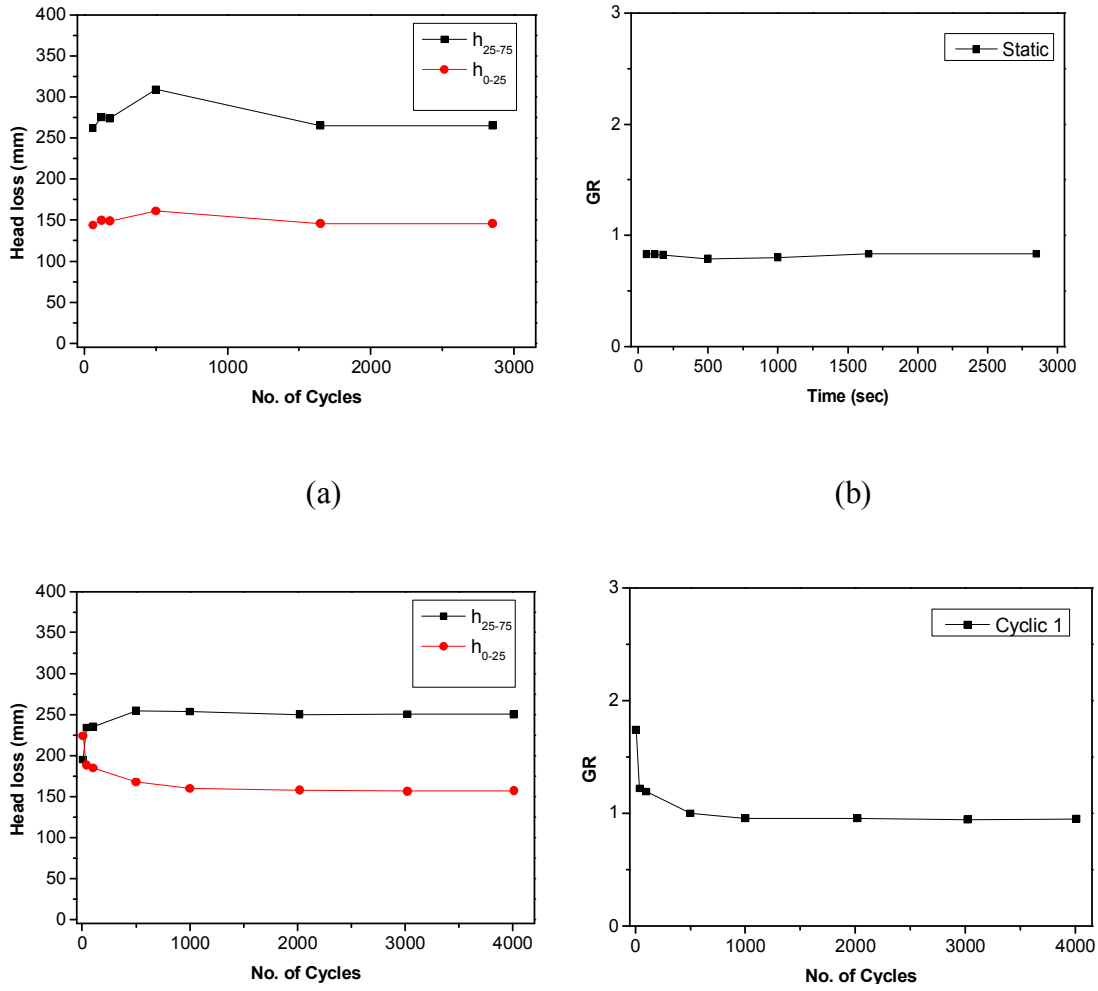


Figure C2.11 F1200M and PFA

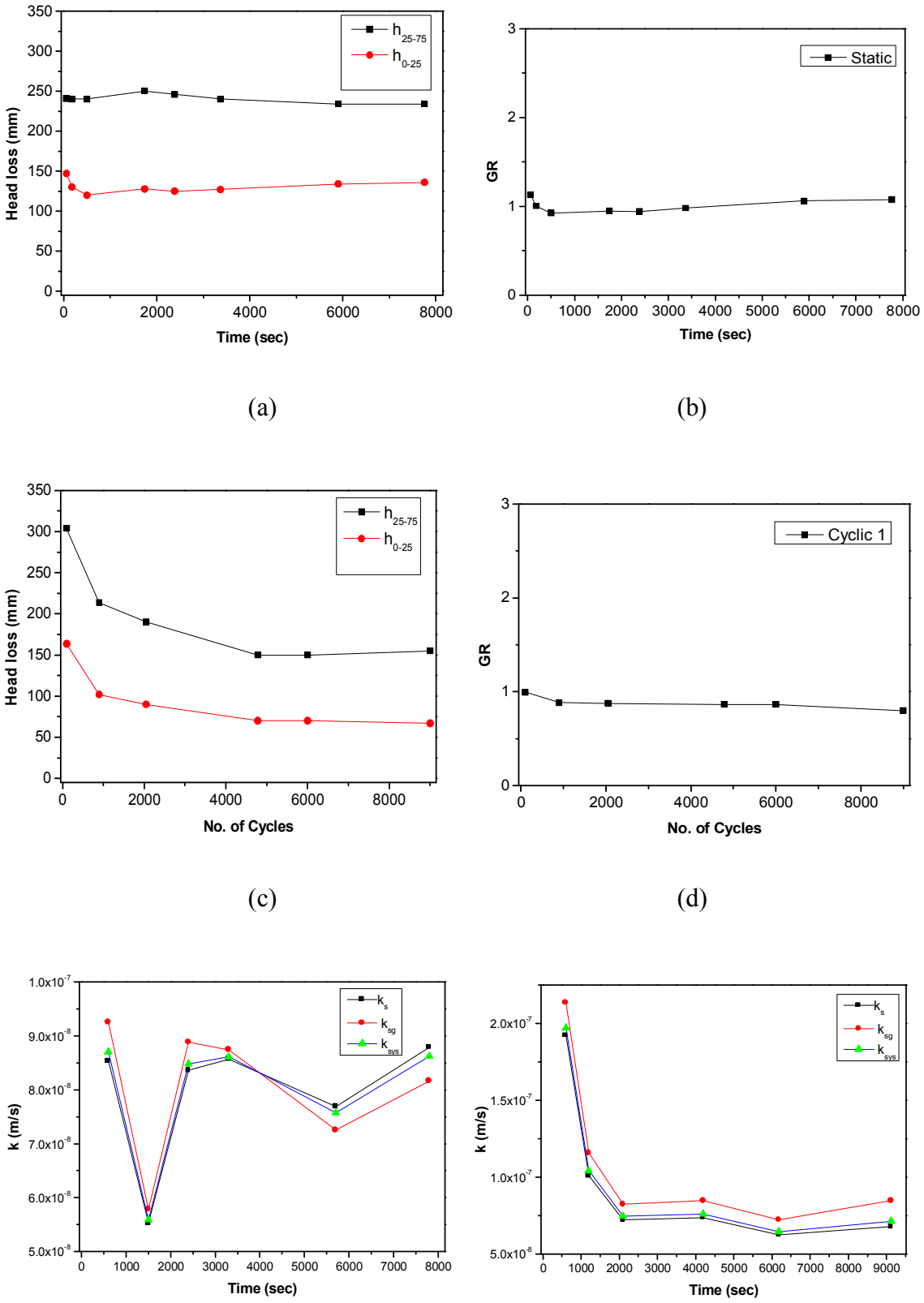
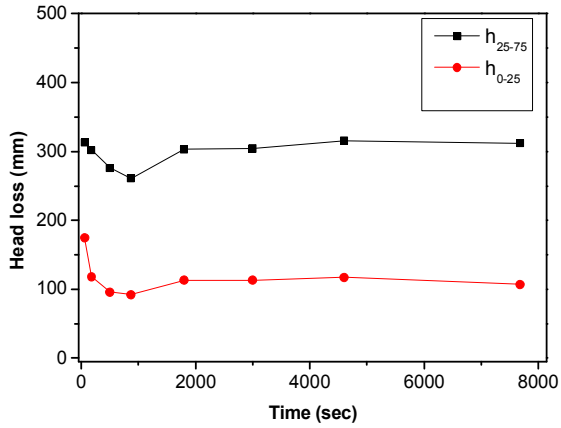
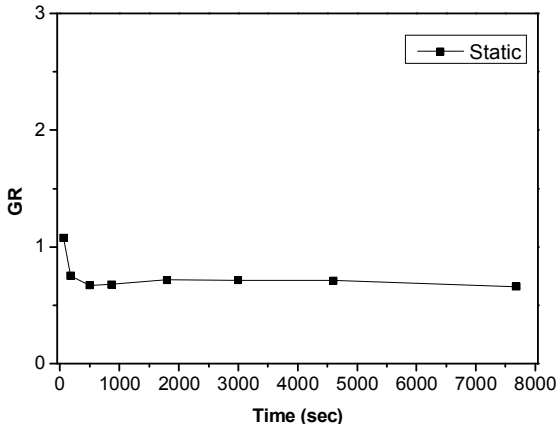


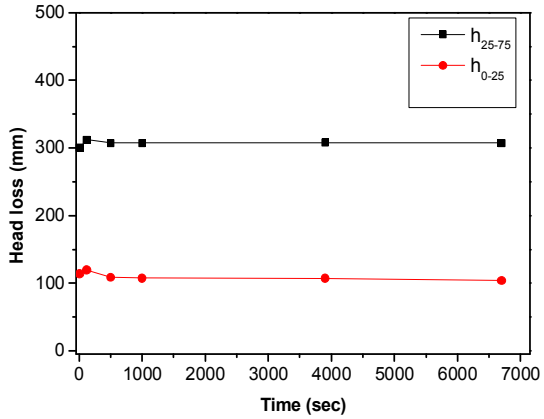
Figure C2.12 NW20 and PFA



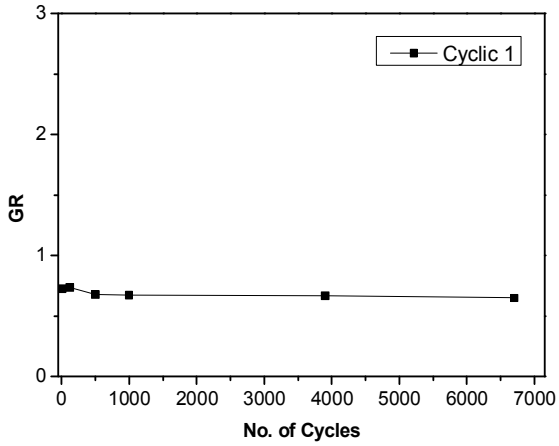
(a)



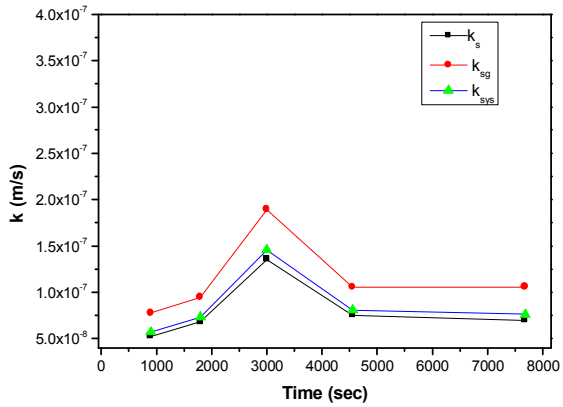
(b)



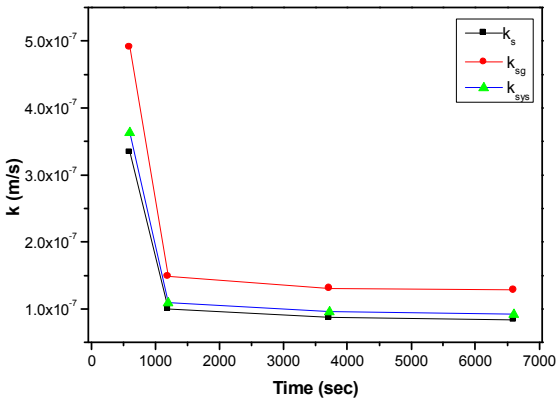
(c)



(d)



(e)



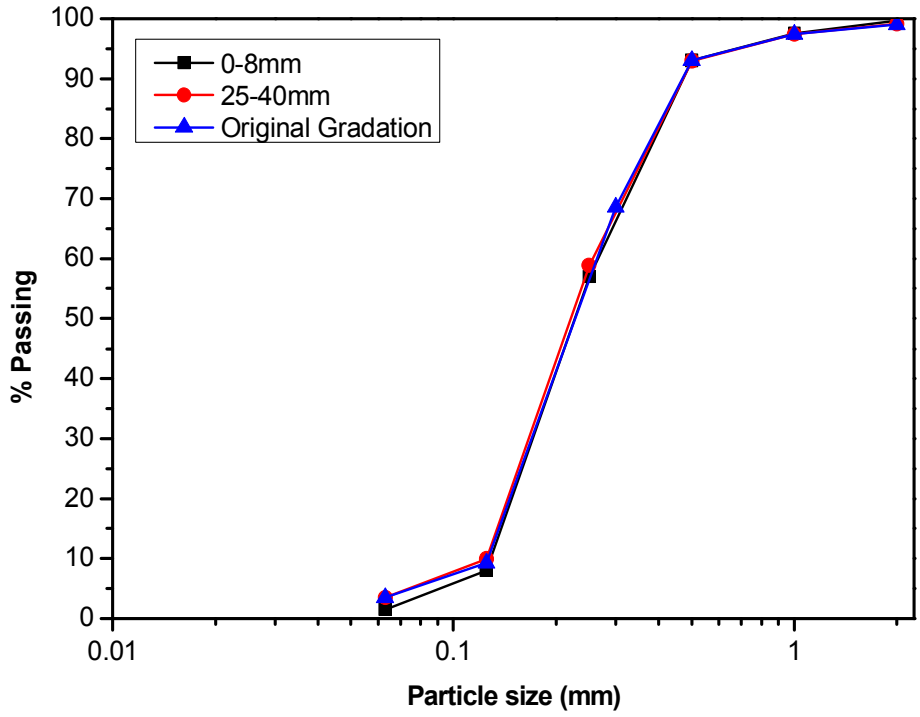
(f)

Figure C2.13 ST170 and PFA

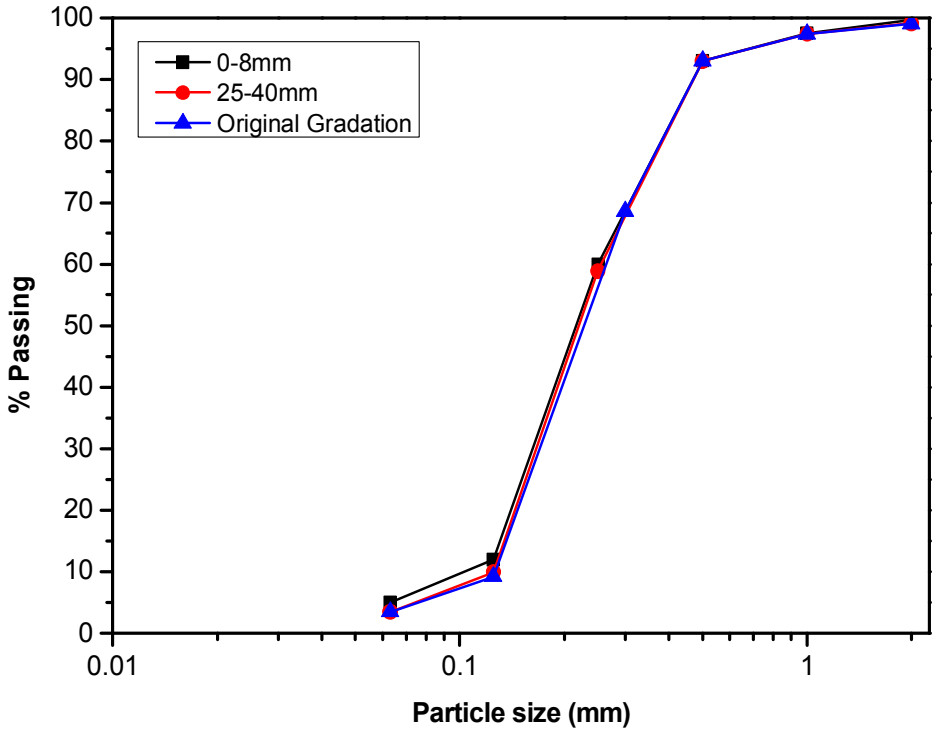
Appendix D: Pre and Post-Test Gradation

The pre and post-test gradations of narrow and broadly-graded soils are presented in chapter 5, in the form of tables. The gradation curves in the form of figures that may be of interest are presented here. The gradation curves for narrow graded soils are presented in section D1 and the broadly-graded results are presented in section D2.

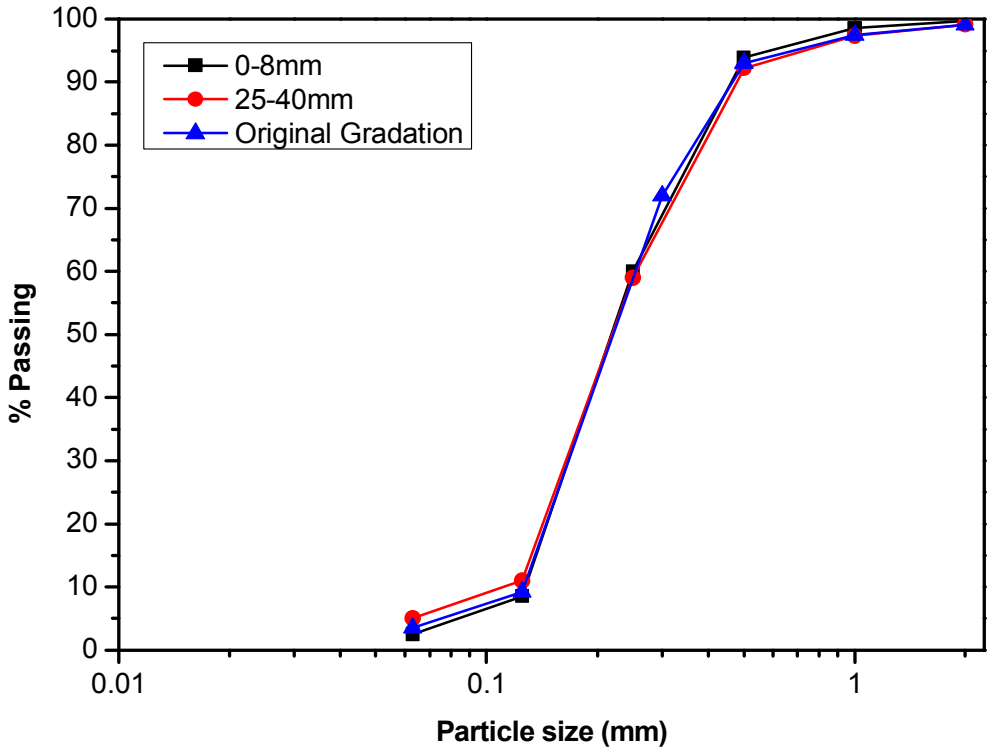
D1: Narrow Graded Soils



(a) NW8 and Medium Sand

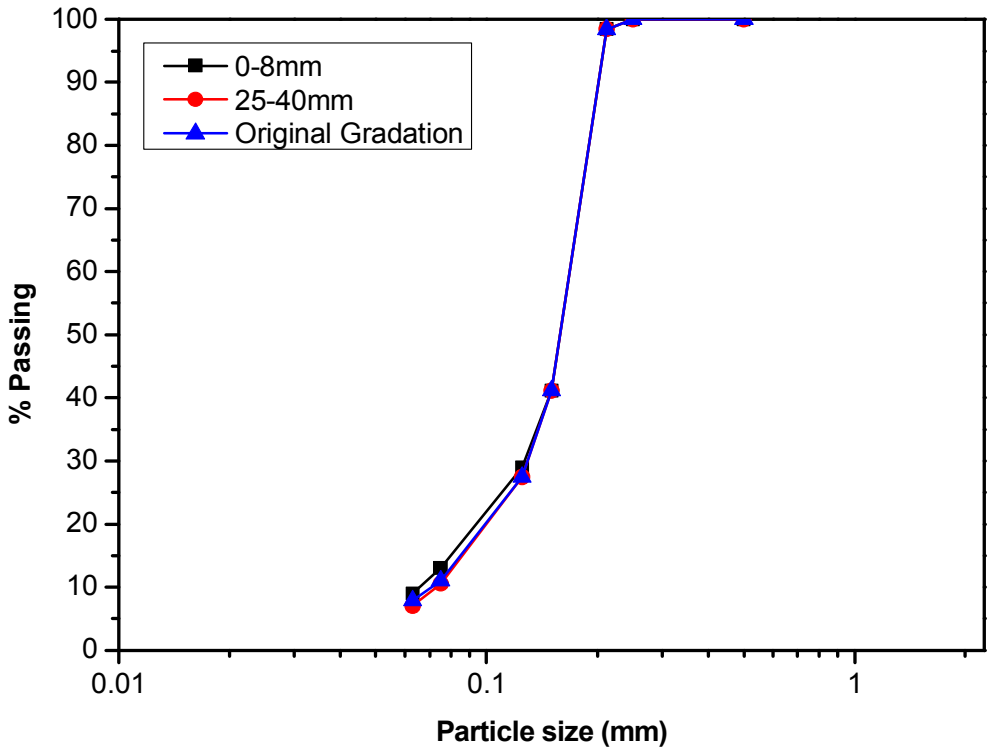


(b) NW20 and Medium Sand

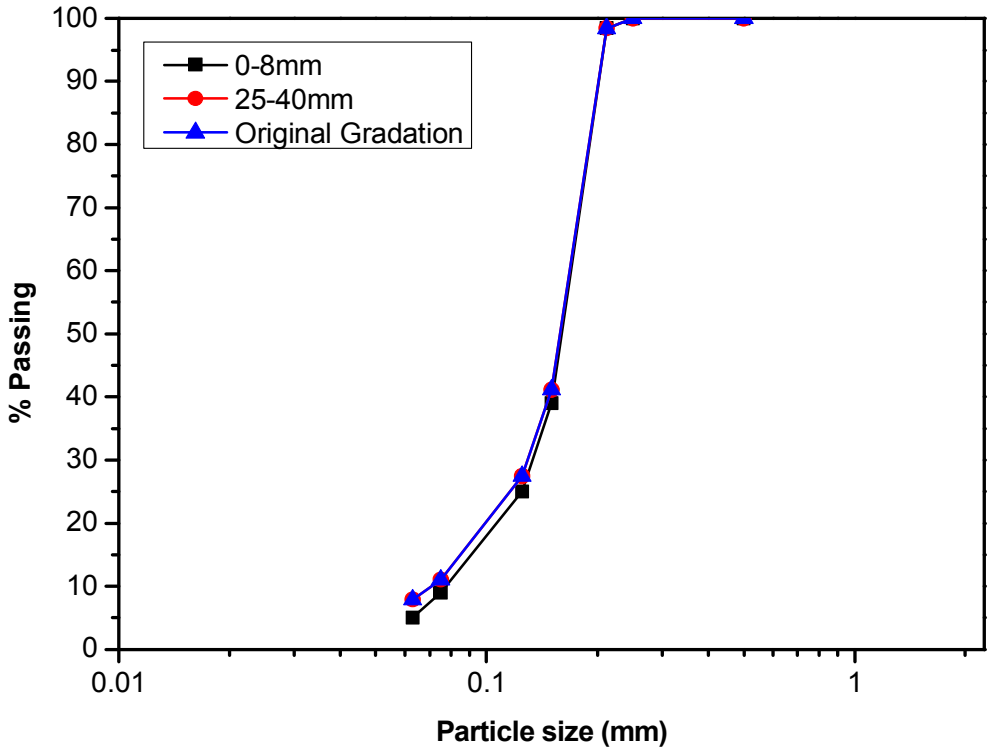


(c) ST170 and Medium Sand

Figure D1.1 Medium Sand

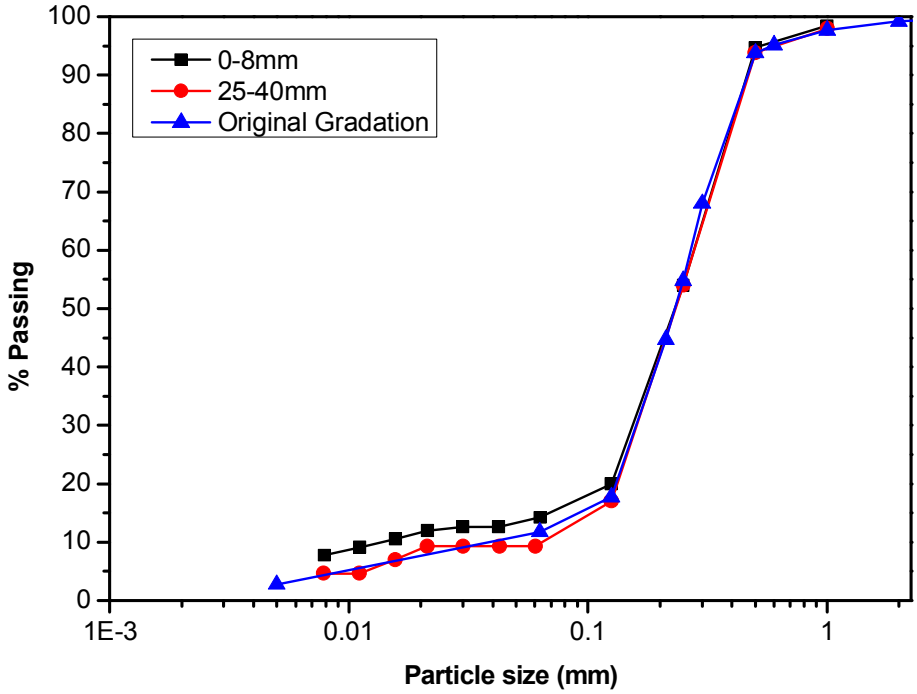


(a) NW20 and Fine Sand

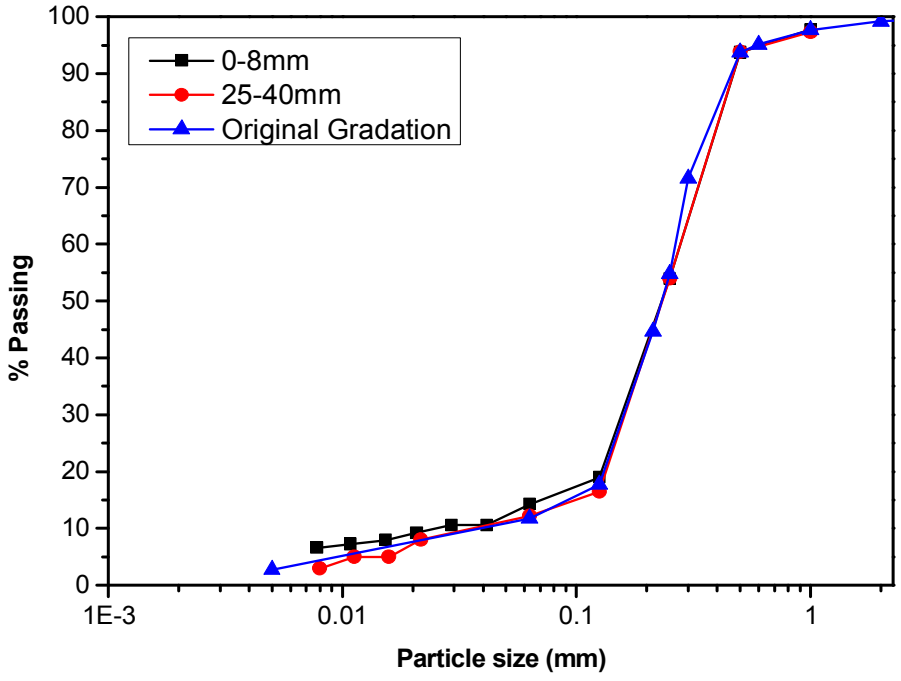


(b) NW8 and Fine Sand

Figure D1.2 Fine Sand



(a) NW20 and 90% Sand 10% PFA



(b) NW8 and 90% Sand 10% PFA

Figure D1.3 Fine Sand

D2: Broadly-Graded Soils

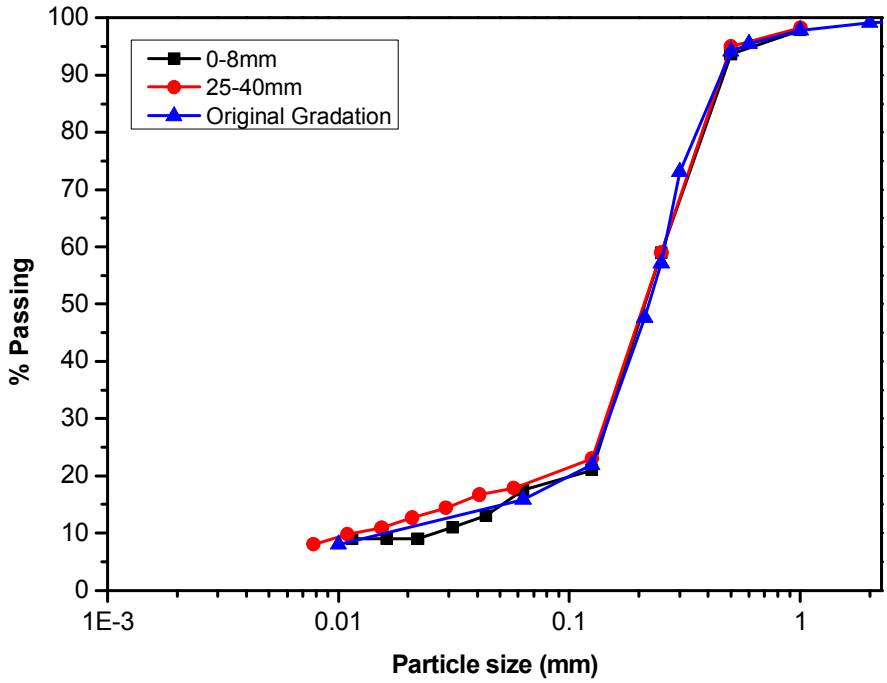
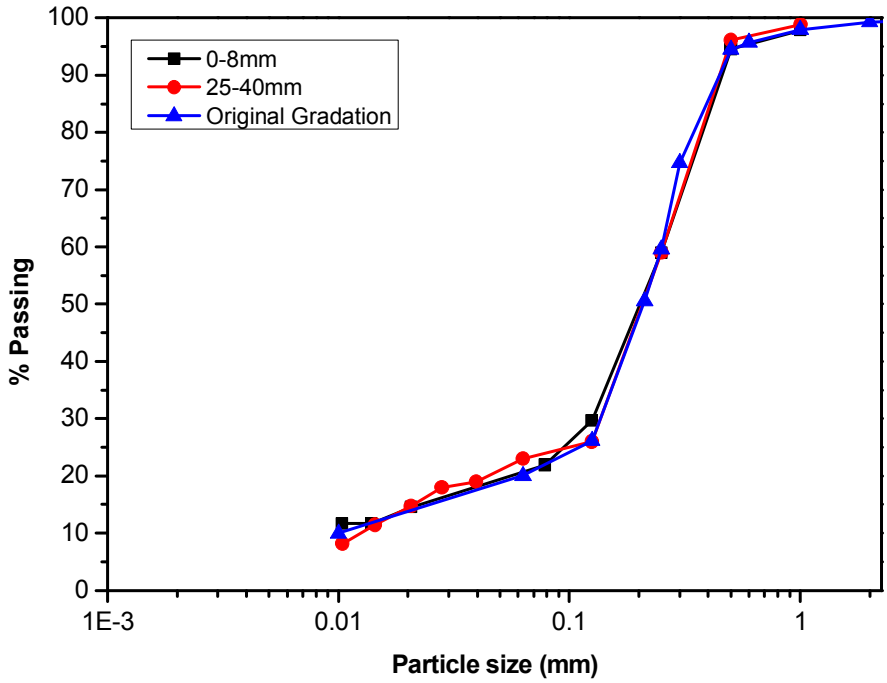
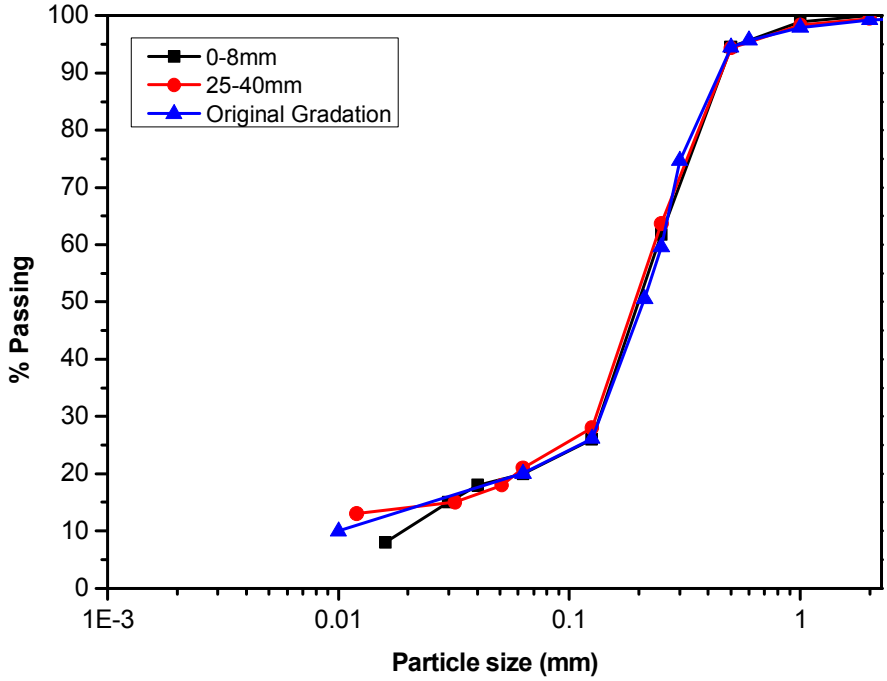


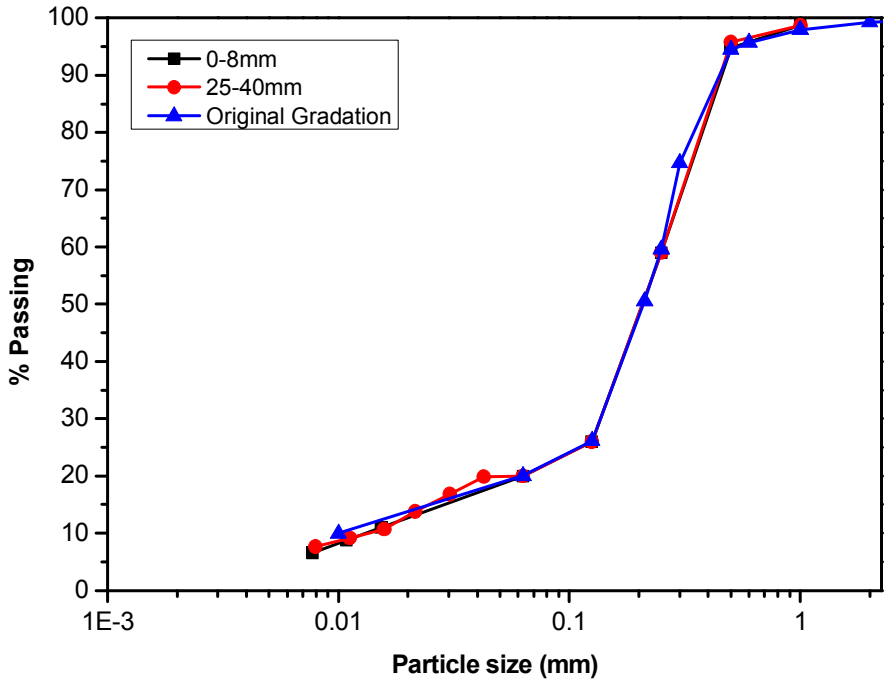
Figure D2.1 NW20 and 85% sand 15% PFA



(a) F1200M and 80% sand 20% PFA



(b) NW20 and 80% sand 20% PFA



(c) NW20 and 80% sand 20% PFA

Figure D2.2 80% sand 20% PFA

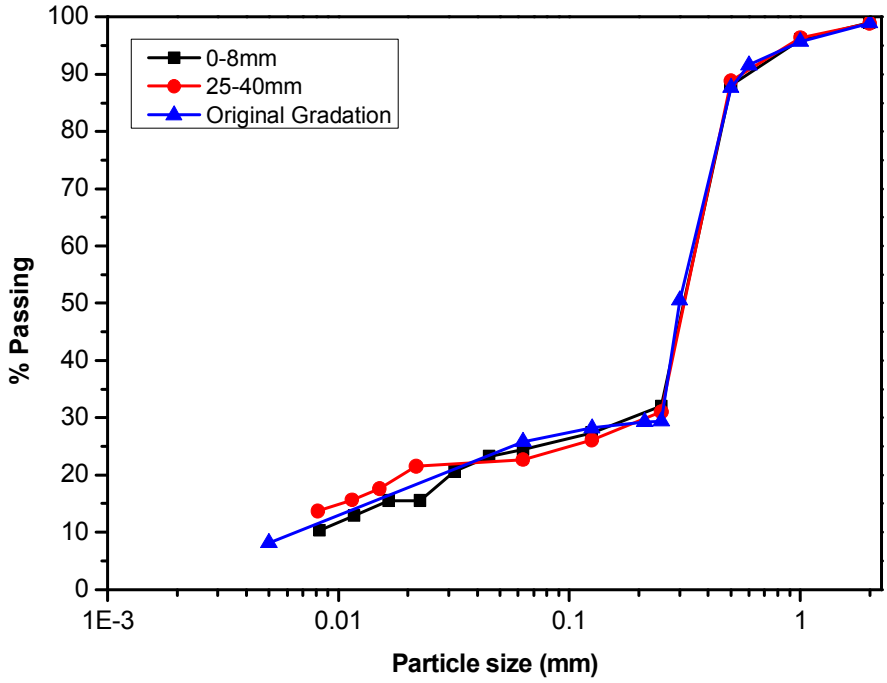
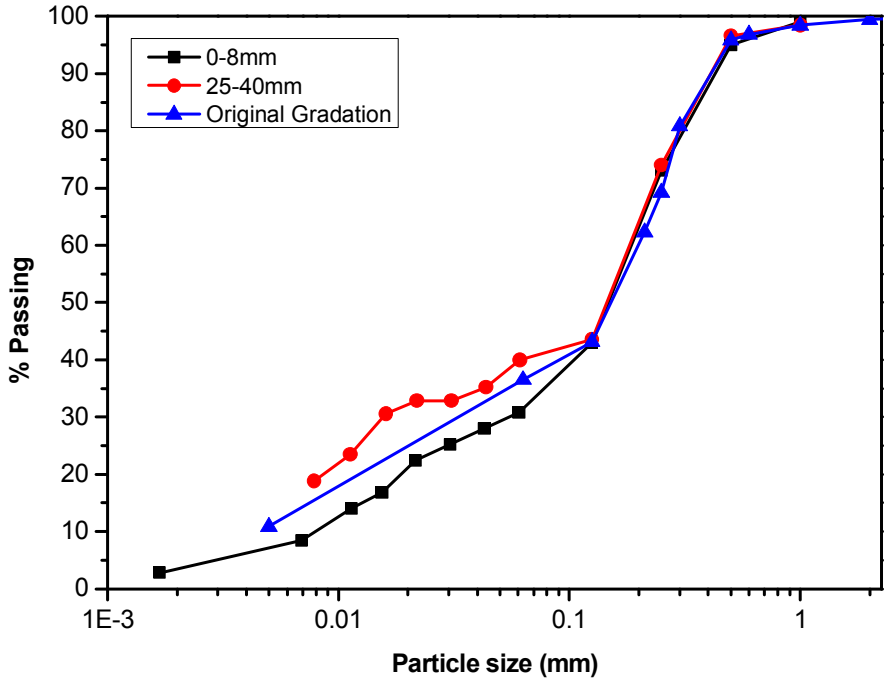
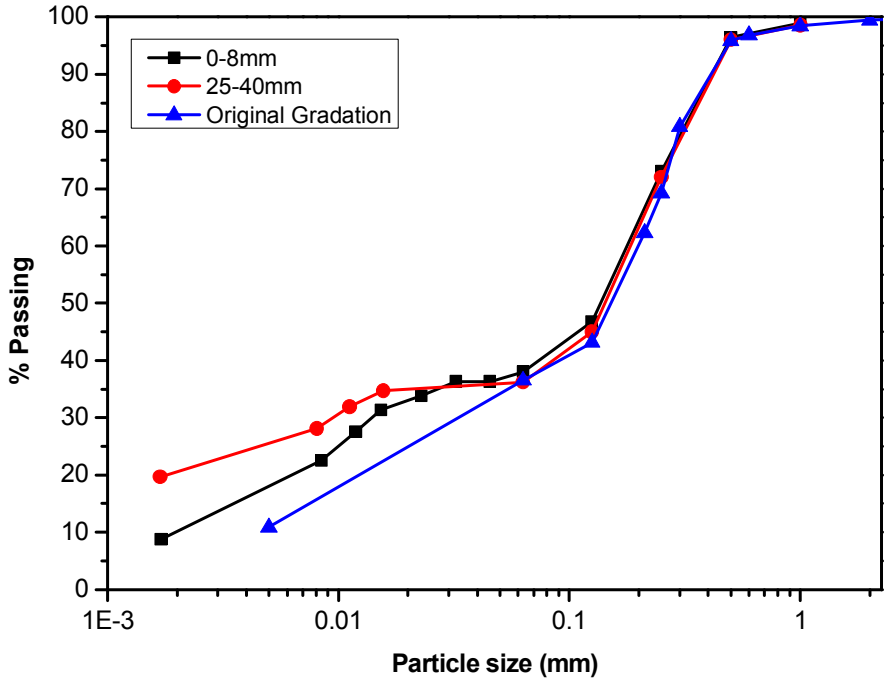


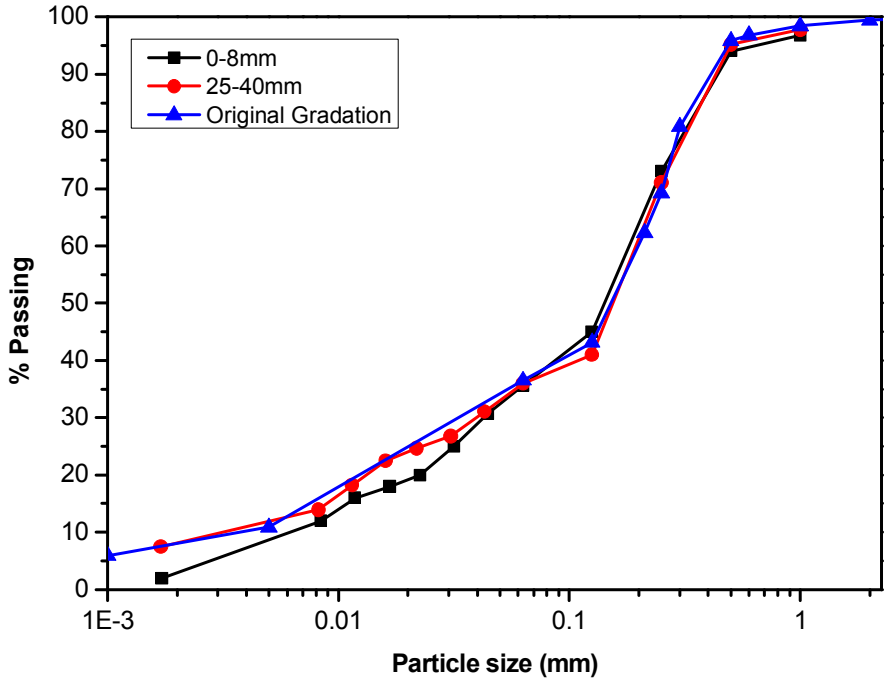
Figure D2.3 F1200M and 70% sand 30% PFA



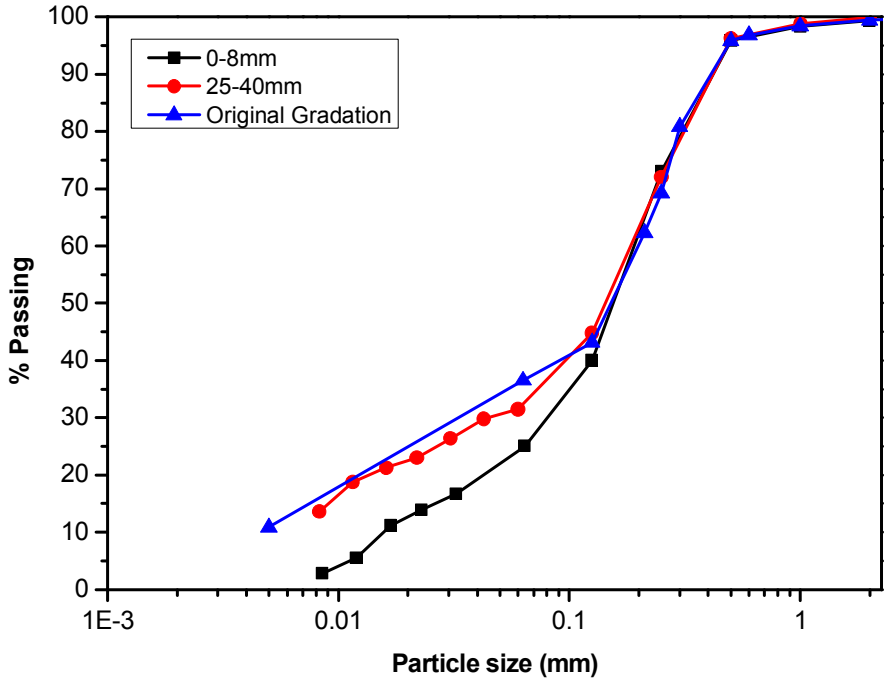
(a) F1200M and 60% sand 40% PFA



(b) NW20 and 60% sand 40% PFA



(c) ST170 and 60% sand 40% PFA



(d) NW8 and 60% sand 40% PFA

Figure D2.4 60% sand 40% PFA

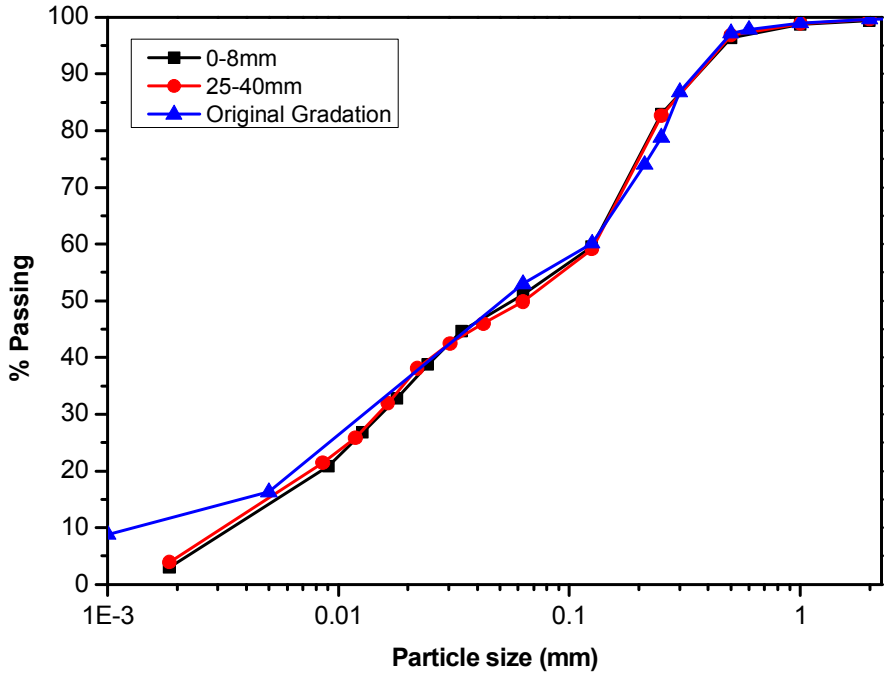
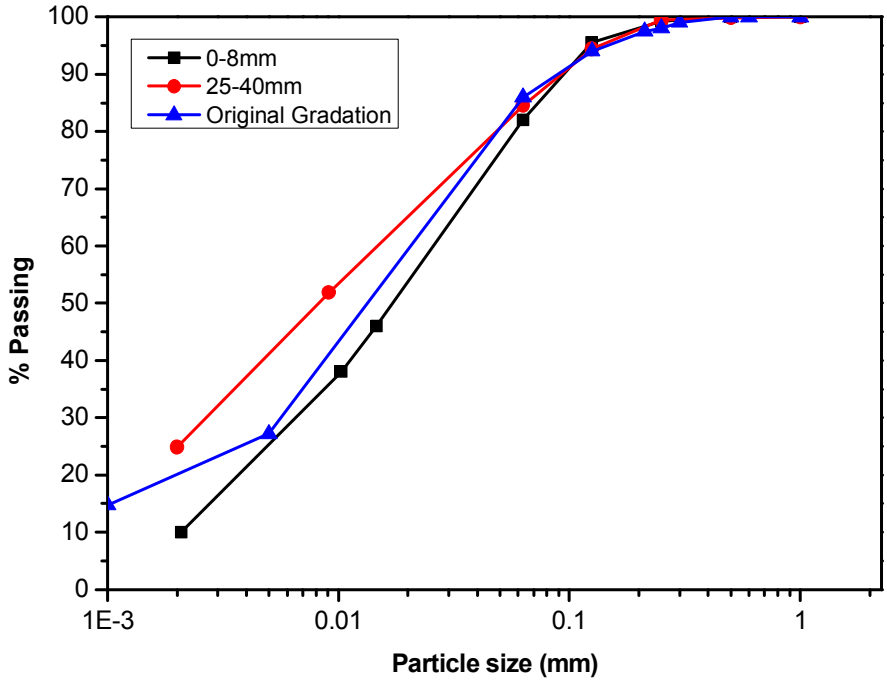
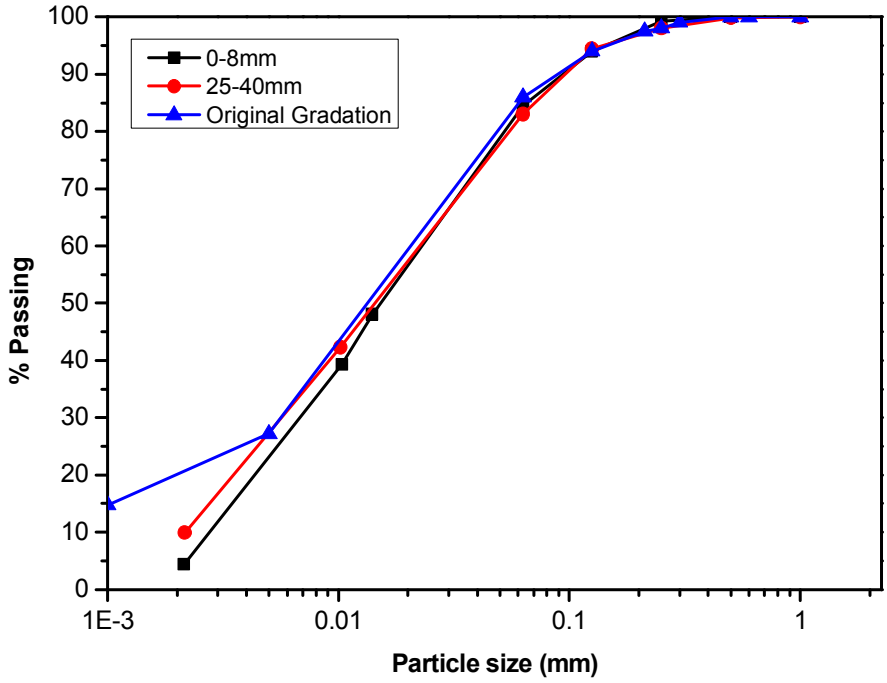


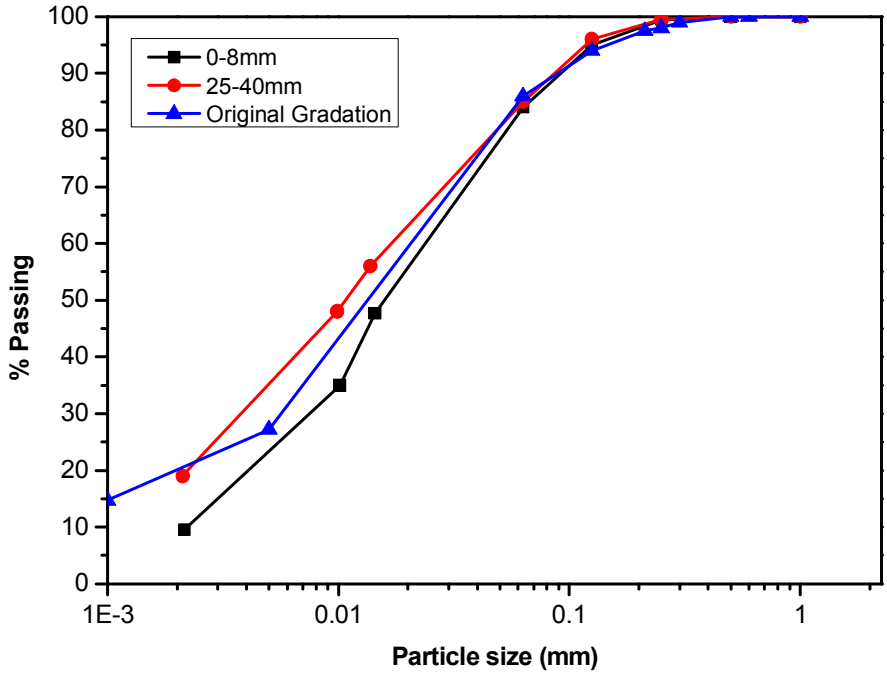
Figure D2.5 NW20 and 40% sand 60% PFA



(a) NW20 and PFA



(b) ST170 and PFA



(c) F1200M and PFA

Figure D2.6 PFA

Appendix E: Summary of all filtration tests

Geotextile / Soil	Soil Type	$\frac{O_{90}}{d_{85}}$	$\frac{C_{50}}{d_{85}}$	$\frac{O_{90}}{d_{30}}$	$\frac{C_{50}}{d_{30}}$	$\frac{O_{90}}{d_{15}}$	$\frac{C_{50}}{d_{15}}$	GR				KR				Particles Passed		Partial Clogging Level 'λ'	Filtration Result
								Static	Cyc1	Cyc2	Cyc3	Static	Cyc1	Cyc2	Cyc3	Mass g/m²	% Original Gradation		
NW8/ Medium Sand	NG	0.29	-	0.63	-	0.8	-	0.83	0.69	-	-	1.30	1.11	-	-	311	<4	1.07	NP/NB
NW20/ Medium Sand	NG	0.17	0.17	0.37	0.38	0.47	0.38	1.27	1.51	-	-	1.07	1.09	-	-	180	<4	0.56	B
ST170/ Medium Sand	NG	0.17	0.14	0.37	0.31	0.47	0.31	0.9	0.89	0.9	0.61	0.95	0.97	0.97	0.90	189	<4	0.79	NP/NB
NW20/ Fine Sand	NG	0.36	0.37	0.5	1.04	0.82	0.85	1	1.15	1.15	1.31	1.00	1.17	1.14	1.34	154	<8	0.38	B
NW8/ Fine Sand	NG	0.62	-	0.86	-	1.41	-	0.38	0.46	0.45	0.43	0.85	0.87	0.88	0.89	215	<8	1.33	NP/NB
NW20/ 90% Sand 10% PFA	NG	0.18	0.18	0.41	0.42	0.61	0.63	1.79	1.73	1.72	1.97	1.18	1.21	1.20	1.22	143	6	0.55	B
NW8/ 90% Sand 10% PFA	NG	0.3	-	0.71	-	1.04	-	1.66	1.65	1.65	1.65	1.18	1.17	1.17	1.21	171	8	1.11	B
NW20/ 85% Sand 15% PFA	BG	0.18	0.18	0.44	0.45	1.27	1.31	0.85	0.68	0.69	0.74	0.96	0.91	0.89	0.94	125	11	0.31	NP/NB
F1200M/ 80% Sand 20% PFA	BG	0.16	-	0.4	-	2	-	1.38	1.27	-	-	1.19	1.15	-	-	259	11	0.3	B

Geotextile / Soil	Soil Type	$\frac{O_{90}}{d_{85}}$	$\frac{C_{50}}{d_{85}}$	$\frac{O_{90}}{d_{30}}$	$\frac{C_{50}}{d_{30}}$	$\frac{O_{90}}{d_{15}}$	$\frac{C_{50}}{d_{15}}$	GR				KR				Particles Passed		Partial Clogging Level 'λ'	Filtration Result
								Static	Cyc1	Cyc2	Cyc3	Static	Cyc1	Cyc2	Cyc3	Mass g/m^2	% Original Gradation		
NW20/ 80% Sand 20% PFA	BG	0.18	0.19	0.47	0.48	2.33	2.40	1.54	1.41	-	-	1.14	1.09	-	-	290	12	0.88	B
NW8/ 80% Sand 20% PFA	BG	0.32	-	0.8	-	4	-	1.44	1.42	-	-	1.03	1.02	-	-	310	13	1	NP/NB
F1200M/ 70% Sand 30% PFA	BG	0.13	-	0.23	-	4	-	0.8	0.73	-	-	1.00	0.98	0.98	1.00	143	15	0.74	NP/NB
F1200M/ 60% Sand 40% PFA	BG	0.18	-	1.76	-	7.5	-	0.62	0.61	-	-	0.94	0.93	-	-	300	18	0.35	NP/NB
NW20/ 60% Sand 40% PFA	BG	0.21	0.21	2.06	2.12	8.75	9	0.77	0.4	-	-	0.93	0.87	-	-	480	30	0.75	P
ST170/ 60% Sand 40% PFA	BG	0.21	0.17	2.06	1.74	8.75	7.4	1.08	0.73	-	-	1.01	0.93	-	-	370	27	1.02	NP/NB
NW8/ 60% Sand 40% PFA	BG	0.35	-	3.53	-	15	-	0.54	0.52	-	-	0.88	0.9	-	-	2707	32	1.56	P
NW20/ 40% Sand 60% PFA	BG	0.25	0.25	5	5.14	14	14.4	1.47	0.87	-	-	1.13	0.98	-	-	275	32	1.31	P
F1200M/ PFA	BG	0.95	-	10	-	60	-	0.83	0.95	-	-	0.96	0.99	-	-	392	45	0.67	P

Geotextile / Soil	Soil Type	$\frac{O_{90}}{d_{85}}$	$\frac{C_{50}}{d_{85}}$	$\frac{O_{90}}{d_{30}}$	$\frac{C_{50}}{d_{30}}$	$\frac{O_{90}}{d_{15}}$	$\frac{C_{50}}{d_{15}}$	GR				KR				Particles Passed		Partial Clogging Level 'λ'	Filtration Result
								Static	Cyc1	Cyc2	Cyc3	Static	Cyc1	Cyc2	Cyc3	Mass g/m²	% Original Gradation		
ST170/ PFA	BG	1.11	0.94	11.67	9.83	70	59	0.66	0.65	-	-	0.92	0.95	-	-	410	47	1.79	P
NW20/ PFA	BG	1.11	1.14	11.67	12	70	72	1.08	0.80	-	-	1.02	0.96	-	-	450	50	1.54	P